SYSTEM-LEVEL REPOSITORY SENSITIVITY ANALYSES USING TPA VERSION 3.2 CODE

Prepared for

Nuclear Regulatory Commission
Contract NRC-02-97-009

Prepared by

Center for Nuclear Waste Regulatory Analyses
San Antonio, Texas

August 1999

301 ----------Q199908260006

CNWRA 99-002

SYSTEM-LEVEL REPOSITORY SENSITIVITY ANALYSES USING TPA VERSION 3.2 CODE

Prepared for

Nuclear Regulatory Commission
Contract NRC-02-97-009

Prepared by

Sitakanta Mohanty
Richard Codell (NRC)
Robert W. Rice (Consultant)
James Weldy
Yichi Lu (SwRI)
Rose M. Byrne (NRC)
Timothy J. McCartin (NRC)
Mark S. Jarzemba
Gordon W. Wittmeyer

Center for Nuclear Waste Regulatory Analyses
San Antonio, Texas

August 1999

ABSTRACT

To review and quantitatively evaluate the safety case in a potential license application by the U.S. Department of Energy (DOE) for the proposed Yucca Mountain (YM) repository, the Nuclear Regulatory Commission (NRC), with technical assistance from the Center for Nuclear Waste Regulatory Analyses (CNWRA), developed a Total-system Performance Assessment (TPA) code. The most recent versions of the TPA code used in evaluation and calculation of YM performance are 3.2 and 3.2.3. This report describes a series of computations performed using these codes for determining the confidence in the estimation of future repository performance in light of the uncertainty in conceptual models and parameters of those models. This report primarily presents (i) the system-level and process-level results (e.g., intermediate results) to demonstrate trends and variabilities in outputs, (ii) the results of system-level sensitivity and uncertainty analyses using a variety of analysis techniques to determine the parameters that have the most influence on repository performance, and (iii) the relative importance of the integrated subissues in reviewing the DOE total-system assessment. An influential parameter is one that either drives uncertainty in performance, or one to which performance is sensitive. The sensitivity and uncertainty analyses were conducted using numerous TPA code runs (several thousand realizations) for each sensitivity analysis technique. Results of system-level analyses are based on peak dose and peak expected dose to a receptor group 20 km from the repository at two time periods of interest (TPIs): 10,000 yr (the likely compliance period in the draft regulation) and either 50,000 or 100,000 yr [a longer period for investigating any significant effects that may not be evident because of the calculated long waste package (WP) life].

Using the basecase, which included the seismic disruptive event scenario, peak expected doses of 0.003 mrem/yr and 4 mrem/yr were obtained for the 10,000- and 100,000-yr TPIs, respectively. The faulting scenario changed the peak expected dose negligibly. The igneous activity scenario increased the peak expected dose to 0.6 mrem/yr. For both TPIs, it was found that the most influential parameters were (i) the fraction of the repository wetted by infiltrating water, (ii) the fraction of water entering the WP, (iii) the well pumping rate at the 20-km receptor group location, (iv) alluvium retardation factors for radionuclides (specifically, ^{99}Tc and ^{129}I), and (v) the present-day infiltration. The most influential parameters for the 10,000-yr TPI, but not for the 50,000-yr TPI, were the initially defective fraction of WPs and the factor that focuses flow onto the WP. The most influential parameters for the 50,000-yr TPI, but not for the 10,000-yr TPI, were the alluvium retardation factors for radionuclides (specifically, ^{234}U and ^{237}Np). The influential parameters were then compared to the current integrated subissues, which are used by the NRC to focus work on items important to repository performance. Nine out of fourteen of the integrated subissues reflected at least one influential parameter.

The analyses and results are limited by the use of simplifying assumptions, models, and sparse data in certain areas. As a consequence, these results are preliminary. However, the estimations resulting from this study allowed the staff to focus attention on what is likely to be the most important phenomena relative to repository performance and point out deficiencies in the current state of knowledge. The manner in which these analyses were conducted or the assumptions and approaches used should not be construed to express the views, preferences, or positions of the NRC staff regarding the nature of site-specific regulations for YM.

CONTENTS

CONTENTS (cont'd)

CONTENTS (cont'd)

CONTENTS (cont'd)

FIGURES

FIGURES (cont'd)

FIGURES (cont'd)

TABLES

TABLES (cont'd)

ACKNOWLEDGMENTS

This report was prepared to document work performed by the Center for Nuclear Waste Regulatory Analyses (CNWRA) for the Nuclear Regulatory Commission (NRC) under Contract No. NRC-02-97-009. The activities reported here were performed on behalf of the NRC Office of Nuclear Material Safety and Safeguards, Division of Waste Management. The report is an independent product of the CNWRA and does not necessarily reflect the views or regulatory position of the NRC.

The authors wish to thank B. Sagar (CNWRA) and C. Lui (NRC) for their technical reviews and W. Patrick (CNWRA) and K. McConnell (NRC) for their programmatic reviews. Technical support provided by R. Rice (consultant) at various stages of this report is gratefully acknowledged. The effort of J. Firth (NRC), program element manager for the Total System Performance Assessment and Integration (TSPA&I) key technical issue, and C. Lui (NRC) in coordinating the multidisciplinary discussions leading to the identification of important integrated subissues is also recognized. Thanks to R. Janetzke for code quality assurance (QA), and debugging the code when needed, to O. Pensado for observing during the analyses of Total System Performance Assessment-Viability Assessment (TSPA-VA) results and providing insights into Total-system Performance Assessment code outputs behavior, and to M. Smith for helping to regenerate several output tables. Thanks are also expressed to K. Poor of Portage Environmental, Inc. for an informal technical review of the document; J.M. Menchaca, Southwest Research Institute (SwRI), for assistance in debugging and testing the computation of several sensitivity analysis methods; M. Muller (SwRI) for help in generating some of the outputs and plotting results. Some staff also tested the initial version of the code. Their contributions are acknowledged and much appreciated. Thanks are also expressed to B. Long, A. Woods, C. Gray and C. Cudd for editorial reviews and C. Garcia and A. Ramos for their secretarial support.

QUALITY OF DATA, ANALYSES, AND CODE DEVELOPMENT

DATA: CNWRA–generated data contained in this report meet QA requirements described in the CNWRA QA Manual. Data from other sources are freely used. The respective sources of non-CNWRA data should be consulted for determining levels of QA.

ANALYSES AND CODES: The TPA Version 3.2, 3.2.3, and 3.2MM codes have been developed following the procedures described in the CNWRA Technical Operating Procedure (TOP), TOP-018, which implements the QA requirements contained in the CNWRA QA Manual. The TPA Version 3.2MM code reflects a minor modification to the Version 3.2 code for use in conjunction with the Morris method. Codes used in conducting the Morris method and Fourier Amplitude Sensitivity Test have also been developed following procedures described in TOP-018.

EXECUTIVE SUMMARY

To review and quantitatively evaluate the safety case in a potential license application by the U.S. Department of Energy (DOE) for the proposed Yucca Mountain (YM) repository, the Nuclear Regulatory Commission (NRC), with technical assistance from the Center for Nuclear Waste Regulatory Analyses (CNWRA), developed a Total-system Performance Assessment (TPA) code. To date, three reports have been written by the NRC staff on performance assessment (PA) for the proposed YM repository. The first, referred to as iterative performance assessment (IPA) Phase 1 (Codell et al., 1992), assembled and demonstrated the NRC assessment methodology. The second NRC Total System Performance Assessment (TSPA), IPA Phase 2 (Wescott et al., 1995), used the TPA Version 2.0 code to investigate the features, events, and processes influencing isolation performance of the proposed YM repository. Information obtained in these IPA analyses was used in NRC reviews of early DOE TSPAs for YM. The third NRC TSPA (Nuclear Regulatory Commission, 1999) used the TPA Version 3.1 code (Mohanty and McCartin, 1998) to determine whether or not the NRC would be able to quantitatively evaluate the soundness of the conclusions reached by the DOE in their viability assessment (VA). Revisions were made to the TPA code leading to the development of the most recent version of the code, TPA Version 3.2 code (Mohanty and McCartin, 1998), which was used in evaluating the TSPA-VA. This report documents the most recent system- and process-level sensitivity and uncertainty analyses performed by the NRC and the CNWRA in conjunction with the review of the TSPA-VA. This report presents

- a brief description of the conceptual models implemented in the TPA code
- an in-depth discussion of basecase results for a single realization using the mean parameter values as well as for a full Monte Carlo run, deterministic results from alternative conceptual models, deterministic results from disruptive scenarios, and a proposed method for combining basecase and disruptive scenario results
- the results of system-level sensitivity and uncertainty analyses using statistical and nonstatistical techniques to determine the parameters that have the most influence on repository performance
- the results from the comparative studies of alternative conceptual models and combinations of models explicitly incorporated in the TPA Version 3.2 code or that can be mimicked through adjustment of input parameters to determine model and parameter uncertainties
- an estimation of the relative importance of the integrated subissues to focus staff effort
- a documentation of improvements in NRC staff capabilities in performance assessment based on the insights gained from process- and system-level results and sensitivity analyses.

Most calculations were made using the basecase data set in which 246 out of 838 parameters were sampled from specified ranges and distributions that represent data uncertainty and variability. To develop a better understanding of the trends of the outputs at a process level, results from a single realization (using the mean value data set) were also analyzed. Calculations to date using the basecase data set (the basecase is defined as the undisturbed scenario along with the effects of rockfall due to seismicity with multiple realizations) indicate peak expected doses of 0.003 mrem/yr in 10,000 yr (the proposed compliance period) and 4 mrem/yr

in 100,000 yr[1]. For a time period of interest (TPI) of 10,000 yr, primarily six radionuclides (^{237}Np, ^{129}I, ^{99}Tc, ^{234}U, ^{36}Cl, and ^{79}Se) contributed to the peak expected dose. For a TPI of 100,000 yr, four radionuclides (^{237}Np, ^{234}U, ^{99}Tc, and ^{129}I) were the primary contributors to peak expected dose with 92 percent of the contribution coming solely from ^{237}Np. Igneous activity is the primary contributor to the peak expected dose during the 10,000-yr TPI, estimated to be 0.6 mrem/yr. The faulting disruptive event is a negligible contributor to the peak expected dose.

The sensitivity and uncertainty analyses were conducted using numerous (several thousands for each analysis method) TPA code runs. The sensitivity and uncertainty of repository performance to specific parameters were evaluated using a number of different statistical tests. The statistical tests examined the sensitivity of repository performance to individual parameters in an effort to identify, as comprehensively as possible, those parameters most important for understanding repository performance. This helped to focus the review of the VA and prepare for the forthcoming review of the TSPA-site recommendation (SR). Sensitivity analyses used peak dose, expressed as total effective dose equivalent, for each TPA run as the performance measure. The use of peak dose eliminated the time dependency of the performance measure, thus simplifying the analyses. Alternative conceptual model studies used case-by-case analyses with peak expected dose from multiple realizations as the performance measure.

This report identifies and presents influential parameters for twoTPIs—10,000 and 50,000 yr. An influential parameter is one that either drives uncertainty in performance, or one to which the estimated performance is sensitive. For both TPIs, several parameters were found most influential for the basecase. The influential parameters include

- Areal fraction of the repository wetted by water infiltrating into the repository
- The fraction of water infiltrating into the repository from the unsaturated zone above the repository that will enter the waste package (WP) and contribute to the release of radionuclides
- Well pumping rate at the 20-km receptor group location
- Alluvium sorption properties (i.e., R_ds) for ^{99}Tc and ^{129}I
- Present-day areal average mean annual infiltration above the repository

In addition, the parameters influential for the 10,000-yr TPI, but not influential for the 50,000 yr, are

- Initially defective fraction of WPs
- A flow-focusing factor that expresses the flow reaching a wetted WP

The only parameters significant for the 50,000-yr TPI, but not influential for the 10,000 yr, are the alluvium R_ds for ^{234}U and ^{237}Np.

---

[1]The time period of interest of 100,000 yr used in presenting the basecase results is different from that used in the sensitivity analyses (10,000 and 50,000 yr), primarily because the basecase results were also used in reviewing the Department of Energy Total System Performance Assessment-Viability Assessment results, which extended to 100,000 yr and beyond.

The influential parameters were used to focus the review of the VA and were also traced back to the integrated subissues used by the NRC to focus its high-level waste program on aspects important to repository performance (Nuclear Regulatory Commission, 1998). Nine out of fourteen integrated subissues have at least one influential parameter (including the integrated subissues related to disruptive scenarios), based on the results of the TPA Version 3.2 code. It should be noted that the staff has not yet developed appropriate techniques for conducting sensitivity analyses of results from the disruptive scenarios with appropriate consideration of probability weighting. Therefore, the sensitivity analyses results from disruptive scenarios are used as such (i.e., without probability weighting) for crosswalking the influential parameters with the integrated subissues. The integrated subissues deserve careful examination because the current models delay any significant radionuclide releases past the 10,000-yr TPI. The delay is primarily attributable to (i) corrosion-resistant material of the inner overpack pushing the WP failure time beyond 10,000 yr, (ii) thermal reflux delaying the onset of flow into the repository, (iii) WP filling time delaying the radionuclide release time by hundreds to thousands of years, and (iv) radionuclide sorption in the alluvium causing significant delay in the arrival time of radionuclides.

This TSPA serves to aid the NRC staff in focusing their review of DOE TSPAs, especially those for the VA and SR, on those models and parameters that could significantly influence the estimated system performance. It should be noted that the results presented in the following chapters are based on numerous simplifying assumptions and use only limited site-specific data. Consequently, the numerical results should not be taken as representative of the performance of the proposed repository at Yucca Mountain, Nevada. Conclusions drawn from the analyses presented in this report may change as the models and assumptions are updated based on revised design, ongoing site characterization, recommendations from reviewers and experts, new regulatory requirements, and improved model conceptualization and data interpretation by staff. The analysis also contains uncertainties regarding conceptual models for consequences and scenarios. Finally, this report should be considered as an interim demonstration of some of the methods that the NRC staff has developed to review a performance assessment submitted by DOE as part of any potential license application. Thus, at the conclusion of some future TSPA effort, instructions to the NRC staff will be developed and documented regarding which specific compliance determination methods will be used to review a DOE performance assessment. Neither the manner in which these analyses were conducted nor the assumptions and approaches used should be construed to express the views, preferences, or positions of the NRC staff regarding the nature of site-specific regulations for YM.

1 INTRODUCTION

In accordance with the provisions of the Nuclear Waste Policy Act (NWPA) of 1982, as amended, and the Energy Policy Act (EnPA) of 1992, the Nuclear Regulatory Commission (NRC) is responsible for evaluating the license application for a proposed geologic repository constructed for emplacement of high-level nuclear waste (HLW) [i.e., commercial spent fuel (SF), several types of U.S. Department of Energy (DOE) and U.S. Navy SF, and vitrified HLW] at Yucca Mountain (YM), Nevada. In support and preparation of its regulatory review activities outlined in the NWPA and EnPA, the NRC staff is conducting detailed technical performance assessments (PAs) to understand and identify the potentially important isolation characteristics and capabilities of the proposed repository system at the YM site based on the available information.

This PA activity, which is part of an ongoing process at the NRC to prepare for the review of a potential DOE license application for the proposed HLW disposal facility at YM, includes regular interactions between the NRC and DOE on the topic of PA. For example, NRC staff comments on model abstraction related to the Total System Performance Assessment-Viability Assessment (TSPA-VA) were relayed to the DOE in a letter to Dr. S. Brocoum dated July 6, 1998 (Bell, 1998). Furthermore, the DOE, NRC, and various stakeholders regularly interact on the topic of PA through technical exchanges.

As part of these Iterative Performance Assessment (IPA) activities, the NRC and its support contractor, the Center for Nuclear Waste Regulatory Analyses (CNWRA), are using the enhanced Total-system Performance Assessment (TPA) computer code. The TPA code, which evolves with each IPA phase, is designed to simulate the behavior of the geologic repository taking into account the essential characteristics of the natural and engineered barrier systems (EBS), and changes in knowledge about the geologic setting and design. This document presents system-level sensitivity and uncertainty analyses using the latest version of the TPA code, Version 3.2.

The NRC previously conducted analyses of repository performance (Codell et al., 1992; Wescott et al., 1995). For the latest iteration, Version 3.2 of the TPA code was developed as a more general and versatile computer code that more readily can accommodate changes to the design of the proposed YM repository. This version (i) accommodates the repository design outlined in the TSPA-VA (U.S. Department of Energy, 1998) [e.g., repository layout and waste package (WP) emplacement and design], (ii) quantifies total system performance related to the proposed compliance performance measure [the peak expected dose, expressed as total effective dose equivalent (TEDE), in the time period of interest (TPI)] expected in the forthcoming U.S. Environmental Protection Agency (EPA) standard and as proposed in the draft NRC site-specific regulations (Nuclear Regulatory Commission, 1999a), and (iii) includes recent site data and improved conceptual models. In addition, because approaches to estimate the performance of geologic repositories and site and repository design data continue to evolve, the TPA Version 3.2 code was developed with the flexibility to perform alternative calculations. Some of the examples include

- Evaluate alternative repository and design features
- Analyze the effect of different areal mass loadings
- Assess the significance of various disruptive scenario classes
- Evaluate radionuclide dilution in the saturated zone (SZ)
- Compute the dose as a function of time for a 10,000-yr or longer TPI
- Evaluate alternative SF dissolution models

1.1 BACKGROUND

The PAs for geologic repositories are based on conceptual models of physical processes (embodied in computer codes) and parameters derived from field and laboratory data or expert elicitation. Because of the variability and sparsity of measured data and the underlying uncertainty involved with modeling physical processes for many thousands of years, the results of any PA are uncertain. Therefore, an important aspect of conducting a PA is quantifying the sensitivity of the results to, and the uncertainty associated with, the input parameters. An analysis of PA code output sensitivity and uncertainty will provide information delineating which input parameters most affect the model results. A better understanding of the parameters that have the most influence on model results can be used to improve the code and build confidence in the numerical results produced by the code. Likewise, identification of the most influential parameters and those parameters that drive uncertainty provides a means of comparing and evaluating different PA models and indicates where future design, site characterization, and analysis activities should be focused.

The staff developed a systematic approach to reviewing the DOE TSPAs. As currently envisioned, the approach is hierarchical, as illustrated in figure 1-1. The focal point is the overall repository system where the performance measure is anticipated to be the expected annual dose to the average member of the critical group during the performance TPI. To facilitate review of the DOE TSPAs, staff will examine the contribution to performance from each of three repository subsystems—engineered, geosphere, and biosphere—as shown in the second tier of figure 1-1. Each of these subsystems is further subdivided into discrete components of the respective subsystems—engineered barriers that make up the engineered system; unsaturated zone (UZ) flow and transport, SZ flow and transport, and direct release to the biosphere; and the dose calculation for the biosphere. This characterization of components is not strictly based on the physical aspects of the system but stems from the perspective of dose or risk calculations for total system performance evaluation. Recognizing there are many different ways of dividing the overall system into smaller and analyzable components, this particular division is primarily based on the natural progress of radionuclide release and transport to a receptor group at the YM site and takes advantage of the results of past NRC IPA and reviews of the DOE TSPAs. At the base of the hierarchy are the key elements of the repository system that need to be appropriately abstracted into a TSPA. These key elements of subsystem abstraction (KESA), in general, are the integrated processes, features, and events that could affect system performance. In conformance with recently proposed changes to the structure of the NRC program for resolving issues related to the HLW repository program, the KESAs are now known as the integrated subissues.

1.1.1 Previous Iterative Performance Assessment Analyses

To date, three reports have been written by NRC staff on PA for the proposed YM repository. The first, referred to as IPA Phase 1 (Codell et al., 1992), assembled and demonstrated the NRC assessment methodology. IPA Phase 1 examined the sensitivity and uncertainty in radionuclide releases to the accessible environment for a geologic repository in unsaturated tuff. The second NRC TSPA, IPA Phase 2 (Wescott et al., 1995), was performed using the TPA Version 2.0 code to investigate the features, events, and processes influencing isolation performance of the proposed YM repository. Information obtained in these IPA analyses was used in NRC reviews of early DOE TSPAs for YM. The overall performance measures for the geologic repository used in IPA Phase 2 were cumulative total releases of radionuclides (normalized release) to the accessible environment and radiation dose (effective dose equivalent) to the exposed population. The third NRC TSPA (Nuclear Regulatory Commission, 1999b) was performed using the TPA Version 3.1 code to determine whether or not the NRC would be able to quantitatively evaluate the conclusions reached by the DOE in their VA. Subsequent to developing and testing the TPA Version 3.1 code, detailed sensitivity and

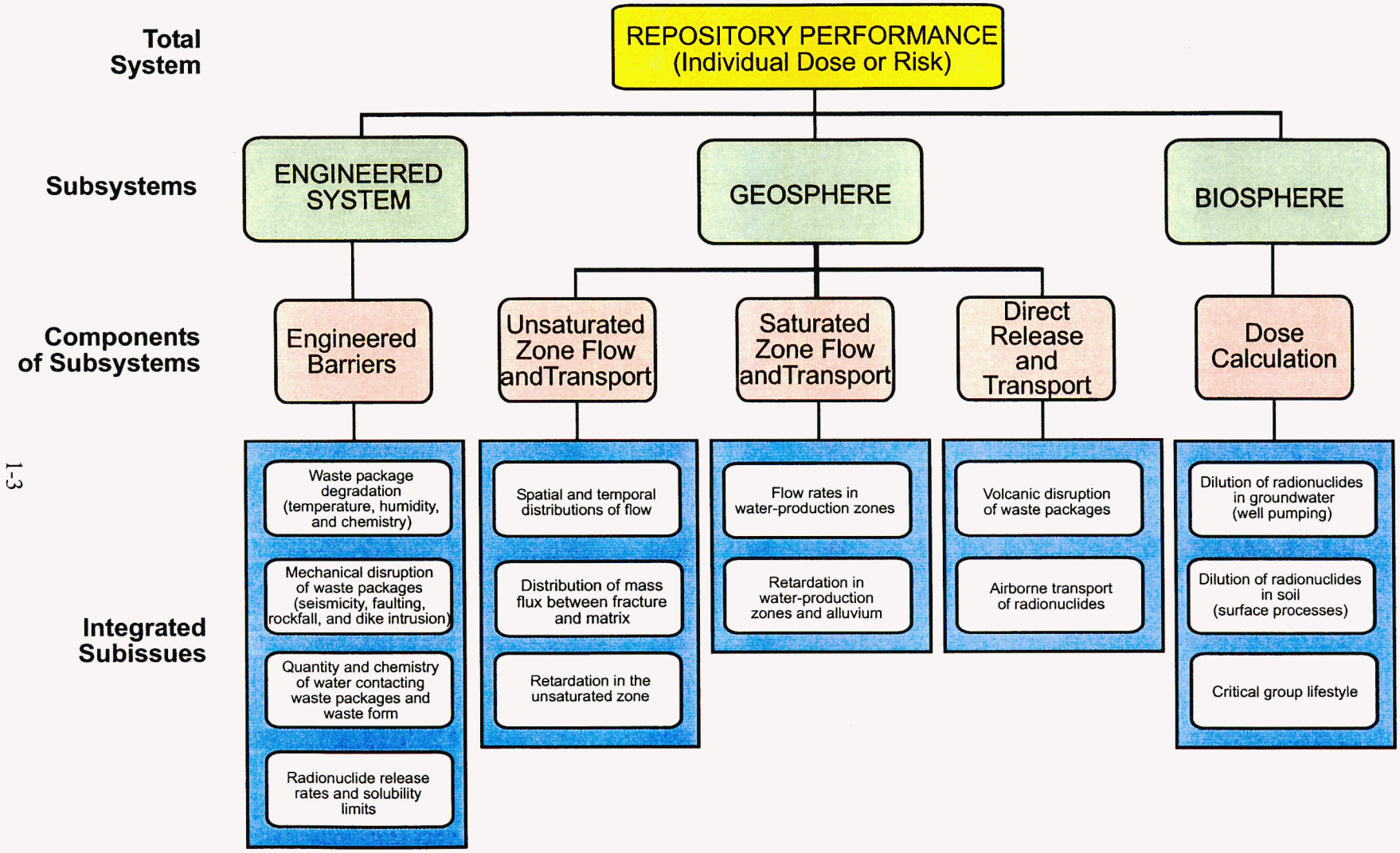

Figure 1-1. Flowdown diagram showing the subsystems and the integrated subissues

uncertainty analyses were undertaken (Nuclear Regulatory Commission, 1999b) that indicated the need for further refinement of the TPA code prior to its use to evaluate the DOE TSPA-VA (Department of Energy, 1998). Revisions were made to the TPA code leading to the development of the current TPA Version 3.2 code, which was used in the evaluation of the TSPA-VA.

In addition, the TSPA analyses are used to better focus NRC activities on those factors of greatest importance to repository performance. The draft site-specific rule developed by the NRC for the proposed YM repository is a risk-informed, performance-based rule. Therefore, the NRC review of a potential license application to build and operate a deep geologic repository at YM necessarily will focus on those physical aspects of the repository system of greatest importance to radiological safety. The results from this study, in part, will be used to focus and direct the review strategy outlined by the NRC in its Yucca Mountain Review Plan (YMRP).

1.1.2 Iterative Performance Assessment Phase 1 Sensitivity and Uncertainty Analyses

Four sensitivity or uncertainty analyses were performed for IPA Phase 1 (Codell et al., 1992): (i) demonstration of the effect of individual parameters on the resultant complementary cumulative distribution function (CCDF) for cumulative release to the accessible environment, (ii) use of stepwise linear regression to estimate sensitivity of key parameters in the consequence models, (iii) determination of relative importance of individual radionuclides in the waste, and (iv) sensitivity of CCDFs to performance of the natural and engineered barriers. The sensitivity and uncertainty analyses considered only groundwater pathway releases, not those from human intrusion or airborne release through igneous activity. Gaseous release of radionuclides was not part of the IPA Phase 1 TSPA results but was included as an auxiliary analysis.

Although IPA Phase 1 conducted full sensitivity and uncertainty analyses for the groundwater pathway, only CCDFs for cumulative release were generated for the scenario cases (basecase, basecase with human intrusion, and basecase with pluvial conditions with and without human intrusion). Cumulative release refers to the sum of releases of all radionuclides during the TPI. The CCDFs reflected the uncertainty in the sampled parameters propagated through the analysis. Peak dose was not calculated as a performance measure for the IPA Phase 1 study.

1.1.3 Iterative Performance Assessment Phase 2 Sensitivity and Uncertainty Analyses

In IPA Phase 2 (Wescott et al., 1995), model results were evaluated to develop regression equations describing TSPA model output and to analyze input parameter sensitivity. Techniques used to develop a regression equation that emulated the TPA model included transformation of data (Iman and Conover, 1979; Seitz et al., 1991); test for heteroscedasity (residual variation—Draper and Smith, 1981; Bowen and Bennett, 1988; Sen and Srivastava, 1990); and Mallows' C_p statistic (Sen and Srivastava, 1990). In addition to techniques used in previous PA work (e.g., the stepwise linear regression), several techniques were evaluated to determine parameter importance and sensitivity, including Kolmogorov-Smirnov (K-S) and Signs tests (Bowen and Bennett, 1988) and differential analysis (Helton et al., 1991).

Phase 2 IPA included a number of disruptive scenarios. These scenarios included igneous activity, seismicity, faulting, climate change, and exploratory drilling. Sensitivity and uncertainty analyses were conducted on the undisturbed case as well as on the other scenario cases. These analyses were conducted

with radionuclide release to the accessible environment and integrated population dose as the output variables, in contrast to peak expected dose described in this report.

1.1.4 Total-System Performance Assessment Version 3.1 Sensitivity and Uncertainty Analyses

For the TPA Version 3.1 code (Nuclear Regulatory Commission, 1999b), a variety of analytical procedures were implemented to assess the sensitivity of the estimated peak dose due to variations in the values of model parameters as well as to changes resulting from use of alternative conceptual models. Scaled sensitivity coefficients were obtained by univariate and stepwise, multiple linear regression, and by standard differential analysis. To make linear regression models as accurate as possible, the dependent (peak dose) and independent (sample parameter values) variables were transformed using four methods: (i) normalization, in which the variable is divided by its mean; (ii) standardization, in which the difference between the variable and its mean is divided by the standard deviation of the variable; (iii) rank transformation, in which the value of the variable is replaced by its numerical rank; and (iv) logarithmic transformation, in which a multiplicative model is converted to an additive model. The statistical significance of the scaled sensitivity coefficients obtained by stepwise regression was determined using Student's t-statistic. The importance or influence of each parameter was ranked by the order in which the stepwise procedure selected the parameter for inclusion as an explanatory variable in the regression equation and by the use of K-S and Sign tests.

Sensitivity coefficients were calculated for both 10,000- and 50,000-yr TPIs and for waste canisters constructed with an inner corrosion-resistant layer of either Alloy 625 or Alloy C-22 leading to the identification of four distinct sets of important parameters. The effects of employing alternative conceptual models were also investigated for a number of the repository subsystems. Alternative conceptual models that were considered include (i) backfilling of the repository, (ii) matrix diffusion in the rock matrix, (iii) credit for protection of the fuel provided by zircaloy cladding, (iv) focusing the flow of water to a smaller number of WPs, (v) use of the flowthrough model for SF dissolution and transport, (vi) radionuclide release rates based on natural analogs for SF, (vii) no credit for sorption of radionuclides, and (viii) instantaneous failure of all WPs.

Based on the results of the sensitivity and uncertainty analyses, preliminary conclusions were drawn about the relative importance of the integrated subissues or KESAs. For the 10,000-yr TPI, the most important integrated subissues are those for WP corrosion and the quantity and chemistry of water contacting the WPs. When Alloy C-22 is used, corrosion of the WPs is minimal during the 10,000-yr TPI, and mechanical disruption of the WPs is the most important integrated subissue. For the 50,000-yr TPI, the integrated subissues related to dilution of radionuclides in groundwater through well pumping and retardation in water production zones and alluvium are of increased importance.

1.2 PURPOSE OF CURRENT ANALYSIS

Similar to the sensitivity and uncertainty analyses conducted for previous IPA phases and the TPA Version 3.1 code, multiple sensitivity and uncertainty analyses have been conducted using the TPA Version 3.2 code. Sensitivity is defined as the relative change in output for a unit change of input, and uncertainty is the comparative change in overall output range because of input value uncertainty. Sensitivity and uncertainty analyses described in this report have been used to

- Focus staff reviews of the DOE TSPA-VA on those factors most significant to total-system performance.

- Determine the input parameters in the TPA Version 3.2 code that are most influential to the estimated peak dose for the TPI at the receptor location by using a number of techniques. Although process-level sensitivity and uncertainty analyses have been conducted with the TPA code to determine the parameters most important in a given key technical issue (KTI) (e.g., unsaturated and saturated flow under isothermal conditions, igneous activity), this report summarizes analyses conducted to determine the most influential parameters at the total system level.

- Estimate the relative importance of the integrated subissues or KESAs.

- Continue improving staff capabilities, including improving the TPA code, for conducting independent evaluation of future DOE TSPAs for the site recommendation and license application for the proposed YM repository.

Since the release of the TPA Version 3.1.4 code, which was used in the TPA Version 3.1 code sensitivity analyses (Nuclear Regulatory Commission, 1999b), several major improvements were incorporated into the TPA code and associated input data sets that may have a significant affect on the sensitivity analysis results. Most of these changes were based on new information provided by the DOE after the completion of the TPA Version 3.1.4 code. For example, the DOE decision to replace Alloy 625 with Alloy C-22 as the material for the inner overpack in WP required substantial changes to the TPA model abstraction and its associated model parameters. The second basis for improvements resulted from experience gained from the process- and system-level sensitivity analyses using TPA Versions 3.1.1–3.1.4. Specific changes that were made to the TPA Version 3.1.4 code to obtain the new TPA Version 3.2 code include

- Accounting for the effect of secondary mineral formation on SF dissolution

- Considering the effects of a concrete tunnel invert on the transport of radionuclides

- Introducing correlation between sampled radionuclide sorption parameters for chemically similar species to reflect realization-to-realization homogeneity of water chemistry

- Assessing the significance of the radionuclide inventory between the fuel pellet and the cladding (gap inventory)

- Refining the model used to estimate mechanical failure of the WP from seismically induced rockfall

- Allowing the user to specify the volume of SF wetted (i.e., bathtub height) so that alternate WP failure modes can be better modeled

- Revising the code to implement parameter value distributions that reflect the most current data

1.3 REPORT ORGANIZATION

This report documents the most recent system-level sensitivity and uncertainty analyses performed by the NRC and the CNWRA that were conducted using the TPA Version 3.2 code. Chapter 2 provides a brief description of the TPA Version 3.2 code. Chapter 3 presents an in-depth discussion of basecase results for a single realization using the mean parameter values as well as for a full Monte Carlo run, deterministic results from alternative conceptual models, deterministic results from disruptive scenarios, and a proposed method for combining basecase and disruptive scenario results.

Chapter 4 describes the system-level sensitivity studies, which were conducted in two parts. A set of alternative conceptual models and disruptive scenario cases were compared to evaluate the relative importance of specific components and assumptions used in the model. Evaluating the influence of individual components of the model in this way, where the full set of parameter values is used and a more comprehensive range of repository behavior is modeled, allows the relative importance of the components to be investigated. The sensitivity and uncertainty of repository performance to specific parameters were evaluated using a number of different statistical tests because no single test is completely comprehensive. The use of numerous statistical tests (described in this chapter and appendices A–C and E) to examine the sensitivity of repository performance to individual parameters is intended to identify, as comprehensively as possible, those parameters most important for understanding repository performance.

Evaluation of important parameters based on the system-level sensitivity studies is provided in chapter 5. Here, the important parameters and the alternative conceptual model investigations are related to the NRC integrated subissues or KESAs. Conclusions resulting from this study are described in detail in chapter 6. Appendix D describes the abbreviated parameter names used throughout the report.

1.4 CAVEATS

Because it is not possible to model a system as complex as a geologic repository in a complete and exhaustive manner, a number of assumptions and limitations are used directly, or are implicit, in the analyses conducted in this report. These assumptions and limitations are listed next.

- Any underlying assumptions, limitations, and bases used to construct the models in the TPA Version 3.2 code also apply to these analyses. These models are described in chapter 2 and discussed in greater detail in the TPA Version 3.2 Code User's Guide (Mohanty and McCartin, 1998).

- The results are limited by the use of simplifying assumptions, models, and sparse data in certain areas. As a consequence, these results are preliminary. Moreover, the manner in which these analyses were conducted or the assumptions and approaches used should not be construed to express the views, preferences, or positions of the NRC staff regarding the ongoing efforts to develop site-specific regulations for YM.

2 OVERVIEW OF THE TOTAL-SYSTEM PERFORMANCE ASSESSMENT CONCEPTUAL MODELS IN THE TPA VERSION 3.2 CODE

Analysis of repository performance is anticipated to be complex with substantial uncertainties because of the first-of-a-kind nature of the repository, extended period of performance, and reliance on engineered and natural barriers. The TPA analysis focuses on the postclosure performance of the proposed HLW repository at YM over long time periods (e.g., 10,000 yr). To attempt to quantify the uncertainty in estimating repository performance over long time periods, the TPA analysis is conducted in a probabilistic manner in which many realizations are calculated using input parameter sets sampled from probability distributions. Therefore, detailed simulation models that include all the process couplings, heterogeneities, and complexities are not incorporated into PA models to maintain reasonable computer execution times with modest hardware resources. Though a probabilistic code, the TPA analysis can also be performed in a deterministic mode.

The TPA Version 3.2 code is used in this analysis to obtain deterministic and probabilistic estimates of dose for specified time periods (e.g., regulatory compliance TPI and beyond) at designated receptor locations (e.g., 20 km down-gradient of YM). The TPA Version 3.2 code, which is specifically tailored for evaluation of performance of the proposed repository at YM, is an update of the code used in the NRC IPA Phase 2 study. Conceptual models used in the previous version of the TPA code have been documented in Mohanty and McCartin (1999)[1] and for the 3.2 version in Mohanty and McCartin (1998).

A key part in developing the model used in the TPA Version 3.2 code is determining the level of detail in the processes, design, and attributes of the site necessary to produce a credible analysis that provides meaningful insights into performance without an unreasonable computational burden. A discussion of the repository system and the basecase conceptual models is presented in this section to provide a general overview of the TPA Version 3.2 code. This chapter also includes descriptions of the alternative conceptual models analyzed in chapters 3 and 4.

The TPA Version 3.2 Code User's Guide contains more detailed information on the conceptual and mathematical models and the code structure (Mohanty and McCartin, 1998). A simplified flow chart illustrating the structure of the TPA Version 3.2 code is presented in figure 2-1. The TPA input parameter values and the bases for their selection are presented in appendix A of the same User's Guide.

2.1 CONCEPTUALIZATIONS OF REPOSITORY AND GEOLOGIC SETTING

For ease of use and computational efficiency, the TPA Version 3.2 code replaces the intricate repository layout and the complex geologic setting with relatively simple conceptual representations. The repository layout, for example, is represented by an idealized planar feature discretized into a set of subareas, while the geology is replaced by a sequence of homogeneous layers. Properties and environmental conditions for each subarea are assumed uniform. Except for the influence of the thermal load, flow

[1]Mohanty, S., and T.J. McCartin, eds. 1999. *NRC Sensitivity and Uncertainty Analyses for a Proposed HLW Repository at Yucca Mountain, Nevada Using TPA 3.1. Volume I: Conceptual Models and Data.* NUREG–1668. Washington, DC: Nuclear Regulatory Commission. To be published.

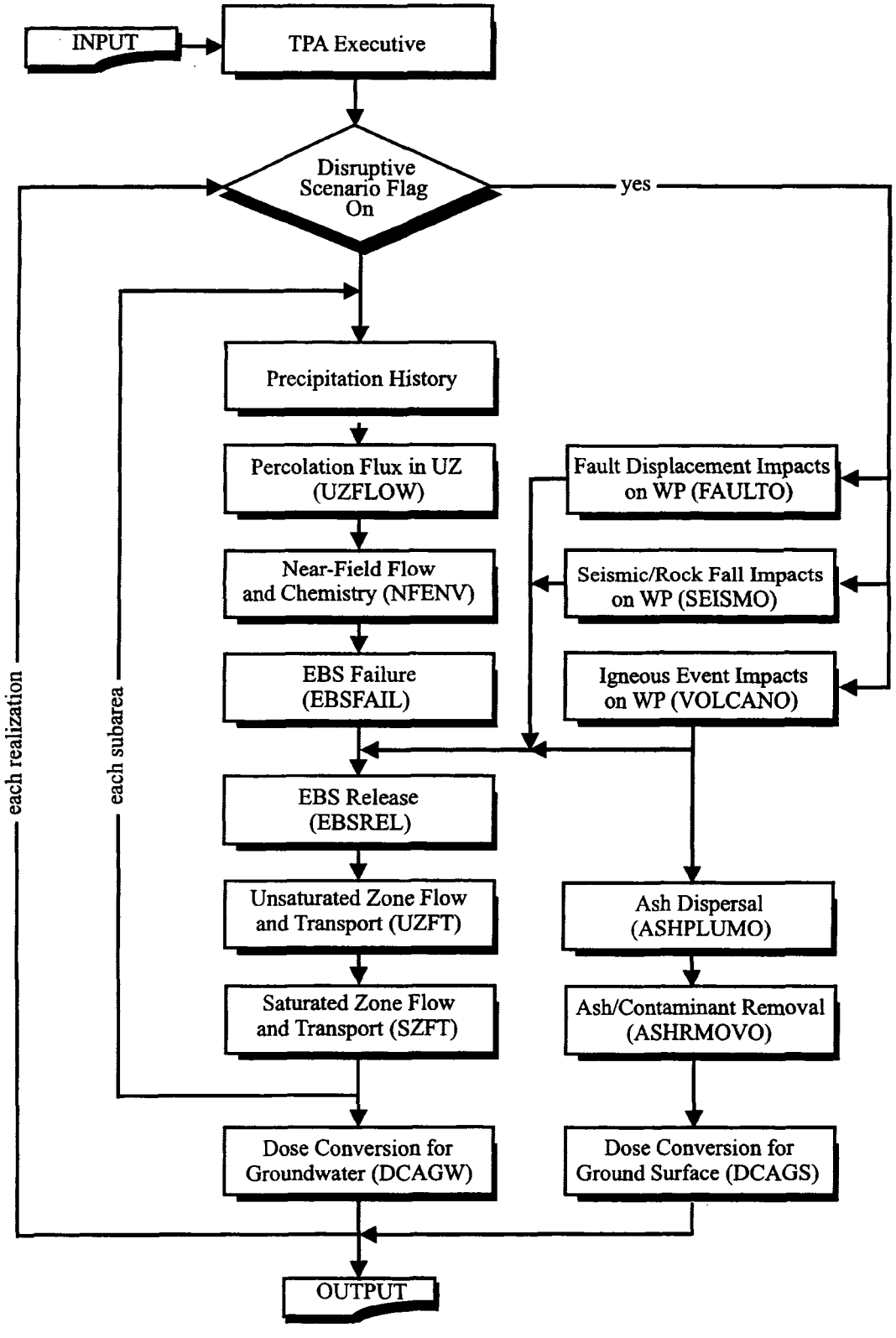

Figure 2-1. Flow diagram for TPA Version 3.2 code

and transport processes in and below a given subarea are independent of processes in other subareas. Thus, flow is entirely vertical with no lateral diversion in the UZ.

As illustrated in figure 2-2, quadrilateral subareas of uniform thickness are used to represent individual subregions of the repository. In the current application, the repository is divided into seven subareas; however, the TPA Version 3.2 code has the capability to use much finer discretizations of both the repository and the geologic setting beneath it. The number of WPs in each subarea is assumed proportional to the fraction of the total repository area represented. Radionuclide releases from the EBS are calculated by modeling a single prototypical WP for each subarea and for each failure type. Performance characteristics of the WP and subsequent release in each subarea are calculated by considering the evolution of such characteristics as climatic conditions, water flux, thermal and chemical conditions, and geologic processes (e.g., seismicity, fault displacement, and igneous activity). Breaching of the WP by human intrusion and the associated release is not considered in the TPA Version 3.2 code.

The geologic setting is composed of the UZ (i.e., geologic media between the ground surface and the water table) and the SZ (i.e., groundwater aquifer beneath the repository, extending to the location of the receptor group). For simplicity, the stratigraphy is assumed laterally continuous and uniform within a subarea but differing from subarea to subarea. This simplification implies that, in general, flow in the UZ is primarily vertical with little or no lateral diversion of flow along hydrostratigraphic units. The geologic setting also includes features, events, and processes, such as seismicity, tectonism (faulting), and igneous activity (intrusive and extrusive) that may adversely affect the performance of the repository. Seismicity, tectonism, and intrusive igneous activity affect the performance characteristics of the WP and contribute to groundwater releases.

To model flow and transport in the SZ, the TPA conceptual model consists of four distinct streamtubes over the width of the repository footprint normal to UZ flow. Each of the seven streamtubes in the UZ is connected to one of the four streamtubes in the SZ, based on proximity. Radionuclide releases from each of the UZ streamtubes provide the source term to the SZ streamtubes. The SZ streamtubes are treated as separate conduits and have flow velocities that vary along the individual flow paths. The mass flowrate of radionuclides exiting all SZ streamtubes at the well head is used to calculate annual dose to the average member of the receptor group. The annual dose computation accounts for all releases in the groundwater pathway at the location of the receptor group, the spatial extent of the releases in the SZ at the location of the receptor group, the extent of the production zone containing the radionuclides (all radionuclides are assumed released in one production zone), and the influence of the pumping rate attributed to water use by the receptor group.

Direct release of radionuclides to the accessible environment because of an extrusive igneous event is also modeled in the TPA Version 3.2 code. The physical characteristics of the extrusion and the assumption of a uniform distribution of WPs in the repository are used to determine the number of WPs affected by the event. Radionuclides are transported to the receptor location based on characteristics of the eruption and meteorological conditions. The areal density of radionuclides in the soil, resulting from the deposition of volcanic ash containing SF particles, is then calculated. This soil concentration is used in computing the annual dose to the average member of the receptor group.

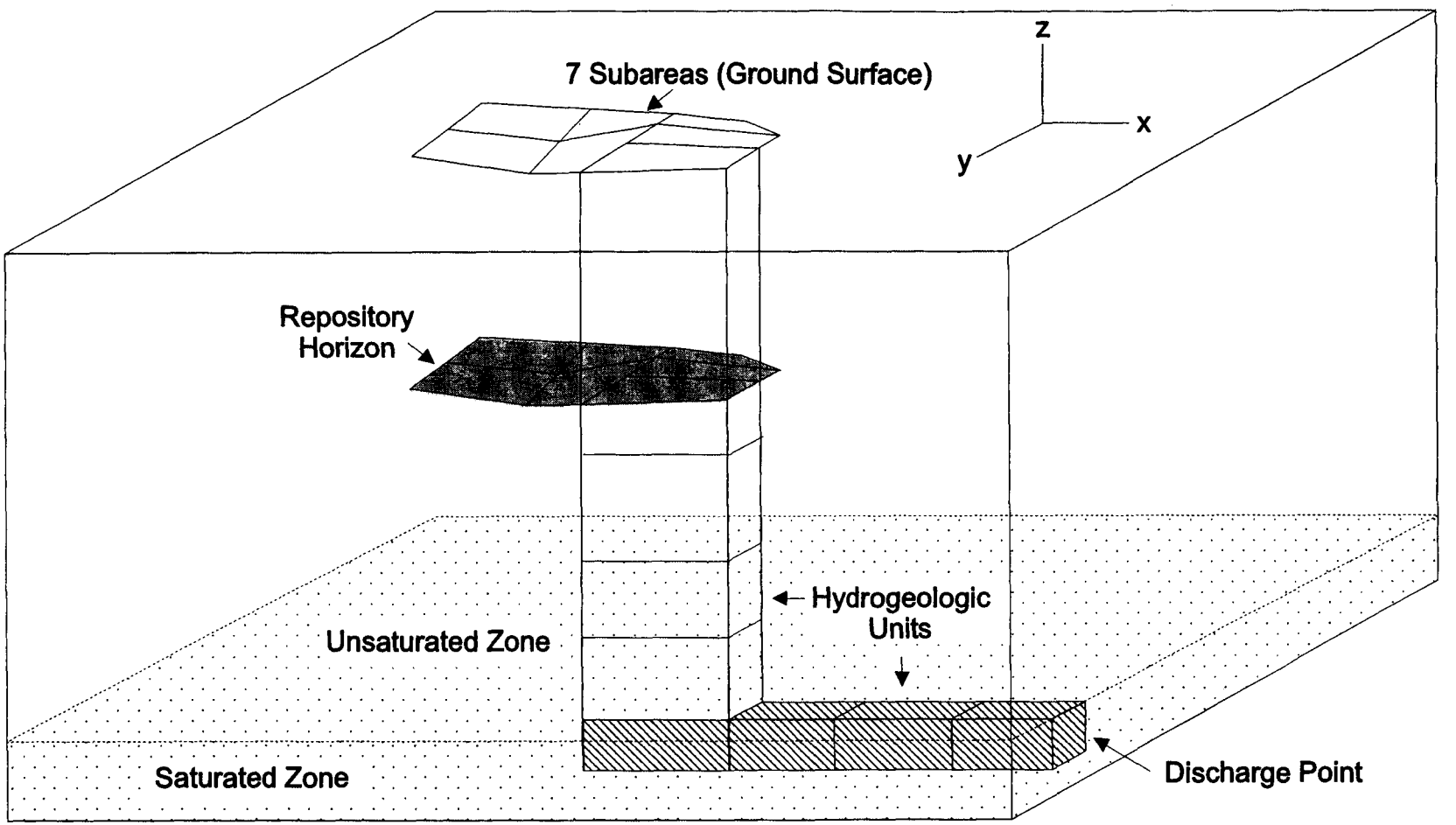

Figure 2-2. Conceptualization of the repository system

2.2 CONCEPTUAL MODELS IMPLEMENTED IN THE TOTAL-SYSTEM PERFORMANCE ASSESSMENT COMPUTER CODE

In developing the TPA Version 3.2 code, several conceptual models were formulated, integrated, and implemented in various abstracted mathematical models. These basic conceptual models, which describe the interactions and couplings of the physical and chemical processes believed present in a proposed geologic repository at YM, can be grouped into the following generic categories:

- Infiltration and deep percolation
- Near-field environment
- Radionuclide releases from the EBS
- Aqueous-phase radionuclide transport in the UZ and SZ
- Airborne transport from direct radionuclide releases
- Exposure pathways and reference biosphere

These conceptual models are designed to apply to the current DOE repository design and specific site characteristics of the YM area and provide flexibility for examining alternative designs and uncertainties in site and engineered material performance. In some of these generic categories, alternative conceptual models also have been incorporated into the code.

These conceptual models are used to represent a range of system states including disruptive events. The consequences of disruptive events (e.g., seismicity, fault displacement, and igneous activity) are evaluated with the TPA Version 3.2 code by assessing the effects on EBS failure (producing releases to groundwater), direct releases of radionuclides (airborne releases to the biosphere), or both. The probability of occurrence of a disruptive event combined with the resulting consequences are used to calculate a risk curve separate from the TPA Version 3.2 code execution.

The following discussion provides a general overview of the key aspects of the major conceptual models implemented in the TPA Version 3.2 code. More detailed descriptions of these models, including the mathematical basis, assumptions, and calculational methodologies, are presented in the TPA Version 3.2 Code User's Guide (Mohanty and McCartin, 1998).

2.2.1 Infiltration and Deep Percolation

A one-dimensional (1D) modeling approach is used in the TPA Version 3.2 code to describe the movement of meteoric water at the land surface vertically downward (i.e., without lateral flow) through the UZ, to the repository horizon, and ultimately to the water table. In the 1D conceptual model, the deep percolation flux (q_{perc}) is constrained to be equal to the shallow infiltration rate (q_{infil}). The annual average q_{infil} is estimated based on

- Present-day shallow-infiltration rate
- Change in climate with time
- Elevation and soil depth over the repository subarea

Uncertainty in the present-day infiltration rate estimate is accounted for in the TPA Version 3.2 code by treating it as a statistically sampled input parameter. Temporal variations are incorporated by varying the present-day infiltration rate over the 100,000-yr TPI assumed for long-term climatic changes. The effects

of site-specific soil cover thickness and elevation are used to reflect the spatial variation over each of the subareas.

The temporal and spatial variations of q_{infil} were developed through consideration of paleo-climatic information and results from detailed process-level auxiliary analysis (Stothoff et al., 1997). The q_{infil} response function depends on two independent variables, present-day mean annual precipitation (MAP) and mean annual temperature (MAT), as well as the present-day infiltration rate. After computing q_{infil}, the water flux at the repository horizon is then partitioned into

- Water flux diverted around the WP
- Water flux entering the failed WP

Thus, for the purposes of the TPA Version 3.2 code, the net water flux carrying dissolved radionuclides is a fraction of the total water flux arriving at the repository. It is this net water flux that is used in the TPA Version 3.2 code to calculate the radionuclide source term for each subarea.

2.2.2 Near-Field Environment

Physical and chemical processes in the near field of the repository, such as heat transfer, water-rock geochemical interactions, and refluxing of condensate water, are expected to affect WP performance. In the TPA Version 3.2 code, a range of near-field characteristics is depicted in the abstracted mathematical models for heat and water flow and table look-ups for chemical parameters. To estimate WP failure times and radionuclide release rates, the near-field environment is characterized by

- Drift wall rock and WP surface temperatures
- Relative humidity (RH) (defined in the TPA code as the ratio of vapor pressure at the drift rock wall to the vapor pressure at the WP surface)
- Water chemistry (e.g., pH, chloride concentration, and carbonate ion concentration)
- Water reflux during the thermal phase

The average rock temperature in the repository horizon is calculated assuming a conduction-only model (i.e., the time history of temperature for each subarea is calculated accounting for the amount of emplaced waste) and no ventilation in the drifts. The WP surface temperature is calculated using a multimode heat transfer (i.e., conduction, convection, and radiation) model. Vapor pressure is computed using the standard thermodynamic equation relating vapor pressure to temperature.

Estimates of the pH and chloride concentration histories of water films on the WP surface were developed in a separate process-level auxiliary analysis using the multicomponent geochemical module of the MULTIFLO code (Lichtner and Seth, 1996). MULTIFLO was applied to calculate the pH and chloride concentration for water percolating through the matrix of the tuffaceous rock. Because the chloride concentration in the water film is likely to be higher than that in the rock mass, the chloride history is scaled by a statistically sampled parameter that varies between 1 and 30 where 30 scales the peak chloride concentration to its solubility limit. The TPA Version 3.2 code provides the option of either using a look-up table that uses the temperature-dependent pH (not currently used) and chloride concentration generated with

the MULTIFLO code or specifying constant values in the input file. In general, the user selects code options by changing flag and variable values in the code input file.

The amount of water percolating through the drifts varies over time primarily because of the coupled processes of heat transfer and fluid flow (e.g., vaporization, condensation, and refluxing). Water refluxing produced by these thermohydrologic effects is important during the first few thousand years, after which natural percolation determines the rate of water flow into the repository. Three water reflux models based on bulk flow balances are included in the TPA Version 3.2 code. The first model considers episodic reflux associated with time-dependent perching above the repository. The second model assumes that the volume of refluxing water will always be sufficient to depress the boiling isotherm in fractures and reach the WP during times when the surface temperature exceeds the boiling point of water. In the third model, the degree to which the boiling isotherm is depressed is a function of the temperature, the thickness of the dryout zone, and the volume of reflux water. These functions vary with time. Each reflux model produces estimates of the total water flux into the repository during the thermal period.

2.2.3 Radionuclide Releases from the Engineered Barrier System

In the TPA Version 3.2 code, the performance of a prototypical WP is modeled for each repository subarea considering the failure time and radionuclide release rates for each of the WP failure categories. When this prototypical WP fails, all WPs in that subarea within a specified failure category are assumed to have failed. The estimation of both WP failure times and liquid releases is dependent on the nature and extent of corrosion, near-field environment, percolation flux in the drift, and external processes that may impose static loads, dynamic loads, or both. WP failures are grouped into three basic categories: (i) corrosion and mechanical, (ii) disruptive event, and (iii) initially defective. After determining the WP failure time, the TPA Version 3.2 code calculates the aqueous-phase radionuclide releases from the WP by considering the dissolution of radionuclides from the SF matrix, advective transport from the WP, and advective and diffusive transport through the invert directly to the UZ beneath the repository.

Corrosion failure of the WP is defined to occur at the time when the inner overpack is fully penetrated by a single pit and the waste form is therefore accessible to water. The abstracted corrosion model uses a conceptual framework that assumes the formation of a water film containing a salt solution but does not explicitly consider water dripping on the container. The corrosion processes considered in the model abstraction are

- Dry air oxidation
- Humid air corrosion
- Aqueous corrosion

WP surface temperature and the chloride concentration in the water film influence the mode, and hence, the rate of corrosion. The predominant mode of corrosion, however, depends on the critical RH as well as the container material. Mechanical failure of the WP is considered the result of fracture of the outer steel overpack due to thermal embrittlement arising from prolonged exposure at temperatures sufficiently elevated to cause substantial degradation of mechanical properties.

Disruptive event failures are taken into account by modeling the effects of events such as seismicity, fault displacement, and igneous activity. In the case of seismicity, the drift is assumed to have no backfill that could prevent rockfalls from mechanically loading and deforming the WP. Because the DOE plans to

not emplace WPs within a setback distance from known and well-characterized faults, displacements along yet undetected faults or new faults that exceed a preestablished threshold are assumed to fail WPs within the fault zone. For igneous activity, simulated magmatic intrusions intersecting the repository are assumed to cause WP failure; WPs within a dike but outside the vent hole are assumed to fail and expose the SF to water while those within the vent hole (the diameter of which is a sampled parameter) are assumed entrained in the magma and released directly to the biosphere. For both igneous activity and fault displacement, failures are modeled by superimposing the physical dimensions of the perturbation (i.e., length, width, and orientation of the fault and the igneous intrusion) on the repository footprint to determine the total number of WPs potentially affected in each repository subarea. Separate failure times are calculated for seismicity, fault displacement, and igneous activity. Because multiple seismic events occur during the 10,000- and 100,000-yr TPIs, seismic failure occurrences are collected into four distinct failure times.

In most applications of the TPA Version 3.2 code, it is assumed a small number of WPs are failed at the time of repository closure. These initially failed WPs are attributed to fabrication defects or damage to the WP as a result of improper emplacement. The average number of initially defective WPs is typically assumed 0.1 percent[2] of the total number of containers.

Radionuclide releases from the WP are calculated by considering the alteration rate of SF (i.e., rate at which radionuclides in fuel become available for release), radionuclide solubility limits, and transport mechanisms out of the WP. The TPA Version 3.2 code incorporates a number of parameters (e.g., fraction of SF that is wet, particle size of the SF, alteration rate of UO_{2+x}, and credit for cladding) that control the release of radionuclides from the SF matrix. The effects of the formation of secondary minerals such as schoepite on SF dissolution are treated separately. After radionuclides are leached from the SF waste form, the calculated releases are adjusted to ensure consistency with the radioelement solubility limits. The gap fraction inventory of radionuclides is available for instantaneous release and therefore, may be a major contributor to peak dose.

A parameter value in the code input file is used to specify the fraction of failed WPs that is wetted in the subarea. This value represents the number of failed WPs available to contribute to the source term. To compute the time-dependent source term, the TPA Version 3.2 code provides two alternative conceptual models: (i) a bathtub model—the WP must fill with water to a certain depth (up to the height of the outlet) before the radionuclides are released—and (ii) a flowthrough model—radionuclides are released by water dripping on the waste form and continuing immediately out of the bottom of the container. For the bathtub model, the WP is treated as a stirred tank, with the tank capacity dependent on the statistically sampled water outlet height. Water will fill the WP until the capacity (height) is reached and, thereafter, the amount of water entering the WP will equal the amount of water flowing out. Water leaving the WP transports dissolved radionuclides into the UZ below the repository. The water capacity of the bathtub is assumed unique to the failure modes and to subareas (except for faulting and igneous activity failures). Releases from WPs will travel through the invert before exiting the EBS. If the physical properties of the construction material for the invert are conducive, the radionuclide species could be sorbed, thus reducing the magnitude of radionuclide release from the near field. The flowthrough model is a variant of the bathtub model except water does not have to first fill the bathtub before release; instead, radionuclides are released as soon as water enters the WP.

---

[2]Tschoepe, E.C. et al. (1994) suggests fabricated metallic component reliabilities of 99.9– 99.99 percent.

2.2.4 Treatment of Aqueous-Phase Transport in the Unsaturated and Saturated Zones

Movement of aqueous-phase radionuclides from the repository horizon, through the UZ, SZ, and ultimately to the receptor group, is modeled in the TPA Version 3.2 code using the streamtube approach described in section 2.1. Each streamtube encompasses one or more repository subareas and is composed of a vertical section from the repository to the water table and horizontal sections in the SZ. The transport module NEFTRAN II (Olague et al., 1991) simulates the spectrum of processes (e.g., advection, dispersion, matrix diffusion, sorption, and decay) occurring within individual streamtubes. For the set of radionuclides specified in the code input file, the UZ and SZ modules simulate their vertical transport through the UZ and horizontal transport through the SZ.

Time-dependent flow velocities in the UZ are calculated using the hydraulic properties of each major hydrostratigraphic unit. The UZ transport module simulates the transport of radiocontaminants through either the porous rock matrix or fractures.[3] Radionuclide retardation by chemical sorption in the rock matrix is also included in the model; however, retardation on fracture surfaces is neglected.

Although groundwater flow in the SZ is assumed at steady state, radionuclide transport within individual streamtubes is time-dependent because the source term varies with time. Streamtubes in the SZ exhibit variable cross sections along the flow path; this variable streamtube geometry was determined from a separate two-dimensional (2D) modeling study of the subregional flow (Baca et al., 1996). The conceptual model of the SZ assumes that flow in the tuff aquifer is in localized conductive zones (i.e., permeable fracture zones) while flow in the alluvium is presumed uniformly distributed in the alluvial aquifer. Although the streamtube approach neglects dilution effects arising from lateral dispersion, credit is taken for sorption in the alluvium, which is likely to retard aqueous-phase transport of many radionuclides. Additionally, matrix diffusion from flowing pores and fractures into the more-or-less stagnant matrix pore water within the rock is included in the SZ transport model.

2.2.5 Airborne Transport from Direct Releases

Radiologic risks associated with the extrusive component of igneous activity are calculated in the TPA Version 3.2 code by modeling airborne releases of radionuclides for simulated extrusive events. The igneous activity module assumes that the magma intercepts WPs, moves upward to the land surface, and then ejects the ash and SF mixture into the atmosphere. The physical characteristics of each simulated extrusion (e.g., vent size, event energetics, and duration) and the atmospheric conditions are treated as statistical parameters in calculations of ash dispersal and deposition patterns, ash blanket thickness, and radionuclide soil concentrations. The three primary factors determining the ash plume geometry and transport rates are

- Power and duration (of the eruption)
- Wind speed and direction
- SF particle sizes

---

[3]Transport though rock matrix takes place if the percolation rate, q_{perc}, is less than the hydraulic conductivity of the rock matrix, K_{matrix}, or through fractures when q_{perc} exceeds K_{matrix}.

The ash transport model developed by Suzuki (1983) was modified by Jarzemba et al. (1997) and incorporated into the TPA Version 3.2 code to calculate distribution of the released radionuclides. The time-dependent radionuclide areal densities are calculated taking into account the thickness of the ash blanket, leaching and erosion rates, and radionuclide decay rates. The calculated doses attributed to direct releases are strongly influenced by the time of the event (early events result in larger doses, in part, due to the contribution to the estimated doses from short-lived fission products present in the SF).

2.2.6 Exposure Pathways and Reference Biosphere

Dose calculations are performed in the TPA Version 3.2 code for exposure pathways that consider an average person of a designated receptor group. These calculations express dose in rem/yr or mrem/yr. Alternative receptor groups are currently included in the exposure scenario. One receptor group is a farming community 20 km from the repository location while the second is a residential community at a specified distance, typically less than 20 km. The average member of the designated receptor group is assumed exposed to radionuclides transported through the groundwater pathway, air pathway, or both as a result of direct releases arising from the extrusive component of igneous activity.

Geographic location and lifestyle characteristics assigned to each receptor group are two primary aspects defining the receptor group and are specified in the TPA Version 3.2 code by selection of appropriate input options. In addition, the farming community receptor group is assumed to include persons that use the contaminated water for

- Drinking (i.e., 2 L/day)
- Agriculture typical of Amargosa Valley area practices (e.g., growing alfalfa and gardening)

The farming community receptor group is assumed exposed to surface contamination through

- Consumption of contaminated farm products (i.e., ingestion)
- Breathing air with ash-SF particles (i.e., inhalation)
- Direct contact

In contrast, the residential receptor group is assumed composed of persons who use contaminated groundwater only for drinking, but are also exposed to surface contamination (created by ash-SF particle deposition from the extrusive component of igneous activity) through inhalation and direct exposure.

Site-specific dose conversion factors (DCFs) for each radionuclide and pathway are contained in TPA data files. These DCFs are used to convert radionuclide concentrations in the groundwater and soil to doses. The individual DCFs are mean values[4] generated through separate pathway calculations using the GENII-S code (Leigh et al., 1993). In the groundwater pathway, for example, the DCFs are applied to the concentrations at the well head. Two separate sets of DCFs are included in the TPA Version 3.2 code to represent two distinct reference biospheres associated with the present arid climate (nonpluvial) and the projected future pluvial climate. The determination of whether the climate is nonpluvial or pluvial is based on the Köppen Geiger climate classification model (Strahler, 1969). In addition to computing the dose history for each stochastic simulation, the TPA Version 3.2 code scans these dose calculations to identify the magnitude and timing of the peak dose within a specified TPI.

---

[4]The justification for using mean values can be found in Mohanty and McCartin (1998).

2.3 BASECASE DEFINITION AND ALTERNATIVE CONCEPTUAL MODELS

The conceptual models available in the TPA Version 3.2 code are briefly presented in the previous sections. The option to evaluate alternatives to the basecase conceptual models is included in the TPA Version 3.2 code. The following sections list the set of conceptual models selected for the basecase studies and also describe the alternatives to the basecase models analyzed for mean input values in chapter 3 and sampled distributions in chapter 4.

2.3.1 Basecase

The basecase input data set reflects current repository design features and likely parameter-range estimates for evaluation of processes affecting repository performance. The set of conceptual models that constitute the basecase against which alternative conceptual models are evaluated in the sensitivity/uncertainty analyses include

- No cladding protection
- Dissolution of SF based on J-13 well-water chemistry
- Bathtub model (i.e., pooling of water in the WP after failure) for determination of water mass balance and fuel wetting of the failed WP
- No matrix diffusion of contaminants in UZ and SZ

A complete list of the input parameters used for the basecase can be found in appendix A in the TPA Version 3.2 code User's Guide (Mohanty and McCartin, 1998). Climate change and seismicity are considered as integral components of the basecase and, therefore, alternative conceptual models to the components are not considered in the analyses.

2.3.2 Alternative Conceptual Models

Various alternative conceptual models are investigated to determine the sensitivity of repository performance to changes in WP design, radionuclide release mechanisms, and radionuclide transport models. These alternative model runs are conducted with the TPA Version 3.2 code and do not include disruptive events (faulting or igneous activity). The alternative models used in this analysis are grouped according to fuel wetting assumptions, fuel-dissolution models, and transport assumptions. For the analyses presented in this report, the repository performance is defined as dose for the mean value data set and as the peak of the expected dose from the multiple-realization results in the TPI.

2.3.2.1 Fuel-Dissolution Models

The TPA Version 3.2 code contains four models (Model 1–Model 4) for the dissolution rate of the SF that has come into contact with water. The basecase model uses Model 2 (Mohanty and McCartin, 1998), which is based on the dissolution rate of SF in J-13 water containing silica and calcium ions. The alternative dissolution models are listed next. Some of the alternatives are combined with fuel wetting alternatives as well.

Fuel-Dissolution Model 1

The first alternative fuel-dissolution model (IModel = 1) has an increased SF dissolution rate at high carbonate concentrations (Mohanty and McCartin, 1998) and reduced silicate and calcium concentrations in the water entering the WP.

Fuel-Dissolution Model 3 (Natural Analog)

In this alternative conceptual model, fuel dissolution and contaminant release rates are based on maximum likely rates inferred from measurements at the Peña Blanca, Mexico, natural analog site (Mohanty and McCartin, 1998). For this alternative, the uranium dissolution rate for fully exposed fuel is 24 kg/yr from the entire repository, but is further limited by the fraction of wetted WPs and the fuel wetting factors. The two factors range from 0 to 1 and are sampled. This alternative conceptual model is invoked by setting IModel = 3.

Fuel-Dissolution on Model 4 (Schoepite Dissolution)

The schoepite-alternative conceptual model assumes that all radionuclides released from the SF matrix are captured in the secondary uranium mineral schoepite (Mohanty and McCartin, 1998) and are subsequently released at a limit controlled by schoepite solubility. This model is specified by setting IModel = 4.

2.3.2.2 Fuel Wetting Assumptions

This grouping includes alternative conceptual models related to the way SF in the WP is contacted by water. These five alternative models utilize combinations of the flowthrough and dissolution-rate models, and also TPA input parameters for the amount of water and fraction of the subarea wetted by impinging water.

Flowthrough Model with Fuel-Dissolution Model 2

This alternative conceptual model evaluates the flowthrough option in which water enters WPs through corrosion pits but does not pool in the container. In the bathtub model used in the basecase, the fraction of fuel wetted is determined by the bathtub height (determined by the position of the exit port which is a corrosion pit), which is sampled and ranges from 0 to 1. In the flowthrough model, the fraction of fuel wetted is unrelated to the water level in the WP. Additionally, the fraction of fuel wetted is likely much smaller and depends on poorly understood phenomena such as dripping patterns, surface tension, and vapor-phase wetting. This alternative conceptual model is invoked by specifying a smaller range for the parameter Fmult* (one-tenth of the normal range for the basecase),[5] to simulate a smaller fraction of wet fuel surface. In this model, solubility limits for the radionuclides might become important because of the limited amount of water in contact with the fuel.

[5]Fmult* is the fraction of water infiltrating to the repository from the unsaturated zone above the repository that will enter the waste package and contribute to the release of radionuclides. Water dripping toward the drifts may be diverted around the drift because of capillary action, may be diverted down the side of the drift, or may not enter the waste package for other reasons.

Flowthrough Model with Fuel-Dissolution Model 1

This alternative conceptual model uses the flowthrough model and IModel = 1 (carbonate-dissolution model), which assumes that silicate and calcium will be depleted from much of the water entering the WP by reaction with the fuel and metal in its path.

Focused Flow

The basecase conceptual model assumes that all parts of a repository subarea will receive an equal quantity of infiltrating water. This alternative conceptual model accounts for the possibility that water infiltration reaching the WPs will be focused or funneled by discrete fractures, which will wet some of the WPs more heavily than others. This alternative model is evoked by increasing the range of Fmult* by a factor of 4 (from 0.01–0.2 to 0.04–0.8), while decreasing the fraction of WPs wetted by a factor of one-fourth (from 0–1 to 0–0.25). This has the effect of funneling the same quantity of water for each subarea to one-fourth the number of WPs.

Cladding Credit Plus Spent Fuel-Dissolution Model 1

The basecase conceptual model assumes that once the inner and outer overpack containers have been breached, SF is exposed and available for dissolution and transport. This assumption ignores any protection afforded the fuel from intact and partially failed cladding. In this alternative model, the effect of cladding protection is simulated by setting the SF wetted fraction to a constant value of 0.005 for the entire TPI.

Grain-Size Model with Fuel-Dissolution Model 1

This conceptual model uses the grain size from the uranium dioxide fuel instead of the particle size to determine surface area, which leads to a higher dissolution rate because of the increased surface area. This alternative conceptual model combines the fuel-dissolution rate model 1 for relatively fast dissolution by carbonate water, with the large surface area provided by assuming that the fuel surface area is determined by the grain size. Both these assumptions are used in the DOE TSPA-VA model (U.S. Department of Energy, 1998) for radionuclide release from SF.

2.3.2.3 Transport Alternatives

The transport assumptions in the basecase UZ and SZ conceptual models are investigated with three alternative models. These assumptions affect the releases and time of release from the EBS, UZ, and SZ.

No Retardation of Pu, Am, and Th

This alternative conceptual model demonstrates the contribution to repository performance of retardation of Pu, Am, and Th in the geosphere, and the effect on the groundwater doses if this sorption was removed. Once released from failed WPs, Pu, Am, and Th are assumed to travel at the same speed as water through the EBS, UZ, and SZ to the receptor location. This alternative model is invoked by setting equilibrium coefficients (K_d) to zero and retardation coefficients (R_d) to unity for these elements. This model is a gross approximation of potential contribution from colloids that could move through the geosphere unretarded if filtration processes were not considered.

No-Invert Model

The TPA Version 3.2 code contains a model that takes into account the effect of flow and retardation through the invert material beneath the WPs. This function is normally activated. The no-invert alternative model negates the effect of the invert. This is accomplished by setting the variable *InvertBypass* equal to 1 in the code input file.

Matrix Diffusion

This conceptual model assumes that matrix diffusion will occur in the tuff SZ transport legs where there is fracture flow. Matrix diffusion is specified by setting the parameter *DiffusionRateSTFF* as a loguniform distribution ranging from 0.01 to 1.0 yr^{-1}. Two other factors involved in the matrix diffusion alternative are the immobile porosity and the retardation coefficients in the immobile phase. The default values in appendix A of the TPA Version 3.2 Code User's Guide (Mohanty and McCartin, 1998) are used to evaluate this conceptual mode.

3 ANALYSIS OF TOTAL-SYSTEM BEHAVIOR

In this chapter, the relationships between repository performance and the key input parameters and intermediate results are presented. The mean values and distributions for the uncertain TPA input parameters are summarized in tables 3-1 to 3-18.

In the single-realization case, mean values for the TPA input parameters are used and the results evaluated over the 10,000- and the 100,000-yr TPIs. The single-realization simulation establishes a baseline to investigate the behavior of the total system at the process level (e.g., WP lifetime and SZ travel time) and the repository performance as measured by groundwater dose. Additionally, the repository performance is related to the key input parameters and intermediate results in a deterministic mode.

Following the discussion of results from the single-realization simulation, a description of the variability in the TPA results from multiple realizations is presented. The variability in the behavior of the total system at the process level and the repository performance are analyzed in multiple realizations using distributions for the TPA input parameters. For example, the variability in dose is related to the release rate from the EBS. Both the single- and multiple-realization basecase analyses provide background information and form the framework to evaluate and quantify the sensitivity of repository performance to TPA input parameters presented in chapter 4. After the multiple-realization results, the TPA outputs from alternative conceptual models and disruptive events are presented. This chapter concludes with a discussion of a methodology used to calculate risks from the disruptive events.

3.1 SINGLE-REALIZATION DETERMINISTIC ANALYSES

This section examines repository behavior for a single realization to illustrate how a component influences both the dose and the behavior of other components. For the single realization, all input parameters are specified at mean (or expected) values. It should be noted that the annual dose obtained from using the mean value data set most likely will not be the same as the expected annual dose (which is the performance measure) obtained from multiple-realizations because of the nonlinear dependency of dose on input parameters.

The general representation of waste emplacement at YM is a total of 62,800 MTUs in an area of 3,060,000 m^2 (approximately 3,000 m long and 1,000 m wide). Assuming a payload of 9.76 MTU per WP and an equivalence between the SF and other types of wastes, such as DOE waste and glass waste, approximately 6,427 WPs will be needed for waste disposal. The initial inventory activity is approximately 200×10^6 Ci (7.4×10^{18} Bq). WPs with a 5.682-m length and a 1.802-m diameter are emplaced in drifts 5 m in diameter, spaced 22.5 m apart. The average age of the SF is 26 yr. The descriptions of the mean values for the key parameters used in various process-level calculations are presented in each of the following sections.

3.1.1 Unsaturated Zone Flow

Detailed modeling (Stothoff, 1999) suggests that climate conditions could significantly affect the flow of water in the UZ and into the repository. As a consequence, the amount of water contacting a WP, which affects the release rate of radionuclides from the EBS and the transport of the radionuclides in the UZ, may also be significantly influenced.

In the TPA Version 3.2 code,[1] precipitation is assumed to vary from present-day to pluvial conditions over a period of 100,000 yr. For the mean value data set, figure 3-1 shows the MAP changes from about 160 to 330 mm/yr, while the infiltrating water enters the UZ from 5 to 110 mm/yr. Based on the Köppen Geiger system of climate classification (Strahler, 1969) implemented in the TPA code to determine the onset of the pluvial period, approximately 90 percent of the 100,000-yr TPI is characterized by pluvial conditions and 10 percent of the time is represented by the present-day climate.

For higher flow rates, there are generally larger releases because of the greater amount of water available to dissolve and transport radionuclides out of the WP. Increasing flow rates in the UZ are not only expected to transport a larger mass of radionuclides from the EBS, but also lead to higher doses. The mean values of the parameters used to calculate the time-varying infiltration rates in the UZ are presented in table 3-1.

3.1.2 Near-Field Environment

The near-field thermal conditions may alter the flow of water into the repository, which influences the quantity of water that contacts, dissolves, and transports the SF out of the EBS. The near-field chemical environment in conjunction with the thermal environment affects WP corrosion and determines quantity and time history of water entering the WP. These near-field conditions and the flow of water onto the WPs are discussed in the following sections.

3.1.2.1 Repository-Scale Thermohydrology

Radioactive decay of SF generates heat that perturbs ambient percolation conditions. The heat evaporates water and creates a dryout zone around the drift. Above the repository horizon, the water vapor condenses and flows back toward the repository, thus creating a reflux zone. The reflux zone is maintained until the near-field temperature falls below boiling. When the temperature falls below boiling or water from the condensate zone penetrates the dryout zone, water flows into the drift. Water entering the drift may impinge on the WP and contribute to WP corrosion failure. After the WP fails, water contacts the SF and is transported out of the EBS into the UZ.

Of the three reflux models in the TPA code indicated in the previous chapter, the third model was used in the basecase. This model estimates the depth that water will penetrate the boiling isotherm as a function of dryout zone thickness and the volume of water flowing from the condensate zone. Table 3-2 presents the mean values of parameters used in the reflux calculations.

Figure 3-2 presents, except for early times, subarea-to-subarea variations in the volume of water contacting WPs, which behave similarly to the infiltration rates in figure 3-1. Figure 3-2 also shows slight differences in the seepage flux between subareas and a consistency in the general behavior of the seepage flux for all seven subareas with subarea 3 having the largest seepage flux attributable to the effects of elevation and soil thickness.

The spike in figure 3-2 at early times illustrates a large change in the seepage flux that occurs because of a higher thermal perturbation. Although this thermal perturbation takes place prior to corrosion failures, the modified infiltration rate could affect releases from initially defective failures or seismically induced

[1]The specific version of the code used in developing this chapter is 3.2.3.

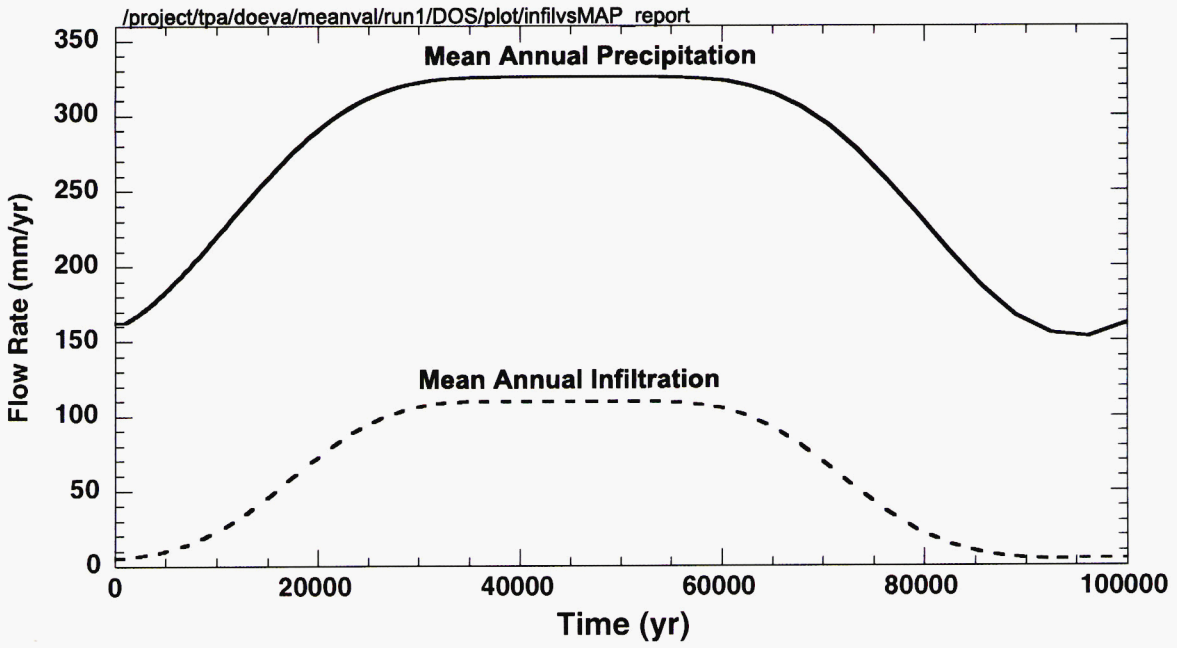

Figure 3-1. Mean annual precipitation and infiltration at the repository horizon averaged over all subareas and encompassing both the current and pluvial periods for the mean value data set

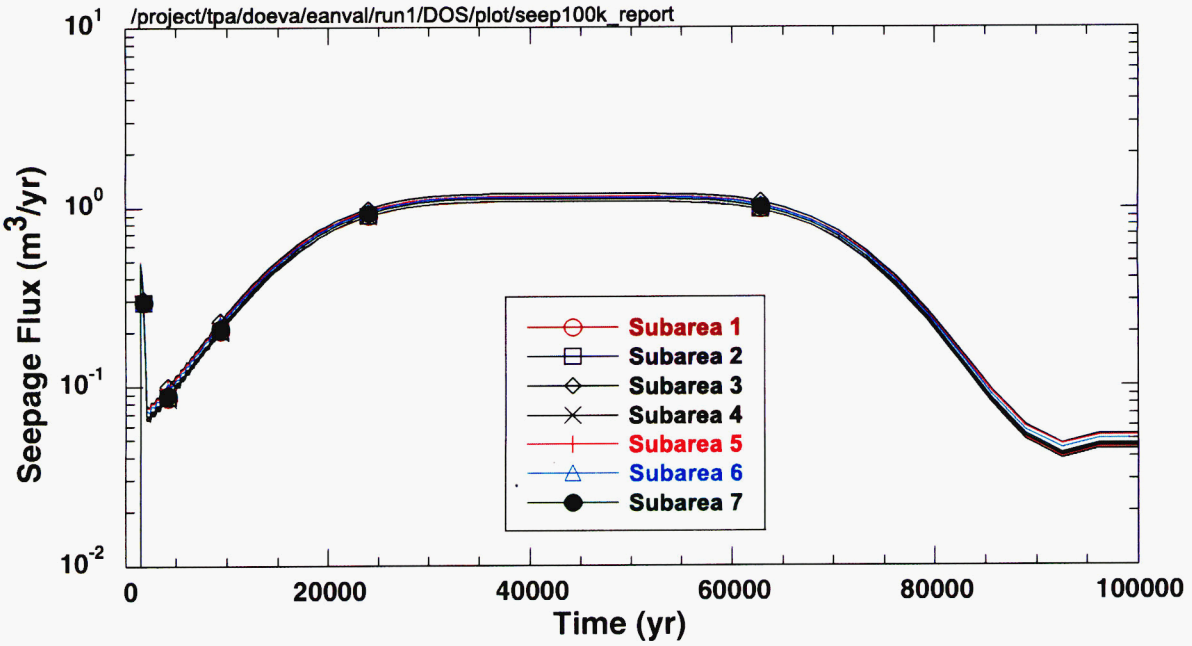

Figure 3-2. Effect of the thermal perturbation on the near-field seepage rate in each subarea for the mean value data set

Table 3-1. Mean values and sampled distributions of parameters for infiltration calculations

Parameter	Mean Value	Distribution
Areally averaged mean annual infiltration for the initial (current) climate	5.50 mm/yr	Uniform; 1.0, 10.0
Mean average precipitation multiplier at glacial maximum	2.00	Uniform; 1.5, 2.5
Mean average temperature increase at glacial maximum	-7.50 °C	Uniform; -10.0, -5.0

Table 3-2. Mean values and sampled distributions of parameters for determining repository-scale and drift-scale thermohydrology. The hyphen in the last column indicates a constant value for the parameter distribution.

Parameter	Mean Value	Distribution
Length of reflux zone	2.00×10^{1} m	—
Maximum flux in reflux zone	1.00×10^{-9} m/s	—
Perched bucket volume per subarea-area	5.00×10^{-1} m^3/m^2	—
Fraction of condensate removed	1.00×10^{-4} /yr	Log-uniform; 1.0×10^{-8}, 1.0
Fraction of condensate toward repository	5.00×10^{-1} /yr	Uniform; 0.0, 1.0
Fraction of condensate toward repository removed	1.00×10^{-4} /yr	Log-uniform; 1.0×10^{-8}, 1.0
Density of water at boiling	9.61×10^{2} kg/m^3	—
Enthalpy of phase change for water	2.40×10^{6} J/kg	—
Temperature gradient in vicinity of boiling isotherm	5.05×10^{1} K/m	Uniform; 1.0, 100.0
Ambient repository temperature	2.00×10^{1} °C	—
Mass density of Yucca Mountain rock	2.58×10^{3} kg/m^3	—
Specific heat of Yucca Mountain rock	8.40×10^{2} J/(kg-K)	—
Thermal conductivity of Yucca Mountain rock	2.00 W/(m-K)	Uniform; 1.8, 2.2
Emissivity of drift wall	8.00×10^{-1}	—
Emissivity of waste package	7.00×10^{-1}	—
Thermal conductivity of floor	6.00×10^{-1} W/(m-°C)	—
Effective thermal conductivity of unbackfilled drift	9.00×10^{-1} W/(m-°C)	—
Time of emplacement of backfill	1.00×10^{5} yr	—
Effective thermal conductivity of backfill	6.0×10^{-1} W/(m-°C)	—
Thermal conductivity of inner stainless steel wall	1.50×10^{1} W/(m-°C)	—
Thermal conductivity of outer carbon steel wall	5.00×10^{1} W/(m-°C)	—
Effective thermal conductivity of basket and spent fuel in waste package	1.00 W/(m-°C)	—
Elevation of repository horizon	1.07×10^{3} m	—
Elevation of ground surface	1.40×10^{3} m	—

failures. The duration of the thermal perturbation is small compared to long simulation periods such as 10^5 yr, however, it may be significant for the 10,000-yr TPI. The subarea average infiltration rate in the UZ is provided in figure 3-3. Water flowing into the drift and water entering the WP are also illustrated in this figure. The effects of the thermal perturbation on the flow rate are evident in this figure for approximately 3,000-yr. Once the infiltration into the repository begins, the rate increases by a factor of approximately 5 compared to the ambient infiltration rate. The thermal augmentation of flow for the mean values data set case lasts about 1,000-yr. Significant infiltration into the repository is delayed until approximately 2,000-yr. Afterward, the thermal effects no longer influence the UZ flow above the repository.

3.1.2.2 Drift-Scale Thermohydrology

Waste package surface temperature, drift wall temperature, and WP surface RH are computed for each subarea. The mean TPA input parameters used to compute these values are presented in table 3-2. Figure 3-4 illustrates the subarea-to-subarea differences in the WP surface temperature and figure 3-5 shows WP surface RH. For the mean value data set presented in table 3-2, the highest temperature of approximately 150 °C is observed at about 100 yr. The temperature remains above ambient temperature even at 100,000 yr. Subareas 1 and 2 are the largest subareas and subarea 7 is the smallest, located away from the center of the repository and with an elongated shape. Thus, in subareas 1 and 2, WPs cool much slower compared to subarea 7. Subarea 7 exhibits the greatest differences in temperature and RH when compared to subareas 1 through 6.

Subarea-dependent temperature and RH values from the near field are also used by the WP degradation model to determine the WP failure time. Consequently, the WP failure time may be different for each subarea. For the drift-scale thermohydrology, the climatic conditions were considered irrelevant because fluid flow was not modeled in the temperature and RH calculations. Fluid flow was not accounted for in the temperature and RH calculations, because its effect was found to be insignificant in the detailed calculations using equivalent continuum modeling conducted outside the TPA code.

3.1.2.3 Near-Field Geochemical Environment

The near-field geochemical environment is represented by the time-dependent chloride concentration that interacts with the WP and wasteform inside the drift. The parameters available to the TPA analysis are the chloride concentration, oxygen partial pressure, the solution pH, and the total dissolved carbonate. Figure 3-6 shows the time history of chloride concentration used by the TPA program, which was calculated with the MULTIFLO (Lichtner and Seth, 1996) computer program and supplied in tabular form to the TPA code. The chloride concentration is calculated based on an initial fluid composition corresponding to J-13 well water and represents the time-dependent composition of water available at the drift wall. The chloride multiplication factor in table 3-3 (mean value of 15.5) modifies the time-dependent chloride concentration curve presented in figure 3-6. The chloride multiplication factor is intended to account for the uncertainty in estimating the water chemistry; the parameter values (chloride concentration) and MULTIFLO results are considered to be the lower bound for chloride concentration.

3.1.3 Waste Package Degradation

Because radionuclide releases begin only after WP failure, the lifetime of a WP significantly affects repository performance. The WP degradation rate is strongly dependent on the behavior of the inner and outer container materials. The inner and outer WP materials are specified as carbon steel and Alloy C-22, respectively, based on the DOE TSPA-VA design (U.S. Department of Energy, 1998). The mean

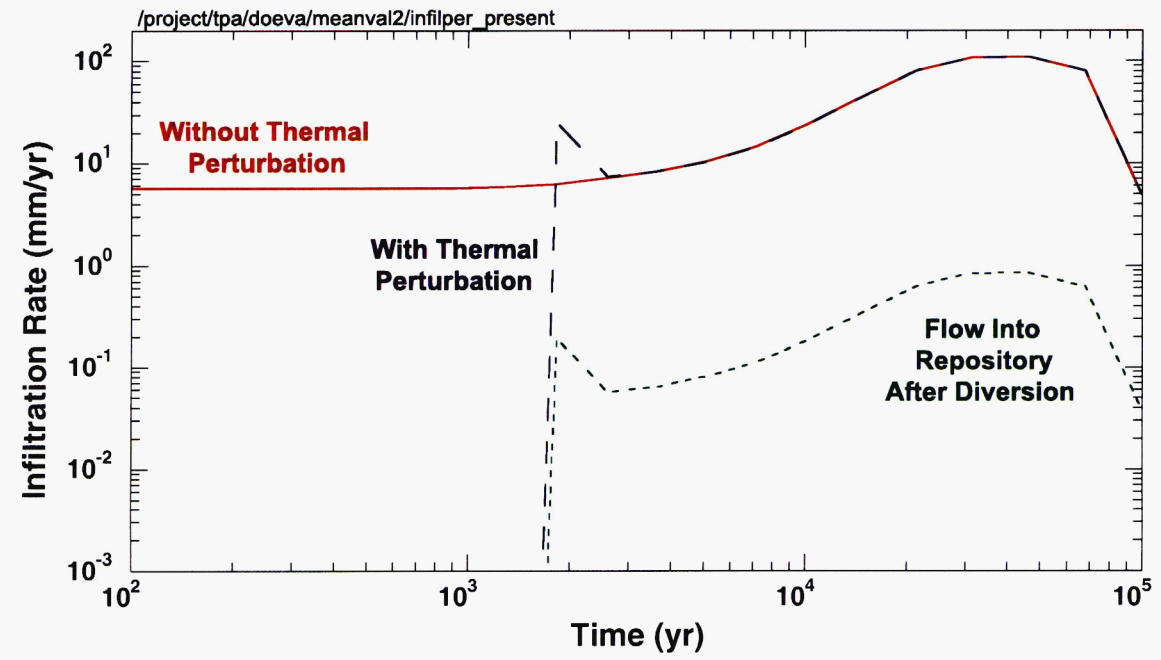

Figure 3-3. Subarea average infiltration rate, flow into the drift, and amount of water entering the waste

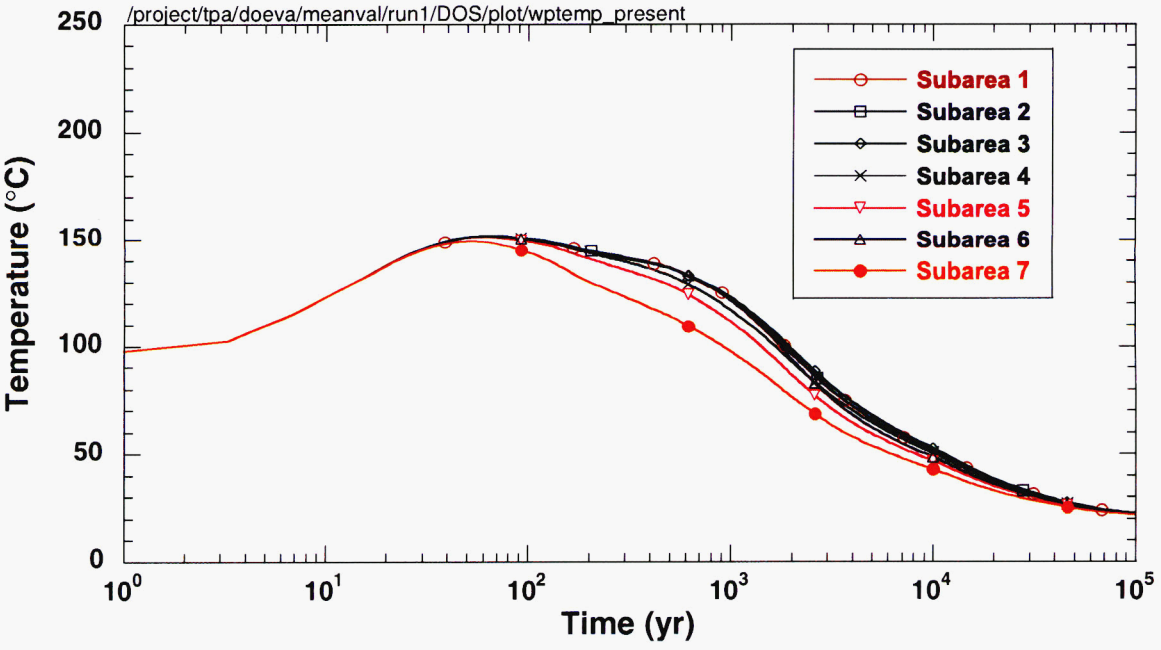

Figure 3-4. Waste package surface temperature in each subarea for the mean value data set

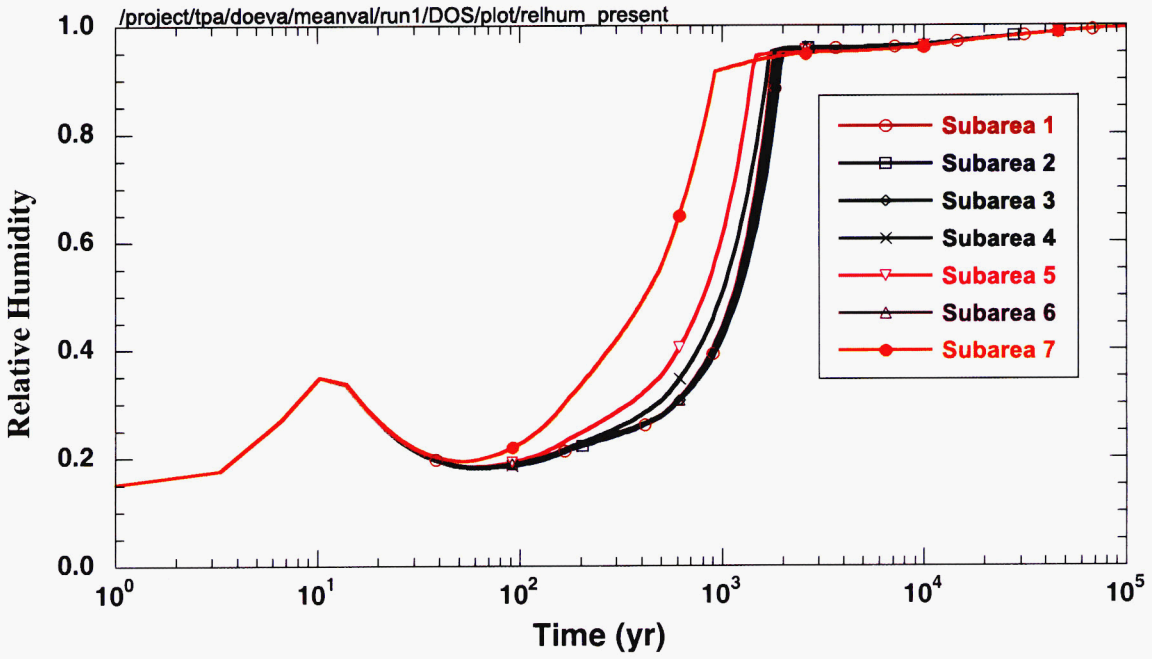

Figure 3-5. Waste package surface relative humidity in each subarea for the mean value data set

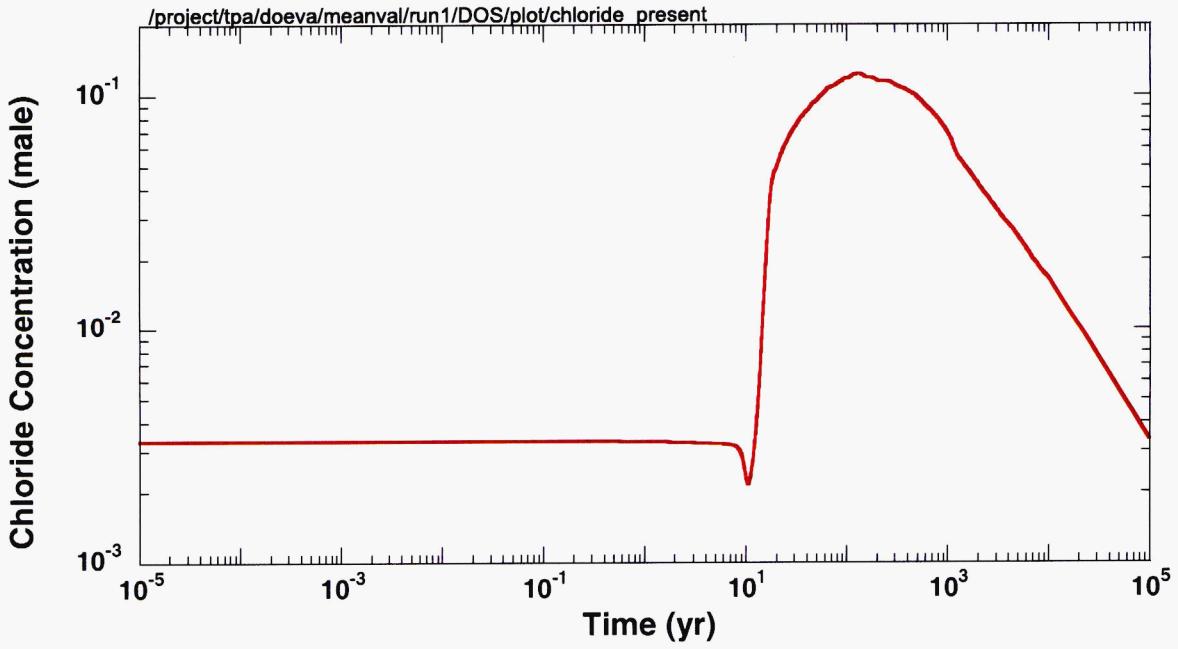

Figure 3-6. Time history of chloride concentration computed by MULTIFLO

Table 3-3. Parameters for determining the corrosion failure of waste packages

Parameter	Mean Value	Distribution
Outer waste package thickness	1.00×10^{-1} m	—
Inner waste package thickness	2.00×10^{-2} m	—
Metal grain radius	1.38×10^{1} μm	—
Grain boundary thickness	7.00×10^{-4} μm	—
Dry oxidation constant	1.00×10^{-5}	—
Critical relative humidity humid air corrosion	5.50×10^{-1}	—
Critical relative humidity aqueous corrosion	8.00×10^{-1}	Normal; 0.75, 0.85
Thickness of water film	2.00×10^{-3} m	Uniform; 0.001, 0.003
Boiling point of water	9.70×10^{1} °C	—
Outer overpack E_{rp} intercept	-6.20×10^{2}	—
Temperature coefficient of outer pack E_{rp} intercept	4.70×10^{-1}	—
Outer overpack E_{rp} slope	-9.52×10^{1}	—
Temperature coefficient of outer pack E_{rp} slope	8.80×10^{-1}	—
Inner overpack E_{rp} intercept	1.14×10^{3}	Uniform; 1040.0, 1240.0
Temp coef of inner pack E_{rp} intercept	0.00e+00	—
Inner overpack E_{rp} slope	0.00e+00	—
Temp coef of inner pack E_{rp} slope	0.00	—
Outer waste package beta kinetics parameter for oxygen	7.50×10^{-1}	—
Outer waste package beta kinetics parameter for water	5.00×10^{-1}	—
Inner waste package beta kinetics parameter for oxygen	7.50×10^{-1}	—
Inner waste package beta kinetics parameter for water	5.00×10^{-1}	—
Outer waste package rate constant for oxygen reduction	3.80×10^{12} C-m/m/yr	—
Outer waste package rate constant for water reduction	1.60×10^{-1} C-m/m^2/yr	—
Outer waste package activation energy for oxygen reduction	3.73×10^{4} J/mol	—
Outer waste package activation energy for water reduction	2.50×10^{4} J/mol	—
Inner waste package rate constant for oxygen reduction	3.00×10^{10} C-m/mol/yr	—
Inner waste package rate constant for water reduction	3.2 C-m/m^2/yr	—
Inner waste package activation energy for oxygen reduction	4.0×10^{4} J/mol	—
Inner waste package activation energy for water reduction	2.50×10^{4} J/mol	—

Table 3-3. Parameters for determining the corrosion failure of waste packages (cont'd)

Parameter	Mean Value	Distribution
Passive current density for waste package outer overpack	3.15×10^{5} C/m^2/yr	—
Passive current density for waste package inner overpack	4.15×10^{4}	Uniform; 2.0×10^{4}, 6.3×10^{4}
Measured galvanic couple potential	-4.60×10^{-1}	—
Coefficient for localized corrosion of outer	4.76×10^{-3}	Uniform; 8.66×10^{-4}, 8.66×10^{-3}
Exponent for localized corrosion of outer overpack	4.5×10^{-1}	—
Humid air corrosion rate	1.16×10^{-5} m/yr	—
Localized corrosion rate of inner overpack	2.5×10^{-4} m/yr	—
Fractional coupling strength	0.0	—
Factor for defining choice of critical potential	0.0	—
Critical chloride concentration for first layer	3.0×10^{-4} mol/L	—
Critical chloride concentration for second layer	1.00 mol/L	—
Chloride multiplication factor	1.55×10^{1}	Uniform; 1.0, 30.0
Reference pH	9.0	—
Waste package surface scale thickness	0.0 m	—
Tortuosity of scale on waste package	1.0	—
Porosity of scale on waste package	1.0	—
Yield strength	2.05×10^{2} MPa	—
Safety factor	1.4	—
Fracture toughness	2.50×10^{2} MPa/m^2	—

values of the parameters used in computing the WP failure time are presented in table 3-3. Figure 3-7 provides a time evolution of the WP wall thinning and shows WP failure occurring at about 16,500 yr. The two distinct slopes in this figure correspond to the different corrosion rates for the carbon steel and Alloy C-22 materials. The transition point corresponds to the penetration of the outer overpack at approximately 1,700 yr. The figure indicates that an order of magnitude longer WP life is attributable to the inner overpack rather than the outer overpack.

Figure 3-8 shows that, for the mean value data set, 31 WPs are initially defective at year zero. The number of initially defective failures ranges from 1 to 9 WPs in the seven subareas. No seismically induced failure occurs for the mean value data set. The first corrosion failures take place in subareas 5 and 7. A total of 928 WPs fail in these subareas at 16,300 yr. The next corrosion failure occurs in subareas 1 to 4 and 6, with a total of 5,468 WPs failing at 17,000 yr.

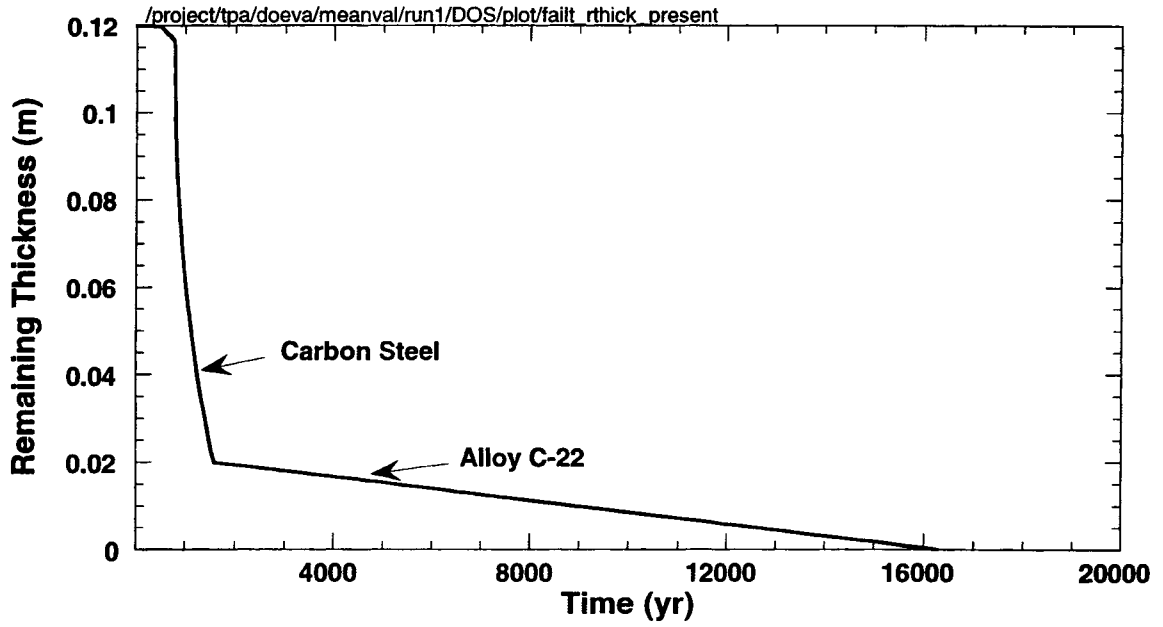

Figure 3-7. Waste package wall thickness as a function of time for the mean value data set

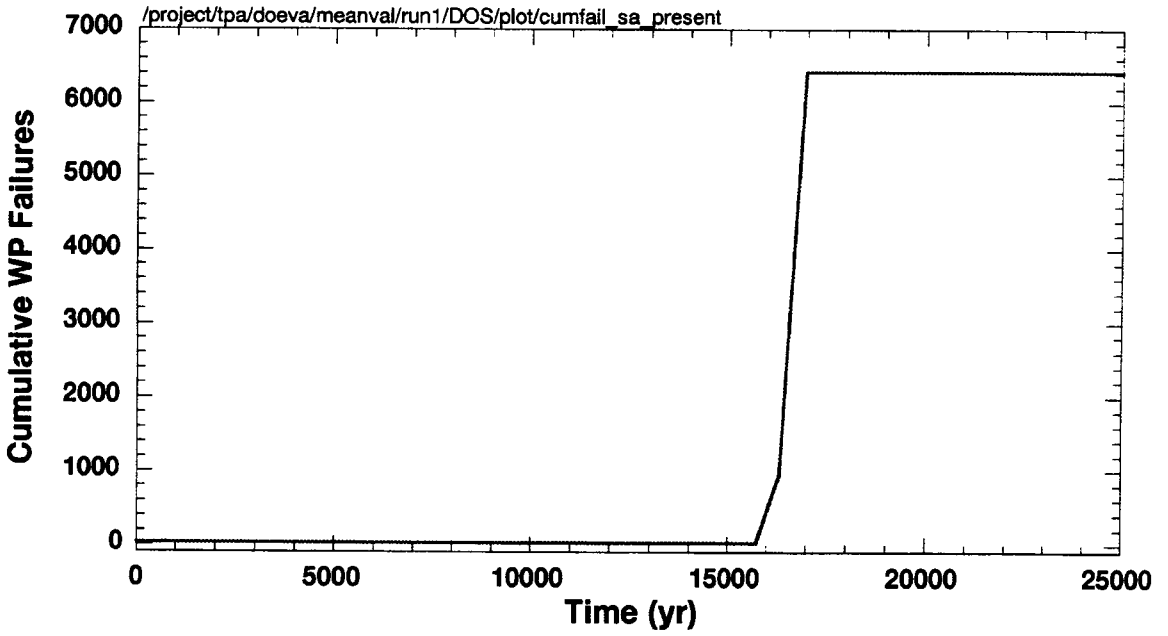

Figure 3-8. Cumulative number of failed waste packages for the mean value data set

3.1.4 Releases from Waste Packages

After WP failure, radionuclide releases are modeled assuming advective mass transfer out of the WP from incoming water. The volume of water contacting the SF is computed from a combination of flow in the near-field environment and two flow factors. The first flow factor represents the fraction of dripping water, which may be focused to reach the WP. The second flow factor represents the fraction of the water reaching the WP that enters the WP. The flow rate into the WP is used in the bathtub model to determine radionuclide release rates. The mean value parameters used in the calculation of radionuclide release rates from the EBS are presented in tables 3-4 and 3-5.

Because radionuclides have different chemical, physical, and biological properties that affect the mobilization and radiotoxicity, not every radionuclide in the SF is an important contributor to dose. Furthermore, because modeling all radionuclides in the SF significantly increases the computation time, a screening process employing criteria such as contribution to dose was used to determine list of 11 radionuclides. The 11 radionuclides and the decay chains evaluated in the TPA analysis are presented in table 3-6.

3.1.4.1 Cladding Degradation

Cladding must fail for water to contact the SF. Because of lack of adequate knowledge, no explicit mechanism for cladding failure is included in the TPA code. To capture the potential effect of cladding degradation, however, a fraction of the rods inside a WP may be specified to have failed at the time of WP failure. In the basecase, cladding failure is specified at 100 percent of the fuel rods, indicating no cladding protection for the SF (see table 3-4).

3.1.4.2 Spent Fuel Dissolution and Mobilization

Spent fuel dissolution is modeled by defining rate equations for the SF exposed following WP failure and cladding degradation. The rate equation is based on laboratory data in the presence of Ca and Si. The data follow an Arrhenius-type trend that uses the time-varying temperature as the independent parameter. The dissolution rate is calculated from a mass balance on the water flowing into the WP. Because the flow rate is subarea dependent, the dissolution rate varies from subarea to subarea.

The average temperature of the WP surface, calculated in the drift-scale thermohydrology model, is used in the dissolution rate equation. This assumption that the temperature of the WP surface is close to the temperature at the interior of the WP is justified because by the time the WP fails from corrosion (the dominant failure mechanism) at around 17,000 yr, the thermal effects have subsided. The surface area of the SF available for dissolution is about 746 m^2 based on the SF particle size, grain density, and the SF wetted fraction.

As with SF dissolution, the mobilization of the SF also depends on the initial inventory instantaneously released from the gap between SF and cladding into the contacting water as soon as the WP fails. Radionuclide gap fractions are presented in table 3-7.

Table 3-4. Parameters used in determining radionuclide releases from the engineered barrier system

Parameter	Mean	Distribution
Flow model flag (0 = bathtub,1 = flow through)	0.00	—
Flow convergence/divergence factor	1.73×10^{-1}	Lognormal; 0.01, 3.0
Flow multiplication factor	4.47×10^{-2}	Lognormal; 0.01, 0.2
Subarea wet fraction	5.0×10^{-1}	Uniform; 0.0, 1.0
Initial failure time	0.00 yr	—
Defective fraction of waste packages per cell	5.05×10^{-3}	Uniform; 1.0×10^{-4}, 1.0×10^{-2}
Number of SEISMO waste package failure intervals	4.00	—
Beginning of seismic waste package failure intervals	0, 2000, 5000, 10,000 yr	—
Waste package internal volume	4.83 m^3	—
Flow onset temperature	9.99×10^{2} °C	—
Spent fuel density	1.06×10^{4} kg/m^3	—
Surface area model	1.00	—
Spent fuel dissolution model	2.00	—
Oxygen partial pressure	2.10×10^{-1} atm	—
Negative log10 carbonate concentration	3.71 mol/L	—
User leach rate	2.50×10^{-6} kg/yr/m^2	—
Initial radius of spent fuel particle	1.85×10^{-3} m	Normal; 7.0×10^{-4}, 3.0×10^{-3}
Radius of spent fuel grain	1.25×10^{-5}	—
Cladding correction factor	1.0	—
Subgrain fragment radius of UO_2 particle after transgranular fracture	1.25×10^{-6} m	Normal; 5.0×10^{-7}, 2.0×10^{-6}
Thickness of cladding	6.1×10^{-4} m	—
Spent fuel ^{14}C inventory of spent fuel	7.2×10^{-4} Ci/kg	—
Clad ^{14}C inventory of spent fuel	4.89×10^{-4} Ci/kg	—
Zirconium oxide and crud ^{14}C inventory of spent fuel	2.48×10^{-5} Ci/kg	—
Gap and grain boundary inventory of spent fuel	6.2×10^{-6} Ci/kg	—
Spent fuel wetted fraction for all failure types	5.0×10^{-1}	Uniform; 0.0, 1.0
Invert bypass (0 = use ebsfilt,1 = bypass ebsfilt)	0	—
Invert rock porosity	3.0×10^{-1}	—
Invert thickness	7.5×10^{-1} m	—
Invert diffusion coefficient	4.4×10^{-5} m^2/yr	—
Invert matrix permeability	2.0×10^{-17} m^2	Lognormal; 2.0×10^{-18}, 2.0×10^{-16}
Unsaturated zone minimum velocity change factor (fraction)	4.0×10^{-1}	—

Table 3-4. Parameters used in determining radionuclide releases from the engineered barrier system (cont'd)

Parameter	Mean	Distribution
Invert RD		—
^{241}Am	3.00×10^{3}	—
^{14}C	6.10×10^{1}	—
^{36}Cl	1.00	—
^{245}Cm	6.00×10^{3}	—
^{129}I	7.00	—
^{237}Np	1.20×10^{3}	—
^{239}Pu	3.00×10^{3}	—
^{79}Se	1.00	—
^{99}Tc	1.00	—
^{230}Th	3.00×10^{3}	—
^{234}U	6.01×10^{2}	—

Table 3-5. Distributions of solubility limits

Radionuclide	Mean Value (kg/m^3)	Distribution (kg/m^3)
^{241}Am	1.20×10^{-4}	Uniform; 2.4×10^{-8}, 2.4×10^{-4}
^{14}C	1.40×10^{1}	—
^{36}Cl	3.60×10^{1}	—
^{245}Cm	2.40×10^{-4}	—
^{129}I	1.29×10^{2}	—
^{237}Np	2.14×10^{-2}	Log triangular; 1.2×10^{-3}, 3.4×10^{-2},2.4×10^{-1}
^{239}Pu	1.21×10^{-4}	Uniform; 2.4×10^{-6}, 2.4×10^{-4}
^{79}Se	7.90×10^{1}	—
^{99}Tc	9.93×10^{1}	—
^{230}Th	2.30×10^{-4}	—
^{234}U	7.60×10^{-3}	—

Table 3-6. Radionuclide decay chains

Chain Number	Chain
1	$^{245}Cm \rightarrow {}^{241}Am \rightarrow {}^{237}Np$
2	^{239}Pu
3	$^{234}U \rightarrow {}^{230}Th$
4	^{129}I
5	^{99}Tc
6	^{14}C
7	^{79}Se
8	^{36}Cl

Table 3-7. Initial inventory, gap inventory, and half-life of radionuclides in spent nuclear fuel for groundwater release

Radionuclide	Inventory at 10 yr from Reactor (Ci/WP)	Gap Inventory (%)	Half-life (yr)
^{241}Am	1.60×10^{4}	0	4.32×10^{2}
^{14}C	1.30×10^{1}	10	5.73×10^{3}
^{36}Cl	1.14×10^{-1}	12	3.01×10^{5}
^{245}Cm	1.22	0	8.50×10^{3}
^{129}I	2.88×10^{-1}	6	1.57×10^{7}
^{237}Np	2.80	0	2.14×10^{6}
^{239}Pu	3.01×10^{3}	0	2.41×10^{4}
^{79}Se	3.71	6	6.50×10^{4}
^{99}Tc	1.20×10^{2}	1	2.13×10^{5}
^{230}Th	1.26×10^{-3}	0	7.70×10^{4}
^{234}U	1.10×10^{1}	0	2.45×10^{5}

3.1.4.3 Transport in the Engineered Barrier System

The TPA code models advective transport out of the WP and advective and diffusive transport through the invert below the WP. Two different flow rates are used in these transport calculations. The volumetric flow rate of water into the WP is calculated by scaling the seepage flux into the drift with the surface area of the pits. The volumetric flux through the invert is based on the volume of water entering the drift rather than the volume of water entering the WP.

Inside the WP, high solubility nuclides released from the solid matrix are carried out of the WP. However, low-solubility nuclides precipitate out of solution if released from the solid matrix at a concentration exceeding the carrying capacity of water (or solubility limit of a particular nuclide). The volume of water available for dissolution of waste is the amount of water in the failed WP and the difference between the volume of water flowing in and out of the failed WP. Table 3-5 provides solubility limits of the radioelements evaluated in the TPA Version 3.2 code.

In the invert, advective and diffusive transport is modeled through 0.75 m of concrete having a 30-percent porosity. The determination of whether flow through the invert occurs in the matrix or fractures is based on the invert matrix permeability and the average flow rate of water through the invert. Radionuclide sorption is modeled in the concrete invert, and the mean values of the R_ds are presented in table 3-4 together with values for other parameters used to compute transport in the EBS. Colloidal transport of radionuclides is not considered in this calculation.

3.1.5 Unsaturated Zone Transport

In UZ transport calculations, the NEFTRAN II code (Olague et al., 1991) models 1D advection and retardation of radionuclides with chain decay. Inputs to the UZ transport model are the release rates of radionuclides from the EBS, the time-varying flow results from the UZ shown in figure 3-1, and the chemical and physical properties of the hydrostratigraphic units between the repository and the water table (see figure 3-9 and table 3-8).

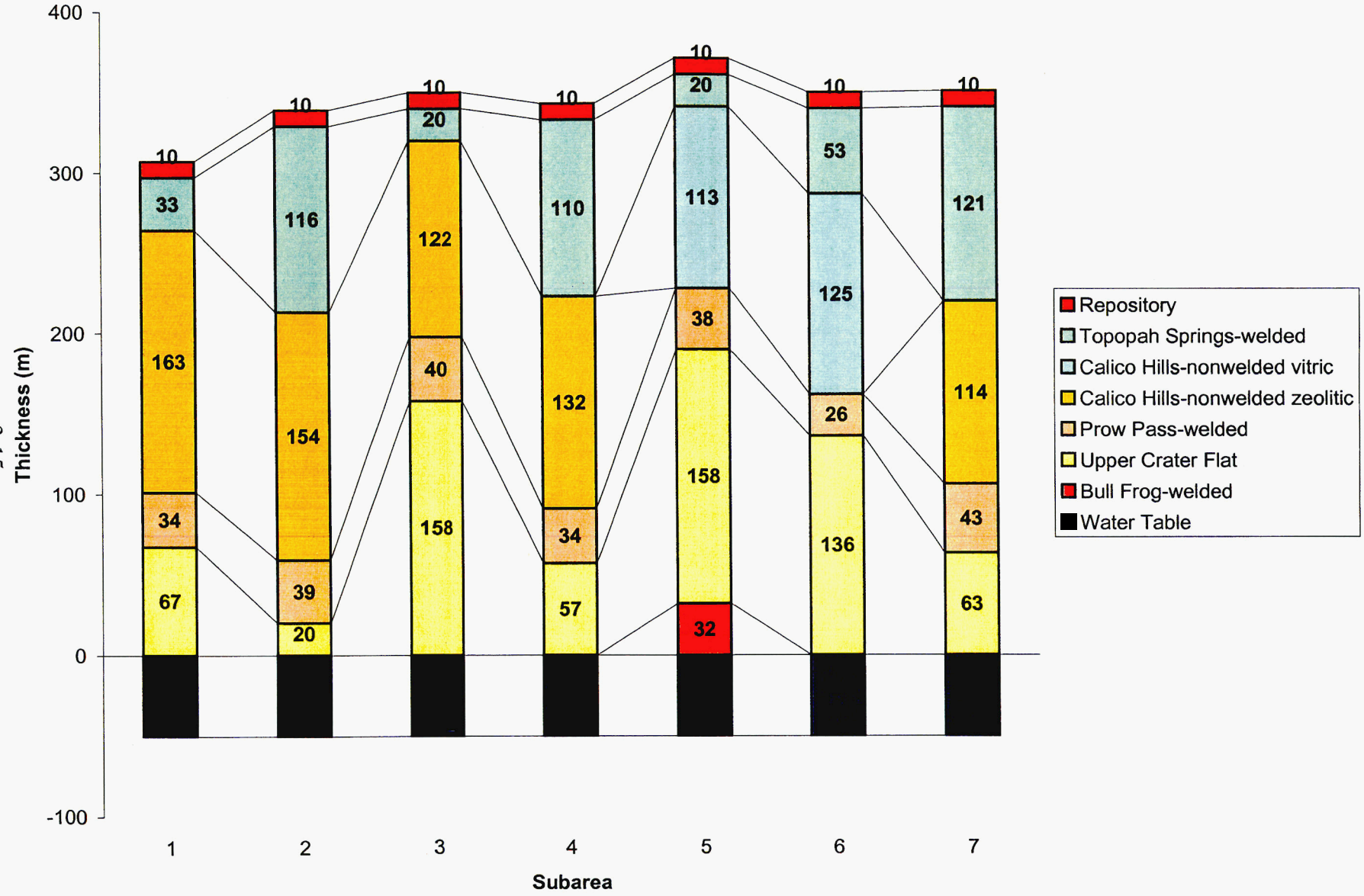

Figure 3-9. Thickness of subarea stratigraphic units

Table 3-8. Mean values and sampled distributions of sorption coefficient, K_d (m^3/kg), parameters. Other parameters for unsaturated zone radionuclide transport are also included. The hyphen in the last column indicates a constant value for the parameter distribution.

Element	Bull Frog welded unit	Calico Hills nonvitric unit	Calico Hills nonzeolitic unit	Prow Pass welded unit	Topopah Spring welded unit	Upper Crater Flat unit
Am	3.89×10^3 (Lognormal; 4.1, 3.7×10^6)	1.25×10^4 (Lognormal; 1.3×10^1, 1.2×10^7)	1.15×10^4 (Lognormal; 1.2×10^1, 1.1×10^7)	9.09×10^3 (Lognormal; 9.5, 8.7×10^6)	3.99×10^3 (Lognormal; 4.2×10^1, 3.8×10^6)	9.54×10^3 (Lognormal; 1.0×10^1, 9.1×10^6)
C	0.00 —	0.00 —	0.00 —	0.00 —	0.00 —	0.00 —
Cl	0.00 —	0.00 —	0.00 —	0.00 —	0.00 —	0.00 —
Cm	0.00 —	0.00 —	0.00 —	0.00 —	0.00 —	0.00 —
I	0.00 —	0.00 —	0.00 —	0.00 —	0.00 —	0.00 —
Np	5.61×10^{-4} (Lognormal; 1.5×10^{-6}, 2.1×10^{-1})	1.78×10^{-3} (Lognormal; 4.8×10^{-6}, 6.6×10^{-1})	1.62×10^{-3} (Lognormal; 4.4×10^{-6}, 6.0×10^{-1})	1.34×10^{-3} (Lognormal; 3.6×10^{-6}, 5.0×10^{-1})	5.93×10^{-4} (Lognormal; 1.6×10^{-6}, 2.2×10^{-1})	1.40×10^{-3} (Lognormal; 3.8×10^{-6}, 5.2×10^{-1})
Pu	6.95×10^{1} (Lognormal; 2.3×10^{-2}, 2.1×10^{1})	2.18 (Lognormal; 7.1×10^{-2}, 6.7×10^{1})	1.99 (Lognormal; 6.5×10^{-2}, 6.1×10^{1})	1.63 (Lognormal; 5.3×10^{-2}, 5.0×10^{1})	7.11×10^{-1} (Lognormal; 2.3×10^{-2}, 2.2×10^{1})	1.71 (Lognormal; 5.6×10^{-1}, 5.2×10^{1})
Se	9.49×10^{-5} (Lognormal; 3.0×10^{-7}, 3.0×10^{-2})	6.32×10^{-5} (Lognormal; 2.0×10^{-7}, 2.0×10^{-2})	4.74×10^{-5} (Lognormal; 1.5×10^{-7}, 1.5×10^{-2})	9.49×10^{-5} (Lognormal; 3.0×10^{-7}, 3.0×-10^{-2})	9.49×10^{-5} (Lognormal; 3.0×10^{-7}, 3.0×10^{-2})	9.49×10^{-5} (Lognormal; 3.0×10^{-7}, 3.0×10^{-2})
Tc	0.00 —	0.00 —	0.00 —	0.00 —	0.00 —	0.00 —
Th	3.36×10^{-1} (Lognormal; 4.7×10^{-5}, 2.4×10^{3})	1.07 (Lognormal; 1.5×10^{-4}, 7.6×10^{3})	9.47×10^{-1} (Lognormal; 1.3×10^{-4}, 6.9×10^{3})	7.92×10^{-1} (Lognormal; 1.1×10^{-4}, 5.7×10^{3})	3.46×10^{-1} (Lognormal; 4.8×10^{-5}, 2.5×10^{3})	8.06×10^{-1} (Lognormal; 1.1×10^{-4}, 5.7×10^{3})
U	2.02×10^{-5} (Lognormal; 1.0×10^{-9}, 2.6)	6.55×10^{-5} (Lognormal; 1.3×10^{-9}, 3.3)	6.00×10^{-5} (Lognormal; 1.2×10^{-9}, 3.0)	4.90×10^{-5} (Lognormal; 9.6×10^{-10}, 2.5)	2.15×10^{-5} (Lognormal; 4.2×10^{-10}, 1.1)	5.10×10^{-5} (Lognormal; 1.0×10^{-9}, 2.6)

Table 3-8. Mean values and sampled distributions of sorption coefficient, K_d (m^3/kg), parameters. Other parameters for unsaturated zone radionuclide transport are also included. (cont'd)

Parameter	Mean	Distribution
Matrix Permeability		
Topopah Springs—welded	2.00×10^{-19} m^2	Lognormal; 2.0×10^{-20}, 2.0×10^{-18}
Calico Hills—nonwelded vitric	2.00×10^{-14} m^2	Lognormal; 2.0×10^{-15}, 2.0×10^{-13}
Calico Hills—nonwelded zeolitic	5.00×10^{-18} m^2	Lognormal; 5.0×10^{-19}, 5.0×10^{-17}
Prow Pass—welded	1.00×10^{-17} m^2	Lognormal; 1.0×10^{-18}, 1.0×10^{-16}
Upper Crater Flat	3.00×10^{-18} m^2	Lognormal; 3.0×10^{-19}, 3.0×10^{-17}
Bull Frog—welded	2.00×10^{-19} m^2	Lognormal; 2.0×10^{-20}, 2.0×10^{-18}
Unsaturated Fracture Zone	1.94×10^{-17} m^2	Lognormal; 1.8×10^{-18}, 2.1×10^{-16}
Matrix Porosity		
Topopah Springs—welded	1.20×10^{-1}	—
Calico Hills—nonwelded vitric	3.30×10^{-1}	—
Calico Hills—nonwelded zeolitic	3.20×10^{-1}	—
Prow Pass—welded	2.80×10^{-1}	—
Upper Crater Flat	2.80×10^{-1}	—
Bull Frog—welded	1.20×10^{-1}	—
Unsaturated Fracture Zone	1.20×10^{-1}	—
Matrix Beta		
Topopah Springs—welded	1.50	—
Calico Hills—nonwelded vitric	1.30	—
Calico Hills—nonwelded zeolitic	2.30e+00	—
Prow Pass—welded	1.50e+00	—
Upper Crater Flat	1.40e+00	—
Bull Frog—welded	1.70	—
Unsaturated Fracture Zone	2.30	—
Matrix Grain Density		
Topopah Springs—welded	2.46×10^3 kg/m^3	—
Calico Hills—nonwelded vitric	2.26×10^3 kg/m^3	—
Calico Hills—nonwelded zeolitic	2.40×10^3 kg/m^3	—
Prow Pass—welded	2.54×10^3 kg/m^3	—

Table 3-8. Mean values and sampled distributions of sorption coefficient, K_d (m^3/kg), parameters. Other parameters for unsaturated zone radionuclide transport are also included. (cont'd)

Parameters	Mean	Distribution
Matrix Grain Density		
Upper Crater Flat	2.42×10^3 kg/m^3	—
Bull Frog—welded	2.57×10^3 kg/m^3	—
Unsaturated Fracture Zone	2.63×10^3 kg/m^3	—
Fracture Permeability		
Topopah Springs—welded	8.00×10^{-13} m^2	Lognormal; 8.0×10^{-15}, 8.0×10^{-11}
Calico Hills—nonwelded vitric	8.00×10^{-13} m^2	Lognormal; 8.0×10^{-15}, 8.0×10^{-11}
Calico Hills—nonwelded zeolitic	6.00×10^{-13} m^2	Lognormal; 6.0×10^{-15}, 6.0×10^{-11}
Prow Pass—welded	6.00×10^{-13} m^2	Lognormal; 6.0×10^{-15}, 6.0×10^{-11}
Upper Crater Flat	6.00×10^{-13} m^2	Lognormal; 6.0×10^{-15}, 6.0×10^{-11}
Bull Frog—welded	3.00×10^{-13} m^2	Lognormal; 3.0×10^{-15}, 3.0×10^{-11}
Unsaturated Fracture Zone	1.00×10^{-12} m^2	Lognormal; 1.0×10^{-13}, 1.0×10^{-11}
Fracture porosity for all units	3.16×10^{-3}	Lognormal; 1.0×10^{-3}, 1.0×10^{-2}
Fracture beta for all units	3.00	—
Matrix and fracture longitudinal dispersivity as a fraction of unit	1.00×10^{-1}	—

The water table elevation remains constant in the TPA calculations. Thus, the thickness of the UZ does not change with time even during the pluvial climate. Sorption in fractures is neglected because of the fast travel times, whereas sorption in the matrix is modeled using the sorption coefficients presented in table 3-8. The effects of matrix diffusion on transport in the UZ are not modeled.

Figure 3-10 shows the release rate for ^{36}Cl. Because ^{36}Cl moves unretarded, comparison of the times of the release rates in this figure indirectly illustrate the UZ and SZ travel times. The EBS and UZ release rates are nearly the same, indicating that the UZ does not significantly delay groundwater transport.

3.1.6 Saturated Zone Flow and Transport

For each subarea, radionuclide transport out of the EBS and into the UZ and the SZ can be conceptualized as occurring in a single streamtube that originates in the repository, extends to the water table, and continues to the receptor location. In the SZ, streamtubes begin at the water table directly below the repository and continue to the receptor location. Each subarea in the repository is assigned to the nearest streamtube. Subareas 1 and 2 are mapped to streamtube D, subareas 3 and 4 are mapped to streamtube B and subareas 5, 6, and 7 are mapped to streamtube A. Figure 3-11 shows the subareas and streamtubes used for the SZ transport model, and table 3-9 provides the length of the SZ flow path by subarea. The groundwater travel times (GWTT) from the point where the radionuclides enter the SZ to the receptor location are 6,000 yr for subareas 1 and 2 (streamtube D); 2,700 yr for subareas 3 and 4 (streamtube B); and 2,800 yr for subareas 5, 6, and 7 (streamtube A). Large variations in the GWTT are primarily the result of variations in the streamtube length, width, and flow rates. There are no subareas mapped to streamtube C, consequently, streamtube C, which contains 26 percent of the total SZ flow, serves to dilute the concentration of radionuclides in the groundwater. The total SZ flow rate in all the streamtubes is 2.56×10^5 m^3/yr. The relative contributions of streamtubes A, B, and D to the total SZ flow are 27, 29, and 18 percent.

The release rate at the outlet of the streamtubes is determined using the sum of the release rates from all the streamtubes and is dependent on the time-varying concentration at the inlet. Figure 3-10 shows the SZ release rates for ^{36}Cl, which is not retarded in the SZ. When compared to the time of peak UZ release rate, this figure also indicates the GWTT through the SZ is on the order of a few thousand years.

The source term for the SZ transport model is the time-varying radionuclide release rate from the UZ calculations. Other inputs to the SZ transport model include the physical and chemical properties of the tuff and alluvium and the streamtube flow rates, widths, and lengths. The mean values for the SZ input parameters are presented in table 3-9.

3.1.7 Dose to the Receptor Group

The receptor location for the basecase data set is 20 km from the repository. At 20 km, the mean value for the pumping rate is 1.21×10^7 m^3/yr, which is sufficient to capture the entire contaminant plume. Because the TPA code assumes the volume of water pumped is constant throughout the TPI, values for the concentration of the well water exhibit the same behavior as the SZ release rates. For example, to convert from ^{36}Cl release rates in figure 3-10 to concentration, the release rates are divided by the well pumping rate to compute the well water concentrations.

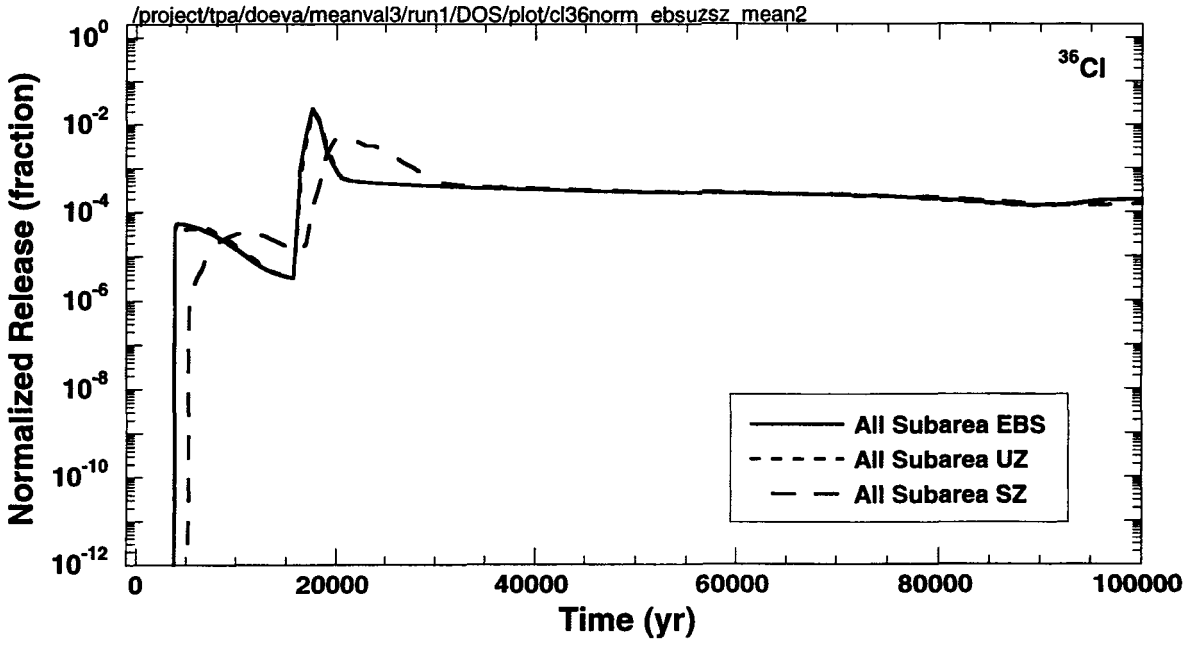

Figure 3-10. ^{36}Cl normalized release rates from the engineered barrier system, unsaturated zone and saturated zone for the mean value data set

The groundwater dose is determined by multiplying the concentration of the nuclides in the pumped water with the DCF. The mass of radionuclides captured by pumping is diluted in the volume of water extracted from the pumping well and converted from a groundwater concentration to a dose using DCFs. The dose to an individual of the receptor group originates from drinking and irrigation water used by an average adult living in Amargosa Valley. The groundwater pathway DCFs for the 11 radionuclides used in the basecase mean value data set are summarized in table 3-10.

3.2 RESULTS FROM THE MEAN VALUE DATA SET

This section illustrates the behavior of the total-system with the mean value of parameters and how the individual dose is influenced by the various subsystem models and parameters. Time history plots of key system parameters for both doses and release rates at various subsystem boundaries are presented in this section for the mean value single-realization case.

Subarea	Streamtube
1	D
2	D
3	B
4	B
5	A
6	A
7	A

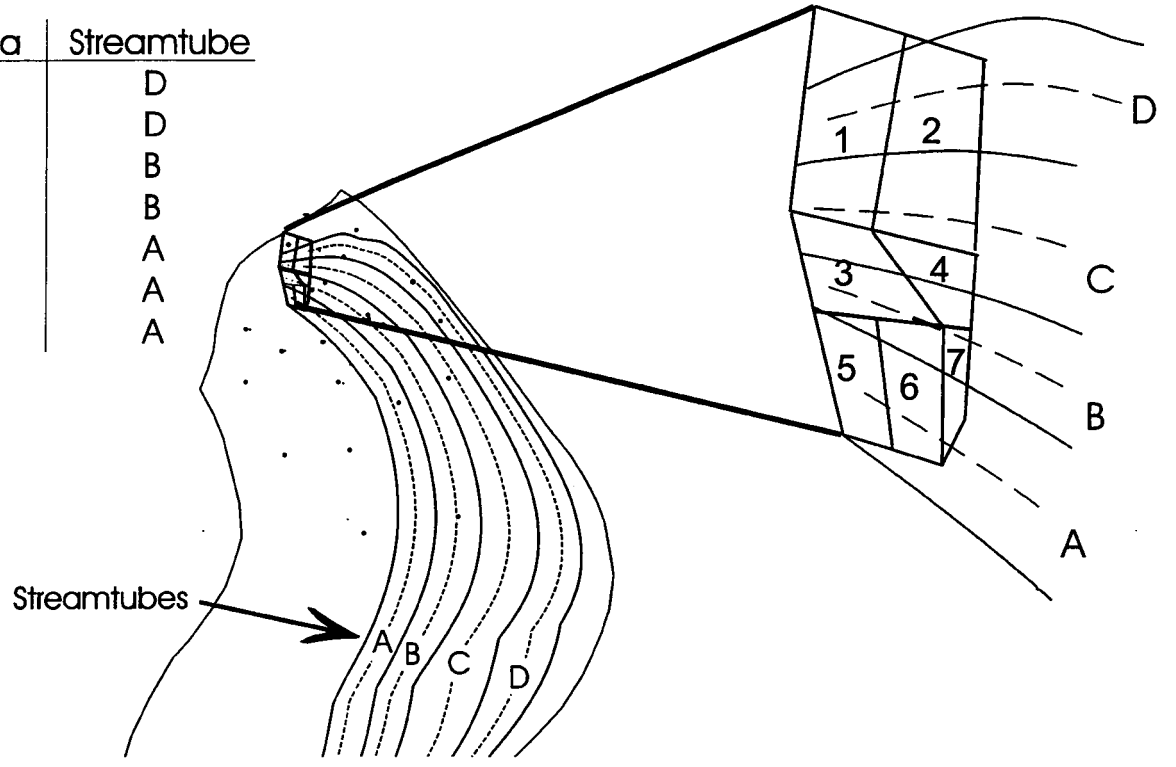

Figure 3-11. Saturated zone streamtubes assigned to each subarea

Table 3-9. Parameter values used for saturated zone flow and radionuclide transport in total-system performance assessment

Parameter	Mean	Distribution
Mixing zone dispersion fraction	1.00×10^{-2}	—
Tuff dispersion fraction	1.00×10^{-2}	—
Alluvium dispersion fraction	1.00×10^{-1}	—
Tuff fracture porosity	3.16×10^{-3}	Log-uniform; 1.0×10^{-3}, 1.0×10^{-2}
Alluvium matrix porosity	1.25×10^{-1}	Uniform; 1.0×10^{-1}, 1.5×10^{-1}
Immobile R_d for tuff for ^{241}Am	1.80×10^{4}	Not used because matrix diffusion = 0
Immobile porosity for tuff	1.00×10^{-2}	—
Diffusion rate for tuff	0.00	—
Fracture R_d for tuff for all nuclides	1.00	—
Min residence time for tuff	1.00×10^{1} yr	—
Min residence time for alluvium	1.00×10^{1} yr	—
Well pumping rate at receptor group at 20 km	8.75×10^{6} gal/day	—
Mixing zone thickness at 20 km	1.25×10^{2} m	—
Alluvium Matrix R_d		
^{241}Am	7.14×10^{7}	Lognormal; 7.5×10^{4}, 6.8×10^{10}
^{14}C	1.00	—
^{36}Cl	1.00	—
^{245}Cm	7.50×10^{4}	—
^{129}I	2.00	Log-uniform; 1.0, 4.0
^{237}Np	6.24×10^{1}	Lognormal; 1.0, 3.9×10^{3}
^{239}Pu	1.28×10^{4}	Lognormal; 4.2×10^{2}, 3.9×10^{5}
^{79}Se	2.24×10^{1}	Log-uniform; 1.0, 500.0
^{99}Tc	5.48	Log-uniform; 1.0, 30.0
^{230}Th	9.25×10^{3}	Lognormal; 1.9, 4.5×10^{7}
^{234}U	1.38×10^{2}	Lognormal; 1.0, 1.9×10^{4}
Streamtube Flow Properties	**Length (m)**	**Streamtube**
Subarea 1	29,200	D
Subarea 2	28,600	D
Subarea 3	25,200	B
Subarea 4	24,600	B
Subarea 5	23,400	A
Subarea 6	23,000	A
Subarea 7	22,500	A

Table 3-10. Biosphere dose conversion factors for groundwater at the 20-km receptor location

Radionuclide	Nonpluvial DCF (rem/year)/(Ci/m^3)	Pluvial DCF (rem/year)/(Ci/m^3)
^{241}Am	6.11×10^6	4.31×10^6
^{14}C	1.35×10^4	8.60×10^3
^{36}Cl	4.52×10^4	3.02×10^4
^{245}Cm	6.32×10^6	4.51×10^6
^{129}I	1.27×10^6	7.90×10^5
^{237}Np	9.01×10^6	6.43×10^6
^{239}Pu	6.00×10^6	4.30×10^6
^{79}Se	2.51×10^4	1.68×10^4
^{99}Tc	4.74×10^3	3.29×10^3
^{230}Th	9.32×10^5	6.61×10^5
^{234}U	5.06×10^5	3.66×10^5

The dose to an average individual residing 20 km downgradient of the repository is presented in figure 3-12 for radionuclides with doses greater than 10^{-6} mrem/yr (10^{-11} Sv/yr). The results are presented for the first 10,000 and 100,000 yr, respectively. The period of 100,000 yr is chosen so that the effects of one cycle of the pluvial climate and the effects of WP corrosion, which occur after the 10,000-yr TPI, can be studied.

A peak total dose of about 0.002 mrem/yr (2×10^{-8} Sv/yr) was calculated during the 10,000-yr TPI. The dose is dominated in the 10,000-yr TPI by ^{129}I and ^{36}Cl, which are nonsorbing nuclides with relatively long half-lives. For the 100,000-yr TPI, a peak total dose of 0.3 mrem/yr (3×10^{-6} Sv/yr) occurred at 23,000 yr, and the dose was dominated by the nuclides ^{129}I, ^{99}Tc, and ^{36}Cl. A discussion of the TPA results from the 10,000- and 100,000-yr TPIs, with and without the faulting and igneous activity disruptive events, follows in the next two sections.

3.2.1 Ten Thousand-Year Releases and Dose

As evident from figure 3-8 and explained in section 3.1.3, all basecase releases in 10,000 yr would arise from initially defective WP failures. Although initially defective failure takes place at the zero year, releases do not occur until approximately 3,400 yr later. Prior to 3,400 yr, refluxing water enters and fills the failed WP. Once the WP fills, water overflows from the WP, and radionuclides leave the failed WP.

The time histories of radionuclide releases at the downgradient boundaries of the EBS, the UZ, and the SZ are provided in figure 3-13. In general, the release rates from the EBS in figure 3-13(a) for the soluble radionuclides drop within a few years after the peak release, because of radioactive decay and because the removal of radionuclides from the WP decreases the inventory available for release. Other radionuclides, such as ^{234}U, ^{237}Np, ^{239}Pu, and ^{230}Th, which are less soluble, and have relatively longer half-lives, exhibit increasing release rates in the 10,000-yr TPI. The radionuclide ^{241}Am also has a low solubility, however, with a relatively short half-life of 432 yr, the release rate decreases to match the release rate of its parent ^{245}Cm and establishes secular equilibrium.

There is no initial increase in the EBS release rates observed from the instantaneous release of the gap fraction inventory. Moreover, climatic change from current to pluvial conditions could be a key event that

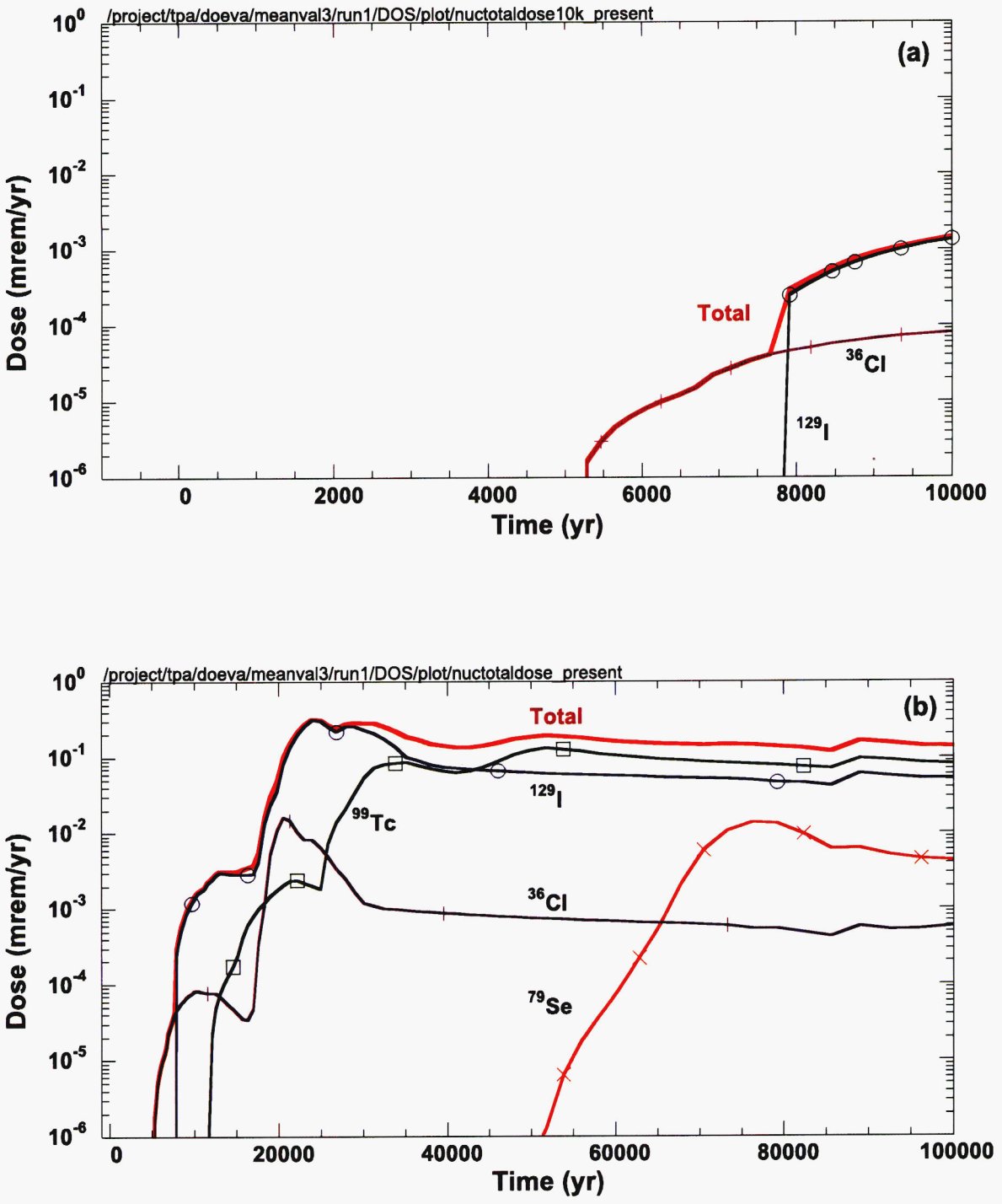

Figure 3-12. Groundwater dose to an average individual as a function of time at the receptor location 20 km downgradient of the repository for the mean value data set in the (a) 10,000-yr and (b) 100,000-yr time periods of interest

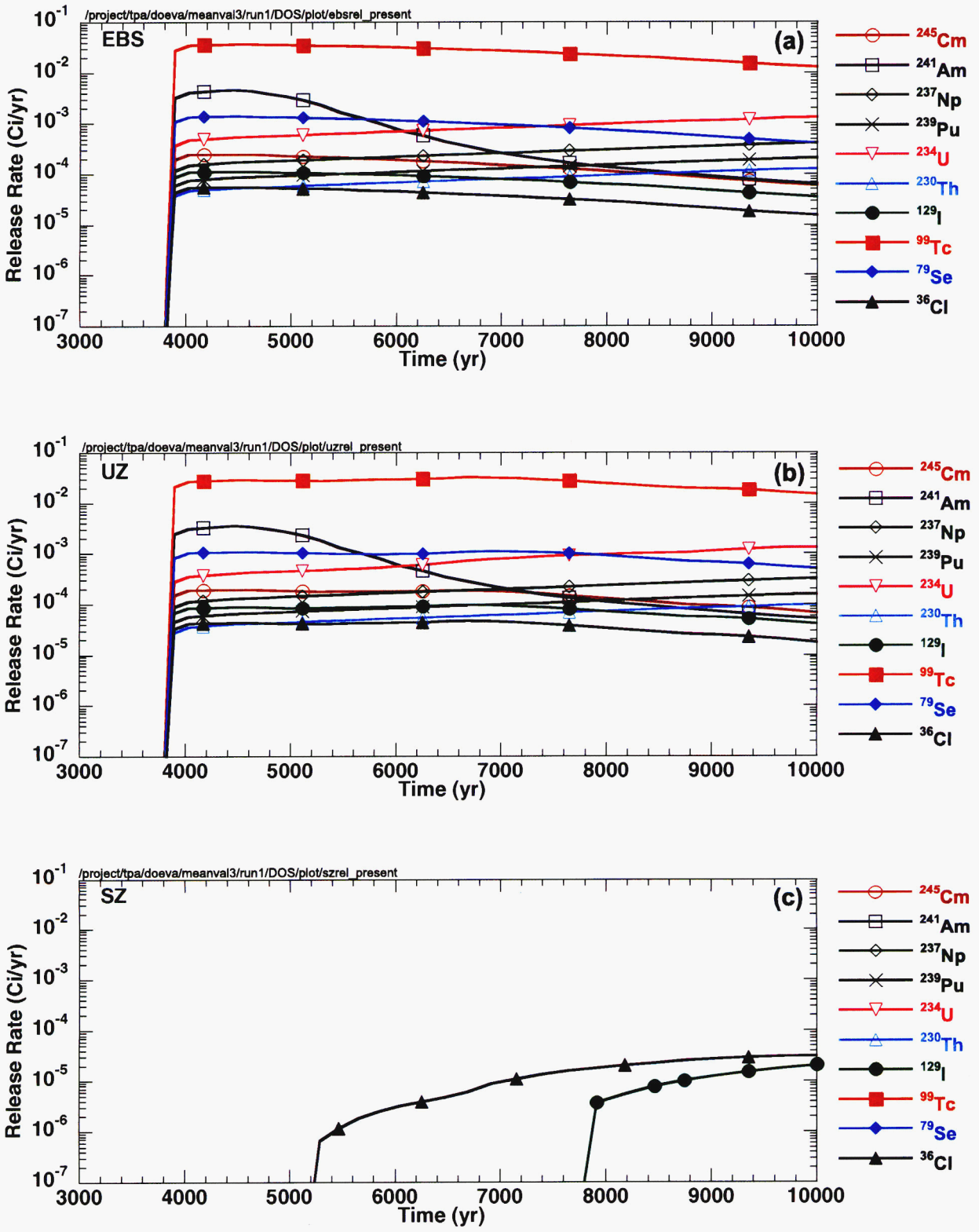

Figure 3-13. Release rates in the 10,000-yr time period of interest from the (a) engineered barrier system, (b) unsaturated zone, and (c) saturated zone for the mean value data set

affects performance. The increase in infiltration rate over the 10,000-yr TPI shown in figure 3-1 does not result in increased release rates from the EBS for the highly soluble radionuclides, although an effect is evident for the less soluble radionuclides, as discussed previously.

The similarity between EBS and UZ releases shown in figures 3-13(a) and (b) indicates the UZ as modeled does not significantly influence the releases into the SZ. One might expect the UZ to delay the transport of radionuclides, because the radionuclides must be transported 300 m from the repository to the water table.

The GWTT through the UZ is only 20 yr (i.e., fracture flow) for all subareas except subareas 5 and 6, which have a travel time of about 1,400 yr (i.e., matrix flow). Consequently, for subareas 1 through 4 and subarea 7, which encompass almost 80 percent of the SF inventory, the UZ does not delay radionuclide transport subsequent to release from the EBS. For the remaining 20 percent of the SF inventory, the 1,400-yr GWTT is relatively small compared to the 10,000-yr TPI.

The SZ illustrated in figure 3-13(c) reveals releases of only ^{99}Tc, ^{129}I, and ^{36}Cl in the 10,000-yr TPI. As provided in table 3-9, these radionuclides have the weakest sorbing properties in the SZ alluvium. The SZ release rates presented in figure 3-13(c) can also be compared with figure 3-13(b) to evaluate the effects of flow and transport in the SZ. The GWTT computed using the streamtube flow rates and lengths in the SZ is about 3,700 yr. However, sorption in the alluvium significantly increases the travel time for most of the radionuclides.

As illustrated in figure 3-12(a), the groundwater pathway dose at 10,000 yr is dominated by ^{129}I and ^{36}Cl. These nuclides contribute the most to dose because of no or little retardation during transport, a large initial inventory, long half-lives compared to the 10,000-yr time frame of interest, relatively large DCFs, and high solubilities. Tables 3-5 and 3-7 through 3-10 provide a summary of the mean values for these parameters. To obtain a perspective of the magnitude of the dose, a total dose of 1 nanorem/yr (10^{-11} Sv/yr) does not appear until 4,500 yr in the time evolution of dose curve in figure 3-12(a). Furthermore, the SZ release rate for ^{129}I corresponding to 2 μCi/yr does not occur until 6,500 yr, at which time the dose from ^{129}I is 1/10th of a μrem/yr. The only nuclides that contribute more than a nanorem/yr (10^{-11} Sv/yr) to dose in 10,000 yr are ^{129}I and ^{36}Cl, which exhibit the peak doses at the end of the 10,000-yr TPI.

The dose histories for a particular faulting event and a particular igneous event are presented in figures 3-14(a) and (b). It must be made very clear that the purpose of the following discussion is not to compare the incremental risk posed by the faulting crust or the igneous event, but rather to illustrate the behavior of the underlying model abstractions for faulting and igneous activity. To determine the risk one would need to multiply the additional doses due to faulting and igneous activity by their respective annual probabilities of occurrence (5×10^{-6} and 1×10^{-7}). For the mean value data set, there are no faulting events because the mean value of the threshold displacement is greater than the mean value of the credible displacement along a fault. However, if the threshold is made smaller than the mean value of the credible displacement, the faulting event occurs at about 4,900 yr and causes the failure of 162 WPs. Figure 3-14(a) shows the groundwater dose from the forced faulting event is approximately twice the dose without a faulting event at 10,000 yr. The difference between the results arises solely due to the release of SF from WPs failed by faulting.

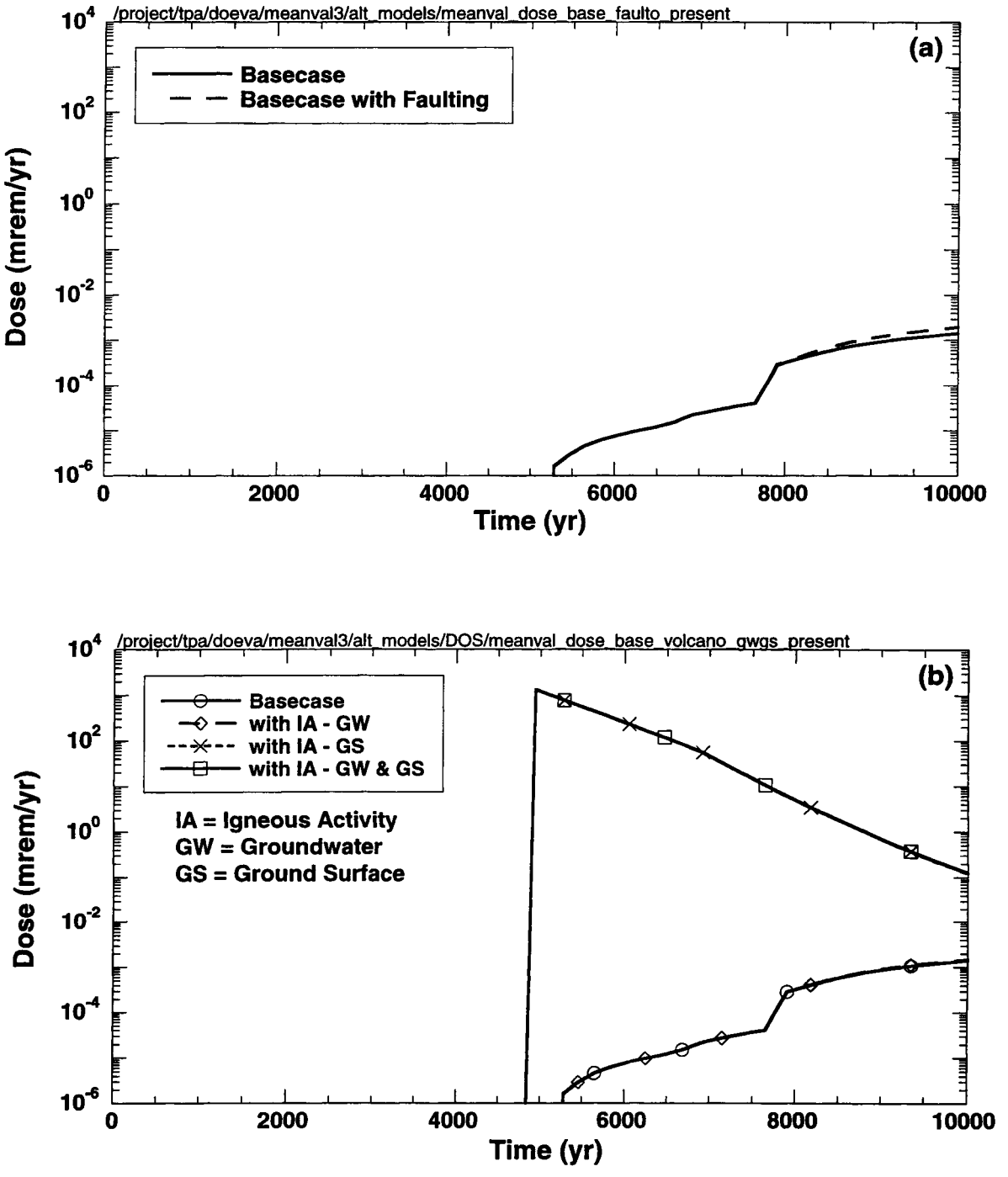

Figure 3-14. Groundwater dose in 10,000-yr time period of interest with and without (a) faulting and (b) igneous activity disruptive events for the mean value data set without probability weighting. The ground surface dose is shown for releases caused by extrusive igneous activity.

The groundwater dose from igneous activity in figure 3-14(b) behaves similarly to the dose from faulting events. The increase in groundwater dose from igneous activity is smaller than that for faulting events because only 31 WPs are failed by the intrusive igneous activity compared to 162 WPs failed by the faulting event in the mean value single-realization case. Extrusive igneous events also result in a peak ground surface dose of about 1,000 mrem/yr at 4,900 yr, which is the time of the volcanic event, and the dose exponentially decreases thereafter.

The following section presents a discussion of the TPA results from the 100,000-yr TPI for dose, release rates, and other intermediate values such as corrosion failure time. The results for the 100,000-yr TPI are different from the results for the 10,000-yr TPI, partly because all WPs fail from corrosion before 17,000 yr.

3.2.2 One Hundred Thousand-Year Releases and Dose

Figure 3-8 provides the performance of the EBS showing the number of failed WPs during the 100,000-yr TPI. Initially defective failures in all subareas account for 31 WPs, while of those remaining, 928 WPs in subareas 5 and 7 fail from corrosion at 16,300 yr; and 5,468 WPs in subareas 1, 2, 3, 4, and 6 fail from corrosion at 17,000 yr. Thus, all 6,427 WPs in the repository fail by 17,000 yr. Table 3-3 provides a summary of the TPA input parameters that determine the WP failure time.

The release rate histories for all 11 radionuclides at the three boundaries (i.e., EBS, UZ, and SZ presented in figure 3-15) reflect the time required for the initially defective WPs to fill with water (3,400 yr) and release radionuclides, together with the corrosion failure time of 17,000 yr. The WPs failed by corrosion fill relatively faster and release radionuclides relatively faster compared to initially defective failures because the thermal reflux period has passed and the pluvial period has taken effect. The first peak releases begin at about 4,000 yr and the second peak occurs before 20,000 yr. Just as with the 10,000-yr TPI in figure 3-13, release rates for radionuclides are impacted by sorption coefficients, half-lives, initial inventories, solubilities, and DCFs. Values for these parameters are presented in tables 3-5 and 3-7 through 3-10.

When water starts to leave the WP after it has filled with water, the releases of ^{99}Tc, ^{129}I, and the other highly soluble radionuclides represent the accumulation of the radionuclides in water that occurs as the WP fills. The peak releases for these highly soluble radionuclides occur after the WP fills with water at 3,400 yr. As seen in figure 3-15 for the less soluble radionuclides such as ^{237}Np, the release rate peaks at the end of the 10,000-yr TPI. This implies that the solubility limit is controlling the release rate. Because ^{237}Np leaves the WP at the solubility limit, the release rate from the WP is proportional to the rate of water flow through the WP. With a half-life of 2.14×10^6 yr, the ^{237}Np inventory is available for release throughout the simulation period. This effect is observable in figure 3-15(a) from 3,400 yr to the corrosion failure time at 17,000 yr. After 17,000 yr, radionuclide releases decrease (i.e., not solubility-limited) following the peak releases at approximately 17,000 yr. The decrease in release rates for the radionuclides with low solubilities can be attributed to high flow rates during the pluvial period. ^{239}Pu is another actinide that is solubility-limited in ambient YM pore waters. Therefore, release rates from the EBS should be similar to ^{237}Np as shown in figure 3-15(a).

The plot in figure 3-15(b) represents the release rates from the seven subareas summed over all nuclides at the water table. Comparison of the EBS and UZ release rates in figures 3-15(a) and (b) shows that the UZ has little delaying effect, not only on the transport of ^{99}Tc, a nonsorbing nuclide, but also on the transport of the other 10 radionuclides. As discussed in the previous section, the UZ does not significantly affect the release rates because flow mainly occurs in fractures with no retardation.

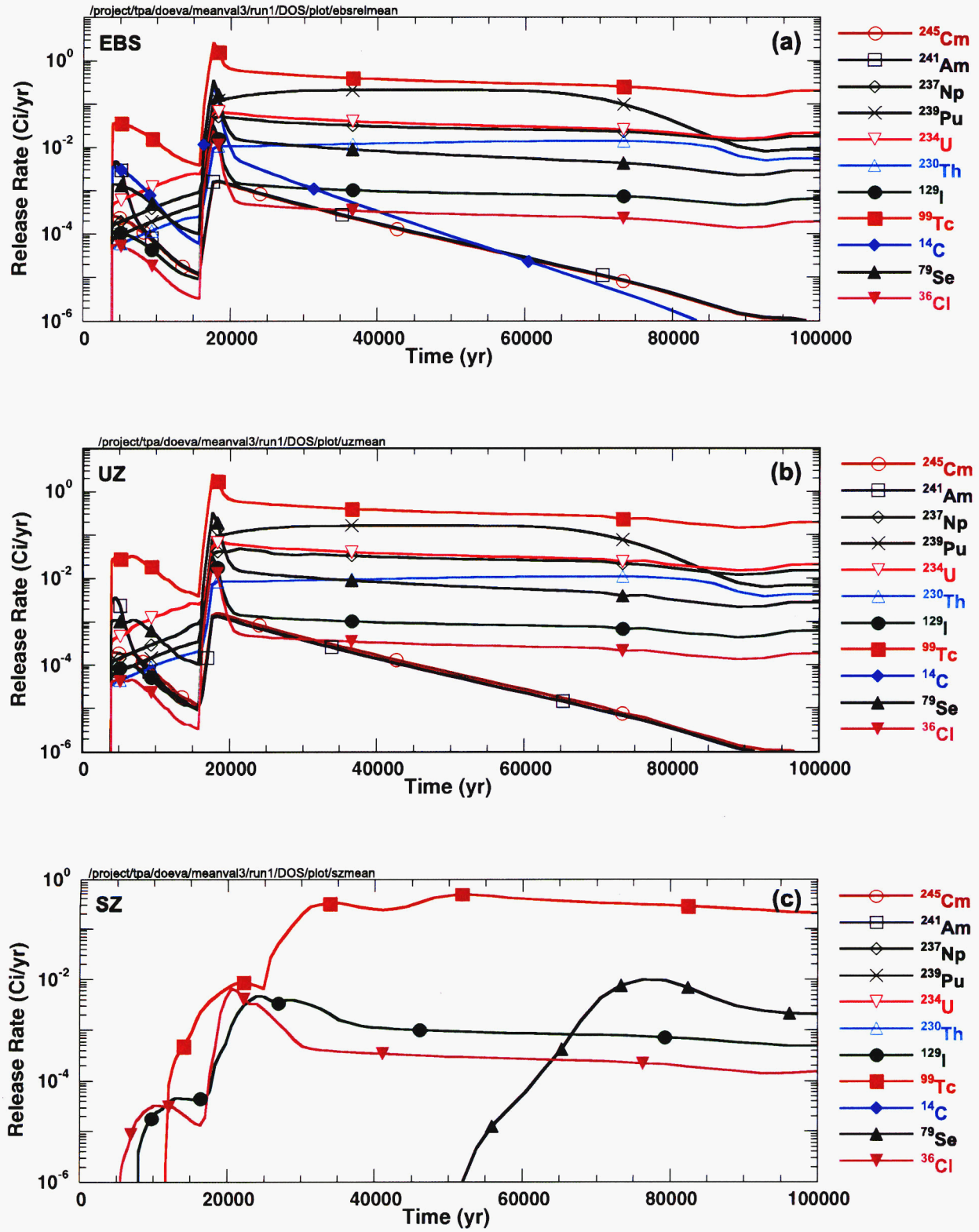

Figure 3-15. Release rates in 100,000 yr from the (a) engineered barrier system, (b) unsaturated zone, and (c) saturated zone for the mean value data set

Figure 3-15(c) illustrates the performance of the SZ in the 100,000-yr TPI. The figure shows the SZ release rates at a distance of 20 km from the repository. In the SZ, sorption significantly affects the release rates. The only radionuclides that arrive at the receptor location with a release rate greater than 10^{-6} Ci/yr are ^{99}Tc, ^{79}Se, ^{129}I, and ^{36}Cl. Retardation of the remaining seven radionuclides in the alluvium delays their time of arrival past the 100,000-yr TPI. The SZ alluvium sorption coefficients for all radionuclides are provided in table 3-9.

The radionuclides contributing to the 100,000-yr dose are completely different than those dominating the 10,000-yr dose. For the 100,000-yr TPI, the dose provided in figure 3-12(b) is dominated by ^{99}Tc and ^{129}I, with smaller contributions from ^{36}Cl and ^{79}Se. The radionuclide contributing the most to the peak dose at 23,000 yr is ^{129}I with minor contributions from ^{99}Tc and ^{136}Cl. Although ^{136}Cl has a relatively long half-life at 3.01×10^5 yr, the chloride inventory is small (see table 3-7). Thus, although contributing significantly to peak dose at 23,000 yr, ^{36}Cl rapidly becomes an insignificant contributor to dose. Figure 3-12(b) also illustrates the impact of retardation in the alluvium on the arrival of radionuclides at the 20-km receptor location. Radionuclides with lower retardation factors arrive earlier than those with higher values. The retardation factors for ^{36}Cl, ^{129}I, ^{99}Tc, and ^{79}Se are 1, 2, 5.5, and 22.4, respectively. The reasons ^{99}Tc and ^{129}I dominate the dose in figure 3-12(b) are (i) high solubility in the water contacting the SF, (ii) almost no retardation, (iii) large initial inventory, (iv) long half-lives, and (v) relatively large DCFs. Tables 3-5 and 3-7 through 3-10 provide summaries of the values for these parameters.

Figures 3-16 and 3-17 present ^{99}Tc and ^{237}Np release rates and ^{99}Tc dose, respectively, by subarea and for the repository. The EBS release rates for ^{99}Tc and ^{237}Np in figure 3-16(a) exhibit similar behavior with the subareas having the largest inventory contributing the most to the total release. The number of WPs in each subarea, which are directly related to the inventory, are 1,663; 1,767; 855; 472; 654; 738; and 278 for subareas 1 through 7, respectively. Subareas 1 and 2 are the largest subareas and show the highest release rates, whereas subarea 7 contains the fewest WPs and has the lowest release rates.

The plots of the UZ releases in figure 3-16(b) indicate that the ^{99}Tc and ^{237}Np release rates are the same as the EBS releases in figure 3-16(a) in all subareas except 5 and 6. Only subareas 5 and 6 have the Calico Hills nonvitric unit (figure 3-9), which has relatively high matrix permeability compared to other units. At the infiltration rate corresponding to the mean value data set, only matrix flow can occur in this unit. Flow occurs in the fractures for subareas 1, 2, 3, 4, and 7 with GWTTs of about 20 yr and no retardation. However, for subareas 5 and 6, the transport of ^{237}Np is retarded in the matrix and the effects of the time-varying UZ flow change the ^{99}Tc and ^{237}Np release rates. As evident in figure 3-16(b), retardation in the matrix produces a greater effect on the ^{237}Np UZ release rates than the release rates for ^{99}Tc, which is not retarded in the UZ matrix.

The SZ release rates for ^{99}Tc in figure 3-16(c) exhibit a delay when compared to the ^{99}Tc UZ release rates in figure 3-16(b). However, the general characteristics of the engineered barrier and UZ releases are preserved insofar as the peak releases arising from initially defective failures and corrosion failures are apparent in the plot. The variability by subarea is also consistent for the ^{99}Tc release rates. There is no ^{237}Np release from the SZ because of retardation in the SZ alluvium.

The groundwater doses for ^{99}Tc by subarea are shown in figure 3-17. The general characteristics of this plot match the SZ release rates for ^{99}Tc in figure 3-16(c). For 100,000 yr, the subareas with the largest ^{99}Tc release rates and dose in figure 3-17 contain the greatest amount of SF (i.e., the subareas listed from the largest to the smallest amount of SF are subareas 2, 1, 3, 6, 5, 4, and 7). The effects of GWTT on dose at the

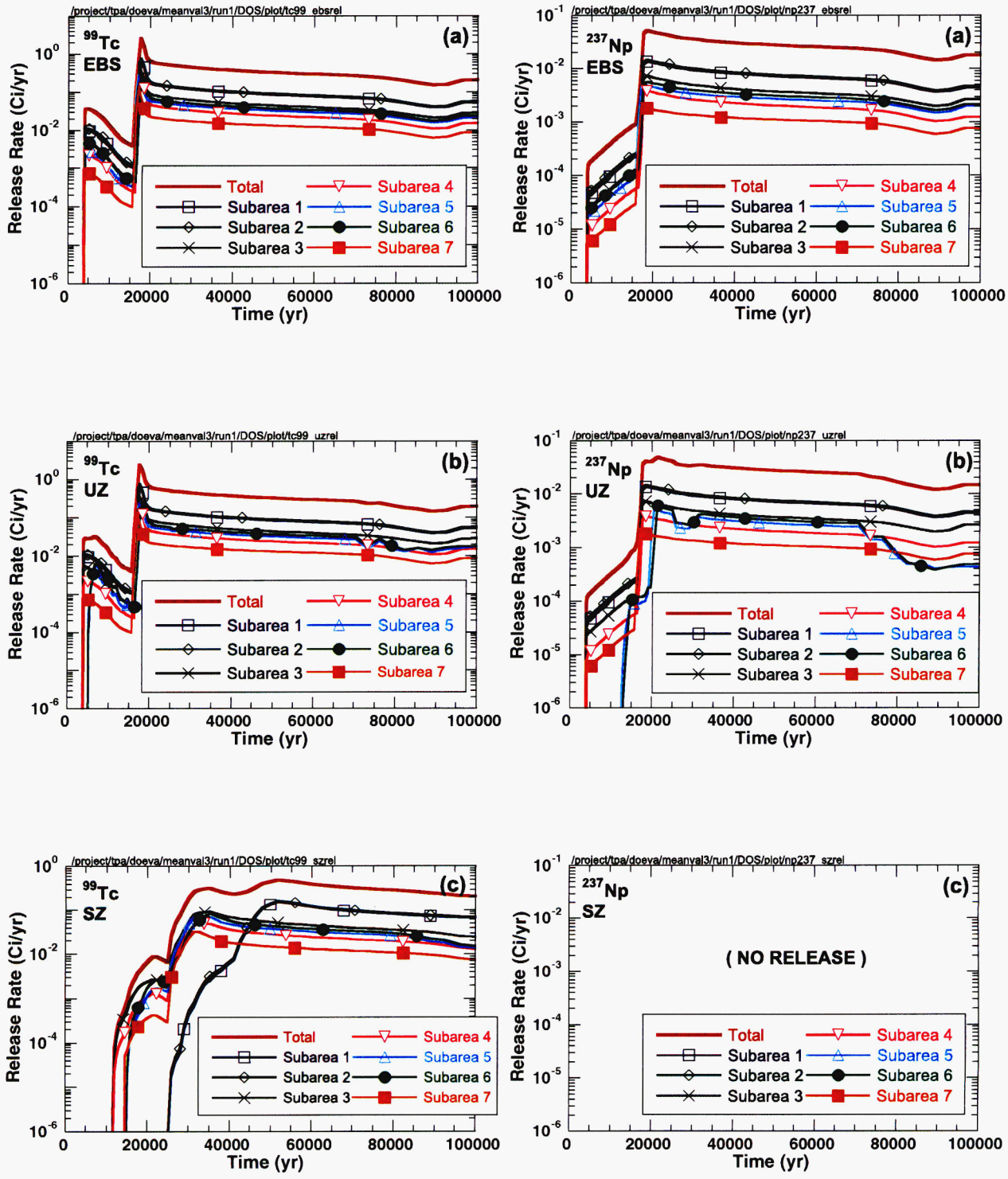

Figure 3-16. ^{237}Np and ^{99}Tc total release and releases by subarea in 100,000 yr from the (a) engineered barrier system, (b) unsaturated zone, and (c) saturated zone for the mean value data set

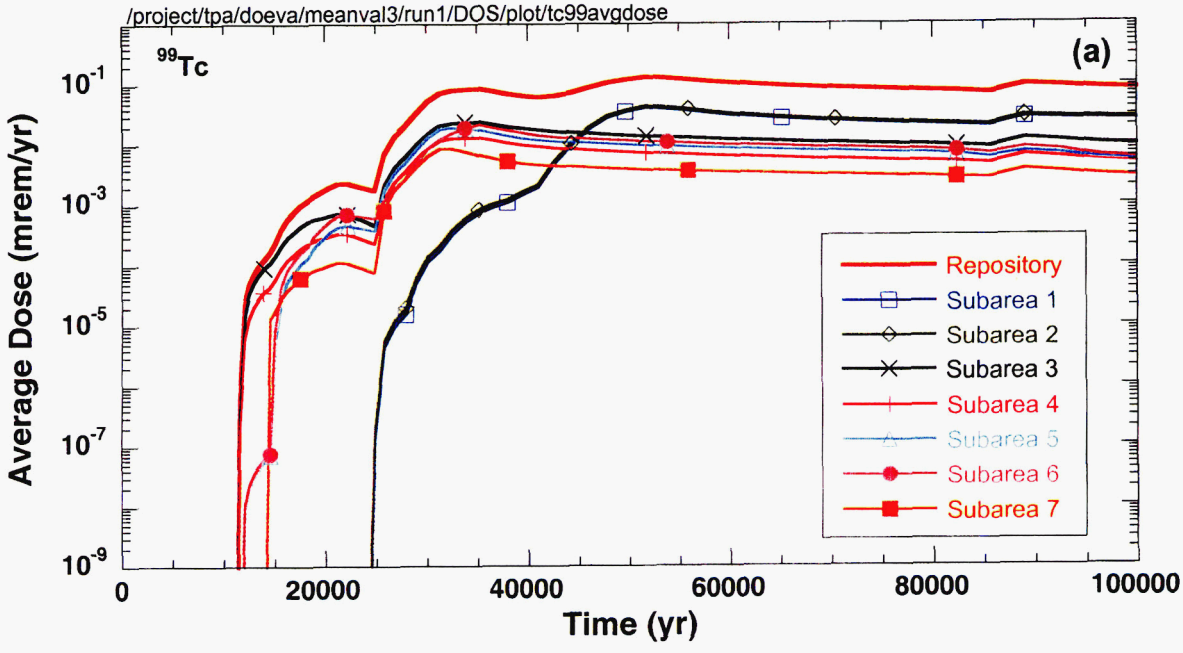

Figure 3-17. ^{99}Tc groundwater doses, total and by subarea, in 100,000 yr for the mean value data set

receptor location is evident in figure 3-18 with the peak dose from subareas 1 and 2 arriving at about 20,000 yr after peak doses from subareas 3 through 7. The SZ travel times vary by subarea because subareas use different streamtubes. Subareas 3 and 4 are assigned to streamtube B and exhibit the shortest SZ travel times, whereas subareas 5, 6, and 7 are assigned to streamtube A, and subareas 1 and 2 use streamtube D. The longest travel times are found in streamtube D (see table 3-9 for streamtube lengths).

The dose history for faulting events and igneous activity[2] over 100,000 yr is presented in figure 3-19. As with the results for the 10,000-yr TPI, using the mean value data set results show no faulting events because the mean value of the threshold displacement is greater than the mean value of the credible displacement along a fault. However, if the threshold is made smaller than the credible displacement, the faulting event occurs at about 4,900 yr and causes the failure of 162 WPs. Figure 3-19(a) shows the groundwater dose from the faulting event is approximately twice the dose without a faulting event from about 10,000 to 17,000 yr. After 17,000 yr, the releases from WPs failed by corrosion dominate the groundwater

[2]These results are presented only to show the process-level trends and must be used in proper context because these are not weighted by appropriate probabilities. The annual probability for the faulting event is 5×10^{-6} and for the igneous event is 1×10^{-7} yr^{-1}.

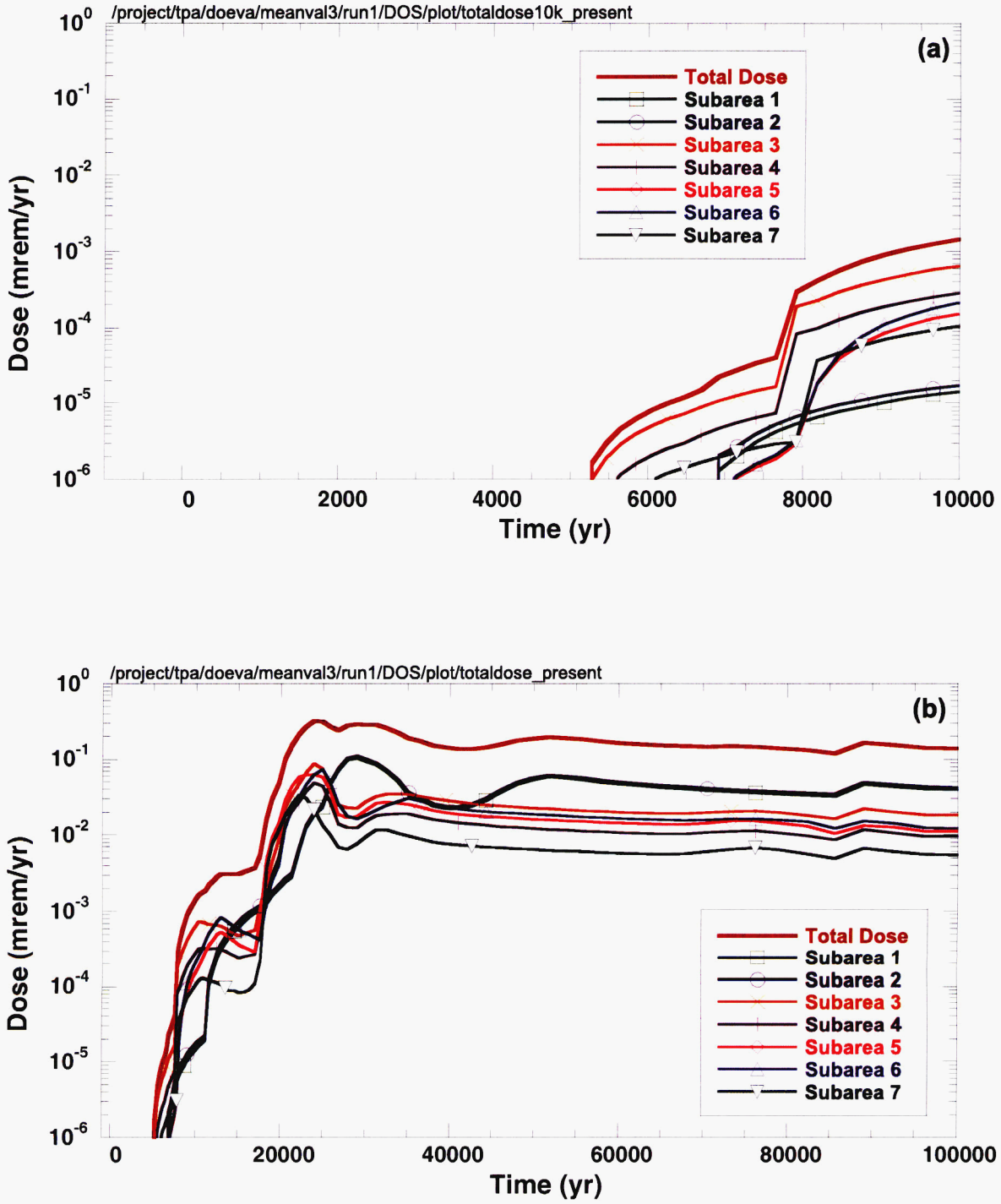

Figure 3-18. Groundwater dose, total and by subarea, in (a) 10,000 and (b) 100,000 yr for the mean value data set

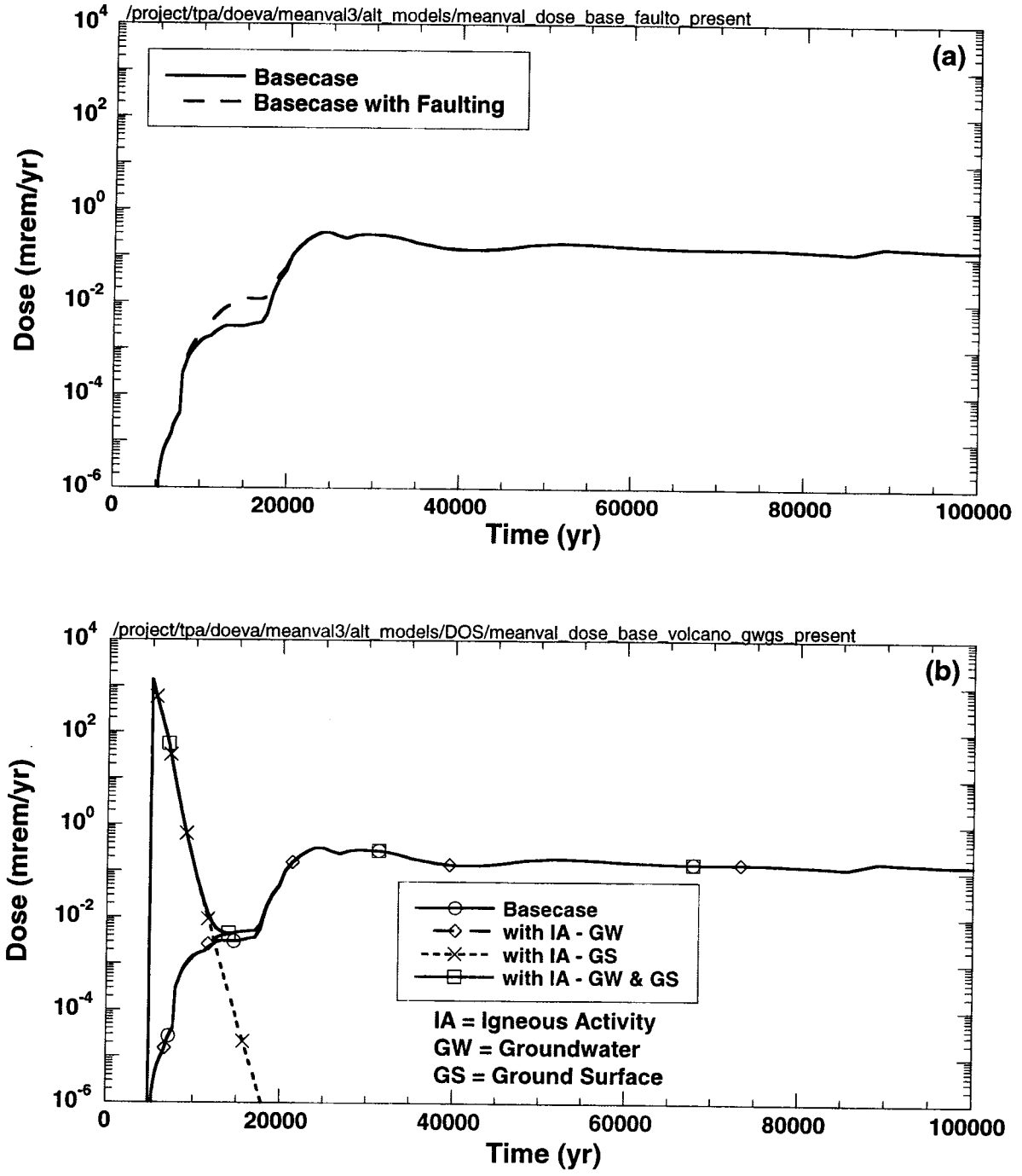

Figure 3-19. Groundwater dose in 100,000 yr with and without (a) faulting and (b) igneous activity disruptive events for the mean value data set without probability weighting. The ground surface dose is shown for releases caused by extrusive igneous activity.

dose, and the results plotted in figure 3-19(a) of the groundwater dose with and without faulting events are not distinguishably different.

The groundwater dose from igneous activity over the 100,000-yr TPI in figure 3-19(b) behaves similarly to the dose from faulting events. As with the results for the 10,000-yr TPI, the increase in groundwater dose from igneous activity for 100,000 yr is smaller than that for faulting events because only 31 WPs are failed by the intrusive igneous activity compared to 162 WPs failed by the faulting event. Extrusive igneous events also result in a ground surface dose that peaks at about 1,000 mrem/yr when the volcanic events occur at 4,900 yr and exponentially decreases thereafter. At about 12,000 yr, the groundwater and ground surface contributions to dose are equal. From 17,000 yr, when all the WPs have failed by corrosion, through 100,000 yr, groundwater dose dominates the receptor dose. The doses presented in figure 3-19 are not probability weighted.

3.3 MULTIPLE REALIZATION ANALYSIS

The performance of the YM repository is evaluated with a probabilistic approach that comprises results from simulations performed with multiple realizations. This approach uses the probabilistic sampling of input data to compute dose at a receptor location 20 km from the repository during time periods of 10,000 and 100,000 yr. While the deterministic approach (previous section) was presented to illustrate in detail how the behavior of the various components or processes influences other components or dose, the probabilistic approach provides a range of results that shows the variation in the output resulting from the combined effects of the variability in the input data. Also, trends not evident in the results from the deterministic data may become evident in the probabilistic results.

Probabilistic sampling is conducted using Latin Hypercube Sampling (LHS) (Iman et al., 1980) for the 250 realizations, which is sufficiently large to obtain convergence in results while maintaining computational efficiency. Each realization uses a set of values generated from probability distribution functions specified in the TPA input file. The probability distribution functions are constructed for the input parameters thought to contain uncertainty and variability using available data and interpretation. Uncertainty arises from a lack of complete information, whereas variability is the natural or inherent variance in the value of a parameter.

The previous section presents TPA results computed with mean values for the distributions specified in the basecase data set. The basecase data set comprises the best available information of the TPA input parameters. In the basecase data set, of the 838 parameters, 592 parameters are defined as constants, and 246 parameters are specified with probability distribution functions. The basis for assigning a constant value or a probability distribution to the parameter depends on various factors. For example, constant values are assigned to parameters that are either well-characterized or have negligible variability. Probability distribution functions are assigned to parameters with either a natural variability or uncertainty that has been observed in data. Expert elicitation also provides a valid basis to assign a constant value or a probability distribution function to a parameter. The selection of the particular distribution type, such as normal, uniform, or beta, depends on the information available for the parameter and may involve either the best fit of data to a distribution or a reasonable assumption of the distribution type. Specification of a probability distribution function in the TPA code consists of a distribution type and limits (e.g., uniform with a minimum of 0 and a maximum of 100 or log-triangular with a minimum of 1.0×10^{-5}, maximum of 1.0×10^{-1}, and a peak of 1.0×10^{-3}). The impact of assuming a particular distribution for a parameter is evaluated in sensitivity analyses.

When the TPA code is executed for a realization of the parameter vector, dose to the receptor is calculated for realization. The results from all Monte Carlo realizations using the LHS sampler are plotted to evaluate the repository performance. For example, dose to the receptor is presented in a scatterplot of peak dose versus time of peak dose, a time history of average and expected dose for all realizations, and a CCDF of peak dose. The expected dose is computed by averaging the doses at an instant of time from all realizations. The resulting curve is a time-dependent dose curve that represents the expected dose. The peak expected dose is the largest expected dose obtained from the expected dose curve versus time. For example, groundwater dose from a single realization using the mean value data set is shown in figure 3-18 and the expected dose from multiple realizations is presented in figure 3-20, which also provides dose from individual realizations. Additionally, the relationship between dose and intermediate results, such as WP failure time, flow of water onto a WP, and radionuclide release rates, is presented for all realizations.

This section provides results from simulations conducted with the TPA Version 3.2 code using the basecase data set with 250 realizations. For the major components of the TPA code, results are summarized and trends presented. The values and distributions of the TPA parameters in the basecase data set used to generate the multiple-realization results are provided in tables 3-1 through 3-10, and the correlated parameters with associated correlation coefficients are presented in table 3-11.

3.3.1 Unsaturated Zone Flow

The variation in the mean, minimum, and maximum infiltration rates is illustrated in figure 3-21. For the mean infiltration rates, a present-day climate exists from 0 to about 3,000 yr and 89,000 to 100,000 yr, with the pluvial climate occurring between 3,000 and 89,000 yr. Figure 3-21 shows that the range from the minimum to the maximum infiltration rates is approximately one order of magnitude. This range is related to the TPA input parameter for the initial infiltration rate, which has a uniform distribution from 1 to 10 mm/yr.

Subarea 3 exhibits the largest infiltration rates, because of higher infiltration at the ground surface above subarea 3 attributable to near-surface processes such as elevation and soil depth, whereas subareas 1, 2, and 4 have the lowest infiltration rates. In any single realization, the largest difference among the subarea infiltration rates is approximately 10 percent. The minimum and maximum pluvial infiltration rates, which occur between about 3,000 and 89,000 yr, vary from about 10 to 280 mm/yr for all realizations and subareas.

In realizations with higher flow rates, there are generally more radionuclides released from the EBS because of a greater amount of water available to dissolve radionuclides. This effect is illustrated in figure 3-22, which provides scatterplots of the cumulative releases of ^{99}Tc and ^{237}Np in 100,000 yr versus the maximum flow rate into the repository for each realization. The variability in the maximum flow rate is slightly more than one order of magnitude, while the cumulative release varies over three orders of magnitude. Although these releases are solubility limited, there is not a one-to-one relationship with the flow rate because of other parameters such as flow factors and the subarea wet fraction that affect the EBS release rate.

Figure 3-23 shows the trend of higher peak groundwater dose for maximum flow rate in both the 10,000- and 100,000-yr TPIs. Higher flow rates in the UZ transport a larger mass of radionuclides from the EBS and result in higher groundwater dose. Although the peak flow rate varies about one order of magnitude, the variability in the peak groundwater dose spans five orders of magnitude.

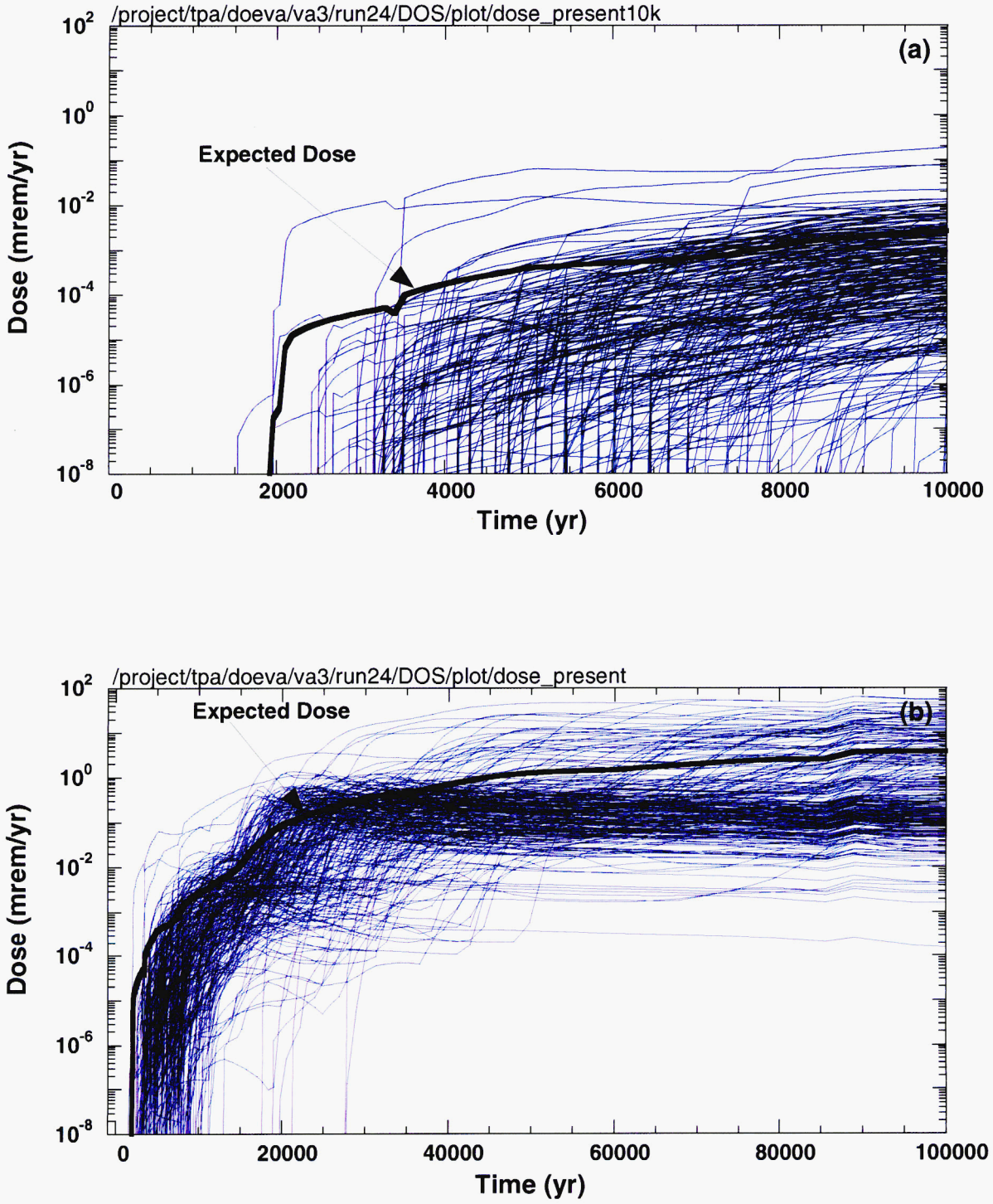

Figure 3-20. Groundwater dose in (a) 10,000 and (b) 100,000 yr, including the average dose, for 250 realizations

Table 3-11. Correlated parameters and correlation coefficients for the multiple realizations

Correlated Parameter 1	Correlated Parameter 2	Correlation
SubAreaWetFraction	ArealAverageMeanAnnualInfiltrationAtStart[mm/yr]	0.631
SubAreaWetFraction	MatrixPermeability_TSw_[m2]	-0.623
FowFactor	ArealAverageMeanAnnualInfiltrationAtStart[mm/yr]	-0.224
FowFactor	MatrixPermeability_TSw_[m2]	0.13
FowFactor	SubAreaWetFraction	-0.366
AlluviumMatrixRD_SAV_Am	AlluviumMatrixRD_SAV_Pu	0.964
AlluviumMatrixRD_SAV_Am	AlluviumMatrixRD_SAV_U	0.346
AlluviumMatrixRD_SAV_Am	AlluviumMatrixRD_SAV_Np	0.837
AlluviumMatrixRD_SAV_Am	AlluviumMatrixRD_SAV_Th	0.112
AlluviumMatrixRD_SAV_Pu	AlluviumMatrixRD_SAV_U	0.489
AlluviumMatrixRD_SAV_Pu	AlluviumMatrixRD_SAV_Np	0.881
AlluviumMatrixRD_SAV_Pu	AlluviumMatrixRD_SAV_Th	0.109
AlluviumMatrixRD_SAV_Np	AlluviumMatrixRD_SAV_Th	0.260
AlluviumMatrixRD_SAV_Np	AlluviumMatrixRD_SAV_U	0.610
AlluviumMatrixRD_SAV_Th	AlluviumMatrixRD_SAV_U	0.165

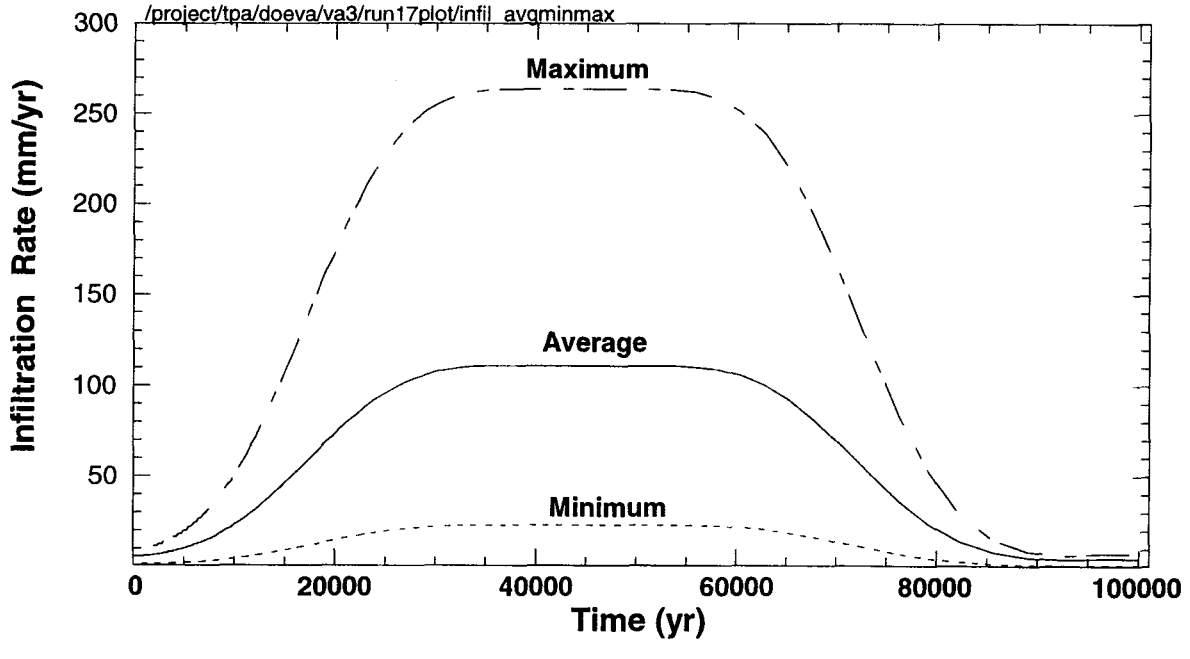

Figure 3-21. Mean, maximum, and minimum infiltration rates in the unsaturated zone for each subarea. The subarea mean infiltration rate is averaged over all 250 realizations.

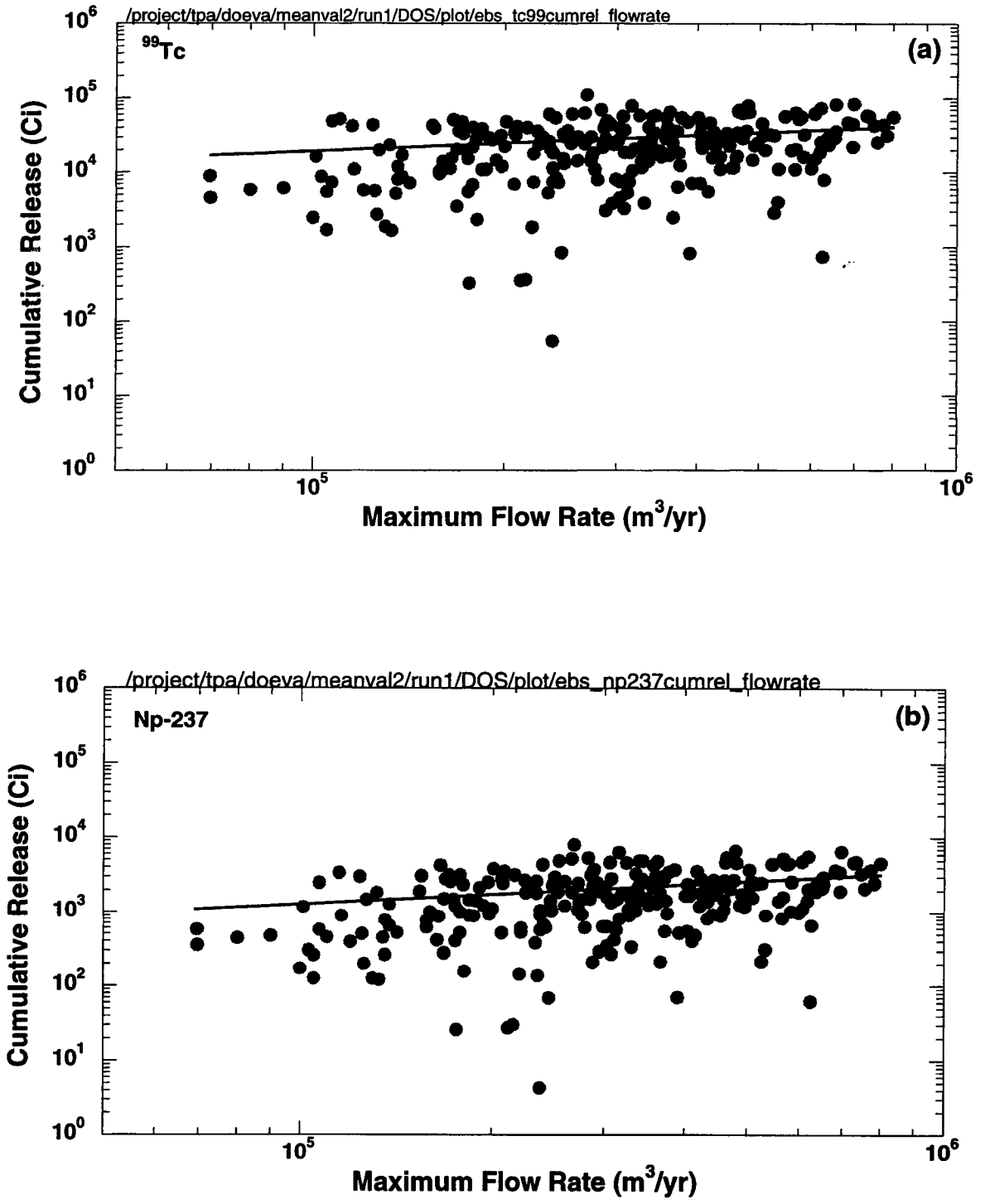

Figure 3-22. Cumulative release rates of ^{99}Tc and ^{237}Np from the engineered barrier system plotted with the maximum flow rate of water into the repository for 250 realizations

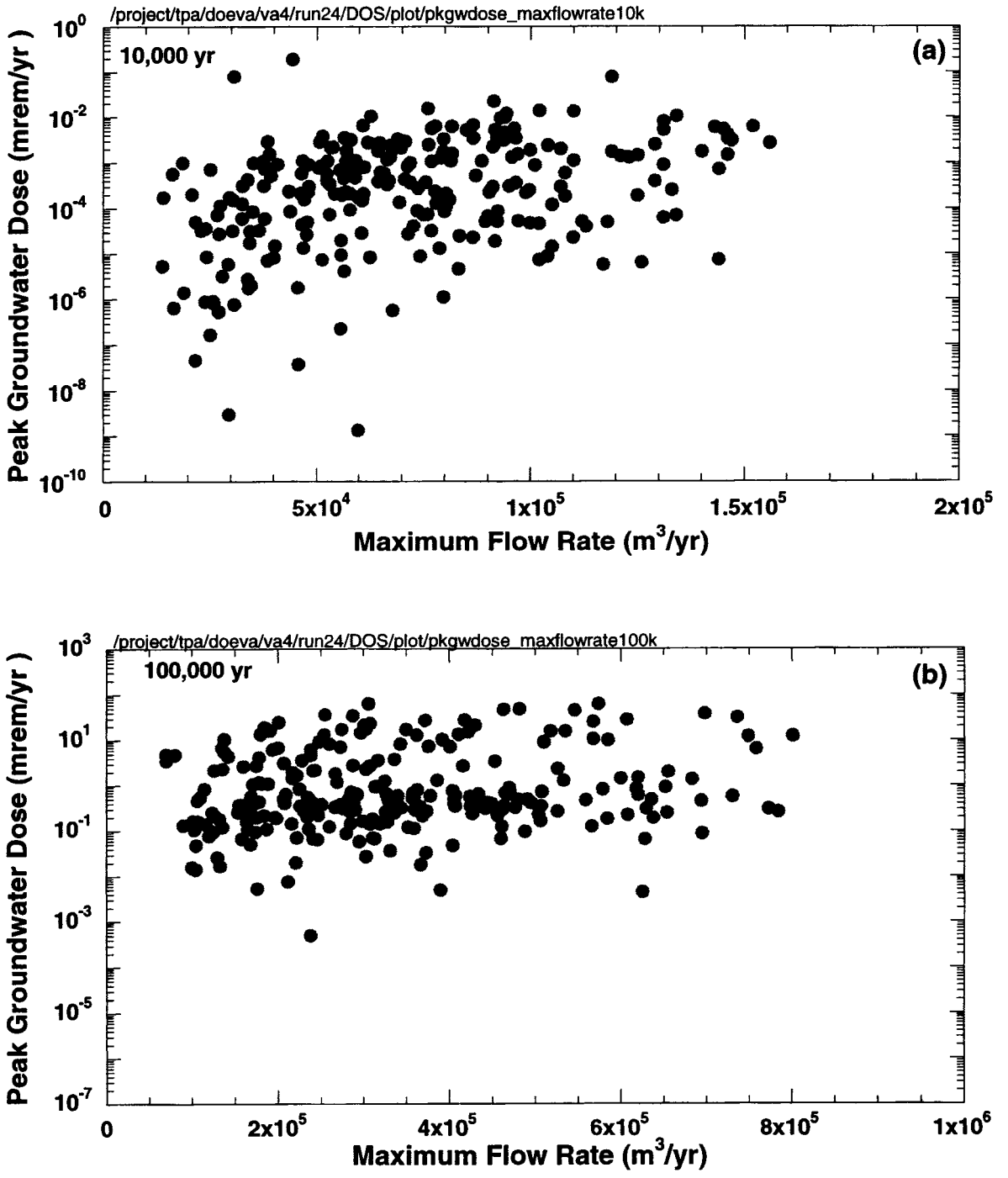

Figure 3-23. Peak groundwater dose in (a) 10,000 and (b) 100,000 yr plotted with the maximum flow rate of water into the repository for 250 realizations

3.3.2 Near-Field Environment

The time history of average WP temperature is provided in figure 3-24(a) for each subarea. The subarea variability in the WP temperature from 10,000 and 100,000 yr is small compared to the difference in temperatures exhibited over about 100–10,000 yr with a maximum difference in average WP temperature about 10 °C at 1,000 yr. In the 100–10,000-yr TPI, the greatest amount of heat is generated from the radioactive decay of SF.

Figure 3-24(b) shows the average, minimum, and maximum WP temperatures for subarea 1. The range between the minimum and maximum temperatures is about 10 °C at 100–1,000 yr. Subareas 2–7 exhibit the same general variability in the average, minimum, and maximum WP temperatures as subarea 1. Inasmuch as the variation from the average temperature among the subareas is less than five percent in figure 3-24, the parameters sampled in the basecase data set do not have a large influence on the range of computed WP temperatures. This small difference could affect corrosion calculations because the corrosion rate is sensitive to the WP temperature.

3.3.3 Waste Package Degradation

In the basecase data set, the outer and inner overpack materials for the WP are specified as carbon steel and Alloy C-22, respectively, consistent with the DOE TSPA-VA design (U.S. Department of Energy, 1998). Figure 3-25 presents results from all realizations and the expected failure curve of WPs failed by corrosion for the probabilistic case. The WP failure times by corrosion range from about 11,000 to 46,000 yr with an average corrosion failure time for 250 realizations of approximately 20,000 yr. There are no WPs failing from corrosion before 10,000 yr. It should be noted that effects of welds and closures, which could substantially decrease WP failure time, have not been considered in this calculation.

The relationship between average WP failure time and both the peak groundwater dose and the time of the peak groundwater dose is presented in figure 3-26. The variability in the peak groundwater dose in figure 3-26(a) ranges over five orders of magnitude, while the average WP failure time is 11,000–46,000 yr. An overall trend of decreasing peak groundwater dose with increasing average WP failure time is observable in this figure. When the WP failure time is delayed, more of the SF inventory decays and the transport time through the UZ and SZ is delayed. Thus, the peak groundwater dose is generally expected to be lower for larger WP failure times.

The average WP failure time and time of peak groundwater dose are provided as a scatterplot in figure 3-26(b). In all instances, the peak groundwater dose occurs after the average WP failure time for 100,000-yr analyses. However, for approximately one-half the realizations, the peak groundwater dose occurs at times greater than 90,000 yr.

3.3.4 Waste Package Release

Water transports radionuclides out of the WP and into the UZ and SZ to the receptor location. Thus, the flow rate of water in the UZ should be positively correlated with the release from the EBS. The relationships between the flow of water into the WP and the release of ^{99}Tc and ^{237}Np are illustrated in figure 3-22. Furthermore, higher release rates contribute to greater peak groundwater doses as shown in figure 3-27 for ^{99}Tc and ^{237}Np in subarea 1. The subarea 1 release rates presented in these figures are representative of release rates from subareas 2 through 7. The ^{99}Tc and ^{237}Np peak release rates and time of

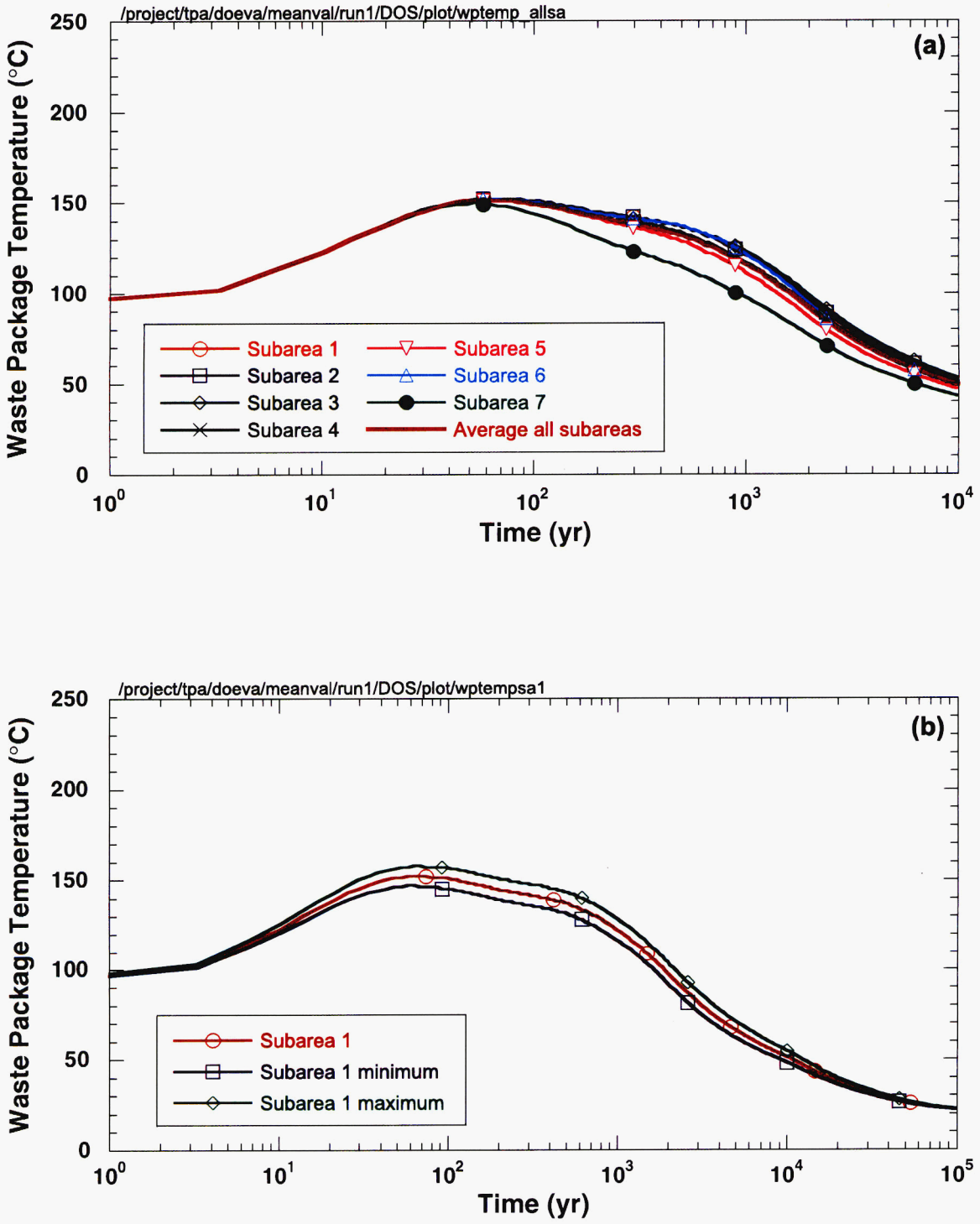

Figure 3-24. Waste package surface temperature (a) averaged over the repository and for each subarea and (b) in subarea 1, the average, minimum, and maximum values for 250 realizations

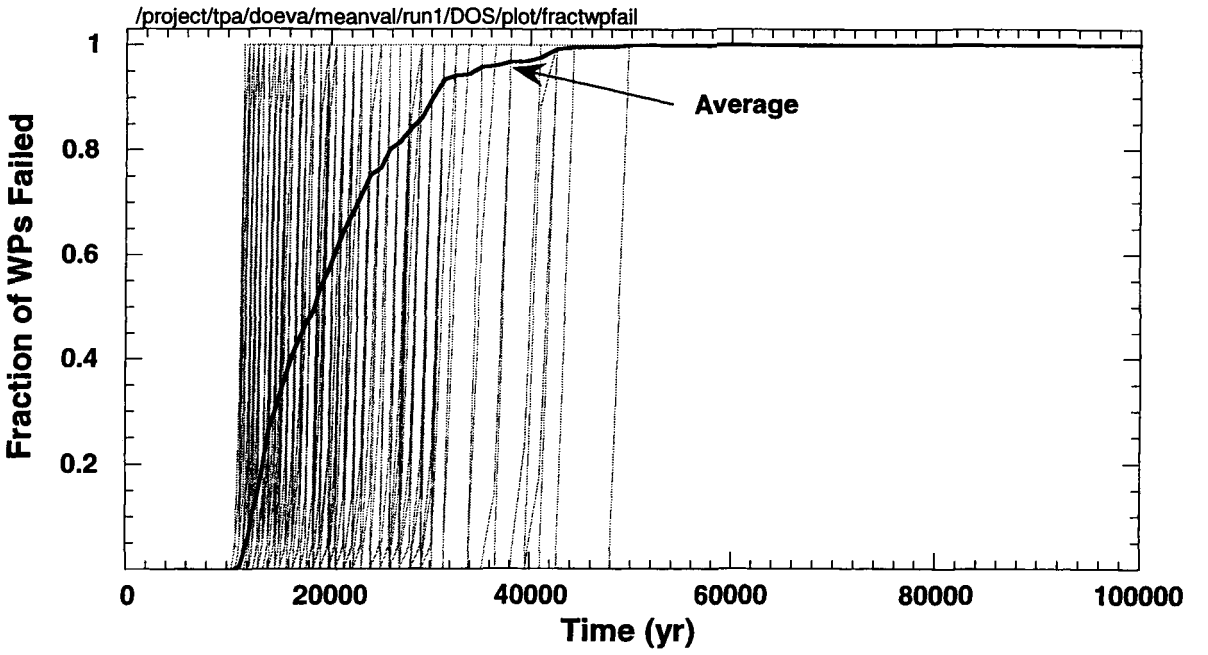

Figure 3-25. Fraction of waste packages failed by corrosion for each of the 250 realizations and the average fraction of failed waste packages

the peak release rates are presented in figure 3-28. This figure shows nearly all the ^{99}Tc and ^{237}Np peak releases occur between 11,000 and 46,000 yr when WPs fail by corrosion. The variability in the peak release rates is slightly less than that for the groundwater dose. The peak release rates of ^{99}Tc and ^{237}Np vary over three to four orders of magnitude, whereas the peak groundwater dose exhibits over five orders of magnitude variability. Factors that influence the radionuclide transport from the EBS to the receptor location, such as well pumping rate and retardation, cause a greater variability in the groundwater dose than the release rate from the EBS.

Figure 3-29 provides the release rate of ^{99}Tc from subarea 1 for 10,000 and 100,000 yr. The results in this figure demonstrate that the variability in the EBS release rates is greater in the first 10,000 yr than in the period between 10,000 and 100,000 yr. It appears that the variability can be attributed to factors such as lower flow rates at times less than 10,000 yr, initially defective failures, and time to fill up the WP. Releases prior to 10,000 yr are from initially defective and seismic failures, while the peak releases observed after 10,000 yr result mainly from corrosion failures. The magnitude of the releases extends over four to five orders of magnitude and arises partly from the variability in the flow rate into the EBS.

The cumulative release of radionuclides from the EBS is plotted in figure 3-30 along with the initial inventory and the UZ and SZ releases. This graph reveals that more radionuclides are released relatively early, with most of the releases occurring during the first 50,000 yr. Radionuclides with a combination of the higher solubility, half-life, and initial inventory, such as ^{99}Tc, exhibit the largest release rates. Source depletion and radioactive decay result in lower releases toward the end of the 100,000-yr TPI.

3.3.5 Unsaturated Zone Transport

Figure 3-31 presents ^{99}Tc, ^{237}Np, and ^{239}Pu average release rates for the basecase data set. In the first 10,000 yr, releases are from initial WP failures. The failure of WPs from corrosion begins after 10,000 yr and

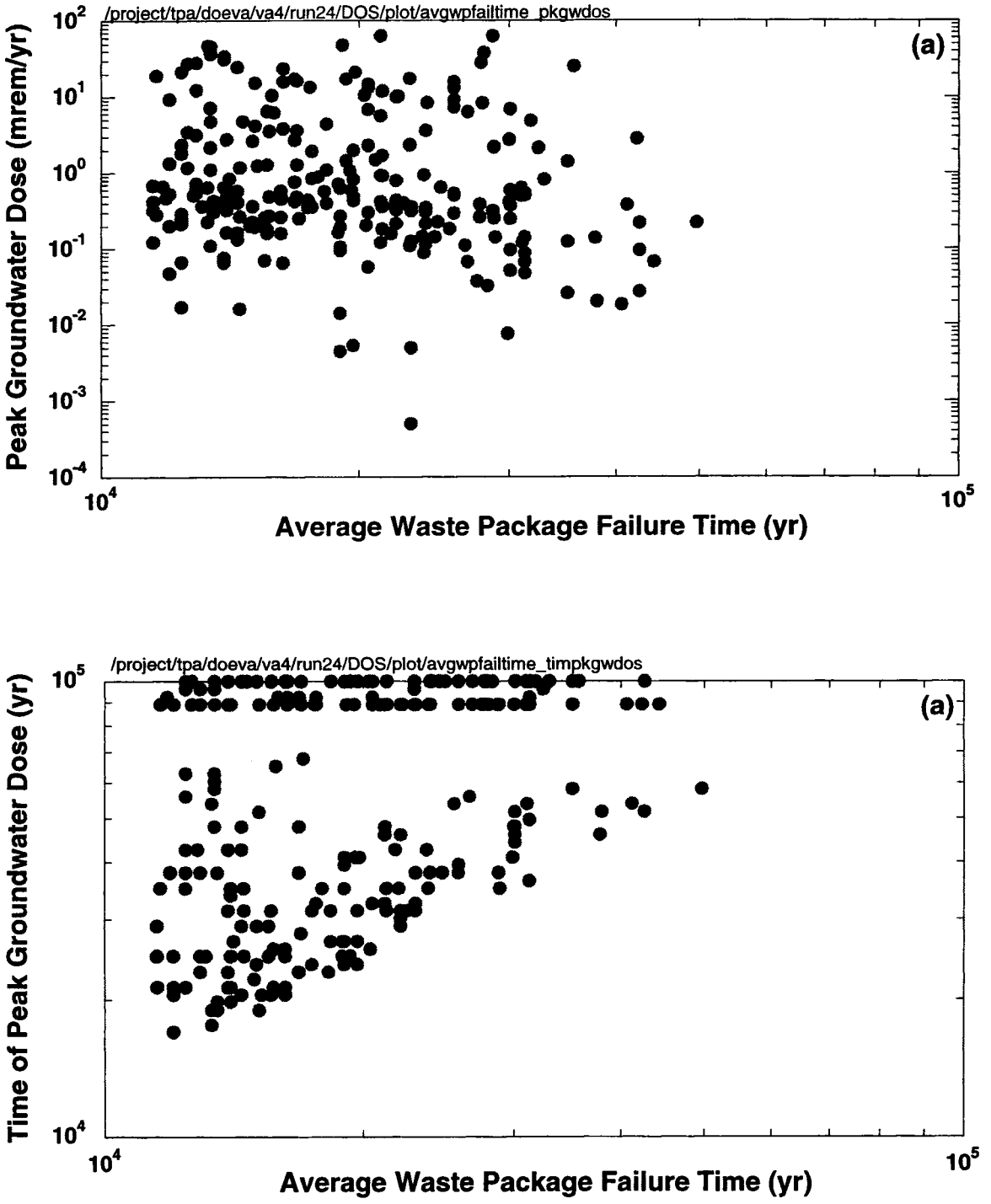

Figure 3-26. Average waste package failure time by corrosion plotted with (a) peak groundwater dose and (b) time of the peak groundwater dose for 250 realizations

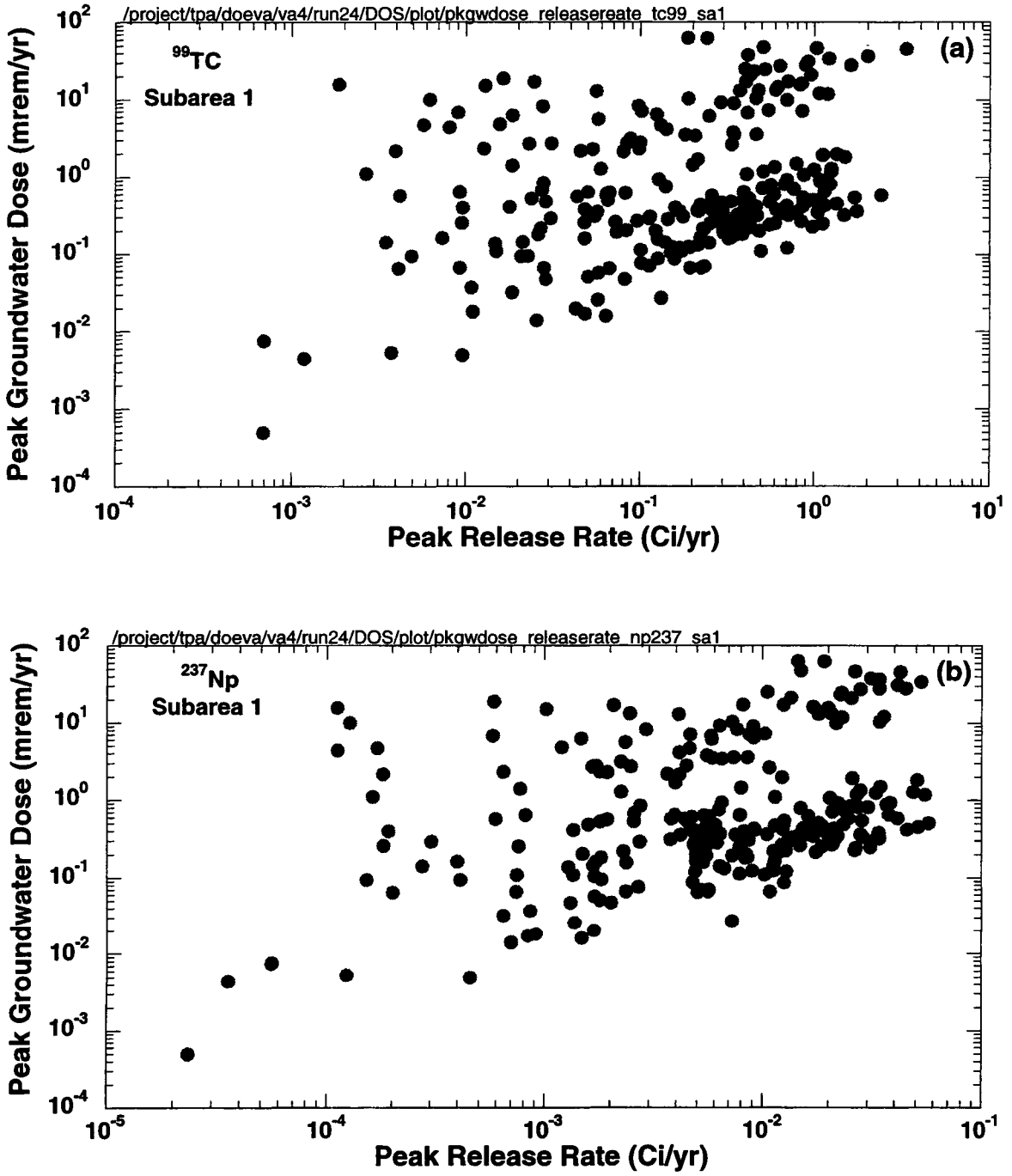

Figure 3-27. Peak groundwater dose and the (a) ^{99}Tc and (b) ^{237}Np peak release rates from subarea 1 for 250 realizations

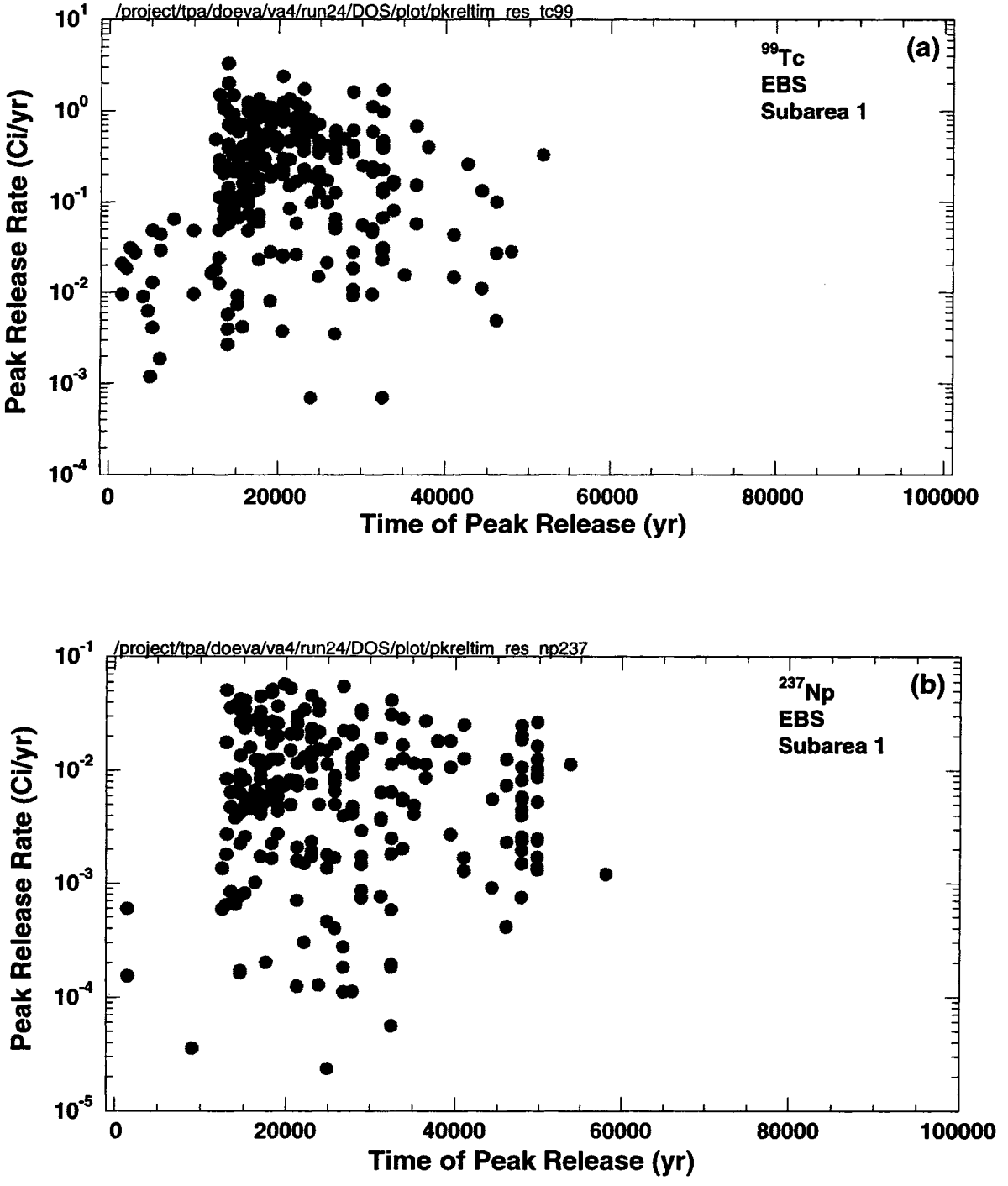

Figure 3-28. Peak release rates from the engineered barrier system and time of the peak release for (a) ^{99}Tc and (b) ^{237}Np in 250 realizations

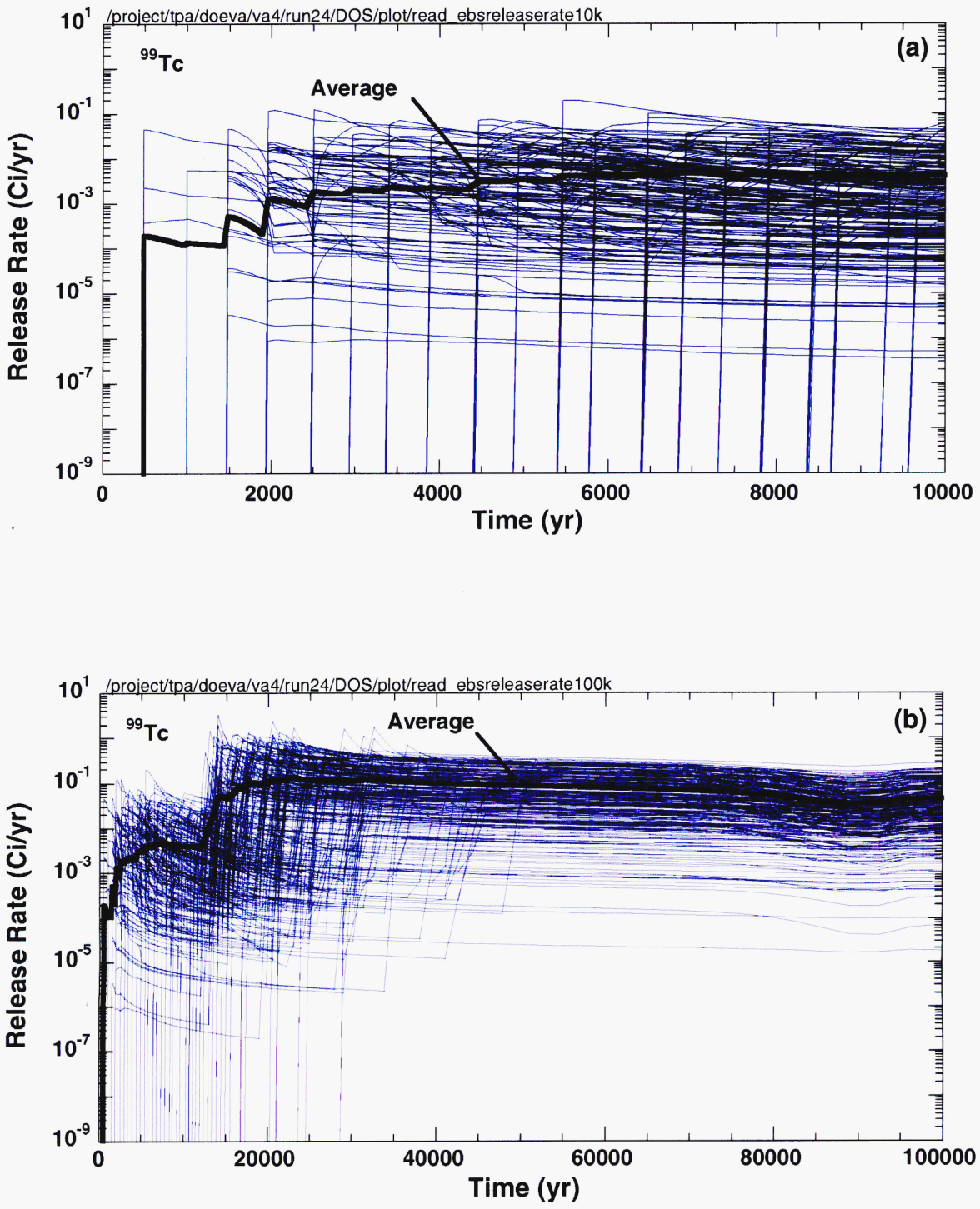

Figure 3-29. ^{99}Tc release rates from the engineered barrier system over (a) 10,000 and (b) 100,000 yr, including the average release rate, in subarea 1 for 250 realizations

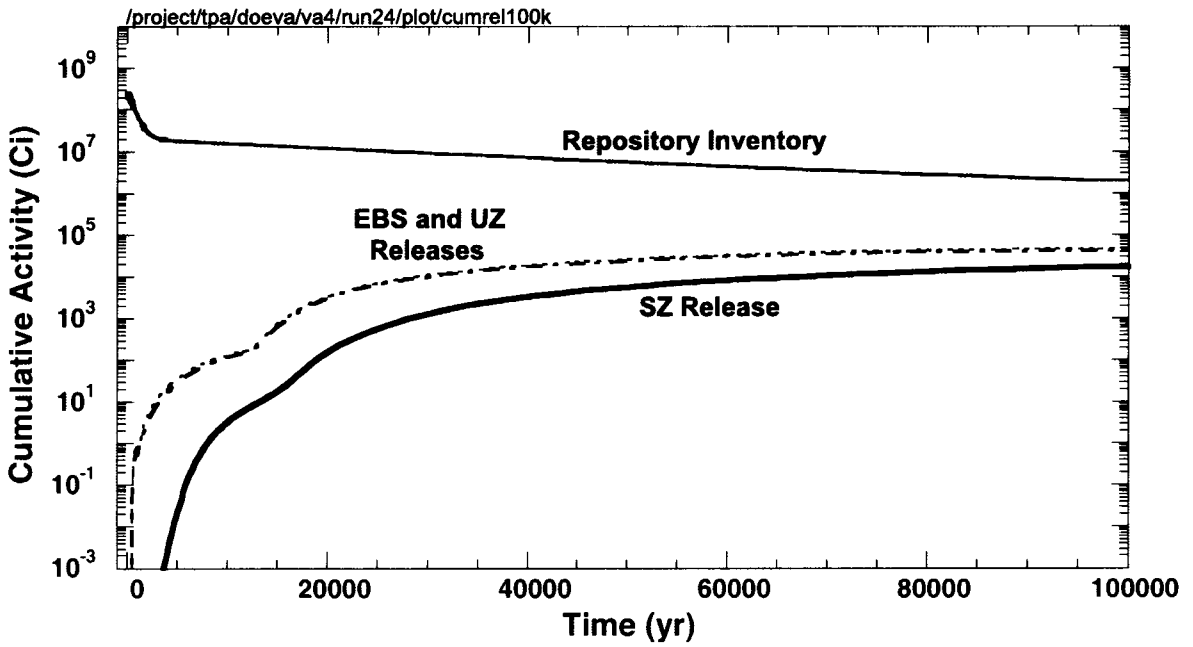

Figure 3-30. Cumulative releases from the engineered barrier system, and the unsaturated and saturated zones, together with the initial inventory in the repository

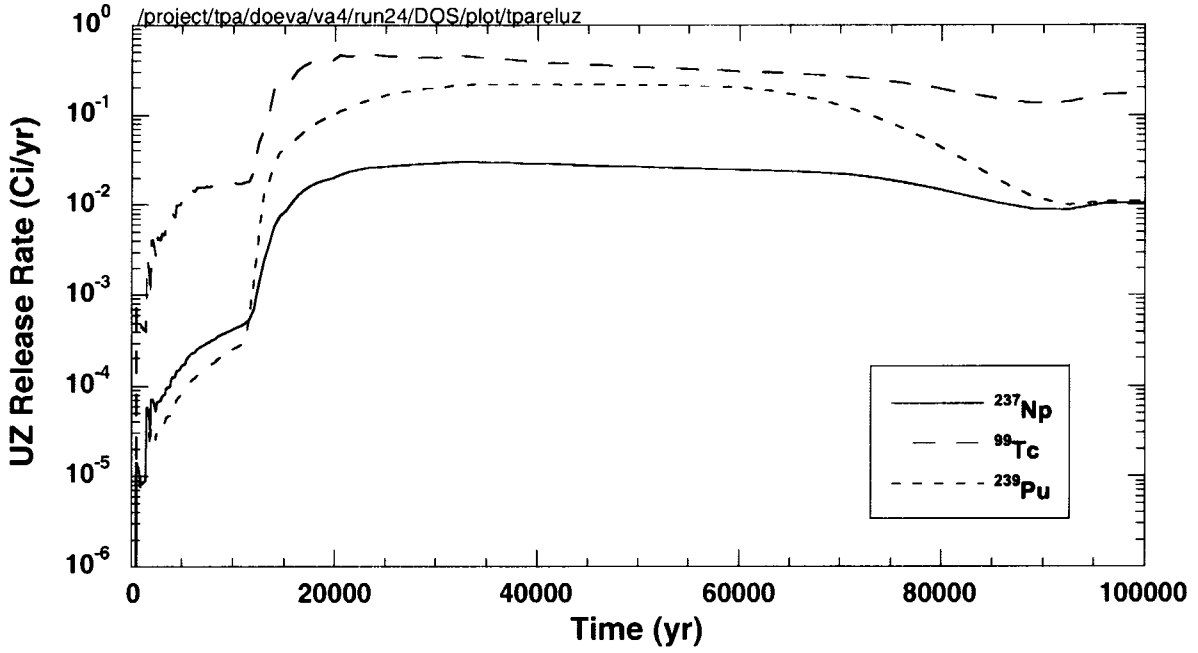

Figure 3-31. Unsaturated zone average release rates of ^{99}Tc, ^{237}Np, and ^{239}Pu for 250 realizations

an increase in the release rates is evident in figure 3-31 from 10,000 to 20,000 yr with the peak average release rate for 250 realizations occurring at approximately 20,000 yr.

The results in figure 3-30 indicate that the UZ releases are only slightly less than the EBS releases and suggest that the effects of the hydrostratigraphic units beneath the repository on the radionuclide release rates are not significant.

Figure 3-32 provides the ^{99}Tc release rate from the UZ for subarea 1 from 10,000 and 100,000 yr. When compared to the EBS release rates in figure 3-29, these results demonstrate that the movement of ^{99}Tc through the UZ is not significantly different. As with the EBS, releases from the UZ prior to 10,000 yr are from initially defective and seismic failures, while the peak releases observed after 10,000 yr result mainly from corrosion failures. The magnitude of the releases extends over four to five orders of magnitude and arises partly from the variability in the flow rate into the EBS.

The conclusion that the UZ has a small effect on the EBS release rates is further supported by the results for the relatively short UZ GWTTs shown in figure 3-33. The average UZ travel time is about 530 yr with a range 200–1,200 yr, which is small compared to the 10,000- and 100,000-yr TPIs. Differences in the travel times arise from distributions specified in the basecase data set for the porosities of the hydrostratigraphic units below the repository and for the climate conditions used to determine the UZ flow rates.

3.3.6 Saturated Zone Flow and Transport

Release rates from the SZ are presented in figure 3-34 for ^{99}Tc, ^{237}Np, and ^{239}Pu. The ^{99}Tc, ^{237}Np, and ^{239}Pu UZ and SZ release rates can be significantly different because of the flow path length and retardation in the SZ alluvium. The path length thickness in the SZ alluvium ranges from 8,000 to 12,000 m, while the UZ path length is about 300 m. Saturated zone retardation occurs in the alluvium. For UZ retardation to occur, flow needs to be in the matrix. Because UZ flow is mainly in fractures, UZ retardation has little effect on delaying radionuclide transport. Additionally, the average retardation factors for Tc, Np, and Pu are 1, 9, and 10,000 in the UZ matrix; and 5, 62, and 13,000 in the SZ alluvium, respectively. Consequently, the longer flow path combined with greater retardation have a larger effect on the SZ release rates than on the UZ release rates. These effects are apparent in the UZ and SZ release rates plotted in figures 3-31 and 3-34. Compared to the releases from the UZ, ^{99}Tc and ^{237}Np releases are smaller from the SZ and, because of a larger retardation factor, there is no Pu released from the SZ in 100,000 yr.

The affect of retardation and the flow path length on the ^{99}Tc SZ release rates for subarea 1 from 10,000 and 100,000 yr is evident when comparing figure 3-35 with the UZ release rates in figure 3-32. Higher retardation factors increase the SZ travel time and shift the release rate to the right (i.e., later time).

The average repository GWTT in the SZ is approximately 3,680 yr compared to about 500 yr for the UZ (see figure 3-33). For each subarea, the minimum travel times vary from 2,130 to 4,730 yr, whereas the maximum travel times range 3,320 to 7,240 yr. Table 3-12 provides a summary of the average, minimum, and maximum SZ GWTTs for the repository and for each subarea. The average for each subarea is obtained using equal weighting of GWTTs from each realization. Similarly, the repository average for all subareas is the mean of subarea averages.

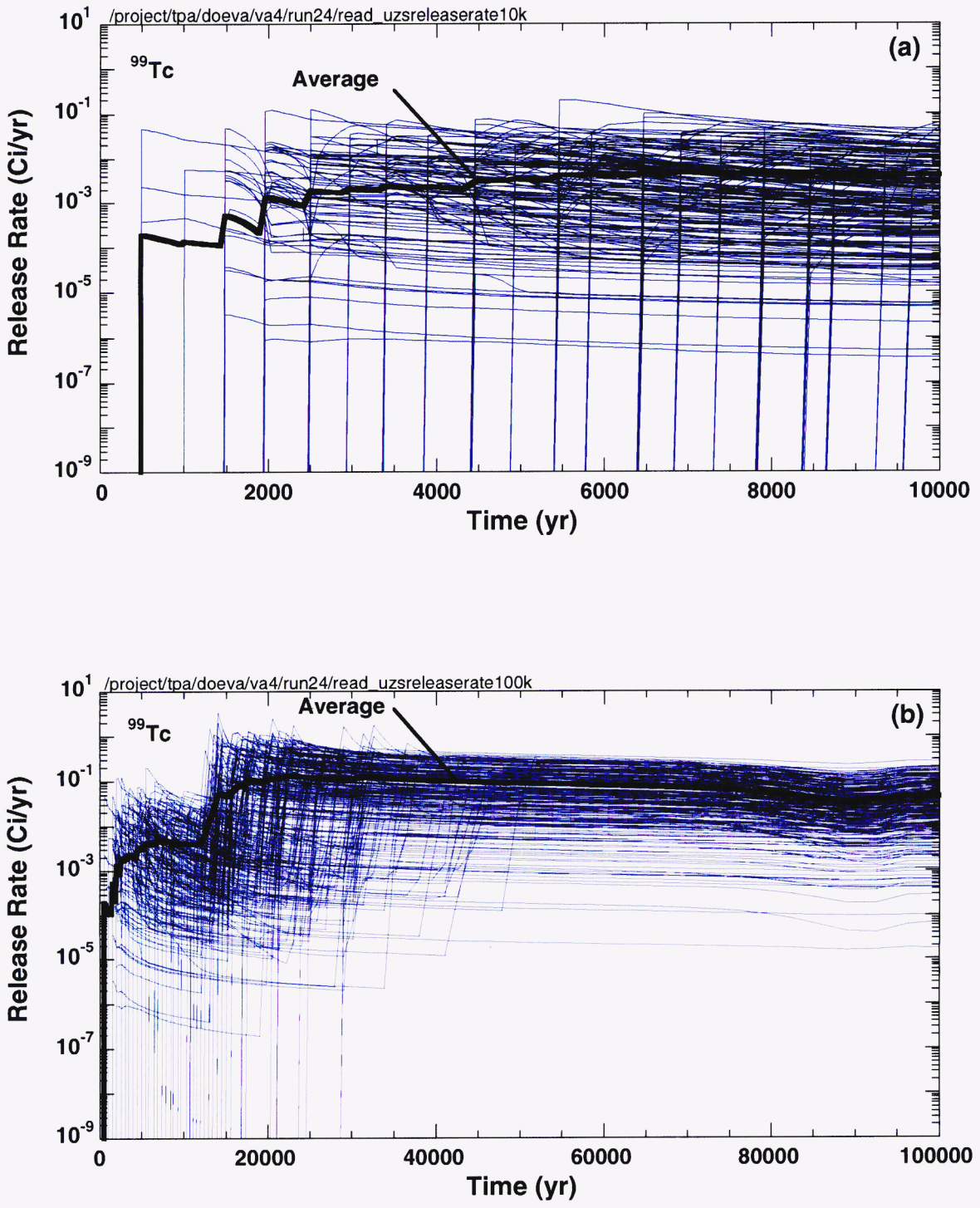

Figure 3-32. Unsaturated zone release rates of ^{99}Tc over (a) 10,000 and (b) 100,000 yr, including the average release rate, in subarea 1 for 250 realizations

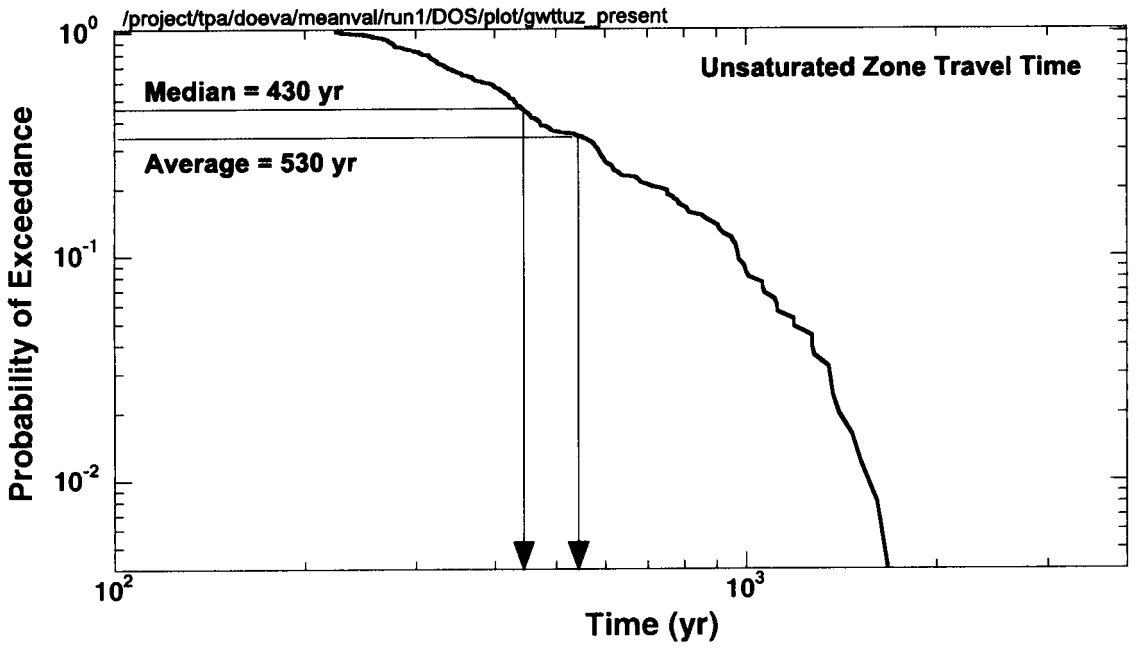

Figure 3-33. Complementary cumulative distribution function of unsaturated zone groundwater travel times for 250 realizations

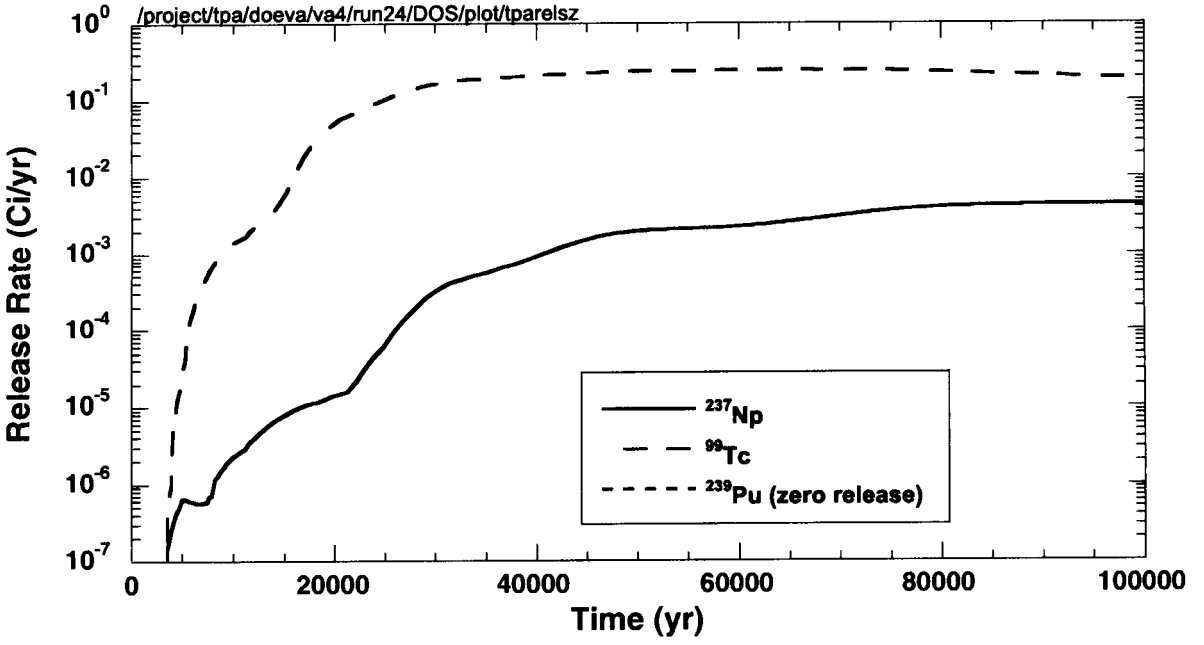

Figure 3-34. Saturated zone average release rates of ^{99}Tc, ^{237}Np, and ^{239}Pu for 250 realizations

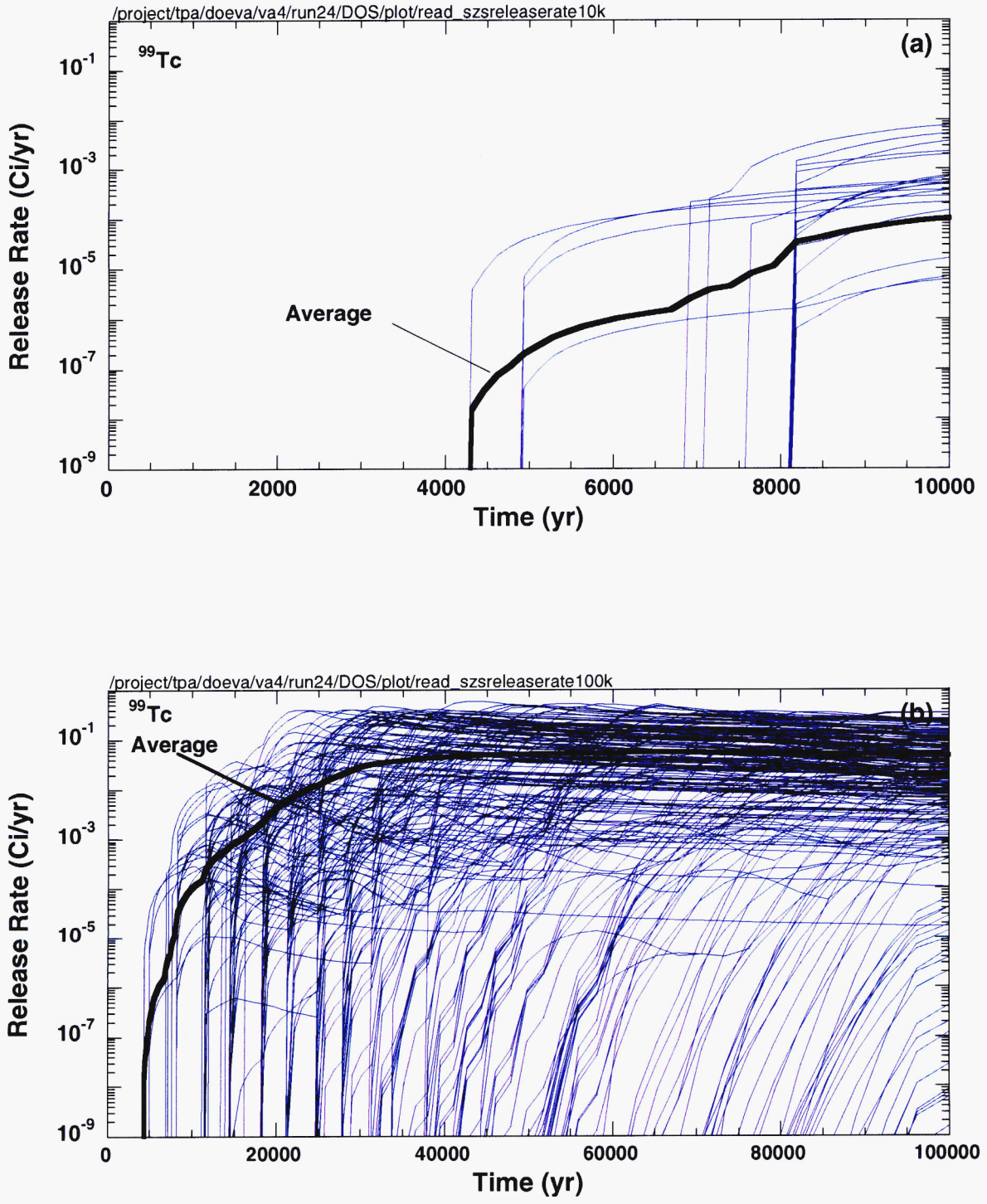

Figure 3-35. Saturated zone release rates of ^{99}Tc over (a) 10,000 and (b) 100,000 yr, including the average release rate, in subarea 1 for 250 realizations

Table 3-12. Average, maximum, and minimum saturated zone groundwater travel times by subarea and average for all subareas from 250 realizations

	Saturated Zone Travel Time (yr)		
Subarea	Minimum	Maximum	Average
1	4,730	7,240	5,990
2	4,730	7,240	5,980
3	2,130	3,330	2,730
4	2,130	3,320	2,720
5	2,180	3,380	2,720
6	2,180	3,380	2,780
7	2,180	3,370	2,770
Average (all subareas)	2,890	4,460	3,680

The variability in the SZ travel times is approximately the same order of magnitude as for the UZ. The repository averaged SZ GWTTs range from about 2,700 to 6,000 yr; for the UZ, GWTTs vary from 200 to 1,200 yr. A CCDF of the SZ GWTTs for all 250 realizations is presented in figure 3-36. For comparison, a CCDF of the UZ travel times can be found in figure 3-33.

3.4 COMPARISON OF DOSES FROM MEAN VALUE DATA SET AND MULTIPLE-REALIZATION CASES

To illustrate the difference between results from a mean value data set and results from multiple realizations, the peak expected dose is computed as a function of time from the multiple realizations. The peak dose from the mean-value data set is 0.002 mrem/yr, whereas the peak expected dose from the multiple-realization case is 0.003 mrem/yr for the 10,000-yr TPI. For the 100,000-yr TPI, the peak dose from the mean value data set is 0.3 mrem/yr compared to 4 mrem/yr peak expected dose for the multiple-realization case. For comparison purposes, the primary nuclides contributing to peak dose are presented in table 3-13.

The major contributors to the peak dose from table 3-13 in the mean value data set for 10,000 yr are ^{129}I and ^{36}Cl; for the multiple-realization case they are ^{237}Np, ^{129}I, ^{99}Tc, and ^{234}U. For the 100,000-yr TPI, the major contributors to the peak dose in the mean value data set are ^{99}Tc, ^{129}I, and ^{79}Se compared to ^{237}Np, ^{234}U, and ^{99}Tc for the multiple realization case. Thus, some radionuclides that are major contributors to peak dose could not be accounted for by the use of the mean value data set. This clearly indicates the inadequacy of the analysis using the mean value data set. However, as indicated before, the mean value data set provides a convenient means for observing deterministic trends in the intermediate outputs.

The variability in dose within realizations is shown in figure 3-20 for 10,000 and 100,000 yr, together with the average dose. The minimum and maximum peak doses vary over five orders of magnitude from about 4×10^{-7} to 0.3 mrem/yr for 10,000 yr and 2×10^{-4} to 50 mrem/yr for 100,000 yr. The doses occurring before 10,000 yr are from initially defective and seismic failures of WPs. From 11,000 to 46,000 yr, corrosion failures occur and contribute to increased dose. At about 85,000 yr, a slight increase in dose is observed, attributable to the arrival of ^{237}Np and switching from DCFs associated with the pluvial climate to a present-day climate.

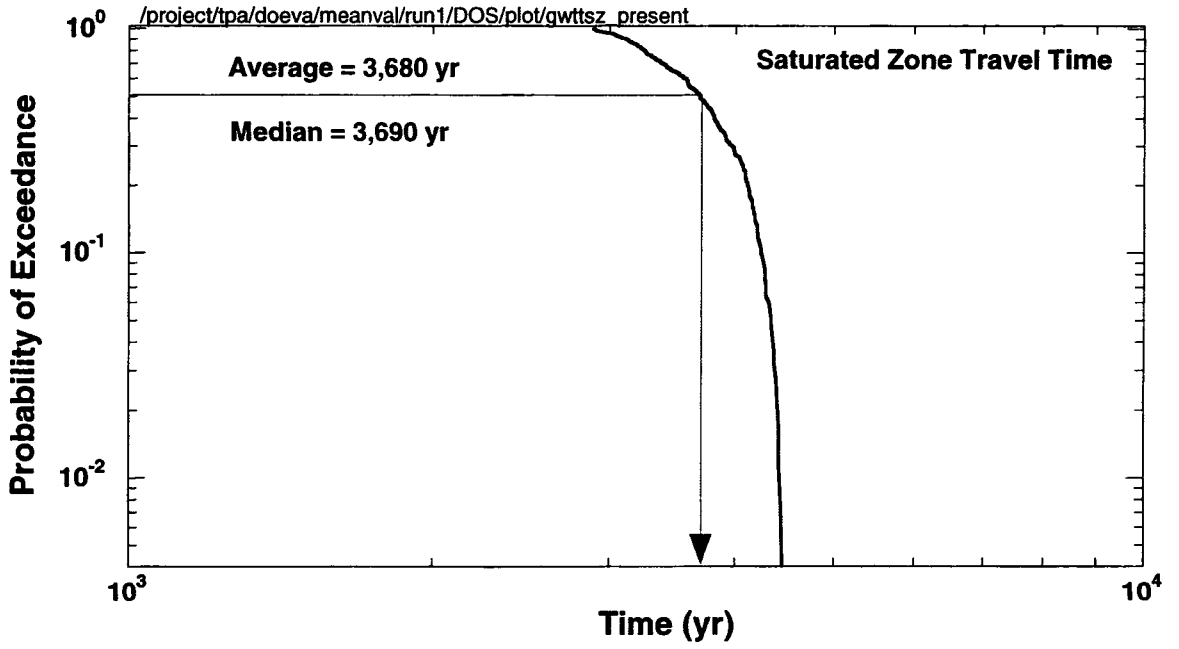

Figure 3-36. Complementary cumulative distribution function of unsaturated zone groundwater travel times for 250 realizations

Table 3-13. Primary nuclides contributing to peak expected dose

	10,000 yr		100,000 yr	
Radionuclide	**Mean Value Data Set**	**Multiple Realization Data Set**	**Mean Value Data Set**	**Multiple Realization Data Set**
^{237}Np	0	0.389	0	0.924
^{129}I	0.95	0.349	0.38	0.015
^{99}Tc	0.0002	0.138	0.59	0.022
^{234}U	0	0.1	0	0.035
^{36}Cl	0.05	0.014	0.004	0
^{79}Se	0	0.010	0.03	0

Figure 3-37 shows the variation in peak dose and the arrival time of the peak dose at the pumping well for ^{99}Tc and ^{237}Np. For more than one-half the realizations, the ^{99}Tc peak dose does not arrive until after 90,000 yr, while the ^{237}Np peak dose does not occur for most realizations until the end of the 100,000-yr TPI. The difference in results arises because ^{99}Tc retardation factors are less than those for ^{237}Np. Although the peak dose is not captured in all realizations, a maximum simulation time of 100,000 yr is long enough to evaluate the peak dose for the 10,000-yr TPI and a significant time period thereafter.

The groundwater dose expressed as a percent of total dose for the radionuclides ^{245}Cm, ^{241}Am, ^{237}Np, ^{239}Pu, ^{234}U, ^{230}Th, ^{129}I, ^{99}Tc, ^{14}C, ^{79}Se, and ^{36}Cl is illustrated in figure 3-38 for all 250 realizations. The radionuclides ^{237}Np, ^{234}U, ^{230}Th, ^{129}I, ^{99}Tc, ^{79}Se, and ^{36}Cl contribute at least 1 percent to the groundwater dose for any single realization. The radionuclides with the greatest consistency in contributing to peak dose in all realizations are ^{237}Np, followed by ^{129}I and ^{99}Tc. The results plotted in figure 3-39 of the expected dose for each nuclide show similar behavior over the 10,000- and 100,000-yr TPI as does figure 3-38 with the same nuclides having the largest contribution to the groundwater dose.

The volume of well water pumped, which is used as the dilution volume for the 20-km receptor group location, is assigned a uniform distribution ranging from 6.2×10^6 to 1.8×10^7 m^3/yr. Figure 3-40 illustrates the relationship between the peak groundwater dose to the receptor in 100,000 yr and the dilution volume for 250 realizations. The scatterplot reveals a slight trend of decreasing peak groundwater dose with dilution volume. The mass release rates from the SZ are converted into a groundwater dose by dividing the mass release rate by the dilution volume and multiplying by the DCF. Consequently, higher dilution volumes should be associated with lower groundwater dose.

3.5 ALTERNATIVE CONCEPTUAL MODELS

This section compares repository performance, as measured by dose, for the mean value data set with doses computed from mean values for alternative conceptual models described in section 2.3. The alternative models include different conceptualizations for fuel dissolution, fuel wetting, and transport. Only the general trends in the groundwater dose of the alternative models relative to the basecase are described in this section. Discussion of the sensitivity of TPA output to a conceptual model using multiple realizations is provided in section 4.4.

Sensitivity of repository performance to the basecase model abstractions was evaluated by performing TPA simulations using alternative conceptual models. Conceptual models can either be activated with flags in the TPA input file, or a conceptual model may be evaluated by modifying TPA input parameters. Both approaches are utilized in this section to specify a conceptual model and to analyze the influences of the conceptual model on groundwater dose. Conceptual models activated with flags in the TPA input file include the four dissolution rate models, the bathtub and flowthrough models, bypassing invert transport, and the particle and grain surface-area models. Parameter values in the TPA input file are modified to evaluate conceptual models for focused flow, matrix diffusion, no retardation, and cladding protection.

Figures 3-41 through 3-43 present groundwater dose in 10,000 and 100,000 yr for the basecase mean value data set together with groundwater doses from the TPA alternative conceptual models. For the conceptual models evaluated using the mean value data set, repository performance spans almost seven orders of magnitude for the 100,000-yr TPI and encompasses the basecase dose. The general trend in groundwater dose exhibited in figures 3-41 through 3-43 indicates a wide range in the sensitivity of groundwater dose to the conceptual model. The alternative models with the most deviation from the basecase dose are the no

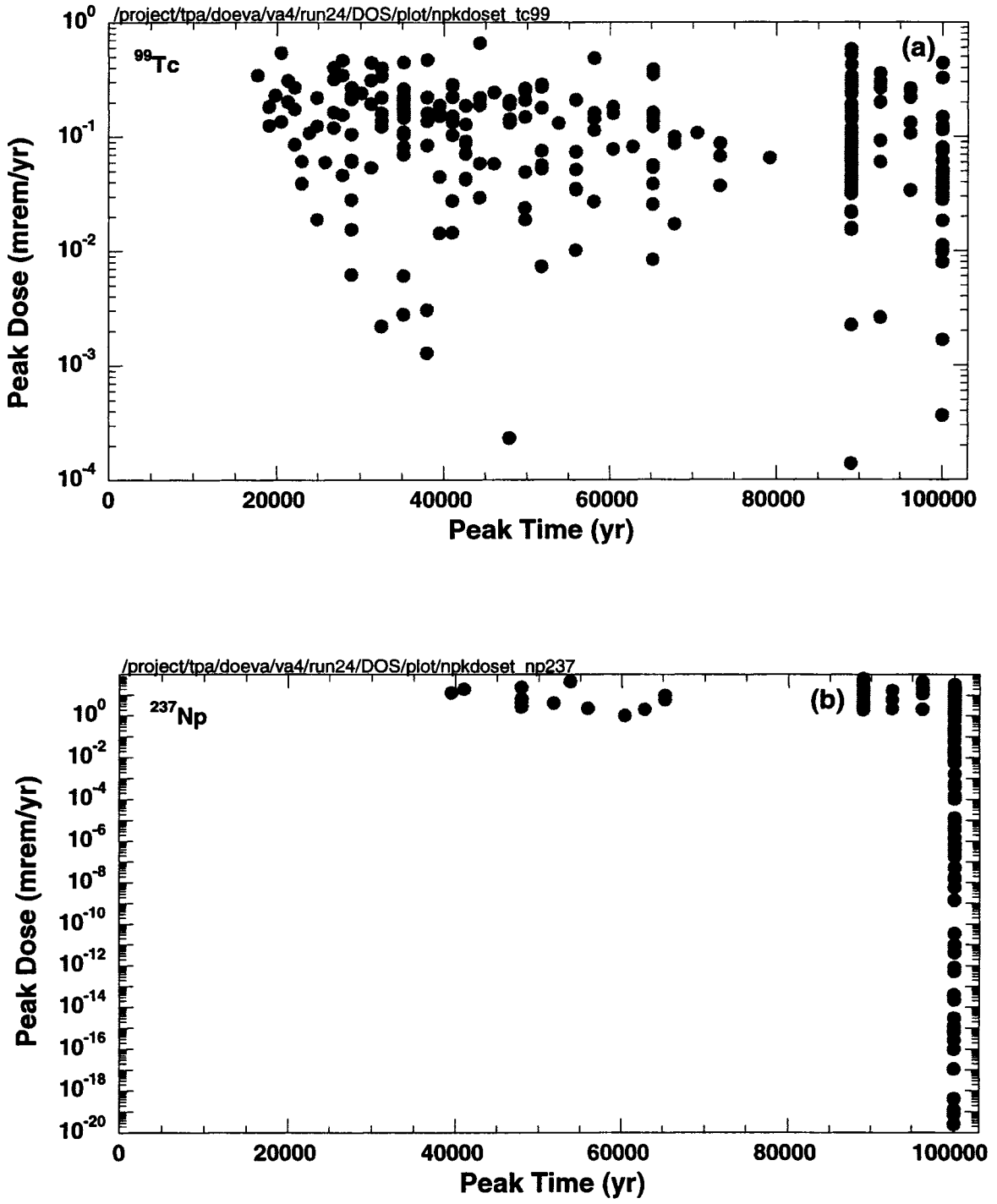

Figure 3-37. Peak groundwater dose of (a) ^{99}Tc and (b) ^{237}Np and time of the peak dose for 250 realizations

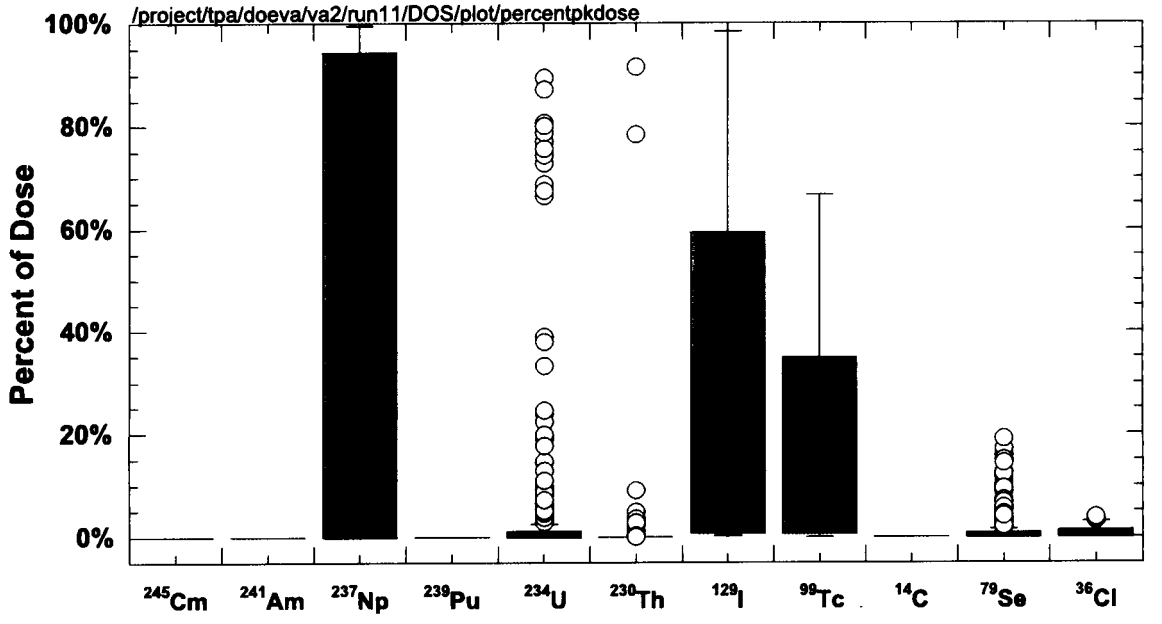

Figure 3-38. Percent each radionuclide contributes to the peak groundwater dose for 250 realizations

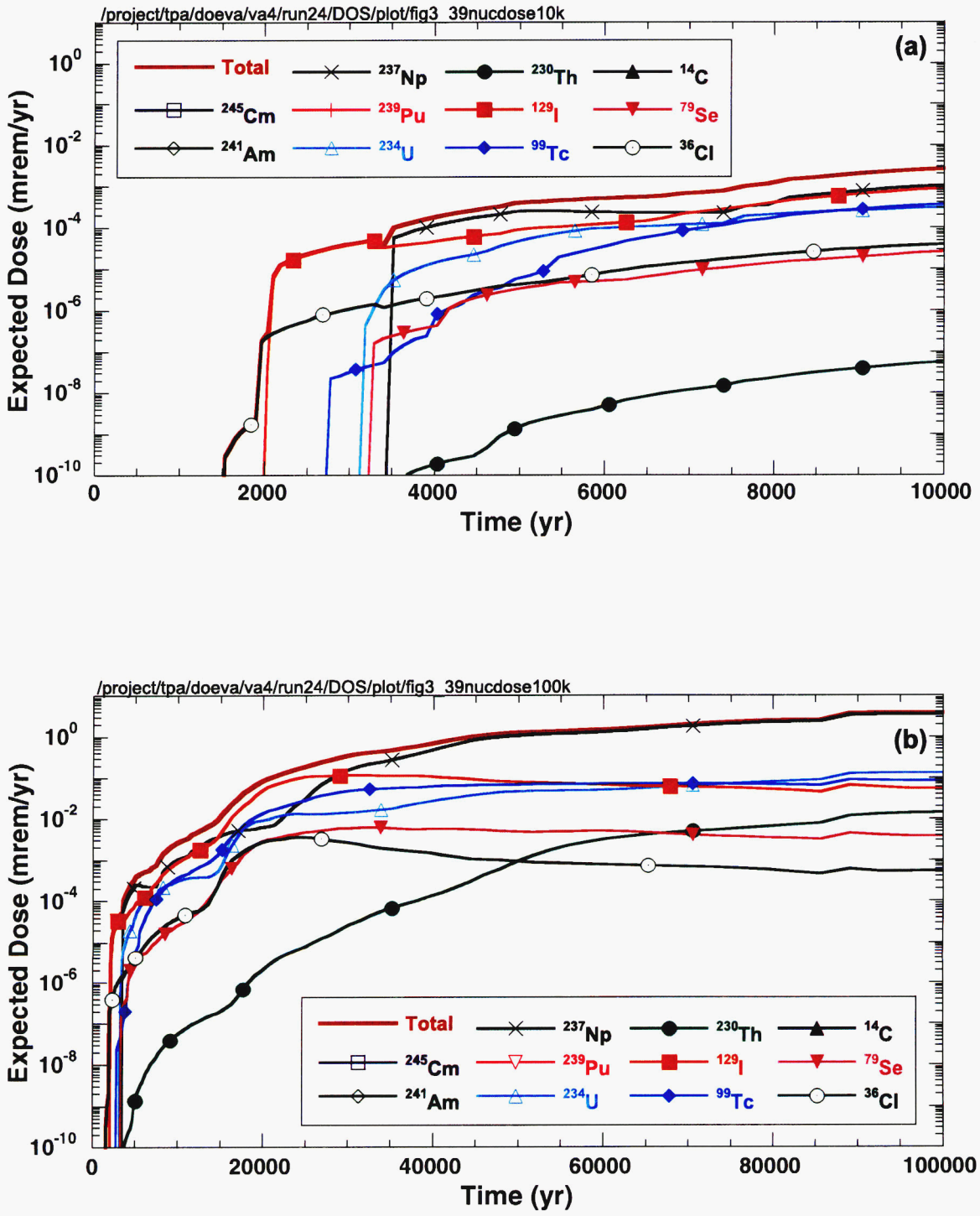

Figure 3-39. Average groundwater dose in (a) 10,000 and (b) 100,000 yr for each nuclide, including the total dose, for 250 realizations

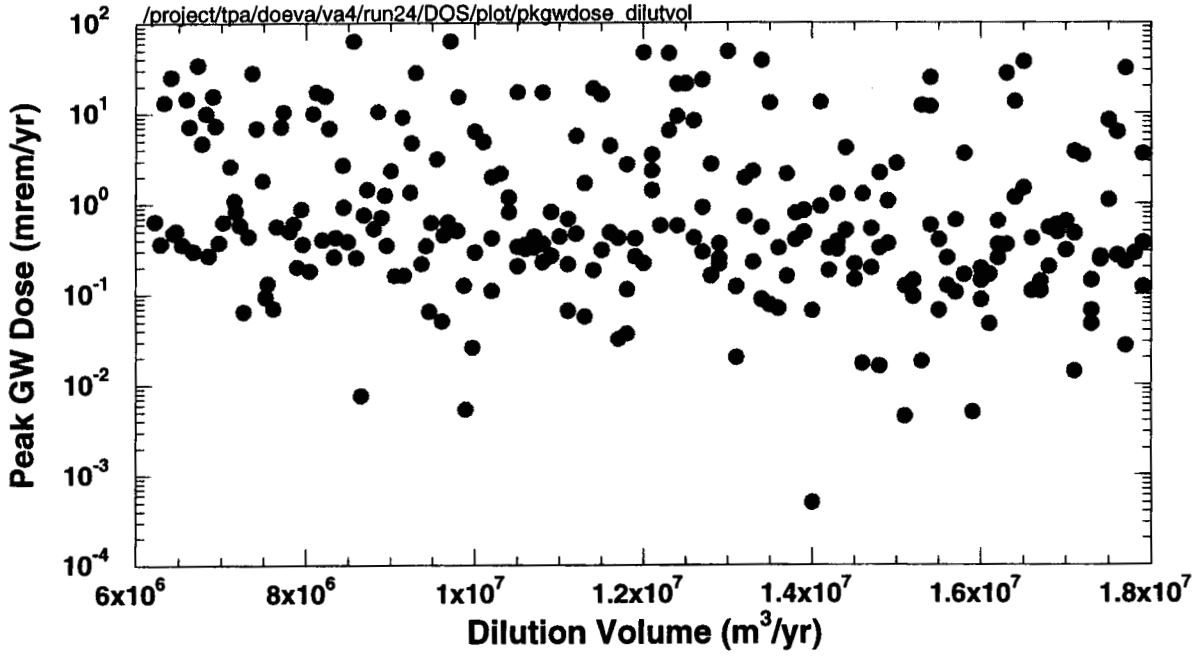

Figure 3-40. Peak groundwater dose and the volume of well water pumped for 250 realizations. The well water dilutes the plume of radionuclides traveling in the saturated zone.

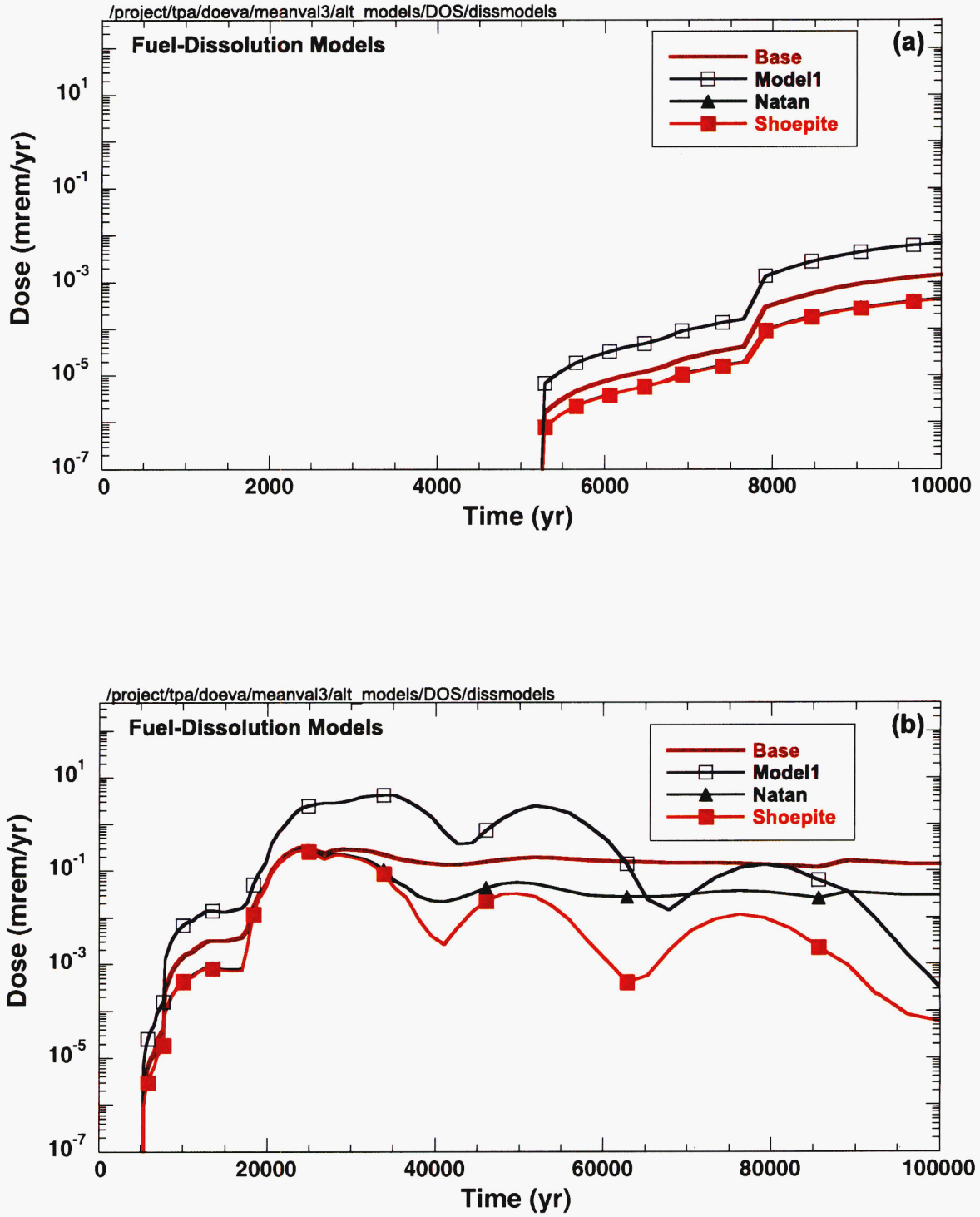

Figure 3-41. Groundwater dose from the basecase and the fuel-dissolution alternative conceptual models for (a) 10,000 and (b) 100,000 yr using the mean value data set

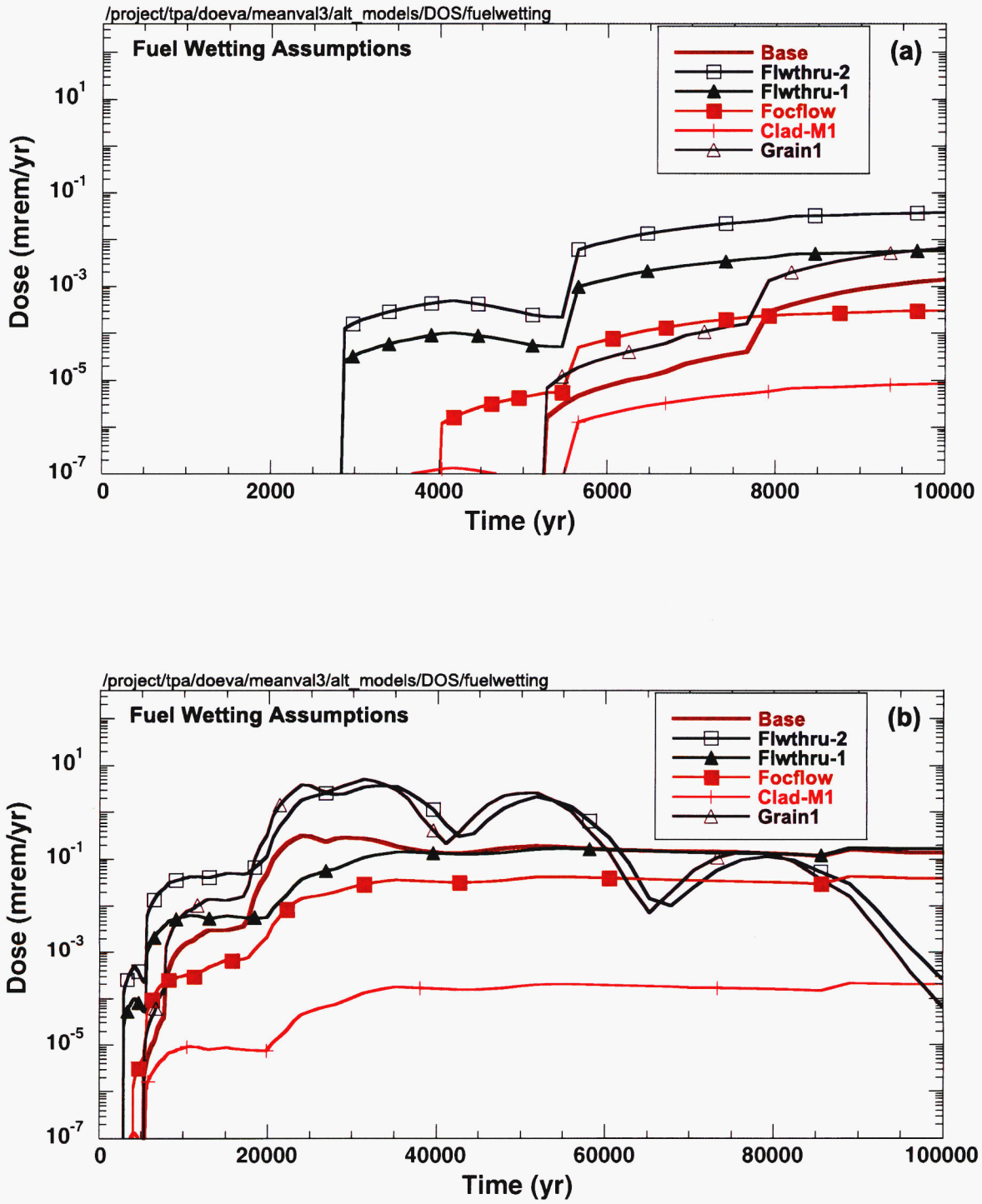

Figure 3-42. Groundwater dose from the basecase and the fuel wetting alternative conceptual models for (a) 10,000 and (b) 100,000 yr using the mean value data set

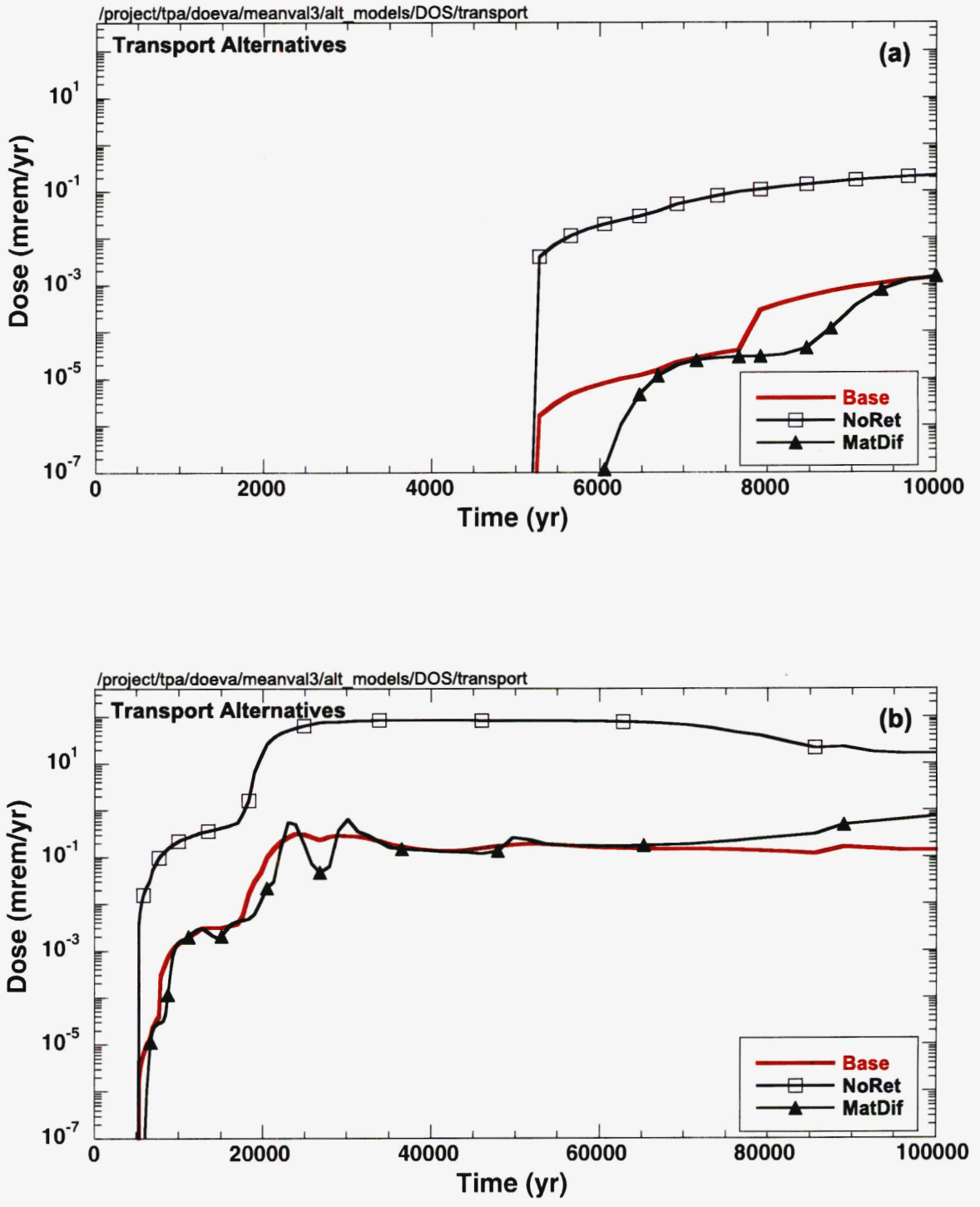

Figure 3-43. Groundwater dose from the basecase and the transport alternative conceptual models for (a) 10,000 and (b) 100,000 yr using the mean value data set

retardation case, which is more than two orders of magnitude greater than the basecase, and the Schoepite and Clad-M1 cases, which are three to four orders of magnitude less than the basecase dose through most of the 100,000-yr TPI. The following sections discuss the alternative conceptual models grouped by fuel dissolution, fuel wetting, and transport assumptions and compare the groundwater dose to the basecase groundwater dose computed with mean values. The TPA Version 3.2 code User's Guide (Mohanty and McCartin, 1998) presents a description of these models.

3.5.1 Fuel-Dissolution Models

Results from TPA simulations using three different fuel-dissolution models are evaluated by comparing the groundwater dose from each of the models with the basecase groundwater doses. The groundwater doses from the basecase and the fuel-dissolution, three-alternative conceptual models are presented in figure 3-41.

3.5.1.1 Fuel-Dissolution Model 1

The groundwater doses in figure 3-41 (labeled as Model1) indicate an earlier release and higher dose than the basecase dose from the beginning of the simulation through about 60,000 yr, while from about 60,000 to 100,000 yr, the basecase dose is greater than the dose computed with the first dissolution rate model. At the end of the 100,000-yr TPI, the dose from the first dissolution rate model is more than two orders of magnitude less than the basecase dose (Model 2 used). Dissolution Model 1 is characterized by a higher release rate resulting from faster dissolution compared to Model 2. But faster dissolution (congruent) results in faster source depletion from the WP for the dissolution-limited radionuclides. Consequently, the release rate for Model 1 becomes less than that for Model 2 at longer times. The dose for this conceptual model follows a sinusoidal pattern after 20,000 yr, attributable to variations in the transport of nuclides to the receptor location not only by nuclide but by subarea. This effect is not evident in the basecase dose, and further studies are underway to explain this behavior.

3.5.1.2 Fuel-Dissolution Model 3 (Natural Analog)

The groundwater doses in figure 3-41 (labeled as Natan), which is same as the results from the schoepite dissolution model, show a slightly later release with lower doses throughout the 100,000-yr TPI than the basecase dose, indicating a slower dissolution rate. Just as with the first dissolution rate model, which exhibits a release rate that peaks and drops quickly, the dose for this conceptual model follows a sinusoidal pattern after 20,000 yr, attributable to differences in the transport of nuclides to the receptor location not only by nuclide but by subarea. The variations in dose for this dissolution model are smaller compared to the first model but greater compared to Model 2. Further studies are under way to explain this behavior.

3.5.1.3 Fuel-Dissolution Model 4 (Schoepite Dissolution)

The groundwater doses in figure 3-41 (labeled as Schoepite) indicate a slightly later release with lower doses throughout the 100,000-yr TPI. Just as with the first and natural analog dissolution rate models, the dose for this conceptual model follows a similar sinusoidal pattern after 20,000 yr, attributable to differences in the transport of nuclides to the receptor location not only by nuclide but by subarea. However, the variations in dose are similar for this dissolution model and the first model, although the groundwater dose at 100,000 yr is more than three orders of magnitude less than the basecase dose. Justification for the trend in the curve is similar to that of the natural analog model. Further studies are under way to explain the trend.

3.5.2 Fuel Wetting Assumptions

The amount of water contacting a WP affects the EBS release rate and the time of the release. This section presents results that investigate the assumptions for fuel wetting with five alternative conceptual models. The groundwater doses computed using these models and the basecase results are provided in figure 3-42.

3.5.2.1 Flowthrough Model with Fuel-Dissolution Model 2

The groundwater doses in figure 3-42 (labeled as Flwthru-2) have an earlier release and higher dose than the basecase dose from the beginning of the simulation through about 20,000 yr. Earlier dose is expected because in the flowthrough model, release from the WP occurs instantaneously (i.e., no time to fill WP). From about 20,000 to 40,000 yr, the basecase dose is greater than the dose computed with this conceptual model. Beyond 40,000 yr, the groundwater doses are almost equal. One of the reasons these two doses are almost equal is that at high flow rates into the WP, the flowthrough model behaves like the bathtub model once the bathtub is full.

3.5.2.2 Flowthrough Model with Fuel-Dissolution Model 1

Groundwater doses in figure 3-42 (labeled as Flwthru-1) indicate an earlier release and higher dose from the beginning of the simulation through about 60,000 yr, while from about 60,000 to 100,000 yr, the basecase dose is greater than the dose computed with the flowthrough model. This behavior is consistent with the faster dissolution rate and source depletion associated with Model 1. At 100,000 yr, the basecase dose is about three orders of magnitude greater than the flowthrough model dose. The greatest difference between these plots is the behavior of the doses over time. The basecase dose exhibits a smoother behavior than the flowthrough model dose, which shows a sinusoidal pattern caused by the arrival of different nuclides and releases from different subareas at the receptor location.

3.5.2.3 Focused Flow

As presented in figure 3-42, the groundwater doses (labeled as Focflow) computed using a focused flow of water onto the WP are greater than the basecase dose before about 7,000 yr, indicating an earlier release. The groundwater doses are approximately one order of magnitude less than the basecase dose from about 7,000 to 100,000 yr. These results are consistent with solubility-limited releases associated with higher flows at earlier times and lower doses thereafter, attributable to fewer wet WPs.

3.5.2.4 Cladding Credit with Model 1

The groundwater doses in figure 3-42 (labeled as Clad-M1) calculated for this conceptual model are less than the groundwater doses for the basecase from about 5,000-yr to the end of the 100,000-yr TPI. Prior to 5,000 yr, the dose with cladding protection is greater than the basecase dose. During the 5,000–100,000-yr period, the general trends in the dose computed with cladding protection follow a sinusoidal pattern that is attributable to subarea and nuclide variability. The groundwater dose for this alternative conceptual model is about six orders of magnitude less than the basecase dose at 100,000 yr.

3.5.2.5 Grain-Size Model with Fuel Dissolution Model 1

Groundwater doses in figure 3-42 (labeled as Grain1) are characterized by an earlier release and higher dose than the basecase dose from the beginning of the simulation through about 60,000 yr. The high dose results from a high dissolution rate, the result of a larger surface area associated with the grain-base model in which grain size as opposed to the particle size is used for determining the surface area over which water contacts SF. From about 60,000 to 100,000 yr, the source becomes depleted and the basecase dose is greater than the dose computed using the grain-based surface area model. At the end of the 100,000-yr TPI, the dose is more than three orders of magnitude less than the basecase dose. The sinusoidal behavior of the dose is attributable to the arrival of different nuclides and releases from different subareas at the receptor location.

3.5.3 Transport Alternatives

The three alternative conceptual models that investigate assumptions of transport in the EBS, UZ, and SZ are assessed in this section. Figure 3-43 presents the groundwater doses for these conceptual models and the basecase dose.

3.5.3.1 No Retardation of Pu, Am, and Th

As presented in figure 3-43, the groundwater doses (labeled as NoRet) calculated assuming no retardation in the UZ and SZ are greater than the basecase dose for the entire 100,000-yr TPI. Moreover, the general characteristics of the groundwater doses are consistent with the dose with no retardation and approximately two orders of magnitude greater than the basecase dose.

3.5.3.2 No-Invert Model

Using the basecase mean value data set, flow through the invert is greater than the concrete permeability, and fracture flow does occur. Thus, the invert does not affect the radionuclide release rates from the EBS. Consequently, the basecase doses and the doses computed when bypassing the invert transport computations using the TPA input file flag are the same.

3.5.3.3 Matrix Diffusion

The groundwater doses presented in figure 3-43 (labeled Matdif) with matrix diffusion are less than the basecase doses from the beginning of the simulation time to about 25,000 yr because of the retention of radionuclides in the matrix lateral to the fracture transport path. From approximately 25,000 to 60,000 yr, the dose exhibits a sinusoidal behavior that appears to be attributable to subarea variations in the arrival time of nuclides at the receptor location that are not present in the basecase groundwater dose. Further investigation is underway to explain this behavior. After 60,000 yr, the groundwater dose computed with matrix diffusion increases, and at 100,000 yr, is almost one order of magnitude greater than the basecase groundwater dose. The increase in dose is caused by the increase in the release rate presumably resulting from the reversal in the diffusion (matrix to fracture). The increasing doses from the matrix diffusion case are nonintuitive, and may be caused by the way the NEFTRAN flow legs are specified in the basecase and alternative models. For the basecase model, the saturated flow pathway is specified as a "composite" flow leg, for which a single equivalent medium represents several hydrogeologic media in series. NEFTRAN does not allow this feature

when the matrix diffusion option is stipulated. Although average travel times are the same for both models, the treatment of dispersion is different.

3.6 DISRUPTIVE EVENTS

The TPA results from faulting and igneous activity are presented in this section for single and multiple realizations. The groundwater doses for the disruptive events and the ground surface doses from igneous activity are compared to doses computed using the basecase data set.

3.6.1 Single-Realization Analysis of Disruptive Events

To determine the number of WPs ruptured by seismically induced rockfalls, which is part of the basecase, the time evolution of seismicity that includes the number, time, and magnitude of seismic events is obtained using the seismic hazard curve presented in figure 3-44. The vertical extent of rockfall associated with different categories of seismic events (figure 3-45), and the joint spacing information (figure 3-46) for computing the rockfall area, are used in determining the rockfall volume. The rockfall volume is then used in computing impact stress which, when inducing a plastic strain on the WP at the contact of impact exceeding 2 percent, will fail the WP. Other associated information is presented in table 3-14 and figure 3-47.

To determine the number of WPs failed by a faulting disruptive event, the TPA code uses the time of the faulting event and the fault length and width information summarized in table 3-15. Faults modeled in the TPA code are hidden faults (i.e., either unknown and unmapped faults or underestimated faults), and thus the TPA calculations recognize that the WPs will be emplaced with an appropriate setback distance from known faults. The conditional probability for a faulting event is 1.69×10^{-4}/yr (Mohanty and McCartin, 1998).

Igneous activity contributes to WP failure for both extrusive and intrusive events. As modeled, extrusive events result in the direct release of radionuclides to the ground surface, whereas intrusive events contribute to groundwater releases. The igneous event occurs between 100- and 10,000-yr postclosure with a recurrent probability of 10^{-7}/yr. The parameters corresponding to the determination of the timing of future igneous events, subsurface areas affected by a volcanic event, and the number of WPs affected by intrusions extending laterally from the volcanic conduit are presented in table 3-16.

After the volcanic event penetrates the repository and exhumes SF, areal density from deposition of ash and radionuclides are computed at the compliance point. Input parameters, such as eruption height, wind velocity, and parameters that determine the transport and deposition of radionuclides in ash, are presented in table 3-16. The radionuclides modeled for extrusive releases, in addition to those evaluated for groundwater transport, are listed in table 3-17 with corresponding initial inventories and half-lives. Parameters associated with surface erosion of radionuclides from the ash blanket deposited following an extrusive igneous event are presented in table 3-18. For the ground surface pathway, the areal densities calculated for each radionuclide computed with the ASHPLUME (Jarzemba et al., 1997) ash transport model are used in determining the dose TEDEs by utilizing the DCFs presented in table 3-19.

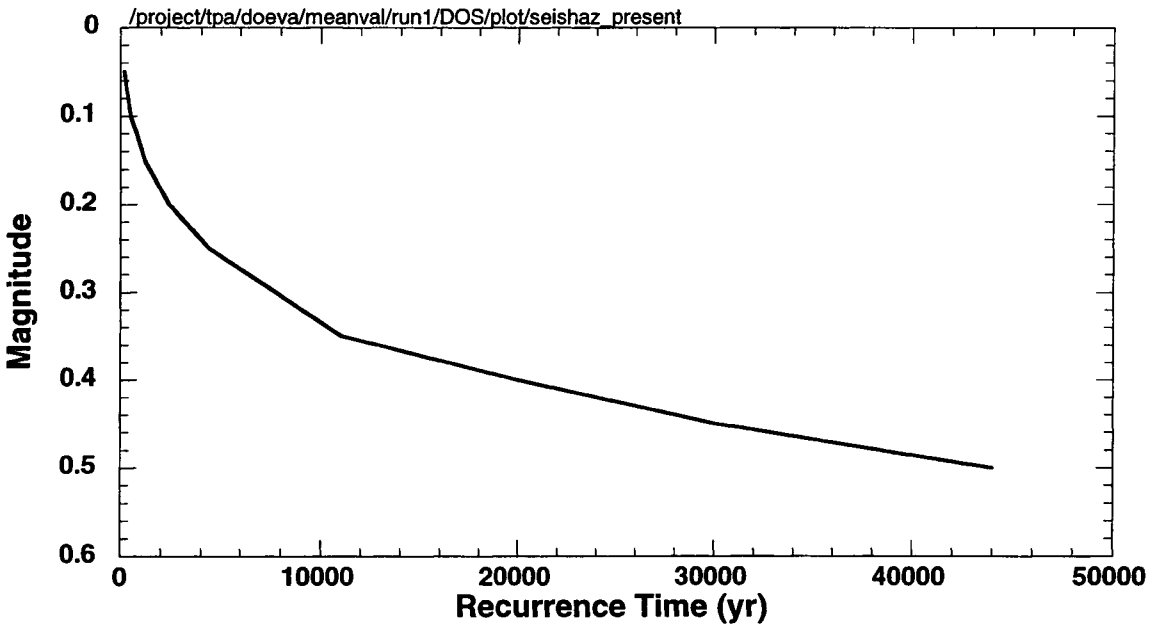

Figure 3-44. Seismic hazard curve comprises ground accelerations and recurrence times used to determine the time of seismic events

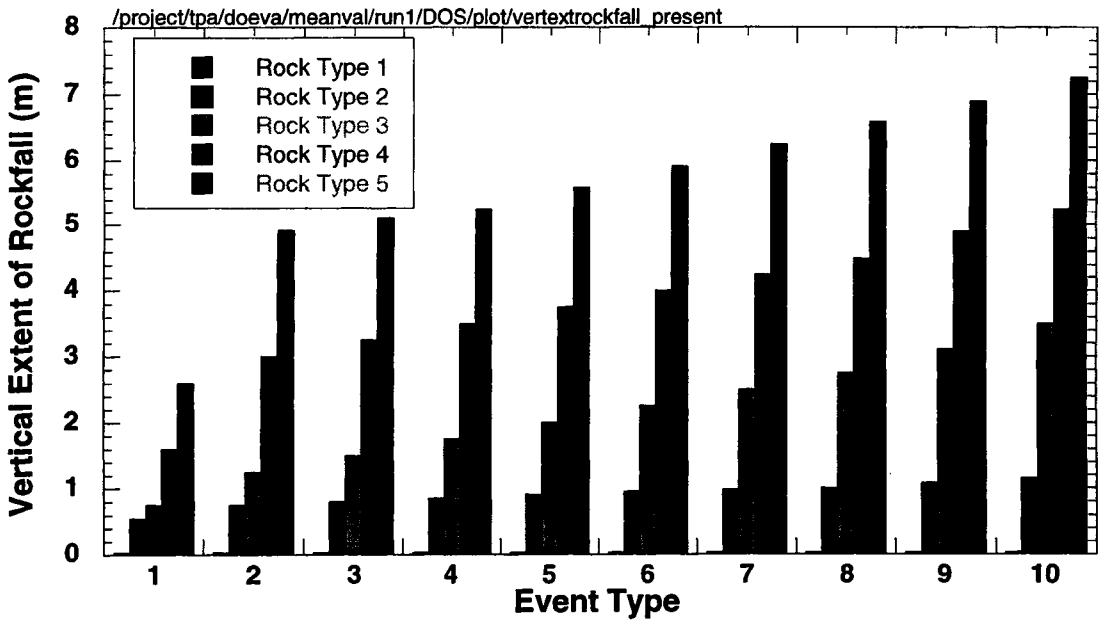

Figure 3-45. Vertical extent of rockfall associated with the five rock types and ten seismic events defined by the seismic hazard curve

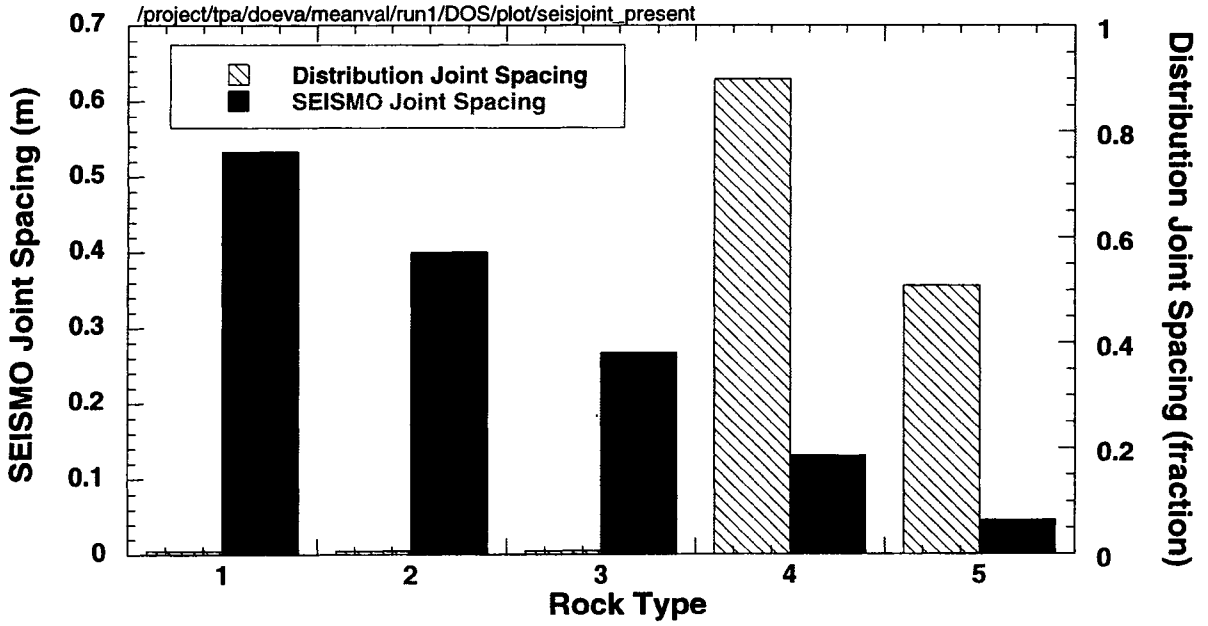

Figure 3-46. Joint spacing of the five rock types and ten seismic events

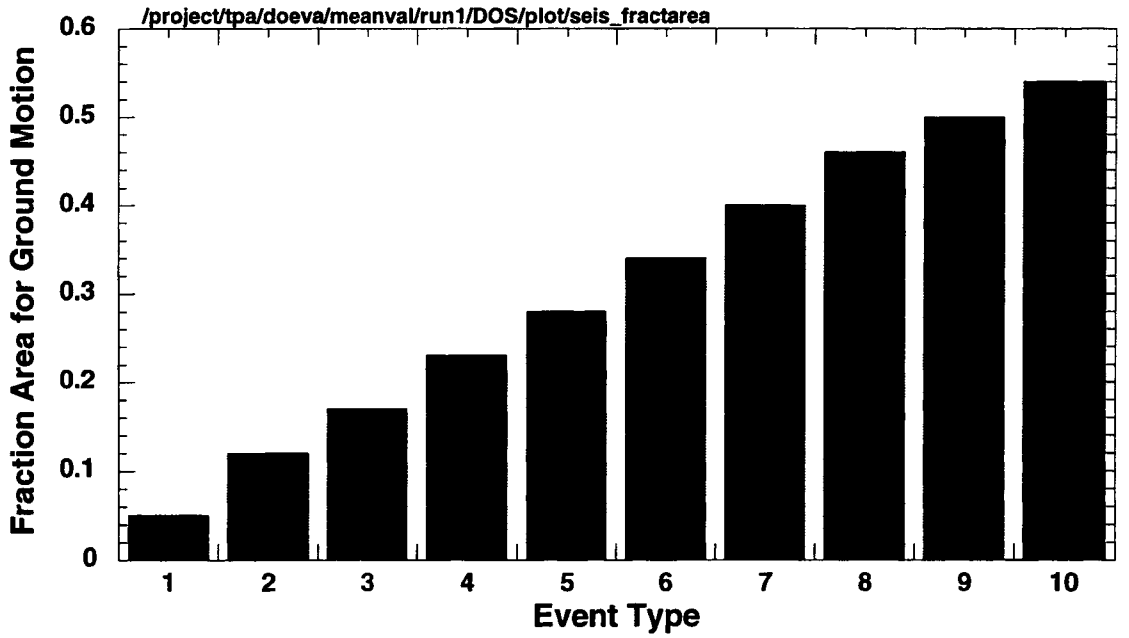

Figure 3-47. Fraction of the area with ground motion for each of the ten seismic events defined by the seismic hazard curve

Table 3-14. Parameters used in determining seismic failure of waste packages

Parameter	Mean Value	Distribution
Waste package stiffness for SEISMO	1.21×10^{10} Pa m	—
Waste package modulus of elasticity for SEISMO	2.07×10^{11} Pa	—
Rock modulus of elasticity for SEISMO	3.45×10^{10} Pa	Normal; 2.76×10^{10}, 4.14×10^{10}
Waste package Poisson ratio for SEISMO	2.00×10^{-1}	—
Rock Poisson ratio for SEISMO	2.00×10^{-1}	Normal; 0.15, 0.25
Rock falling distance for SEISMO	2.00 m	—
Waste package falling distance for SEISMO	3.00×10^{-1} m	—
Waste package number of support pair for SEISMO	2.00	—
Waste package support stiffness for SEISMO	5.50×10^{9} Pa m	—
Waste package ultimate strength	4.50×10^{8} N/m^2	—
Grain density for Topopah Spring - welded for SEISMO	2.55 g/cm^3	—
Waste package yield point	2.00×10^{-3}	—
Waste package plastic elongation	2.00×10^{-2}	—

Table 3-15. Faulting disruptive event parameters

Parameter	Mean Value	Distribution
Time of next faulting event in region of interest	4.89×10^{3} yr	Finite exponential; 100.0, 10000.0, 2.0×10^{-5}
Threshold displacement for fault disruption of waste package	2.00×10^{-1} m	User distribution; 4 values: 0.1, 0.2, 0.3, 0.4
X coordinate of faulting event in region of interest	5.48×10^{5} m	Uniform; 547400.0, 548600.0
Y coordinate of faulting event in region of interest	4.08×10^{6} m	Uniform; 4076200.0, 4079040.0
Probability for NW orientation of faults	5.00×10^{-2}	—
Random number to determine fault orientation	5.00×10^{-1}	Uniform; 0.0, 1.0
NW fault strike orientation measured from North - clockwise	-32.5°	—
NE fault strike orientation measured from North - clockwise	10°	—
NW fault trace length	4.00×10^{3} m	—
NE fault trace length	4.00×10^{3} m	—
NW fault zone width	2.16×10^{1} m	Beta; 0.5, 275.0, 1.25, 15.0
NE fault zone width	2.85×10^{1} m	Beta; 0.5, 365.0, 1.25, 15.0
NW amount of largest credible displacement	1.34×10^{-1} m	—
NE amount of largest credible displacement	1.34×10^{-1} m	—
NW cumulative displacement rate	5.00×10^{-5} mm/yr	—
NE cumulative displacement rate	5.00×10^{-5} mm/yr	—

Table 3-16. Igneous activity parameters

Parameter	Mean Value	Distribution
Time of next volcanic event in region of interest	5.05×10^{3} yr	Finite exponential; 100.0, 10000.0, 1.0×10^{-7}
X location in region of interest	5.48×10^{5} m	—
Y location in region of interest	4.08×10^{6} m	—
Random number to determine if extrusive or intrusive volcanic event	5.00×10^{-1}	Uniform; 0.0, 1.0
Fraction of time volcanic event is extrusive	9.99×10^{-1}	—
Angle of volcanic dike measured from north—clockwise	7.50°	Uniform; 0.0, 15.0
Length of volcanic dike	6.50×10^{3} m	Uniform; 2000.0, 11000.0
Width of volcanic dike	5.50 m	Uniform; 1.0, 10.0
Diameter of volcanic cone	5.13×10^{1} m	Uniform; 24.6, 77.9
Density of air at standard pressure	1.29×10^{-3} g/cm^3	—
Viscosity of air at standard pressure	1.80×10^{-4} g/cm-s	—
Constant relating fall time to eddy diffusivity	4.00×10^{2} cm^2/sec^5/2	—
Maximum particle diameter for particle transport	1.00×10^{1} cm	—
Minimum fuel particulate size	1.00×10^{-4} cm	—
Mode fuel particulate size	1.00×10^{-3} cm	—
Maximum fuel particulate size	1.00×10^{-2} cm	—
Minimum ash density for variation with size	1.20 g/cm^3	—
Maximum ash density for variation with size	2.00 g/cm^3	—
Minimum ash log-diameter for density variation	-2.00	—
Maximum ash log-diameter for density variation	-1.00	—
Particle shape parameter	5.00×10^{-1}	—
Incorporation ratio	3.00×10^{-1}	—
Wind direction	-90°	—
Wind speed	1.20×10^{3} cm/sec	Exponential; 8.3×10^{-4}
Volcanic event duration	6.66×10^{5} sec	Log-uniform; 6.13×10^{4}, 7.24×10^{6}
Volcanic event power	3.02×10^{10} W	Log-uniform; 2.57×10^{9}, 3.55×10^{11}
Volcanic column constant beta	1.00×10^{1}	—
Ash mean particle log-diameter	1.00×10^{-1} cm	Log triangular; 0.01, 0.1, 1.0
Ash particle size distribution standard deviation	1.00	—
Relative rate of blanket removal	1.00×10^{-3} /yr	—
Fraction of precipitation lost to evapotranspiration	6.80×10^{-1}	—
Fraction of irrigation lost to evapotranspiration	5.00×10^{-1}	—
Annual precipitation	8.50×10^{-2} m/yr	—
Annual irrigation	1.52 m/yr	—
Fraction of year soil is saturated due to precipitation	5.40×10^{-3}	—

Table 3-16. Igneous activity parameters (cont'd)

Parameter	Mean Value	Distribution
Fraction of year soil is saturated due to irrigation	2.00×10^{-1}	—
Ash bulk density	1.40 g/cm^3	—
Ash volumetric moisture fraction at saturation	4.00×10^{-1}	—
Depth of the rooting zone	1.50×10^{-1} m	—

Table 3-17. Initial inventory and half-life of *additional* radionuclides considered for ground surface release but not for groundwater release

Radionuclide	Inventory at 10 yr from Reactor (Ci/WP)	Half-life (yr)
^{227}Ac	5.07×10^{-5}	2.18×10^{1}
^{108m}Ag	1.17×10^{-1}	1.27×10^{2}
^{242m}Am	7.31×10^{1}	1.52×10^{2}
^{243}Am	1.50×10^{2}	7.38×10^{3}
^{243}Cm	1.49×10^{2}	2.85×10^{1}
^{244}Cm	1.12×10^{4}	1.81×10^{1}
^{246}Cm	2.50×10^{-1}	4.73×10^{3}
^{135}Cs	3.43	2.30×10^{6}
^{137}Cs	7.46×10^{5}	3.00×10^{1}
^{93}Mo	9.86×10^{-2}	3.50×10^{3}
^{94}Nb	4.92	2.03×10^{4}
^{59}Ni	2.40×10^{1}	8.00×10^{4}
^{63}Ni	2.98×10^{3}	9.20×10^{1}
^{231}Pa	1.90×10^{-4}	3.28×10^{4}
^{210}Pb	4.61×10^{-7}	2.23×10^{1}
^{107}Pd	1.02	6.50×10^{6}
^{240}Pu	4.96×10^{3}	6.54×10^{3}
^{241}Pu	7.26×10^{5}	1.44×10^{1}
^{242}Pu	1.56×10^{1}	3.87×10^{5}
^{238}Pu	2.06×10^{4}	8.77×10^{1}
^{226}Ra	3.58×10^{-6}	1.60×10^{3}
^{151}Sm	3.10×10^{3}	9.00×10^{1}
^{126}Sn	6.99	1.00×10^{5}
^{121m}Sn	7.78	5.00×10^{1}
^{90}Sr	5.18×10^{5}	2.91×10^{1}
^{229}Th	1.36×10^{-6}	7.34×10^{3}
^{232}U	2.42×10^{-1}	7.20×10^{1}
^{233}U	2.34×10^{-4}	1.59×10^{5}
^{235}U	1.65×10^{-1}	7.04×10^{8}
^{236}U	2.34	2.34×10^{7}
^{238}U	3.11	4.47×10^{9}
^{93}Zr	1.81×10^{1}	1.53×10^{6}

Table 3-18. Parameters used in computing ash and radionuclide removal from the ground surface

Element	K_d in Volcanic Ash (cm^3/g)	Solubility in Volcanic Ash (mol/L)
Ac	4.50×10^{2}	1.00×10^{-6}
Am	1.90×10^{3}	1.00×10^{-6}
C	5.00	1.00
Cs	2.80×10^{2}	1.00
Cl	0.00	1.00
Cm	4.00×10^{3}	1.00×10^{-6}
I	1.00	1.00
Pb	2.70×10^{2}	3.20×10^{-7}
Mo	1.00×10^{1}	1.00
Np	5.00	1.00×10^{-4}
Ni	4.00×10^{2}	2.00×10^{-3}
Nb	1.60×10^{2}	1.00×10^{-8}
Pd	5.50×10^{1}	9.50×10^{-4}
Pu	5.50×10^{2}	5.00×10^{-6}
Pa	5.50×10^{2}	3.20×10^{-8}
Ra	5.00×10^{2}	1.00×10^{-7}
Sm	2.45×10^{2}	5.00×10^{-6}
Se	1.50×10^{2}	1.00
Au	5.50×10^{1}	1.00
Sr	1.50×10^{1}	1.30×10^{-4}
Tc	1.00×10^{-1}	1.00
Th	3.20×10^{3}	3.20×10^{-9}
Sb	1.30×10^{2}	5.00×10^{-8}
U	3.50×10^{1}	4.50×10^{-5}
Zr	6.00×10^{2}	3.20×10^{-10}

Other parameters

Parameter	Mean Value	Distribution
Distance cutoff for dose conversion duality in DCAGS module	2.00×10^{1} km	—
Airborne mass load for igneous activity dose calculation	1.00×10^{-3} g/m3	Log-uniform; 1.0×10^{-4}, 1.0×10^{-2}
Occupancy factor for igneous activity dose calculation	2.40×10^{-1}	—
Depth of resuspendable layer	3.00×10^{-1} cm	—

Table 3-19. Biosphere dose conversion factors of all 43 nuclides for ground surface at the 20-km receptor location

Radionuclide	Nonpluvial and Pluvial DCF			
	Direct Exposure (rem/yr)/(Ci/m^2)	Inhalation (rem/yr)/(Ci/m^3)	Ingestion of Animal Products (rem/yr)/(Ci/m^2)	Ingestion of Crops (rem/yr)/(Ci/m^2)
^{227}Ac	3.80	7.02×10^{13}	2.13×10^{2}	4.73×10^{4}
^{108m}Ag	6.20×10^{4}	2.97×10^{9}	3.70	2.40×10^{2}
^{241}Am	6.70×10^{2}	4.66×10^{12}	1.50×10^{1}	9.80×10^{3}
^{242m}Am	7.30×10^{1}	4.46×10^{12}	1.41×10^{1}	9.53×10^{3}
^{243}Am	1.30×10^{3}	4.62×10^{12}	1.50×10^{1}	9.81×10^{3}
^{14}C	3.90×10^{-1}	2.19×10^{7}	0.00	1.70×10^{-1}
^{36}Cl	1.70×10^{1}	2.30×10^{8}	1.70×10^{4}	3.90×10^{4}
^{243}Cm	3.10×10^{3}	3.22×10^{12}	2.80×10^{1}	6.80×10^{3}
^{244}Cm	2.20×10^{1}	2.60×10^{12}	2.30×10^{1}	5.40×10^{3}
^{245}Cm	2.10×10^{3}	4.77×10^{12}	4.20×10^{1}	1.00×10^{4}
^{246}Cm	1.90×10^{1}	4.73×10^{12}	4.20×10^{1}	1.00×10^{4}
^{135}Cs	8.30×10^{-1}	4.77×10^{7}	1.00×10^{2}	5.50×10^{1}
^{137}Cs	1.30×10^{4}	3.35×10^{8}	6.90×10^{2}	3.80×10^{2}
^{129}I	6.20×10^{2}	1.82×10^{9}	2.20×10^{3}	1.60×10^{3}
^{93}Mo	1.30×10^{2}	2.99×10^{8}	1.10×10^{1}	1.90×10^{2}
^{94}Nb	3.70×10^{4}	4.35×10^{9}	2.70×10^{-3}	4.40×10^{1}
^{59}Ni	0.00	2.83×10^{7}	4.30	1.90
^{63}Ni	0.00	6.60×10^{7}	1.20×10^{1}	5.20
^{237}Np	7.30×10^{2}	5.67×10^{12}	6.50×10^{2}	2.50×10^{4}
^{231}Pa	9.80×10^{2}	1.35×10^{13}	3.80×10^{1}	3.30×10^{4}
^{210}Pb	6.20×10^{1}	1.42×10^{11}	1.09×10^{3}	1.96×10^{4}
^{107}Pd	0.00	1.34×10^{8}	1.70	4.70
^{238}Pu	8.30	4.11×10^{12}	4.43	8.60×10^{3}
^{239}Pu	8.80	4.50×10^{12}	4.90	9.50×10^{3}
^{240}Pu	2.00×10^{1}	4.50×10^{12}	4.90	9.50×10^{3}
^{241}Pu	1.30×10^{-1}	8.65×10^{10}	9.51×10^{-2}	1.84×10^{2}
^{242}Pu	1.70×10^{1}	4.31×10^{12}	4.70	9.00×10^{3}
^{226}Ra	1.60×10^{2}	9.00×10^{10}	1.20×10^{3}	3.60×10^{3}
^{79}Se	5.10×10^{-1}	1.03×10^{8}	3.60×10^{1}	6.20×10^{1}
^{151}Sm	1.20×10^{-1}	3.14×10^{8}	1.70×10^{-1}	1.70
^{121m}Sn	1.20×10^{2}	1.21×10^{8}	1.90×10^{1}	1.88×10^{1}
^{126}Sn	1.30×10^{3}	1.05×10^{9}	1.69×10^{2}	1.68×10^{2}
^{90}Sr	6.70	1.36×10^{10}	2.49×10^{3}	6.92×10^{3}
^{99}Tc	1.90	8.73×10^{7}	1.10×10^{2}	2.30×10^{3}
^{229}Th	2.10×10^{3}	2.25×10^{13}	8.53×10^{1}	1.02×10^{4}
^{230}Th	1.80×10^{1}	3.42×10^{12}	1.80	1.50×10^{3}
^{232}U	2.50×10^{1}	6.91×10^{12}	3.82×10^{2}	4.54×10^{3}
^{233}U	1.80×10^{1}	1.42×10^{12}	8.50×10^{1}	9.90×10^{2}
^{234}U	1.80×10^{1}	1.39×10^{12}	8.30×10^{1}	9.80×10^{2}
^{235}U	3.60×10^{3}	1.29×10^{12}	7.82×10^{1}	9.14×10^{2}
^{236}U	1.60×10^{1}	1.32×10^{12}	7.90×10^{1}	9.20×10^{2}
^{238}U	1.30×10^{1}	1.24×10^{12}	7.53×10^{1}	9.02×10^{2}
^{93}Zr	0.00	3.38×10^{9}	1.86×10^{-3}	4.75

3.6.2 Multiple-Realization Analysis of Disruptive Events

The variability in the average dose arising from faulting events and igneous activity for the multiple-realization simulations is presented in this section. The dose history for faulting events for the 100,000-yr TPI without probability weighting is presented in figure 3-48(a). The average groundwater dose from the faulting events is approximately 20 percent greater than the dose without a faulting event at 10,000 yr. However, after 10,000 yr, the releases from WPs failed by corrosion dominate the dose; the groundwater dose with faulting and the basecase in the 100,000-yr TPI are not distinguishable.

The probability-weighted expected dose from igneous activity is presented in figure 3-48(b) together with the groundwater dose computed using the basecase data set. In the 10,000-yr TPI, probability weighted dose from igneous activity is about two to four orders of magnitude greater than the basecase groundwater dose. The next section presents the methodology used to determine the risk arising from faulting and igneous disruptive events.

3.7 CALCULATION OF RISK

Risk is defined in this section as the probability-weighted dose. Doses are calculated from three scenario classes (i) basecase with seismicity, (ii) faulting, and (iii) igneous activity. The probability of the three scenario classes is assumed to sum to unity. This implies that other scenario classes are either too improbable, or have consequences too small, to affect the overall risk materially.

The average risk to a receptor can be computed by summing contributions to dose from each Monte Carlo simulation, weighted by the scenario probability and the conditional probability of each realization within the scenario. The methodology for computing conditional risk (i.e., assuming that the scenario has a probability of one) from scenarios other than extrusive igneous activity is presented in section 3.7.1. The methodology used to determine the conditional risk from scenarios with extrusive igneous activity is described in section 3.7.2. The methodology for combining the conditional risks to an overall risk is presented in section 3.7.3.

3.7.1 Scenarios Other Than Extrusive Igneous Activity

The risk or effective dose equivalent is the product of the consequence (i.e., dose) and the probability that the dose has occurred. Estimates of dose are uncertain because the models and their input parameters are uncertain, as are the times of occurrence of the disruptive events such as faulting and intrusive igneous activity. Monte Carlo analysis is used to account for the uncertainty in parameters and events. The Monte Carlo analysis propagates the uncertainty in model inputs through the conceptual models. A Monte Carlo simulation evaluates a model repeatedly using input values that have been randomly selected from the probability distributions for the input variables. The output of the Monte Carlo analysis is a set of results such as dose versus time, for each of the randomly chosen input sets of values. Generally, each Monte Carlo output result has equal probability. Thus, each dose curve from the Monte Carlo analysis has a probability of occurrence equal to $1/N$, where N is the number of Monte Carlo samples. The analysis in this section does not explicitly include conceptual model uncertainty, other than that captured by changes in the input parameters. Alternative conceptual models are covered in sections 2.3 and 3.5.

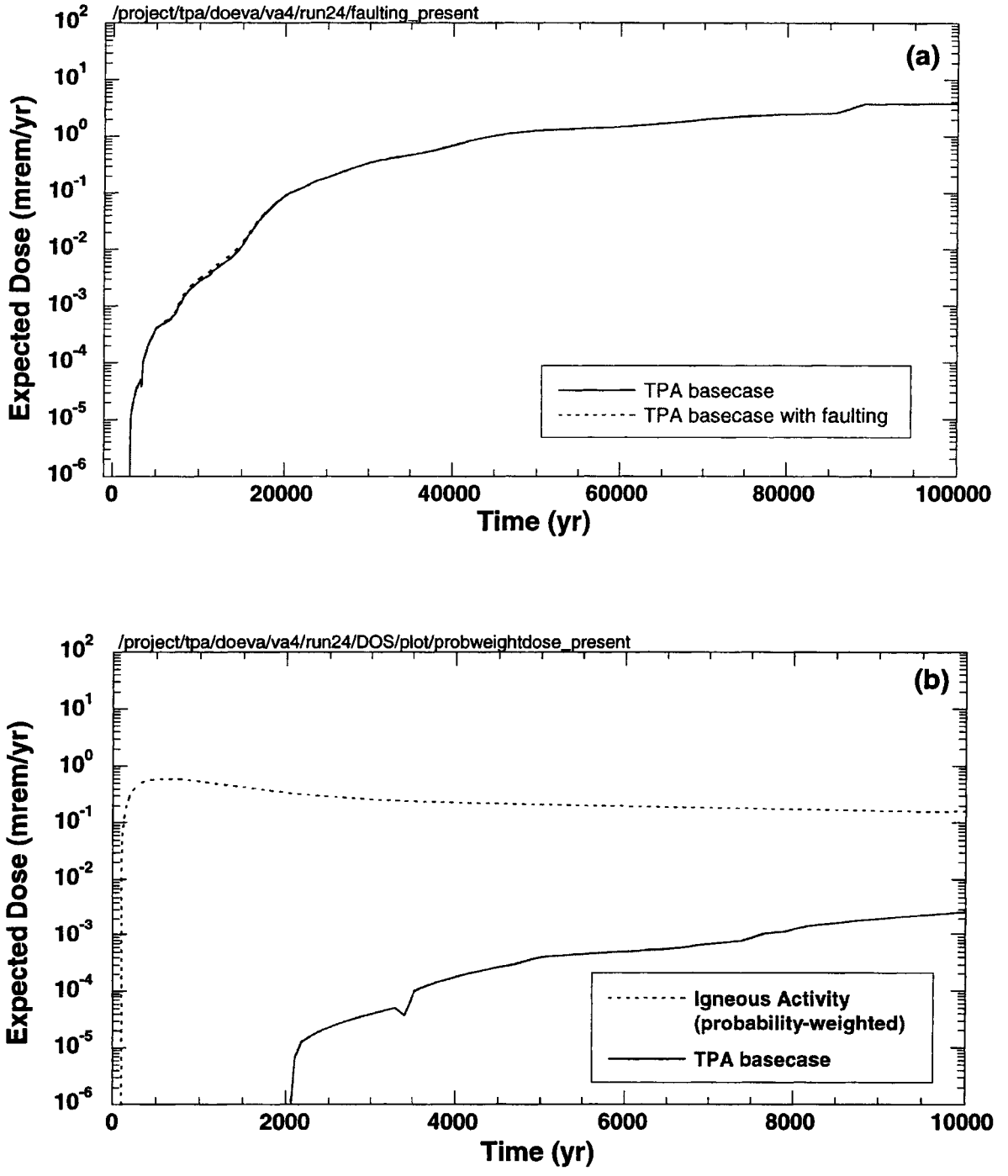

Figure 3-48. Groundwater dose in 10,000 and 100,000 yr with and without (a) faulting and (b) igneous activity in 10,000 yr for 250 realizations. Only the ground surface dose for releases caused by extrusive igneous activity in (b) is probability weighted. The basecase and faulting doses are not probability weighted.

The expected dose-versus-time relationship for scenario j (e.g., intrusive volcanic scenario) can be developed by summing, over all realizations, the probability weighted contributions from the family of dose relationships produced by the N Monte Carlo samples. The mathematical representation of this calculation is

$$\overline{D}_j(t) = \sum_{i=1}^{N} p_i C_{i,j}(t) \tag{3-1}$$

where

$\overline{D}_j(t)$ — average annual dose to the receptor individual as a function of time for the jth scenario

$C_{i,j}$ — dose as a function of time for the ith realization of the jth scenario

p_i — probability assigned to the dose curve for the ith realization. For Monte Carlo sampling, $p_i = (1/N)$

N — number of model simulations that compose the family of dose curves (i.e., N Monte Carlo samples of the model inputs are used to generate N model outputs in the form of dose curves)

The index indicates that the event can occur at any time between [0,t].

3.7.2 Extrusive Igneous Activity Scenario

For the igneous activity scenario, dose consequences are largest for events that occur soon after repository closure, while the relatively short-lived but high-activity radionuclides such as ^{241}Am are still present in significant quantities. Radionuclides can reach the affected population in short times (hours to days), but persist in the environment and also cause lower levels of exposure long after the event (hundreds to thousands of years). The time of occurrence of the event is extremely important to the dose consequences, and is, therefore, included in the probabilistic analysis as one of the sampled parameters. The fact that there are short-term, relatively high consequences and long-term, lower consequences from igneous events complicates the probabilistic analysis by requiring a large number of Monte Carlo samples to resolve the overall expected dose on both the short- and long-term time scales. To get a reasonably converged mean value, hundreds of realizations must be performed at each potential occurrence time, which may be impractical with the present models run in the usual Monte Carlo fashion.

Because the expected dose-versus-time curve is anticipated to be smooth, a much more efficient convolution approach to generating the curve is to develop the expected dose for igneous events at a few, discrete event times and then use linear interpolation between the discrete event times. The procedure for developing the expected dose curve involves the following steps:

- Conduct Event Time Specific Probabilistic Analyses
  Specific occurrences of igneous activity are selected for the evaluation rather than randomly selecting occurrence times in a Monte Carlo approach. A separate probabilistic analysis,

based on the parameter uncertainty, is conducted for each specific occurrence time. In the present model, the event times were 100; 500; and 1,000 to 10,000 yr in 1,000-yr steps.

- Generate Conditional Expected Dose Curves for Specific Event Times
  Each of the separate probabilistic analyses described previously is used to develop a separate conditional expected dose curve for the specified occurrence times using Eq. (3-1).

- Generate Probability Weighted Dose Curve for Specific Event Times
  The probability weighted dose $\overline{D}_n$ for the specific event times is generated by multiplying the conditional dose curves by the probability in a given year that an igneous event occurred (annual probability can be used provided it is constant over time). Figure 3-49 presents the series of probability weighted dose curves calculated in this analysis.

- Generate an Overall Expected Dose Curve
  The expected dose at any given time t is the sum of conditional expected dose $\overline{\Re}$; overall, the expected dose curve due to igneous activity occurring over the TPI is determined by cumulating probability weighted dose over time using the probability weighted dose curves at the 12 specified event times. Equation (3-2) describes how the expected annual dose to the receptor individual is estimated in this approach:

$$\overline{\Re}(t) = \sum_{n=1}^{E} (\Delta t)_n \overline{D}_n(t) \tag{3-2}$$

where

$\overline{\Re}(t)$ — expected annual dose to the receptor individual as a function of time

$D_{n(t)}$ — probability weighted mean dose as a function of time for specific event time n

$(\Delta t)_n$ — increment of time associated with event time n (if events are evaluated on a per year basis, this would be 1yr)

E — number of specific event times used to represent variation in event uncertainty (interpolation between events can be used to generate dose curves for each year).

The probability weighted dose curve calculated with this more efficient approach is presented in Figure 3-50. As expected, the consequences of an igneous event are highest at early times. The probability weighted dose curve goes through a maximum at around 500 yr. This results from the accumulation of dose from potential earlier events.

3.7.3 Combining Conditional Risks to an Overall Risk

The overall risk, $\overline{D}(t)$, is calculated by summing the scenario mean doses weighted by the scenario probability P_j. The mathematical representation of this calculation is

$$\overline{D}(t) = \sum_{j=1}^{M} \overline{D}_j(t) P_j \qquad (3\text{-}3)$$

where

$\overline{D}_j(t)$	—	dose rate from scenario j, averaged over the Monte Carlo realizations
M	—	number of scenario classes
P_j	—	annual probability of scenario j

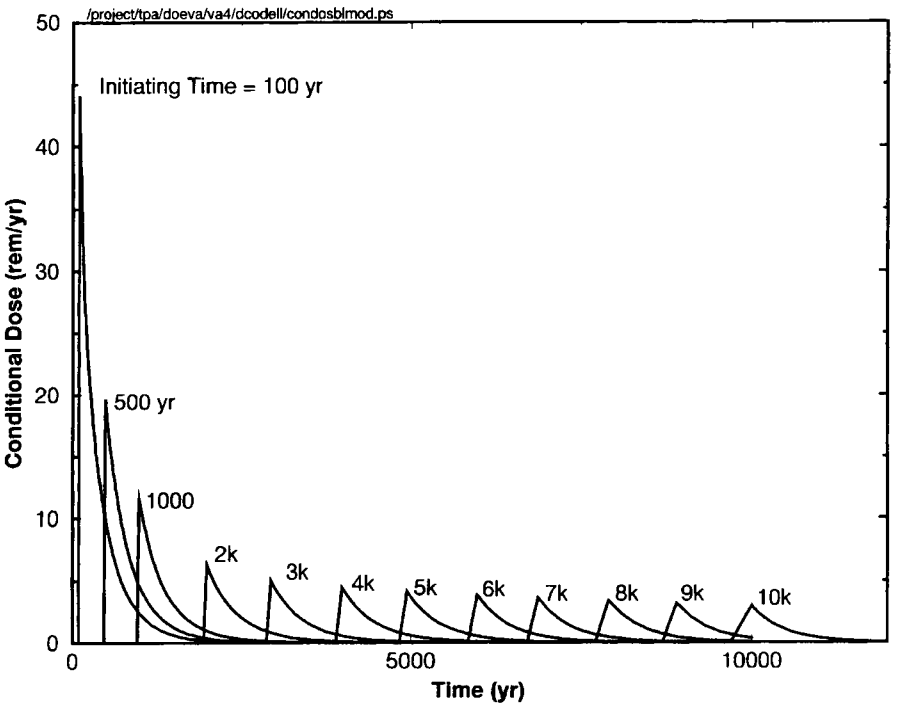

Figure 3-49. Mean dose arising from extrusive igneous activity shown with various times for the volcanic event in 400 realizations

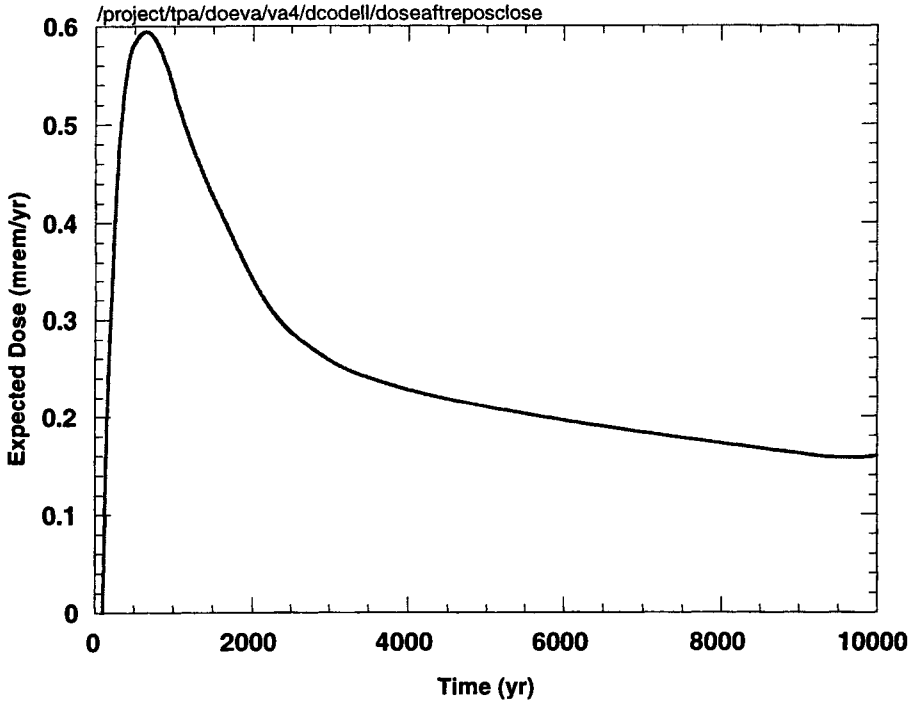

Figure 3-50. Contribution of extrusive igneous activity to the total dose, weighted by an annual probability for the volcanic event of 10^{-7}

4 SYSTEM-LEVEL SENSITIVITY STUDIES

This chapter describes the sensitivity and uncertainty analysis techniques used in conjunction with results of the TPA Version 3.2 code system-level calculations. In general, a sensitive parameter is defined as one that provides a relatively large change in the output variable for a unit change in an input parameter. The goal of the sensitivity analyses presented in this report is to determine the parameters to which peak dose or the TPI shows the most sensitivity. The goal of the uncertainty analyses is to determine the parameters that are driving uncertainty (i.e., variation) in peak dose output. The analyses were conducted primarily for the basecase and to a limited extent for the igneous activity and faulting disruptive events. The analyses conducted herein rely on the models and assumptions used in the TPA Version 3.2 code.[1] For more detailed description of these models and assumptions, the reader is referred to the TPA Version 3.2 Code User's Guide (Mohanty and McCartin, 1998). Conclusions based on these analyses may be updated as the models or assumptions are updated, and certain parameters or processes may become more or less influential.

The sensitivity analyses in this report use peak dose as the output variable for each realization because this result is most likely to demonstrate sensitivity relationships among the independent and dependent variables. The performance measure in the draft version of the YM implementing regulation 10 CFR Part 63 (Nuclear Regulatory Commission, 1999a) is stipulated to be the peak of the average dose history within the 10,000-yr TPI. Although there is an important distinction between these two measures of performance, the use of the peak dose for each realization would not significantly alter the sensitivity analysis conclusions since approximately 90 percent of the realizations have their peak dose at 10,000 yr, and for those realizations with earlier peak doses, the peak dose does not significantly differ from the dose at 10,000 yr.

4.1 SENSITIVITY ANALYSIS TECHNIQUES

Most techniques used herein rely on the Monte Carlo method for probabilistically determining system performance. As mentioned in the previous chapters, the performance measure of the system in the NRC YM repository PA exercises is the peak dose in the TPI to an average member of a receptor group located 20-km from the repository. Many of the input parameters are not precisely known and are spatially variable, so their values are described by probability distributions (figure 4-1). The Monte Carlo technique makes repeated calculations (called realizations) of the possible states for the system, choosing values for the input parameters from their probability distributions. Although 246 input parameters[2] are sampled in the TPA Version 3.2 code, only a few of these parameters contribute significantly to the uncertainty in peak dose because of the great sensitivity of peak dose to the parameters, the large variability of the parameters, or both.

This section describes the techniques used to determine which input parameters in the TPA Version 3.2 Code most influence the results. It is noted that not all techniques described were applied to all cases. For generalization purposes, the output from the system is denoted as y. In general, y is a

[1]The specific version of the total-system performance assessment used in this chapter is 3.2, whereas Version 3.2.3 was used in developing chapter 3. Results from Version 3.2.3 do not affect the peak dose calculation compared to Version 3.2, which is the performance measure used in this chapter.

[2]The actual number of parameters contributing to the variability in peak dose is fewer than 246 depending on which group of conceptual models is used in the calculation. The Latin hypercube sampling module in the TPA Version 3.2 code samples all parameters that are not constant regardless of their use in a specific run.

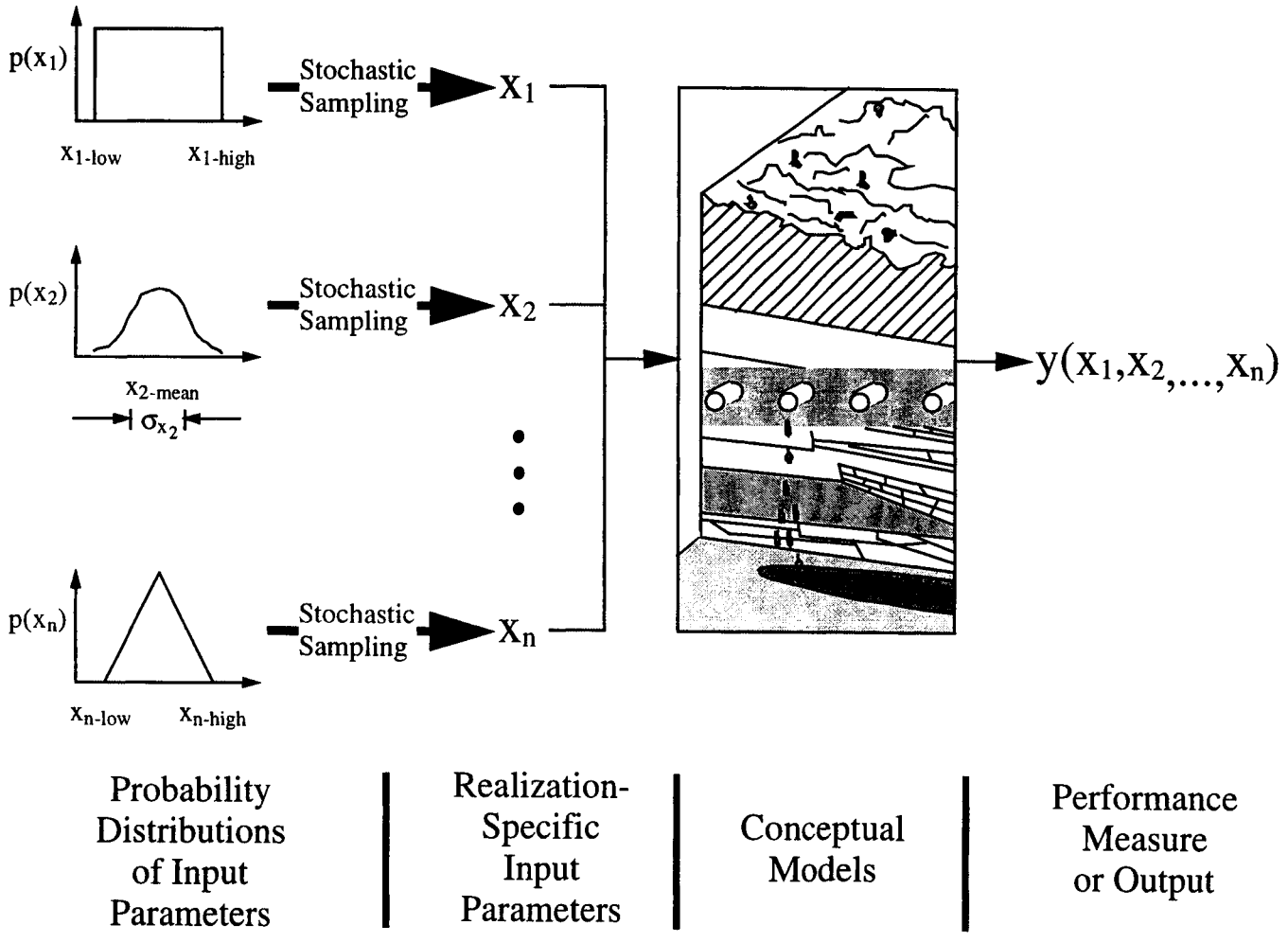

Figure 4-1. A diagram illustrating the use of the Monte Carlo method in performance assessment

function of random parameters, x_i; deterministic parameters, d_k; and model assumptions, a_m. The system output, y, is such that

$$y_j = f\left(x_{1,j}, x_{2,j}, \ldots, x_{I,j}, d_k, a_m\right) \tag{4-1}$$

where j represents the jth realization and I is the total number of sampled parameters in the model. It is assumed that the behavior of the system is simulated by appropriately sampling the random parameters and then computing the system output, y, for each realization of parameter vector (see figure 4-1). For the purposes of this section, which is to outline a method for analyzing simulation output to identify important random parameters and develop understanding of their relationship to the output, it is assumed that the decisions about appropriate model assumptions and deterministic parameters have been made *a priori*. As a result, we do not consider the dependence of y on deterministic parameters and model assumptions any further, and focus on the dependence of y on the x_is only.

4.1.1 Regression Analyses Methods

4.1.1.1 Scatter Plot/Single Linear Regression on One Variable

To understand the nature and strength of relationships between input and output variables of a model, it is often useful to examine scatter plots in which the output variable is plotted against one input variable at a time. As shown in figure 4-2, results of scatter plots give an initial visual indication of nonlinear effects, thresholds, and variables likely to be important to further sensitivity and uncertainty analyses. Single linear regression (i.e., regression with only the first power of one input variable and an intercept) of the output variable with respect to each of the input parameters can give a quantitative measure of the correlation through the coefficient of determination, R^2. This figure can be misleading, however, in cases where the dependencies are not purely of the first order with respect to the input variable. It is noted that linear here and throughout this chapter refers to the functional form of the regression and not the order to which the fitting parameters appear (although the regressions are also linear in the fitting parameters). Even when the output variable is linearly dependent on the input variable being studied, univariate linear regression of Monte Carlo results may fail to show unambiguous correlation because other sampled parameters that affect the output are varying at the same time, and the model is clearly underspecified (i.e., the results depend on more than one variable).

The coefficient of determination, R^2, is small for most variables in the current analyses and is not necessarily a good indicator of the importance of the variables. A better indication of influence is to determine the probability that the slope of the linear regression line is significantly different from zero. This is done with a t-test or t-statistic as described in succeeding sections.

Use of the t-Statistic to Determine Significance of Regression Parameters

The t-statistic is generally used to estimate with a specified confidence level that an estimated parameter value differs from another value. A parameter, x_i, is deemed influential if there is a specified (e.g., 95 percent) confidence that the slope of its regression curve, (m_i), is different from zero (Benjamin and Cornell, 1970).

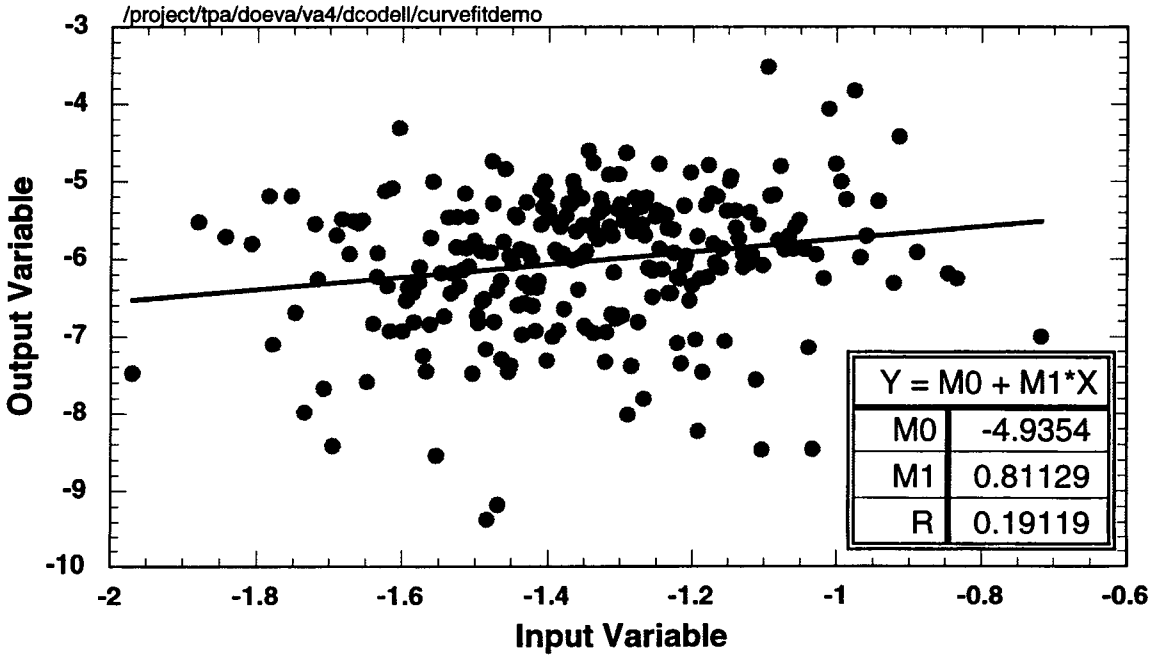

Figure 4-2. Example of a scatter plot/single linear regression

The t-statistic of the slope of a single-variable regression line is defined as

$$t_i = m_i \sqrt{n \frac{S_{i,x}^2}{S^2}} \tag{4-2}$$

where

t_i — t-statistic for regression coefficient i

m_i — estimated value of regression coefficient i (i.e., slope of the best-fit line for dose versus the independent variable, x_i)

S — estimated standard deviation of dose

$S_{i,x}$ — estimated standard deviation of independent variable, x_i

n — number of samples

For the analyses conducted herein, the number of realizations is greater than 250, which provides essentially an infinite number of degrees of freedom for the t-statistic. The critical value to ensure 95-percent confidence that m_i differs from zero under these conditions is 1.96 (Mason et al; 1989). Equation (4-2) is used, therefore, to determine if the absolute value of the t-statistic for each independent variable is greater than 1.96. If not, then the hypothesis that the independent variable was significant is rejected.

The t-statistic was used for the single variable regressions and multiple linear regressions as described in Eq. (4-5).

4.1.1.2 Variable Transformations and Their Attributes

The correlation between input and output variables can be enhanced by transforming the variables. This section describes variable transformations used in this study. In general, variable transformations are used to (i) eliminate dimensionality of the variables, (ii) reduce the role of points at the tails of the distributions, and (iii) properly scale the resulting sensitivities to the variability of the input variables. While transformations generally increase the goodness of the fit analyses, they distort the meaning of the results. For example, transformations such as rank, logarithmic, and power law frequently give unfair weight to small doses, which do not affect the mean results as much as the higher doses. Because the proposed regulations are based on mean doses, regression results based on transformed variables should be used cautiously.

Normalization

In normalization, the input variable, x_i, is transformed by dividing it by its mean value (or another baseline value such as the median, 90th percentile, and such):

$$x_i^* = \frac{x_i}{\overline{x_i}} \tag{4-3}$$

Normalized variables are dimensionless and are scalar multiples of their baseline values. Dimensionless variables allow the comparison of sensitivities to other independent variables with different dimensions. Other types of normalization can also be used and will be shown later in this chapter.

Sensitivity measures based on normalized variables describe only the relative change in the dependent variable (peak dose) to changes in the independent variables. Although this is a useful measure of sensitivity, it does not consider the ranges of the variability of the independent and dependent variables (see standardization, following).

Rank Transformation

If the distributions of input and output are far from a normal distribution, particularly if they have one or two long tails, they are liable to distortions from the effect of outliers. One way to avoid such effects is to arrange the output values according to the rank order, or the samples of each input parameter (Morgan and Henrion, 1990). Rank transformation, a dimensionless transform, replaces the value of a variable by its rank (i.e., the position in a list that has been sorted from largest to smallest values) (Iman and Conover,

1979). Analyses with ranks tend to show a greater sensitivity than results with untransformed variables. If the distribution of doses is skewed toward the low end, which is usually the case, rank transformation gives unfair weights to lower doses.

Logarithmic Transformation

For situations in which input and output variables range over many orders of magnitude, it may be advantageous or even necessary to perform analyses on the logarithm of the variables instead of the variable values themselves. The log transformation is also valuable for creating regression equations, where the subprocesses of the model multiply each other to form the output variable, such as in a transfer function approach. For the present situation in which the dose calculation results from radionuclide releases from the waste form, transport through the geosphere, and uptake by humans, the processes are indeed largely multiplicative rather than additive. Log transforms, therefore, tend to give better fits to the Monte Carlo results than untransformed variables but at the expense of unfair weighting of the smaller doses. The log transformation may be used in conjunction with normalization.

Scaled-Power Transformation

The scaled power transformation is similar to the logarithmic transformation, but often allows a closer approach to normality. For a variable, v, and power, p, (p not equal to 0), the scaled power transformation is (Cook and Weisberg, 1994):

$$v^{(p)} = \frac{(v^p - 1)}{p} \tag{4-4}$$

For $p = 0$, it can be demonstrated that the scaled power transformation reduces to the logarithmic transformation.

The algorithm steps through a range of values of the exponent, p, in small increments and compares the shape of the resultant scaled distribution to the shape of a normal distribution. The staff employed the Lilliefors test for normality (Bowen and Bennett, 1988). The exponent yielding the best fit to the normal distribution is then chosen to scale the variable under consideration. This procedure is used for the independent variables and the dependent variable (peak dose).

The scaled power transformation can be shown graphically for an example of the peak dose for 10,000 yr. Figure 4-3 shows a normal probability plot of dose for 10,000 yr in the 1,000-vector basecase, demonstrating that it is highly skewed. Using Eq. (4-4) with an exponent, $p = 0.1$, transforms the data to a close fit to the normal distribution as shown in figure 4-4. As with the logarithmic transformation, the improved fit is at the expense of an overemphasis on the smaller dose.

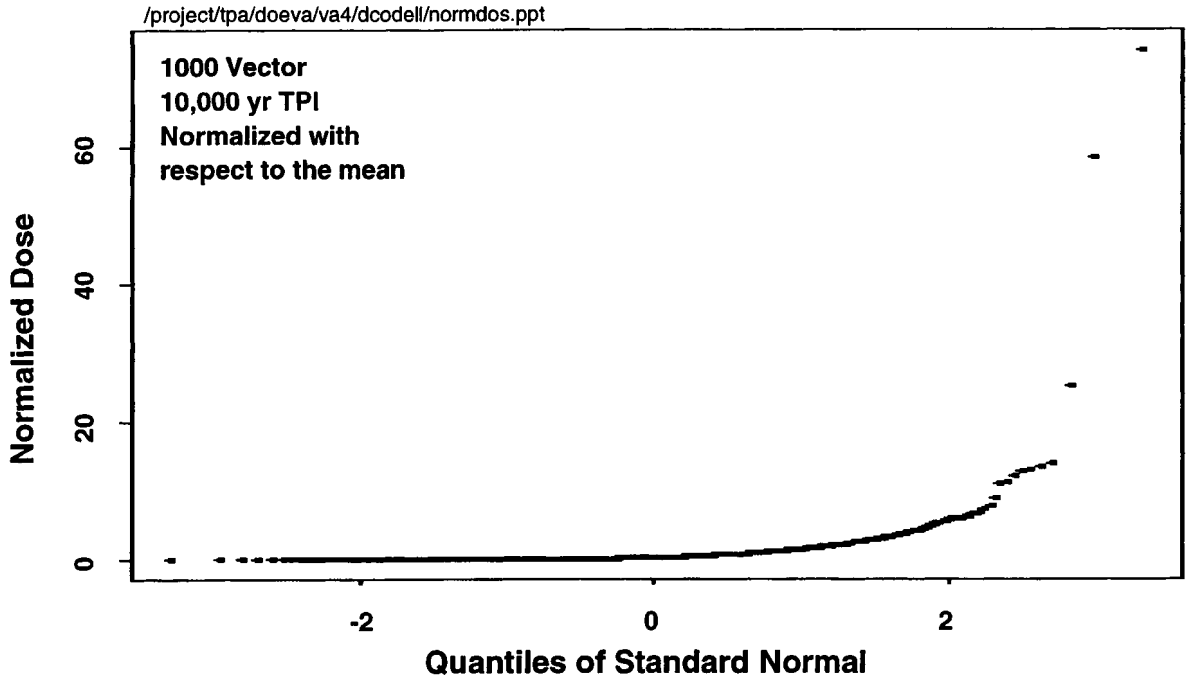

Figure 4-3. Normal probability plot of dose for 10,000 yr in the 1,000-vector basecase

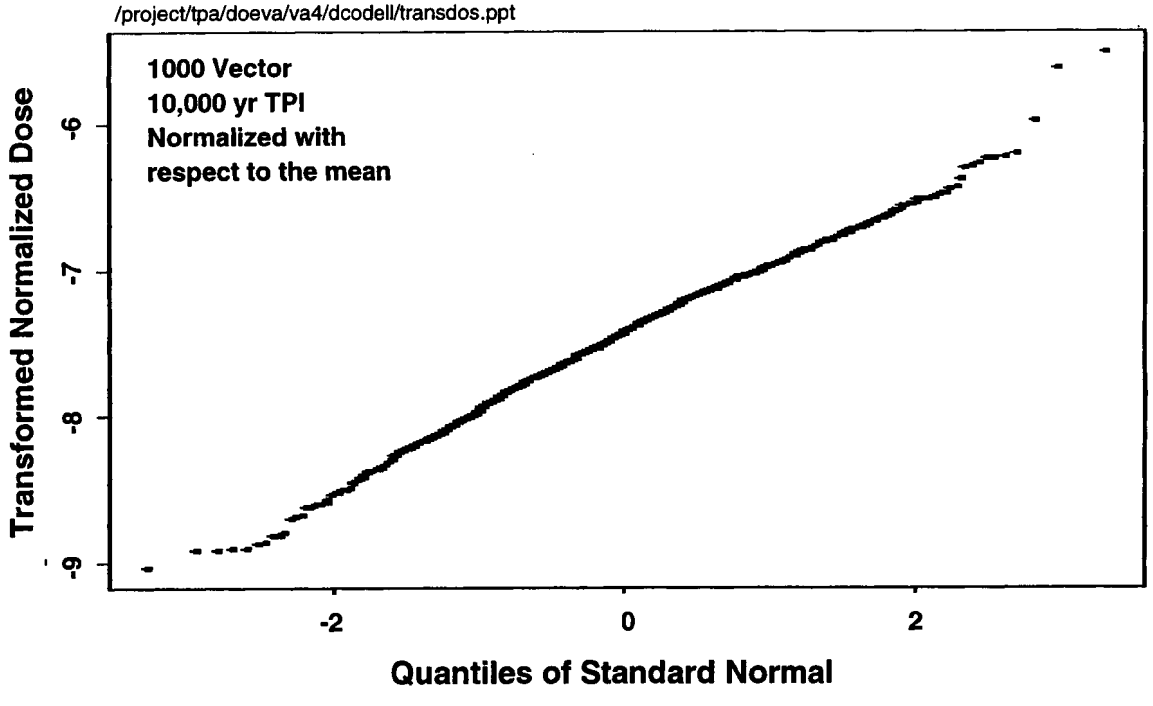

Figure 4-4. Figure showing a close fit to normal distribution after using p = 0.1 transforms

Standardization

The independent and dependent variables can be standardized by subtracting the mean and dividing by the standard deviation

$$x_i^* = \frac{x_i - \bar{x}}{\sigma_x} \tag{4-5}$$

Sensitivity measures based on standardized variables (standardized sensitivities) have the advantage of taking into account the uncertainty (in the standard deviation) of the independent variable. Furthermore, the standardized sensitivities preserve the absolute values of peak dose because the derivatives are divided by the standard deviation for the entire set of calculations, rather than the mean peak dose at the evaluation point. Therefore, the absolute value of changes in mean peak dose is preserved with standardized sensitivities.

Standardized variables can be greater or less than zero, hence they cannot be used directly in the regression analyses using the log-transformed variables. Instead, the standardized sensitivities can be derived from sensitivities based on logs of the normalized variables:

$$\frac{\partial y^*}{\partial x^*} = \frac{\sigma_{x_i}}{\sigma_y}\left(\frac{\partial y}{\partial x_i}\frac{x_i}{y}\right)\frac{y}{x_i} \tag{4-6}$$

where y^* and x^* are the standardized dependent and independent variables as defined by Eq. (4-5). The quantity in parentheses is the sensitivity derived from regression analysis with the logs of the normalized variables. Note that since Eq. (4-6) requires the normalized sensitivities, it necessarily suffers from some of the same disadvantages as normalized sensitivities. Direct linear regression with standardized variables gives the proper weight to all doses.

A modified form of the standardized sensitivities approach was also used in the differential analysis described in section 4.1.2. In this case, only seven points were defined for the parameter space, so the independent variables were standardized by the same standard deviations used in the regression analyses (i.e., the standard deviation based on 250 samples generated in the Monte Carlo analyses). Peak dose did not need to be standardized to show the relative sensitivities to the standardized independent variable. Therefore, those sensitivities have units of dose.

4.1.1.3 Stepwise Multiple Linear Regression

Stepwise multiple linear regression (stepwise regression) determines the most influential input parameters according to how much each input parameter reduces the residual sum of squares (RSS) (Helton, 1991). The form of the regression equation is

$$y = m_1x_1 + m_2x_2 + \ldots + m_nx_n + b \tag{4-7}$$

where

y — dependent variable
x_i — independent variables
m_i — regression coefficients (also known as partial correlation coefficients)
b — intercept

The regression coefficients, m_i, is a measure of linear sensitivity of y to input x_i (Draper and Smith, 1981). The variables may be the raw variables, transformed variables, or ranks. The stepwise algorithm calculates the reduction in RSS for the independent variables in the order that gives the greatest reduction first. In the implementation of the procedure, a multiple linear regression model is fitted to the data in an iterative fashion. The procedure starts with the variable, x_i, that explains most of the variations in the model output, y. Then it adds additional variables (one at a time) to maximize the improvement in fit of the model according to the R^2 value. In the regression model, R^2, the coefficient of determination indicates the fraction of variability in the data explained by all the variability in the model. The sequence in which the inputs are selected is a useful measure of their uncertainty importance, as is the increment in R^2 they produce. Iman and Conover (1979) also suggested the use of partial correlation coefficients, which are measures of the contribution of each uncertain input to the output uncertainty, after removing the effects attributable to other inputs. These coefficients are useful when there are significant correlations between the inputs (Morgan and Henrion, 1990).

The regression coefficients, m_i ,are the partial derivatives of the dependent variable with respect to each of the independent variables. The correlation coefficient reflects the fractions of the variability explained by the individual variables (Zimmerman et al., 1991). The form of the linear regression equation that gave the best fit used the log of the normalized peak dose and the log of the normalized independent variables, x_n:

$$\log\left(\frac{y}{\bar{y}}\right) = b + m_1 \log\frac{x_1}{\bar{x}_1} + m_2 \log\frac{x_2}{\bar{x}_2} + \ldots + m_i \log\frac{x_i}{\bar{x}_i} + \ldots + m_n \log\frac{x_n}{\bar{x}_n} \qquad (4\text{-}8)$$

where

b — intercept
m_i — coefficient of the regression

and the overbars denote the value of the quantities used for normalization (generally the mean value).

When the antilog of both sides of Eq. (4-8) is taken, then the resulting equation becomes

$$\frac{y}{\bar{y}} = 10^b \left(\frac{x_1}{\bar{x}_1}\right)^{m_1} \left(\frac{x_2}{\bar{x}_2}\right)^{m_2} \cdots \left(\frac{x_n}{\bar{x}_n}\right)^{m_n} \qquad (4\text{-}9)$$

After taking the partial derivative of both sides of Eq. (4-9) with respect to the independent variables and rearranging, it reduces to

$$\frac{x_i}{y}\frac{\partial y}{\partial x_i} = m_i \qquad (4\text{-}10)$$

Therefore, the normalized sensitivities are exactly the coefficients of the regression equation using the logs of the normalized peak dose and independent variables. The form of the sensitivities given by Eq. (4-10) is the same measure calculated by the differential method of Eq. (4-12) in section 4.1.2.

4.1.1.4 Application of the Kolmogorov-Smirnov and Sign Tests for Determining Important Parameters

The K-S and Sign tests differ from regression in that they are nonparametric; that is, these tests do not require fitting the data to prespecified functional forms.

The Kolmogorov-Smirnov Test

The K-S test determines if a set of samples was drawn from a given distribution (Bowen and Bennett, 1988). It is used to determine if an independent variable is influential by comparing the distribution of a subset of the independent variables composed of the values from the highest 10 percent of the peak dose realizations to the theoretical distribution of that variable. If the two distributions are equivalent, then peak dose is not sensitive to the variable in question. Conversely, if the distributions are different, then the variable in question does have an effect on peak dose. For the present study, there are 1,000 vectors in the entire set, and the subset consists of the 100 vectors corresponding to the top 10 percent of the peak doses. The distribution of the variable in the 1,000-vector set is taken as the theoretical distribution, although it would also be possible to get the theoretical distribution directly from the generating function specified in the LHS routine. The significance of the K-S test was determined at the 95-percent confidence level.

The Sign Test

The Sign test is another nonparametric test used to determine if a set of data corresponds to a given theoretical distribution (Bowen and Bennett, 1988). It is used in a manner similar to the K-S test. In the Sign test, each observation of the input variable is represented by either a plus sign (+) or a minus sign (−) depending on if it is greater than or less than the median value estimated by the theoretical distribution. The subset of the input parameter values corresponds to the highest 10 percent of the calculated peak doses. The subset is compared to the theoretical distribution, which in this case is assumed represented by the entire set of 1,000 vectors. The significance of the Sign test was determined at the 90 percent confidence level.

4.1.2 Differential Analysis Technique

Regression analysis on the Monte Carlo results can only determine the most influential parameters when those parameters also have large enough correlation coefficients that they are distinguishable from the confounding effects of the simultaneous sampling of all other independent variables. Differential analysis determines sensitivity unambiguously because it deals with changes in only one independent variable at a time. Differential analysis determines sensitivity of parameters only at local points in parameter space and

does not consider the wide range of parameter variations as does the Monte Carlo method. This section describes the results of a differential analysis conducted to determine the most influential parameters with respect to peak dose.

Differential analysis tests were conducted through multiple deterministic runs in which a single input parameter was changed by a known amount compared to its initial baseline value, and all other input parameters were held at a baseline value. The baseline value for the purposes of this report is a sampled value for the input parameter. The sensitivity of a performance measure (in this case peak dose for the TPI) to a parameter is estimated as the first derivative of the performance measure with respect to that parameter

$$\frac{\delta y}{\delta x_i} \approx \frac{y(x_i+\Delta x_i) - y(x_i)}{\Delta x_i} \tag{4-11}$$

Usually Δx_i is relatively small (e.g., 10 percent of the parameter value). These estimates of sensitivity are local (i.e., the value of the derivative may change at different points in the sample space). To partially alleviate this concern, the derivative may be evaluated at several points in the sample space. In the analyses presented herein, the derivative is transformed in one of two ways to allow for comparison of sensitivity coefficients between parameters whose units may differ. The first transformation is described by

$$S_i = \frac{\delta y}{\delta x_i}\frac{\overline{x_i}}{\overline{y}} \tag{4-12}$$

where S_i is the dimensionless normalized sensitivity coefficient. These normalized sensitivity coefficients are in the same form as the sensitivities defined by the regression analyses with the log of the normalized variables. Because S_i does not account for the range of the input parameter, a second transformation of the derivative is also performed where the derivative is multiplied by the standard deviation of the input parameter distribution. This transformation is described by

$$S_\sigma = \frac{\delta y}{\delta x_i}\sigma_{x_i} \tag{4-13}$$

Baseline cases were run with input parameter values set at seven random points within each parameter distribution range selected using the LHS technique. Seven points may not cover the whole space, but this limitation was imposed for expediency purposes.

4.1.3 Morris Method Technique

The Morris method (Morris, 1991) considers $\partial y/\partial x_i$ [3] as a random variable and uses the mean and standard deviation of the random variable to determine the sensitivity of y to x_i. A large value of mean of $\partial y/\partial x_i$ implies that x_i has a large overall influence on y. A large value of standard deviation implies that either x_i has significant interactions with other input parameters (i.e., x_k, $k = 1, 2, ..., I, k \neq i$) or its influence is highly nonlinear. Therefore, both the mean and standard deviation of $\partial y/\partial x_i$ are used to rank the influence of input parameters.

In the Morris method, the random variable, $\partial y/\partial x_i$, is evaluated using the current and the previous values of y:

$$\frac{\partial y}{\partial x_i} = \frac{y(x_1 + \Delta x_1, x_2 + \Delta x_2, \ldots, x_i + \Delta x_i, \ldots, x_I)}{\Delta x_i}$$

$$- \frac{y(x_1 + \Delta x_1, x_2 + \Delta x_2, \ldots, x_i, \ldots, x_I)}{\Delta x_i} \qquad (4\text{-}14)$$

This is in contrast to the differential analysis method in which $\partial y/\partial x_i$ is evaluated using the current and baseline values of y, as presented in Eq. (4-11).

To compute $\partial y/\partial x_i$, a design matrix is constructed using input variables as shown:

$$\begin{bmatrix} x_1 & x_2 & \cdots & x_{i-1} & x_i & x_{i+1} & \cdots & x_I \\ \cdots & \cdots & \cdots & \cdots & \cdots & \cdots & \cdots & \cdots \\ x_1 + \Delta_1 & x_2 + \Delta_2 & \cdots & x_{i-1} + \Delta_{i-1} & x_i & x_{i+1} & \cdots & x_I \\ x_1 + \Delta_1 & x_2 + \Delta_2 & \cdots & x_{i-1} + \Delta_{i-1} & x_i + \Delta_i & x_{i+1} & \cdots & x_I \\ x_1 + \Delta_1 & x_2 + \Delta_2 & \cdots & x_{i-1} + \Delta_{i-1} & x_i + \Delta_i & x_{i+1} + \Delta_{i+1} & \cdots & x_I \\ \cdots & \cdots & \cdots & \cdots & \cdots & \cdots & \cdots & \cdots \\ x_1 + \Delta_1 & x_2 + \Delta_2 & \cdots & x_{i-1} + \Delta_{i-1} & x_i + \Delta_i & x_{i+1} + \Delta_{i+1} & \cdots & x_I + \Delta_I \end{bmatrix} \begin{matrix} 1 \\ \\ i \\ i+1 \\ i+2 \\ \\ I \end{matrix}$$

where $\Delta_i = \Delta x_i$. To construct this matrix, the range of each variable is subdivided into (p-1) intervals using (p-1) equally spaced points. Then x_i values are randomly sampled from these p intervals. It should be noted

---

[3]Strictly speaking, $\partial y/\partial x_i$ should be denoted as $\Delta y / \Delta x_i$ because Δx_i is not necessarily a small value as in the case of differential analysis. Here the notation is maintained to simplify the comparison with the differential analysis method.

that each interval represents the left-most value in the original distribution. The increment Δ is now represented by $\Delta_i = p/2(p-1)$.

To implement the Morris method, the input variables are first normalized using the following transformation such that the transformed input parameters, x_i^*, range from 0 to 1.

$$x_i^* = \frac{x_i - x_{i\min}}{x_{i\max} - x_{i\min}}, \quad i = 1,2,i...,I \tag{4-15}$$

To minimize the influence of the baseline sampling on the parameter sensitivity, seven samples are collected for each random variable $\partial y/\partial x_i$. The steps necessary to obtain the design matrix, which includes these samples are presented in appendix A. This was accomplished by sampling seven baseline realizations using LHS from which seven different design matrices were constructed.

4.1.4 The Fourier Amplitude Sensitivity Test Method

Both the differential analysis and the Morris method handle one input parameter at a time. For a nonlinear computational model, input parameters are likely to have strong interactions. It would be desirable therefore to have a sensitivity analysis method that would investigate the influence of all input parameters at the same time. The Fourier Amplitude Sensitivity Test (FAST) method (Cukier et al., 1973) does this. It first applies trigonometric transforms to the input parameters:

$$x_i = g_i(\sin \omega_i s), \quad i = 1, 2, \ldots, I \tag{4-16}$$

The trigonometric transforms relate each input parameter, x_i, to a unique integer frequency, w_i. All transforms have a common parameter s, where $0 \le s \le 2\pi$. As s varies from 0 to 2π, all the input parameters vary through their ranges simultaneously at different rates controlled by the integer frequencies assigned to them through Eq. (4-16). Equally spaced values of s between 0 and 2π are chosen to generate values of x_i in Eq. (4-16). Because trigonometric transforms and integer frequencies are used in Eq. (4-16), the output, y, becomes periodic in s, and the discrete Fourier analysis can be used to obtain the Fourier coefficients of y with respect to each integer frequency (appendix B). The sensitivity of y to x_i is measured by the magnitudes of the Fourier coefficients with respect to ω_i, and y is considered sensitive to the input parameters with larger magnitudes of Fourier coefficients.

The use of integer frequencies causes some errors due to aliasing among Fourier coefficients. The integer frequencies in Eq. (4-16) were chosen to minimize interactions among Fourier coefficients to ensure, as much as possible, that the particular coefficient, A_i (appendix B), through the particular integer frequency, ω_i, represents only the influence of the corresponding input parameter, x_i. Appendix B explains how the integer frequencies are selected and how the FAST method is implemented. Assuming $0 \le x_i \le 1$, the trigonometric transformation functions used here were

$$x_i = \frac{1}{2} + \frac{1}{\pi} \arcsin[\sin(\omega_i s + r_i)], \quad i = 1,2,\ldots, I \tag{4-17}$$

where r_i, and $i = 1, 2, ..., I$, are random numbers. If the range of variation of a parameter is different from [0, 1], Eq. (4-17) can be modified easily.

Currently, implementation of the FAST method is limited to 50 input parameters. According to Cukier et al. (1975), as many as 43,606 realizations are needed to perform a satisfactory analysis on 50 input parameters to avoid aliasing among any four Fourier amplitudes.

4.1.5 Parameter Tree Method

The parameter tree method examines total system output relative sensitivity and correlations of output to subgroups of input parameters. The parameter trees appear similar to event trees but are different because no specific initiating event is associated with parameter trees. In this technique, the Monte Carlo (or LHS) method is used to examine the possible outcomes of a combination of parameter sets. Bins of realizations are examined where the bins are determined by a commonality of their input parameter states (e.g., all sampled input parameters above their median value).

To analyze the outputs, y_j, in Eq. (4-1) to determine the sensitivity and correlations of output, y, to subgroups of the input parameters, x_n, $n = 1, 2, ..., N$, where $N<I$, a tree structure is developed. The parameter tree partitions input parameter space into bins, each bin forming a branch of the tree based on a partitioning (or branching) criterion as done in an event tree. The simplest branching criterion is a classification based on parameter magnitude that treats sampled input values as either a + or a – depending on whether the sampled value is greater or less than the branching criterion value. The event tree analogy is appropriate if a + is considered a parameter failure and—is considered a parameter success, or vice-versa. Figure 4-5 depicts a general parameter tree. To explain figure 4-5 using a system model, a number of realizations are generated for a given scenario class. Next, the realizations are partitioned into two subsets determined by whether the first influential parameter, x_i, is greater than or less than a specified level. Realizations with a high value are all treated as a + and low as a –, regardless of their position within the subset. Let the number of realizations associated with the two branches be N_{1+} and N_{1-}. Next, the output variable, – 1, is examined for realization associated with each branch of the tree. The number of realizations with y greater than a criterion (e.g., mean) are counted for both the branches. Let these numbers be L_{1+} ($L_{1+} \leq N_{1+}$) and L_{1-} ($L_{1-} \leq N_{1-}$). The difference between L_{1+} / N_{1+} and L_{1-} / N_{1-} is a measure of sensitivity of y to x_j. The procedure is repeated in each of these two subsets with the next influential parameter to be considered and so on until each of the influential parameters is considered. This procedure determines 2^M bins of realizations where M is the number of influential parameters. Note that not every sampled parameter in the system model need be considered if a subset of the sampled parameters satisfactorily explains system behavior of interest. Sensitivity measures similar to those over explained for one parameter are developed for a set of parameters[4]

Another measure of influence of a subset of parameters may be defined through the contribution that realizations in a bin make to specific statistics of the output. For example, one can compute the expected value of y for realizations associated with each branch of the tree and compare these means to the overall mean of y. Statistics other than the mean can be used or probability distributions can be developed for each branch and compared to the overall probability distribution of y. If, for example, the probability of y exceeding a certain limiting value (perhaps specified by regulations) is of interest, one could find the value

---

[4]Jarzemba, M.S., and B. Sagar. 1999. A Parameter Tree approach to estimating system sensitivities to parameter sets. Accepted for publication in *Reliability Engineering & System Safety.*

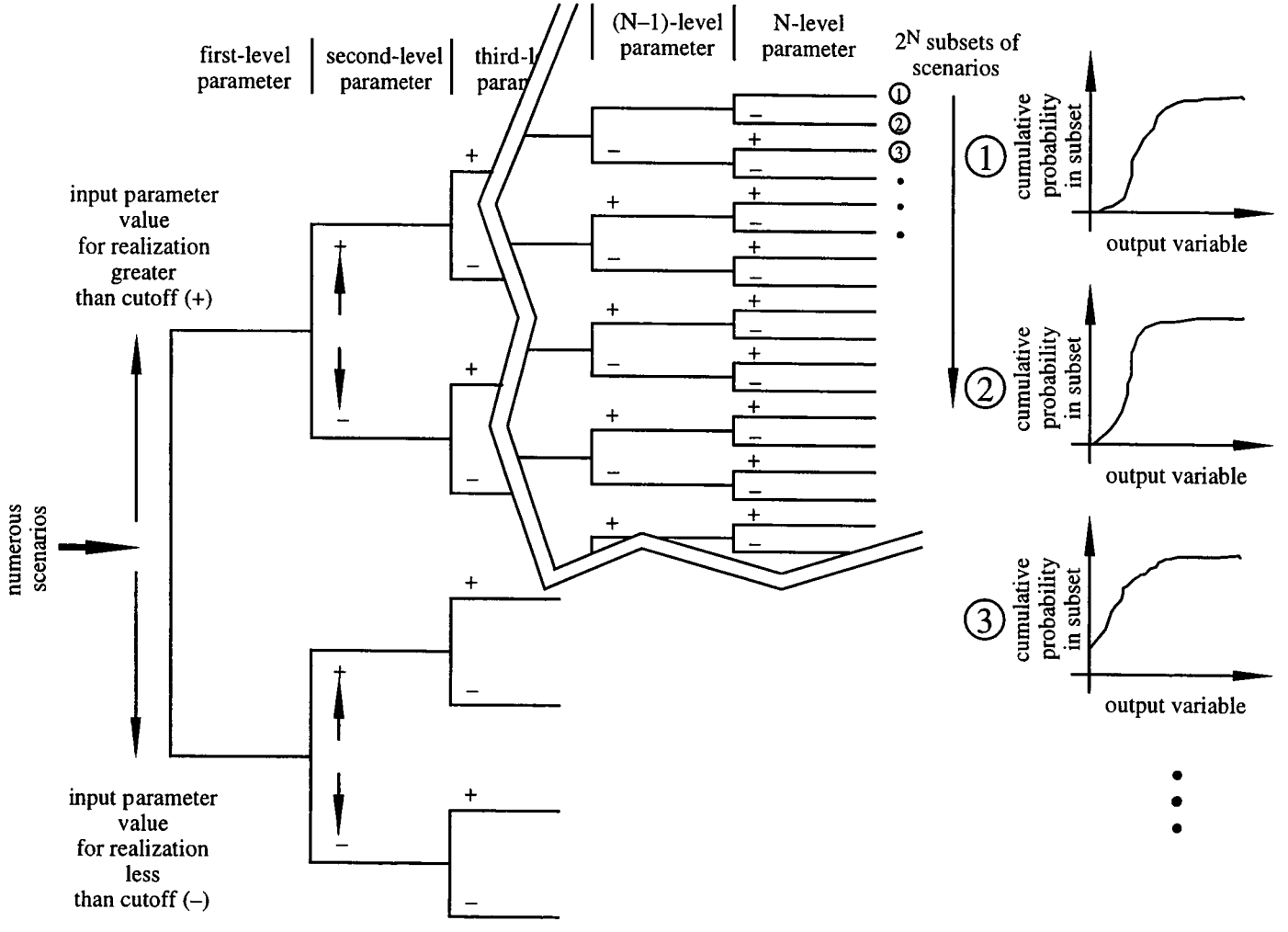

Figure 4-5. General parameter tree

of such exceedance probability for each branch and estimate (in a relative sense) the contribution that each parameter set makes to such a probability. Formally then, if T is a statistic (e.g., mean, mode, median, exceedance probability) of interest, for the second level of the tree, the ratios of $T_{1^+2^+}, T_{1^+2^-}, T_{1^-2^+}, T_{1^-2^-}$ to T or y as a whole provide measures of relative sensitivity.

The branching criterion can be something other than the magnitude of a parameter. One of the more useful possibilities is to assume the system is made up of several components in series such that the output from one component becomes an input to the second and so on. With this conceptualization, the branching criterion can be stated as the magnitude of the output of a component. In this case, each branch of the tree would represent the contribution of a component or a set of components to overall system performance. Relative sensitivity measures could then be defined in exactly the same manner as explained previously.

4.2 ANALYSIS OF SENSITIVITY FROM MONTE CARLO RUNS

This section presents the sensitivity and uncertainty analyses results generated using methods described in the previous section. Statistical results of the 1,000-vector Monte Carlo runs, treated separately from the differential analysis, Morris method, and FAST method will be covered first in this section. Comparison of the results among methods will be presented in subsequent sections.

4.2.1 Procedure for Screening Monte Carlo Sensitivity Results

The Monte Carlo simulation results were screened to estimate which variables were likely to be significantly influential and provide an estimate of the sensitivity coefficients. The sequence by which these procedures were employed is described next.

Preliminary screening analyses—This stage of the analyses used a variety of techniques to determine in gross terms whether an independent variable was possibly related to dose. All variables that passed any of the screening tests are included in the subsequent analyses. For all analyses, zero values of dose were eliminated from the data sets because these were inadmissible for logarithmic and power law transformations. For each TPI (10,000 or 50,000 yr), the following procedures were employed:

- Visual inspection of scatter plots
- t-statistic test for single linear regression of dose versus each variable
  - Normalized variables
  - Log of normalized variables
- Stepwise linear regression
  - Normalized variables
  - Log of normalized variables
  - Scaled power transformed variables
  - Ranks of variables
- Nonparametric tests
  - K-S test
  - Sign test

Linear models—For each TPI, the list of independent variables from any of the preliminary screening analyses was used to construct a linear model, to be fitted by regression to the data, using Eq. (4-7). This was also performed on the logarithmically transformed variables.

Refined screening—The regression coefficients resulting from the linear models were then screened for significance using the t-test. The hypothesis that an independent variable is significant was rejected if the absolute value of t was less than 1.96, corresponding to a 95th percentile confidence limit, for either the normalized or logarithmically transformed variables. Note that the t-test performed on the single-variable regressions in the first step frequently accepted variables that were later screened by the refined analysis.

Transform sensitivity of the variables resulting from refined screening to standardized form—Use Eq. (4-5) to transform the normalized sensitivities resulting from regression of the logarithmically transformed variables to the standardized form.

4.2.1.1 Sensitivity Results from Monte Carlo Analysis

This section presents the sensitivity analyses based on the statistical analysis of a 1,000-vector Monte Carlo analysis of the basecase for 10,000- and 50,000-yr TPI.[5] The screening and regression analyses are summarized in tables 4-1 and 4-2 for the 10,000- and 50,000-yr TPIs, respectively. The column headings in tables 4-1 and 4-2 have the following explanations:

- Variable Name—The abbreviated name of the independent variable appearing potentially sensitive in any of the screening analyses. There is a complete list of the variable names in appendix D.

- Step norm—Variables that appeared to be influential from stepwise regression of the normalized variables.

- Step lnorm—Variables that appeared to be significant for stepwise regression of the log of the normalized variables.

- Step rank—Variables that appeared to be significant from stepwise regression of the ranks of the variables.

[5]The time period of interest of 100,000 yr used in presenting the basecase results is different from that used in the sensitivity analyses (10,000 and 50,000 yr) primarily because the basecase results were also used in reviewing the Department of Energy Total System Performance Assessment-Viability Assessment results, which extended to 100,000 yr and beyond.

Table 4-1. Summary of regression and screening for basecase, 10,000-yr time period of interest

Variable Name	Step Norm	Step Lnorm	Step Rank	Step Lilli	KS + Sign	t-norm	t-lnorm	t-Lilli	In LM Model	t-stat Norm	t-stat Lognorm	Sens ?
AAMAI@S	—	X	X	X	X	X	X	X	X	2.86	8.03	X
MAPM@GM	—	X	X	—	X	X	X	X	X	1.61	3.16	X
MATI@GM	—	—	—	X	—	X	X	X	X	2.13	1.06	X
FOC-R	—	X	X	—	X	—	X	X	X	1.36	0.10	—
FOCTR-R	—	—	—	X	—	—	—	X	—	—	—	—
InnOvrEI	—	—	—	—	X	—	—	—	—	—	—	—
SSMO-RPR	X	—	—	—	—	—	—	—	—	—	—	—
SSMOV201	—	—	—	—	X	—	—	—	—	—	—	—
SSMOV501	X	—	—	—	—	X	—	—	X	1.96	0.15	X
Fow*	X	X	X	X	X	X	X	X	X	4.10	14.60	X
Fmult*	X	X	X	X	X	X	X	X	X	3.01	7.65	X
SbArWt%	X	X	X	X	X	X	X	X	X	32.40	15.37	X
WP-Def%	X	X	X	X	X	X	X	X	X	4.34	12.66	X
InitRSFP	X	X	X	X	—	X	X	X	X	0.09	2.27	X
SfWt%I1	—	—	—	—	X	—	—	—	—	—	—	—
SFWt%I3	X	—	—	—	X	X	—	—	X	2.28	0.91	X
SFWt%S46	X	—	—	—	X	X	—	—	X	2.43	0.37	X
MKDPPwAm	—	—	—	—	X	—	—	—	—	—	—	—
MKDCHzNp	—	—	—	—	X	—	—	—	—	—	—	—
MKDCHzNp	—	—	—	—	X	—	—	—	—	—	—	—
MKDUFZNp	—	—	—	—	X	—	—	—	—	—	—	—
MKDCHzU	—	—	—	—	X	—	—	—	—	—	—	—
MKDCHvPb	—	—	—	—	X	—	—	—	—	—	—	—
MKDBFwPb	—	—	—	—	X	—	—	—	—	—	—	—

Table 4-1. Summary of regression and screening for basecase, 10,000-yr time period of interest (cont'd)

Variable Name	Step Norm	Step Lnorm	Step Rank	Step Lilli	KS + Sign	t-norm	t-lnorm	t-Lilli	In LM Model	t-stat Norm	t-stat Lognorm	Sens ?
MKDBFwSe	X	—	—	—	—	X	—	—	X	2.19	0.78	X
MPrmTSw	—	—	—	—	X	X	X	—	X	0.54	0.35	—
FPrm_CHv	—	—	—	—	X	—	—	—	—	—	—	—
FPrm_BFw	X	—	—	—	—	X	—	—	X	2.28	—	X
ARDSAVAm	—	—	—	—	—	—	—	X	X	0.75	0.49	—
ARDSAVNp	—	X	X	—	X	—	X	—	X	1.43	2.91	X
ARDSAV_I	—	X	X	X	—	—	X	X	X	0.32	4.86	X
ARDSAVTc	X	X	X	X	X	X	—	X	X	2.90	5.04	X
ARDSAV_U	—	—	—	X	X	—	X	X	X	0.22	1.40	—
ARDSAVPu	—	—	—	—	X	—	X	—	—	—	—	—
APrs_SAV	—	—	—	X	—	X	X	—	X	0.09	1.95	X
WPRRG@20	X	X	X	X	X	X	X	X	—	2.90	4.72	X
NWFZnW	—	—	—	—	X	—	—	—	—	—	—	—
NELCDAmt	—	—	—	—	X	—	—	—	—	—	—	—

Table 4-2. Summary of regression and screening for basecase, 50,000-yr time period of interest

Variable Name	Step Norm	Step Lnorm	Step Rank	Step Lilli	KS + Sign	t-norm	t-lnorm	t-Lilli	In LM Model	t-stat Norm	t-stat Lognorm	Sens ?
AAMAI@S	—	—	—	—	X	X	X	X	—	—	—	—
MATI@GM	—	—	—	—	X	—	—	—	—	—	—	—
H2OFThK	—	—	—	X	—	—	—	—	—	—	—	—
AA_2_1	X	X	X	X	—	X	X	X	X	1.67	-31	X
OO-CofLC	X	X	X	X	X	X	X	X	—	—	—	—
SSMO-RE	—	—	—	X	—	—	—	—	—	—	—	—
SSMO-RPR	X	—	—	—	—	X	—	—	—	3.33	9.30	X
SSMO-JS5	—	—	—	—	X	—	—	—	X	-2.22	0.04	X
SSMOV206	X	—	—	—	—	—	—	—	X	0.55	2.00	X
SSMOV408	X	—	—	—	X	X	—	—	X	1.81	0.66	—
Fow*	—	—	—	—	—	—	X	X	—	—	—	—
Fmult*	—	—	—	X	—	—	—	—	X	-0.51	-2.14	X
SbArWt%	X	X	X	X	X	X	X	X	X	2.46	35.20	X
InitRSFP	X	X	X	X	X	X	X	—	X	-2.18	4.20	X
SbGFRATF	—	X	—	—	—	—	—	—	X	-1.79	-2.92	X
SFWt%C1	—	X	X	X	—	—	—	X	X	0.88	3.96	X
SFWt%C2	—	X	X	X	X	—	—	X	X	1.69	3.57	X
SFWt%C3	—	X	X	X	—	—	X	X	X	1.13	4.20	X
SFWt%C5	—	—	X	—	—	—	—	—	—	—	—	—
SFWt%C6	—	—	X	—	—	—	—	—	X	0.22	2.13	X
SFWt%C7	—	X	X	—	—	—	—	—	X	0.28	3.53	X
MKDPPwAm	—	—	—	—	X	—	—	—	—	—	—	—
MKDCHvNp	—	—	—	X	—	—	—	—	X	-0.7	-2.11	X
MPrm_TSw	—	—	—	—	X	X	X	X	—	—	—	—

Table 4-2. Summary of regression results for 50,000-yr time period of interest (cont'd)

Variable Name	Step Norm	Step Lnorm	Step Rank	Step Lilli	KS + Sign	t-norm	t-lnorm	t-Lilli	In LM Model	t-stat Norm	t-stat Lognorm	Sens ?
MPrm_UFZ	X	—	—	—	—	X	—	—	—	—	—	—
FPrs_PPw	X	—	—	—	—	—	—	—	—	—	—	—
ARDSAVAm	X	—	—	—	X	X	X	—	—	—	—	—
ARDSAVNp	X	X	X	X	X	X	X	X	X	-4.16	24.40	X
ARDSAV_I	—	X	X	X	—	—	X	X	X	-0.71	-3.16	X
ARDSAVTc	—	X	X	X	—	—	X	X	X	0.08	-4.6	X
ARDSAV_U	—	—	—	X	X	X	X	X	X	-1.12	-2.57	X
ARDSAVTh	—	—	—	—	X	—	X	X	X	-0.82	1.20	
APrs_SAV	—	X	—	X	—	—	X	X	X	-1.02	-3.29	X
WPRRG@20	X	X	X	X	X	X	X	X	X	-2.2	-9.2	X

- Step Lilli—Variables that appeared to be significant from stepwise regression of the power-law transformed variables.

- KS + Sign—Variables that passed both the K-S and Sign tests.

- t-norm—Variables for which the t-value of a single-variable regression of the normalized variables is greater than 1.96 (95-percent confidence level).

- t-lnorm—Variables for which the t-value of a single-variable regression of the log of the normalized variables is greater than 1.96.

- t-Lilli—Variables for which the t-value of a single-variable regression of the power-law transformed variables is greater than 1.96.

- Include in LM—Variables included in linear models for multiple linear regression.

- t-stat norm—The t-statistic for the variable in the linear model for normalized variables.

- t-stat lognorm—The t-statistic for the variable in the linear model for log of normalized variables.

- Sens ?—The variable had a t-statistic in either the normalized or lognormalized multiple linear regression analysis that exceeded 1.96 (95 percent confidence).

Tables 4-3 and 4-4 summarize the sensitive parameters resulting from linear regression for the 10,000- and 50,000-yr TPIs with using standardized variables that give a truer indication of parameter sensitivity by taking into account the standard deviations of the independent variables sampled in the Monte Carlo analyses. Figures 4-6 and 4-7 present sensitive parameters obtained from step-wise regression analyses using standardized input variables for 10,000 and 50,000 yr, respectively. The ranks of the standardized variables are compared to the ranks from the other sensitivity measures in section 4.3. In these tables, $\bar{x}$ and $\bar{y}$ represent the mean of the input and output variables. Variables σ_{xi} and σ_{yi} in tables 4-3 and 4-4 represent the standard deviations of normalized input and output variables (indicated by x^*_i and y^*_i) . The headings m-norm and m-lognorm represent coefficients from regression equations using normalized variables and lognormalized.

4.2.1.2 Parameter Sensitivity at High End of Peak Doses

Doses at the high end of the calculated range, and their associated parameter sensitivities, may be of more interest than low doses. To develop this idea further, vectors from the basecase were segregated into those with doses higher than a threshold of 10 millirem/yr, and those below for the 50,000-yr TPI. The higher category contained 51 vectors and the lower category contained the balance of 949 vectors.

A t-test was then conducted on means of the independent variables to determine if the means of the two populations are statistically the same at the 95-percent confidence limit. For each independent variable x_1 from the high-dose category and x_2 from the low-dose category, calculate the sample means μ_1, and μ_2, together with the variances σ_1 and σ_2. At the 95-percent significance level, accept the hypothesis if

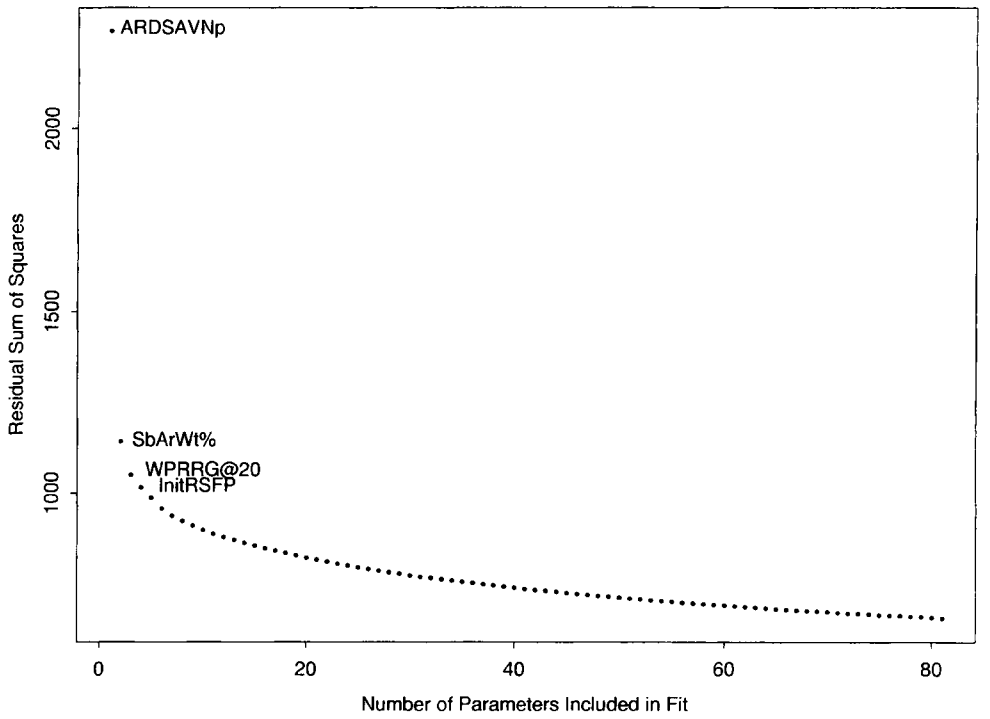

Figure 4-6. Plot of the residual sum of squares versus number of parameters included in the fit for the basecase with a time period of interest of 10,000 yr

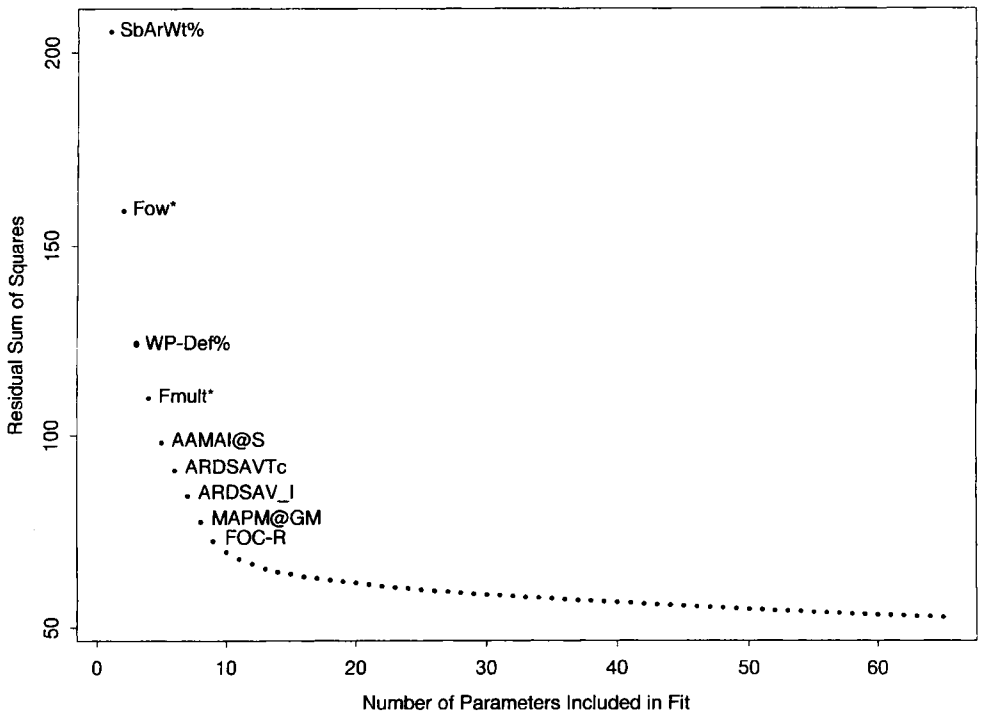

Figure 4-7. Plot of the residual sum of squares versus number of parameters included in the fit for the basecase with a time period of interest of 50,000 yr

Table 4-3. Standardized sensitivities for basecase, 10,000-yr time period of interest

Variable Name	m-norm	$\frac{\sigma_{x_i}}{\sigma_y}\frac{\bar{y}}{\bar{x}_i}$	$\frac{\partial y^*}{\partial x_i^*}$ (norm)	m-lognorm	$\frac{\partial y^*}{\partial x_i^*}$ (lognorm)
AAMAI@s	0.659	0.134	0.088	0.934	0.125
MAPM@GM	1.208	0.042	0.051	1.463	0.061
MATI@GM	1.208	-0.05586	-0.067	0.367	-0.021
SSMOV501	0.485	0.136	0.066	-0.0174	-0.002
Fow*	0.401	0.326	0.131	1.08	0.353
Fmult*	0.64	0.1456	0.093	1.075	0.157
SbArWt%	0.612	0.161	0.099	1.054	0.17
WP-DEF%	0.847	0.164	0.139	1.079	0.177
InitRSFP	0.0492	0.0586	0.003	-0.726	-0.043
SFWt%I1	0.429	0.1684	0.072	0.062	0.01
SFWt%S46	-0.462	0.168	-0.078	-0.025	-0.004
MKDBFwSe	0.11	0.636	0.07	0.016	-0.01
FPrm_BFw	0.104	0.686	0.071	0.013	0.049
ARDSAVNp	-0.0807	0.567	-0.046	-0.148	-0.084
ARDSAV_I	-0.0872	.1149	-0.010	-0.827	-0.095
ARDSAVTc	-0.349	0.264	-0.092	-0.35	-0.092
APrs_SAV	-0.0845	0.0335	0.003	-1.141	-0.038
WPRRG@20	-1.125	0.0818	0.092	-1.08	-0.088

Table 4-4. Standardized sensitivities for basecase, 50,000-yr time period of interest

Variable Name	m-norm	$\frac{\sigma_{x_i}}{\sigma_y}\frac{\bar{y}}{\bar{x}_i}$	$\frac{\partial y^*}{\partial x_i^*}$ (norm)	m-lognorm	$\frac{\partial y^*}{\partial x_i^*}$ (lognorm)
AAMAI@s	0.9314	0.134	0.101	0.8856	0.089
SSMO-RPR	0.0154	0.0292	-0.067	-0.0154	-0.0004
SSMO-JS5	0.4284	0.0389	0.0170	0.5603	0.0.022
SSMOV206	0.5560	0.0989	0.0550	0.0700	0.0007
Fmult*	-0.0837	0.1840	-0.015	-0.135	-0.025
SbArWt%	1.0020	0.2087	0.2090	1.0810	0.2260
InitRSFP	-0.9080	0.0726	-0.066	-0.6052	-0.044
SbGFRATF	-0.7740	0.0700	-0.0540	-0.4374	-0.031
SFWt%C1	0.1448	0.2090	0.0300	0.1210	0.0250

Table 4-4. Standardized sensitivities for basecase, 50,000-yr time period of interest (cont'd)

Variable Name	m-norm	$\frac{\sigma_{x_i}}{\sigma_y}\frac{\bar{y}}{\bar{x}_i}$	$\frac{\partial y^*}{\partial x_i^*}$ (norm)	m-lognorm	$\frac{\partial y^*}{\partial x_i^*}$ (lognorm)
SFWt%C2	0.2445	0.2090	0.0510	0.1080	0.0230
SFWt%C3	0.1631	0.2090	0.0340	0.1284	0.0270
SFWt%C6	0.0319	0.2090	0.0070	0.0706	0.0150
SFWt%C7	0.0403	0.2090	0.0080	0.1083	0.0290
MKDCHvNp	-0.0164	1.2900	-0.021	-0.0338	-0.044
ARDSAVNp	-0.2	0.6930	-0.069	-0.72	-0.499
ARDSAV_I	-0.151	0.1420	-0.008	-0.242	-0.034
ARDSAVTc	-0.0083	0.3270	0.0030	-4.6	-0.047
ARDSAV_U	-0.0407	0.9280	-0.038	-0.0623	-0.058
APrs_SAV	-0.7362	0.0417	-0.031	-0.8617	-0.036
WPRRG@20	-0.6631	0.1010	0.0670	-0.945	0.0040

$$t = \frac{|\mu_1 - \mu_2|}{\sqrt{\sigma_1^2/m_1 + \sigma_2^2/m_2}} < 1.96 \qquad (4\text{-}18)$$

where m_1 and m_2 are the number of samples in sets 1 and 2. The results of this screening are listed in table 4-5.

Note there were several parameters left off the list because they were probably spurious and cannot have had an effect on the results. For example, the water use parameter at 10 km was sampled but not used. Several of the significant parameters were associated with properties of Am and Pu, although neither ^{241}Am nor ^{239}Pu have any doses at all. The effects of the parameters in the models are due in large part to the deliberate correlations of several of the radionuclide retardation parameters, and it is likely that these factors show up because of the large contribution to peak dose of ^{237}Np. In the case of ^{241}Am, some dose also may be indirectly attributed to ^{241}Am decaying to ^{237}Np. Dependence of several of the parameters, particularly MKDUFZAm, MKDUFZ_U, and MPrm_UFZ, are suspicious, since these parameters were sampled but not used. It is likely that these results, and possibly others, are spurious because the relatively small sample size of 51 samples in the high-dose category. The same also is likely to be true for U, since the contribution of ^{234}U to dose is small.

Inspection of the terms that passed this screening and their respective t statistics indicates strong relationships between some of the parameters and relatively high doses, in particular the subarea wet fraction (SbArWt%), matrix permeability of the Topopah Springs welded tuff (MPrm_TSw), and retardation factors for Am, Np, U, and Th.

Table 4-5. t-test on means of high-and low-dose categories for 50,000-yr time period of interest

Variable Name	t value
AAMAI@s	3.79
OOCofLC	3.89
SSMO-RPR	3.13
SSMOV203	2
SbArWt%	7.7
WP-Def%	2.11
SFW%S37	2.15
MKDUFZAm	4.16
MKDUCFNp	3.23
MKD_CHvU	2.88
MKD_CHzU	2.82
MKD_UCFU	2.78
MKDUFZ_U	2.57
MKDTSwTh	2.93
MKDCHvTh	2.93
MKDUCFTh	2.4
MKDBFwTh	3.42
MPrm_TSw	6.14
MPrm_UFz	1.97
FPrs_CHz	2.68
FPrs_PPw	2.12
ARDSAVAm	6.72
ARDSAVNp	15.8
ARDSAVTh	3.98

4.3 ANALYSIS OF SENSITIVITY FROM NONSTATISTICAL METHODS

4.3.1 Results from Differential Analyses

Differential analyses were performed using TPA Version 3.2 code with the basecase. Cases where faulting and igneous activity were activated in the TPA code were modeled separately. A total of 223 input parameter values were perturbed for each series. The input parameters perturbed are defined by a distribution in the basecase tpa.inp input file. The parameters sampled in the tpa.inp file are the ones where a significant amount of uncertainty remains in their value or they have been shown potentially significant to estimating peak dose in the process-level sensitivity analyses.

Seven random sets of input parameters were evaluated. Perturbations to the parameters in these random sets were selected so that the parameter values were maintained in their respectively defined ranges;

the first, second, fourth, fifth, and seventh random set of input parameters were perturbed by +1 percent, while the third and sixth random set of input parameters were perturbed by−1 percent. The selection of random values yields calculations similar to one realization of a probabilistic TPA code run. The percent perturbations are with respect to the baseline (i.e., local) parameter value.

In TPA Version 3.2 code, transport through the UZ stratigraphic units is neglected for those units where groundwater residence time is less than 10 yr, or 10 percent of the residence time for the entire UZ below the repository (Mohanty and McCartin, 1998). Differential analyses, in which UZ transport calculations are omitted because of this assumption, will result in peak dose showing no sensitivity to parameters that describe UZ properties in those stratigraphic units excluded from the transport calculations. For example, when all parameters were set at their mean values, the UZ portion of NEFTRAN was skipped for a majority of the subareas. Thus, sampled UZ flow and transport (UZFT) parameters did not show any sensitivity in these calculations. However, when the transport time in the UZ is short, it is unlikely that any of the UZ parameters would have a substantial effect on the peak dose, so this should not have a significant effect on the results of the differential analysis.

For all sets of the random parameters, the WPs did not fail from either seismicity or corrosion in the 10,000-yr TPI but did fail from corrosion within the 50,000-yr TPI. The baseline dose values in these cases are solely due to initially defective WPs.

Each set of base values was used in a TPA code run to determine the reference value of peak dose necessary to calculate several sensitivity measures. The baseline value peak doses can be found in appendix E.

The results of the differential analysis are shown in the following tables for TPIs of 10,000 and 50,000 yr in appendix E: tables E-1 and E-2 for the basecase, tables E-3 and E-4 for the basecase plus faulting, and table E-5 for the basecase plus igneous activity. The basecase plus igneous activity was not run for the 50,000-yr TPI because the results are not expected to change after the 10,000-yr TPI when groundwater dose dominates and the primary contributors to ground surface dose have decayed. Variables tested but indicating zero sensitivity at all baseline values are not shown in the tables for the basecase.

Tables E-1 through E-5 of appendix E show the sensitivities calculated using four different measures:

(1) The geometric mean of the absolute value of the sensitivity coefficient S_i [see Eq. (4-12)] was calculated for the seven base values. The geometric mean is useful for emphasizing parameters that are sensitive over the entire range of base values. In cases where the sensitivity coefficient was zero (i.e., smaller than the least significant digit in code output) at a base value, the geometric mean is an upper estimate for that parameter.

(2) The arithmetic mean of the absolute values of S_i was calculated for the seven base values.

(3) The highest sensitivity of S_i is calculated at any of the seven points. This sensitivity measure is useful to determine if the parameter is sensitive at any of the seven points.

(4) Arithmetic mean of the derivative is weighted by the standard deviation of the input parameter. This sensitivity measures the response of peak dose to each of the independent variables

weighted by their standard deviation. The standard deviations are determined by the parameter range and distribution used in the Monte Carlo analyses. This measure takes into account the magnitude of the change in peak dose and the uncertainty in the independent variables. For comparison, the normalized sensitivity measure, S_i, is a relative sensitivity where the slope is scaled by the local values of dose and the independent variable. Therefore S_i does not depend on whether the baseline dose is small or large, but only on the change in dose relative to the change in the independent variable.

Measure (4) was used to sort the input parameters in descending order because it reflects both the absolute value of peak dose and the uncertainty in the independent variables. The other three sensitivity measures are also given in the tables provided in appendix E. The lists of influential parameters are generated based on the top 10 parameters for the basecase (i.e., at 10,000- and 50,000-yr TPIs).

The tables in appendix E provide a list of the parameters that showed nonzero sensitivity at any of the seven baseline values about which the derivatives were evaluated. Some of the sensitivities shown, however, were exceedingly small. To focus attention on the parameters to which peak dose showed the largest sensitivity for the current models on which this report is based, tables 4-6 and 4-7 list the influential parameters for the basecase [i.e., the top 10 parameters based on the mean of S_σ as in Eq. (4-13)] for the two TPIs. Table 4-8 lists the influential parameters for the disruptive scenarios for the two TPIs. The influential parameters for the disruptive scenarios were determined by including any parameter whose sensitivity was within one order of magnitude of the most influential parameter from the basecase using measure 4. For the igneous activity scenario, all sampled parameters are influential, and for the faulting scenario, three sampled parameters are influential for the 10,000-yr TPI, but no sampled parameters are influential for the 50,000-yr TPI. The reason for this difference is that the only impact of faulting on the repository is failure of the additional WPs. In the longer TPI, all the WPs fail by corrosion, and the peak dose is dominated by the WPs failed by corrosion.

4.3.2 Results from the Morris Method

The Morris method was applied to the TPA Version 3.2 code with the basecase parameter set. A total of 246 input parameters were investigated. A $1,729 \times 246$ matrix was generated and used in sampling input parameters to the TPA code for the 1,729 realizations. The 1,729 realizations [(246 +1)× 7] produced seven samples for each $\partial y/\partial x_i$, which were used to calculate mean and standard deviation for each $\partial y/\partial x_i$. Seven samples were chosen to be consistent with the differential analysis method.

Figures 4-8 and 4-9 show graphs for the values of mean (abscissa) and standard deviation (ordinate) of $\partial y/\partial x_i$ values for the 10,000- and 50,000-yr TPI. As described earlier, the greater the distance $\partial y/\partial x_i$ for parameter x_i is from zero the more influential the parameter x_i is. Physically, a point with large values of both mean and standard deviation suggests that the corresponding input parameter has not only a strong nonlinear effect itself, but also strong interactive effects with other parameters on the output.

The top ten most influential input parameters identified by the Morris method are listed in table 4-6 for the 10,000 yr TPI and table 4-7 for the 50,000-yr TPI, where each parameter was standardized according to Eq. (4-3). For the 10,000-yr TPI, the listed parameters are either related to thermal reflux or transport properties in alluvium. But for the 50,000-yr TPI, no thermal reflux-related parameters make the top 10 list of influential parameters. The parameter, WPRRG@20 (well pumping rate for farming receptor group located at or beyond 20 km from YM), appears in both 10,000- and 50,000-yr TPIs, as well as some

Table 4-6. Top 10 influential parameters (standardized) from statistical and nonstatistical analyses for 10,000-yr time period of interest

Rank	Normalized Variables	Log-Normalized Variables	Differential Analysis	Morris Method	FAST Method
1	WP-Def%	Fow*	ARDSAVTc	FOCTR-R	WPRRG@20
2	Fow*	WP-Def%	FOCTR-R	FOC-R	ARDSAV_I
3	SbArWt%	SbArWt%	Fow*	FOCTR	AAMAI@S
4	Fmult*	Fmult*	ARDSAV_I	WPRRG@20	Fow*
5	ARDSAVTc	AAMAI@S	SFWt%I3	AAMAI@S	Fmult*
6	WPRRG@20	ARDSAV_I	WP-Def%	ARDSAV_U	MKDBFwSe
7	AAMAI@S	ARDSAVTc	ARDSAVSe	Fow*	SbArWt%
8	SFWt%S46	WPRRG@20	SbArWt%	WP-Def%	ARDSAVNp
9	SFWt%I1	ARDSAVNp	Fmult*	ARDSAV_I	SFWt%I3
10	FPrm_BFw	MAPM@GM	FOC-R	SbArWt%	MATI@GM

Abbreviation	*Description*	*Abbreviation*	*Description*	*Abbreviation*	*Description*
		Fmult*	FmultFactor	SbArWt%	SubAreaWetFraction
AAMAI@S	ArealAverageMeanAnnualInfiltrationAtStart[mm/yr]	FOC-R	FractionOfCondensateRemoved[1/yr]	SFWt%I1	SFWettedFraction_Initial_1
		FOCTR	FractionOfCondensateToward Repository[1/yr]	SFWt%I3	SFWettedFraction_Initial_3
ARDSAV_I	AlluviumMatrixRD_SAV_I	FOCTR-R	FractionOfCondensateToward RepositoryRemoved[1/yr]	SFWt%S46	SFWettedFraction_SEISMO4_6
ARDSAVNp	AlluviumMatrixRD_SAV_Np	Fow*	FowFactor		
ARDSAVSe	AlluviumMatrixRD_SAV_Se	FPrm_BFw	FracturePermeability_BFw_[m2]	WP-Def%	DefectiveFractionOfWPs/cell
		MATI@GM	MeanAverageTemperatureIncreaseA&GlacialMaximum[degC]		
ARDSAVTc	AlluviumMatrixRD_SAV_Tc	MAPM@GM	MeanAveragePrecipitationMultiplierAtGlacialMaximum	WPRRG@20	WellPumpingRateAtReceptorGroup20km [gal/day]
ARDSAV_U	AlluviumMatrixRD_SAV_U	MKDBFwSE	MatrixKD_BFw_Se[m3/kg]		

Table 4-7. Top 10 influential parameters from statistical and nonstatistical analyses for 50,000-yr time period of interest

Rank	Normalized Variables	LogNormalized Variables	Differential Analysis	Morris Method	FAST Method
1	SbArWt%	Fow*	ARDSAVNp	ARDSAVNp	WPRRG@20
2	AAMAI@S	WP-Def%	Fow*	WPRRG@20	AA_2_1
3	WPRRG@20	SbArWt%	OO-CofLC	APrs_SAV	ARDSAV_I
4	ARDSAVNp	Fmult*	AA_2_1	MKD_CHvU	Fmult*
5	SSMO-RPR	AAMAI@S	SbArWt%	SbArWt%	SbArWt%
6	InitRSFP	ARDSAV_I	ARDSAVTc	InitRSFP	SFWt%C3
7	SSMOV206	ARDSAVTc	Fmult*	ARDSAV_U	SFWt%C1
8	SbGFRATF	WPRRG@20	WPRRG@20	SFWt%C3	ARDSAV_U
9	SFWt%C2	ARDSAVNp	APrs_SAV	ARDSAVTc	SFWt%C5
10	ARDSAV_U	MAPM@GM	ARDSAV_I	SFWt%C6	SFWt%C6

Abbreviation	*Description*	*Abbreviation*	*Description*	*Abbreviation*	*Description*
AA_2_1	AA_2_1[C/m2/yr]	Fow*	FowFactor	SFWt%C2	SFWettedFraction_Corrosion_2
AAMAI@S	ArealAverageMeanAnnualInfiltrationAtStart[mm/yr]	InitRSFP	InitialRadiusOfSFParticle[m]	SFWt%C3	SFWettedFraction_Corrosion_3
				SFWt%C5	SFWettedFraction-Corrosion_5
APrs_SAV	AlluviumMatrixPorosity_SAV	MAPM@GM	MeanAveragePrecipitationMultiplierAtGlacialMaximum	SFWt%C6	SFWettedFraction_Corrosion_6
				SSMOpRPR	RockPossonRatioforSEISMO[]
ARDSAV_I	AlluviumMatrixRD_SAV_I	MKD_CHnv	MatrixKD_CHnv[m3/kg]	SSMOV206	VerticalExtentOfRockFall2_6[m]
ARDSAVNp	AlluviumMatrixRD_SAV_Np	OO-CofLC	CoefForLocCorrOfOuterOverpack	WP-Def%	DefectiveFractionOfWPs/cell
ARDSAVTc	AlluviumMatrixRD_SAV_Tc	SbArWt%	SubAreaWetFraction	WPRRG@20	WellPumpingRateAtReceptorGroup20km[gal/day]
ARDSAV_U	AlluviumMatrixRD_SAV_U	SbGFRATF	SubGrainFragmentRadiusAfterTransFrac[m]		
Fmult*	FmultFactor	SFWt%C1	SFWettedFraction_Corrosion_1		

Table 4-8. Most influential parameters from differential analysis for disruptive event scenarios

10,000-yr Time Period of Interest	50,000-yr Time Period of Interest
Igneous Activity Parameters	
VE-Power	VE-Power
ABMLFVDC	ABMLFVDC
VE-Dur	VE-Dur
VEROI-Tn	VEROI-Tn
VC-Dia	VC-Dia
WindSpd	WindSpd
AshMnPLD	AshMnPLD
Faulting Parameters	
FERIO-Tn	None[1]
SFWt%FO	
NEFZnW	

[1]No sensitivities greater than zero

parameters related to transport properties in alluvium. Several SF wet fraction related parameters for corrosion failure appear in table 4-7 for the 50,000-yr TPI but not in table 4-6 for the 10,000-yr TPI.

The ranking of parameters using the Morris method was also examined using normalized Eq. (4-13) and log of normalized parameters. For the top 10 most influential parameters list, the normalization scheme replaced SbArWt% (subarea wet fraction) with APrs_SAV (alluvium matrix porosity) for the 10,000-yr TPI, and the list of influential parameters did not change for the 50,000-yr TPI. However, ranking among the top 10 parameters changed for several parameters for both TPIs. The log of normalized parameters replaced radionuclide parameters ARDSAV_I (AlluviumMatrixRD_SAV_I) and ARDSAV_U (AlluviumMatrixRD_SAV_U) with MAPM@GM (mean average precipitation multiplier at glacial maximum) and SbWt% (subarea wet fraction) for the 10,000-yr TPI. For the 50,000-yr TPI, parameters AA_2_1 (a parameter representing the corrosion rate) SFWt%C4 (SF wet fraction for corrosion failures in subarea 4), and SFWt%C5 (SF wet fraction for corrosion failures in subarea 5) replaced ARDSAV_U (AlluviumMatrixRD_SAV_U), ARDSAVTc, (AlluviumMatrixRD_SAV_Tc), and MKD_CHvU (matrix Kd of U for Calico Hills). The logarithmic transformation also changed the ranking for both TPIs.

4.3.3 Results from the FAST Method

Conducting sensitivity analyses for all 246 sampled parameters in the TPA code using the FAST method is impractical because it would take more than 40,000 realizations for the FAST method to conduct a sensitivity analysis on 50 input parameters. Such a large number of realizations is needed to avoid aliasing among Fourier coefficients (Cukier et al., 1975). Therefore, preliminary screening was necessary to reduce the number of parameters evaluated with the FAST method. In this report, the FAST method is applied to the 18 parameters identified by the statistical screening method presented in the last column of table 4-1 for the 10,000-yr TPI, and the 20 parameters in the last column of table 4-2 for the 50,000-yr TPI. These parameters were selected on the basis of t-statistic of the normalized or lognormalized multiple linear

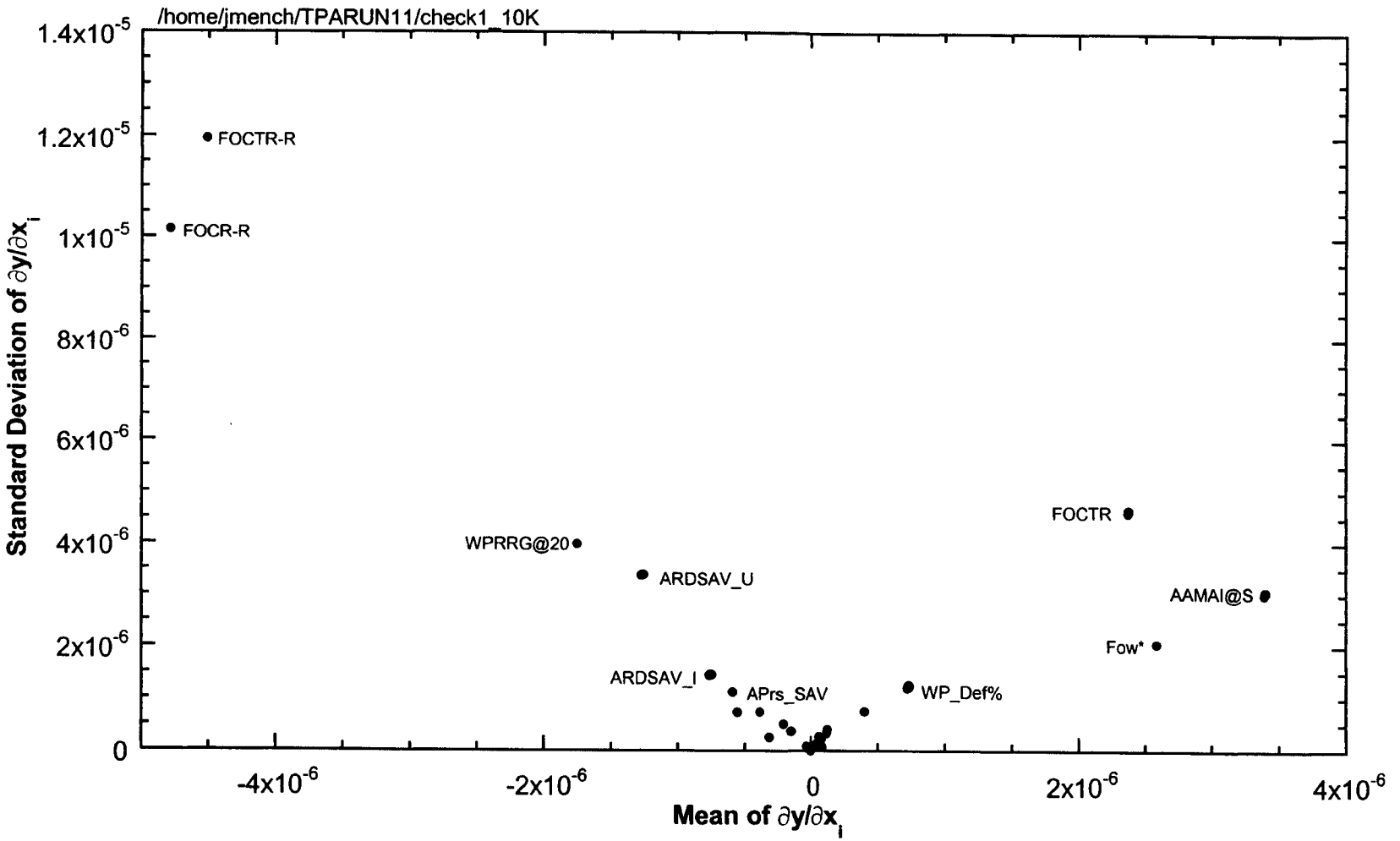

Figure 4-8. Results from the Morris method from the basecase with a time period of interest of 10,000 yr

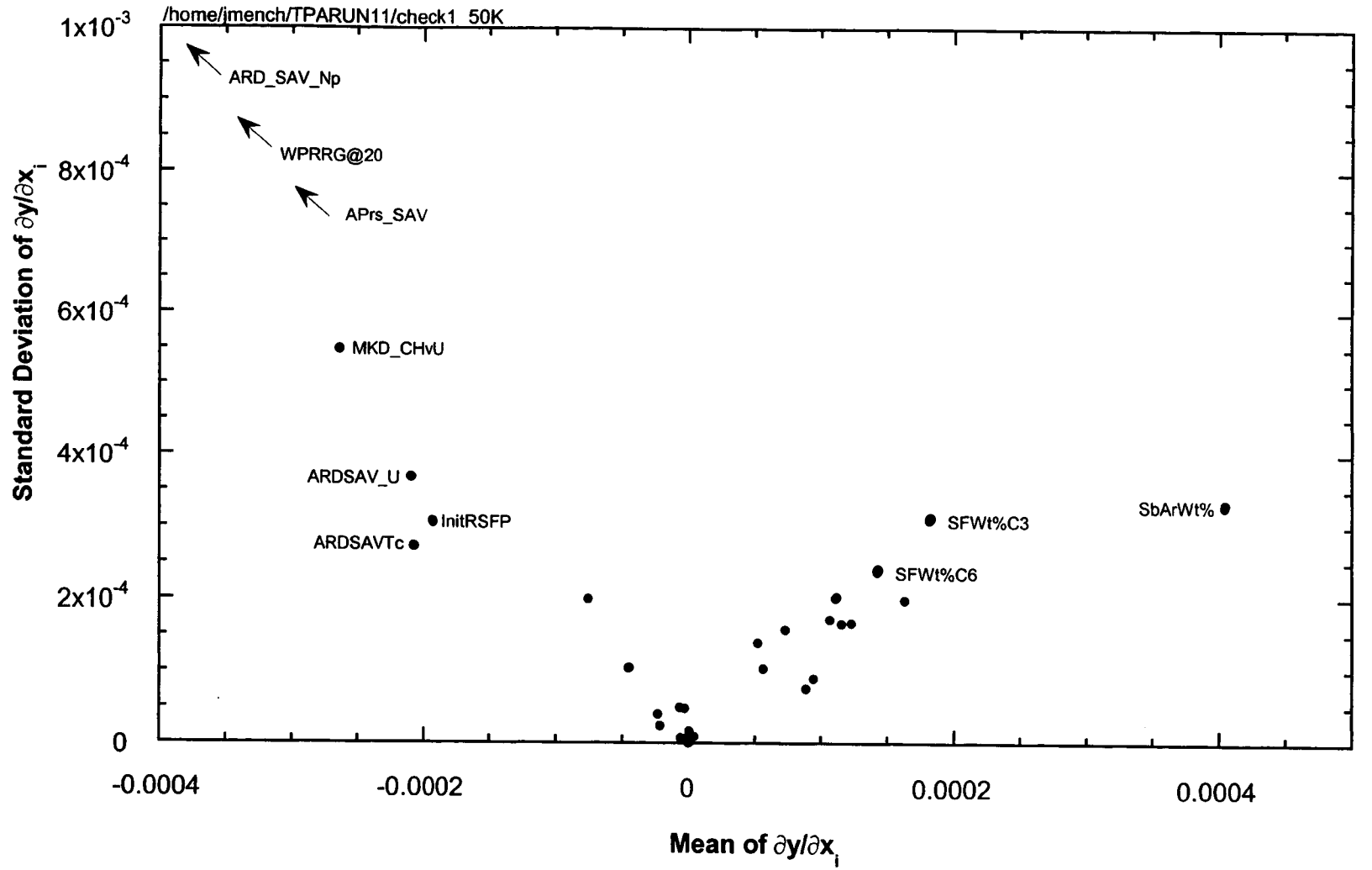

Figure 4-9. Results from the Morris method from the basecase with a time period of interest of 50,000 yr. Arrows indicate that the associated points lie outside the graph.

regression analysis that exceeded 1.96 (95-percent confidence). For the 18 parameters, only 3,310 realizations are needed to avoid aliasing among any four Fourier amplitudes (appendix B). For the 20 parameters, the number of realizations increases to 4,174.To account for the range of an input parameter, each Fourier amplitude was multiplied by the standard deviation of the corresponding input parameter, as defined by Eq. (4-13). The ranking for the top 10 parameters using the FAST method is listed in tables 4-6 and 4-7 for the 10,000- and 50,000-yr TPIs.

It should be noted that the analysis presented here is limited by the initial selection of 20 parameters from the regression analysis. Thus, some influential parameters may be identified by other nonstatistical methods, but not by the FAST method.

4.4 RESULTS FROM THE PARAMETER TREE METHOD

Several trees are presented, each using different branching criteria such as median, mean, and percentiles, for the important input parameters. A stepwise implementation of the approach is also presented. As described previously, the method used for examining system sensitivity to combinations of parameters found to be most important is to treat each realization of a parameter value as either a + or a – depending on whether the realized value is greater than or less than a specified value. This is similar to the procedure followed in a Sign Test (Bowen and Bennet, 1988) as described in section 4.1.1.4. Next, the realizations are sorted based on the commonality of their input parameters being either a + or a –. For example, realizations with all five important input parameters sampled above the median would be placed in the same bin. Similarly, all realizations where the first four parameters are a + and the last one is a – would be placed in another bin and so on.

Figure 4-10 shows the parameter tree based on median values as the branching criterion. A set of 4,000 realizations of the TPA Version 3.2 code was used, and 244 input parameters were sampled for the basecase.[6] Table 4-9 shows some statistical information for the most influential parameters identified by the multiple regression analysis for use in the median-based parameter tree method and the statistics of the output variable. The table presents the median, the mean and the 90th percentile values of the parameter distribution for the identified influential input parameters and the output variable (i.e., peak dose in 10,000 yr). In figure 4-10, column A is the number of realizations of peak dose above the overall median value (i.e., of the 4,000 realizations) in that bin. For example, row one in column A shows that 129 out of 4,000 realizations had all 5 of the important parameters with values above the median. Of these 129 realizations, 128 had peak doses above the median value for all 4,000 realizations (1.84×10^{-5} rem/yr, table 4-9). Column B shows that for these 129 realizations, the mean value of peak dose was 1.20×10^{-4} rem/yr, and column C shows these 129 realizations accounted for 21.07 percent of the population mean of peak doses. This analysis reinforces the notion that these are indeed influential parameters because slightly less than 3 percent of the realizations account for over 21 percent of the mean from all realizations.

[6]The data used in the parameter tree analyses are slightly different from the latest data used in implementing other methods, however, the differences do not contribute to significant changes to the output.

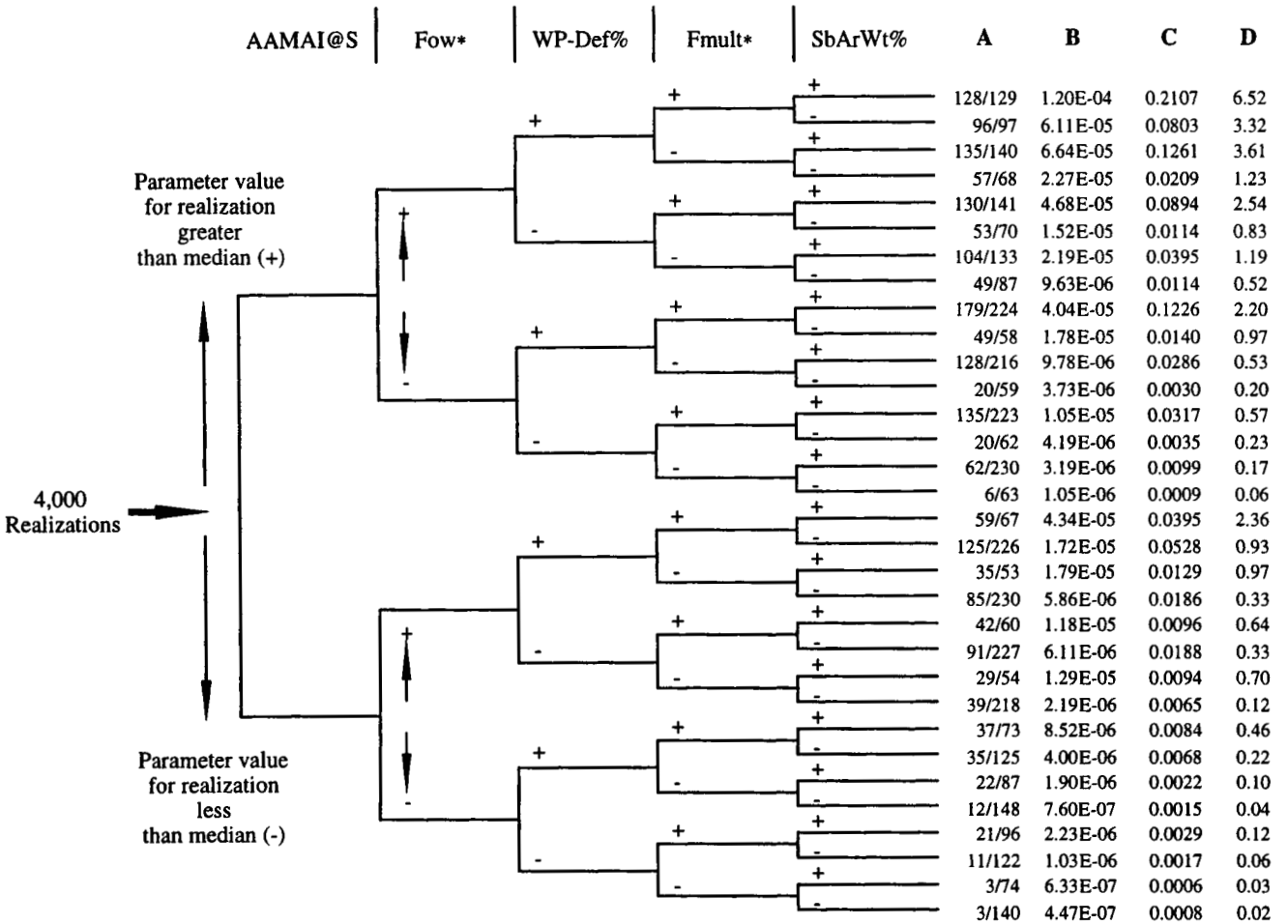

Figure 4-10. Median-based parameter tree describing the technique for examining system sensitivity to groups of parameters

Table 4-9. Statistical information about the 4,000 realizations

Parameter	Median Value	Mean Value	90th Percentile	Distribution Type; Minimum, Maximum Values
AAMAI@S	5.5	5.5	9.1	Uniform; 1,10
Fow*	0.173	0.264	0.566	Lognormal; 0.1, 3.0
WP-Def%$_f$	0.00505	0.00505	0.00901	Uniform; 0.0001,0.01
Fmult*	0.0447	0.0503	0.0833	Lognormal; 0.01,0.2
SbArWt%	0.5	0.5	0.9	Uniform; 0.0,1.0
Peak dose (rem/yr)	2.82×10^{-6}	1.84×10^{-5}	4.97×10^{-5}	—

Column D shows an "importance factor *R*" which is determined as the ratio of the contribution to the overall mean from realizations in that bin to the average contribution of the same number of realizations to the overall mean, that is,

$$R = \frac{\text{fractional contribution to the overall mean dose (Column C)}}{\left(\frac{\text{number of realizations in bin}}{\text{total number of realizations}}\right)} = \frac{\text{mean peak dose in bin (Column B)}}{\text{mean peak dose over all realizations}} \quad (4\text{-}19)$$

All of the data in columns A–D serve as figures of merit for characterizing the group of realizations in a bin. Two other interesting observations can be made about figure 4-10. First, the realizations where none or one of the input parameters is a – account for 67 percent of the mean from all realizations (includes 798 out of 4,000 realizations). Second, only 8 out of 32 bins have importance factors above unity, indicating that the output variable distribution is skewed (the 8 bins include 999 out of 4,000 realizations). Column 2 of table 4-10 presents the sensitivity coefficients for the influential parameters in the median-value based parameter tree. Symbols x_1 to x_5 for this column correspond to the five influential parameters shown in figure 4-10. It is emphasized that these sensitivity coefficients provide only the relative sensitivities. For example, from table 4-10, column 2, one can infer that the system is 1.8 times (0.351/0.192) more sensitive to parameter x_1 than it is to parameter x_5. In the lower portion of table 4-10, the system sensitivities to joint sets of parameters (see appendix C) are presented. As can be seen in the table, the system shows relatively greater sensitivity to parameter sets of increasing size. Again, consider that such results are necessarily dependent on conceptual models embodied in the simulation model as well as on the many fixed value (deterministic) parameters in the TPA code. Other columns of table 4-10 pertain to the parameter trees using other branching schemes presented in the following sections.

4.4.1 Parameter Trees Using Different Branching

Different branching criteria may be used to determine a + or a – value for a given parameter or the output variable as shown in figures 4-11 and 4-12. The most influential parameters identified by multiple

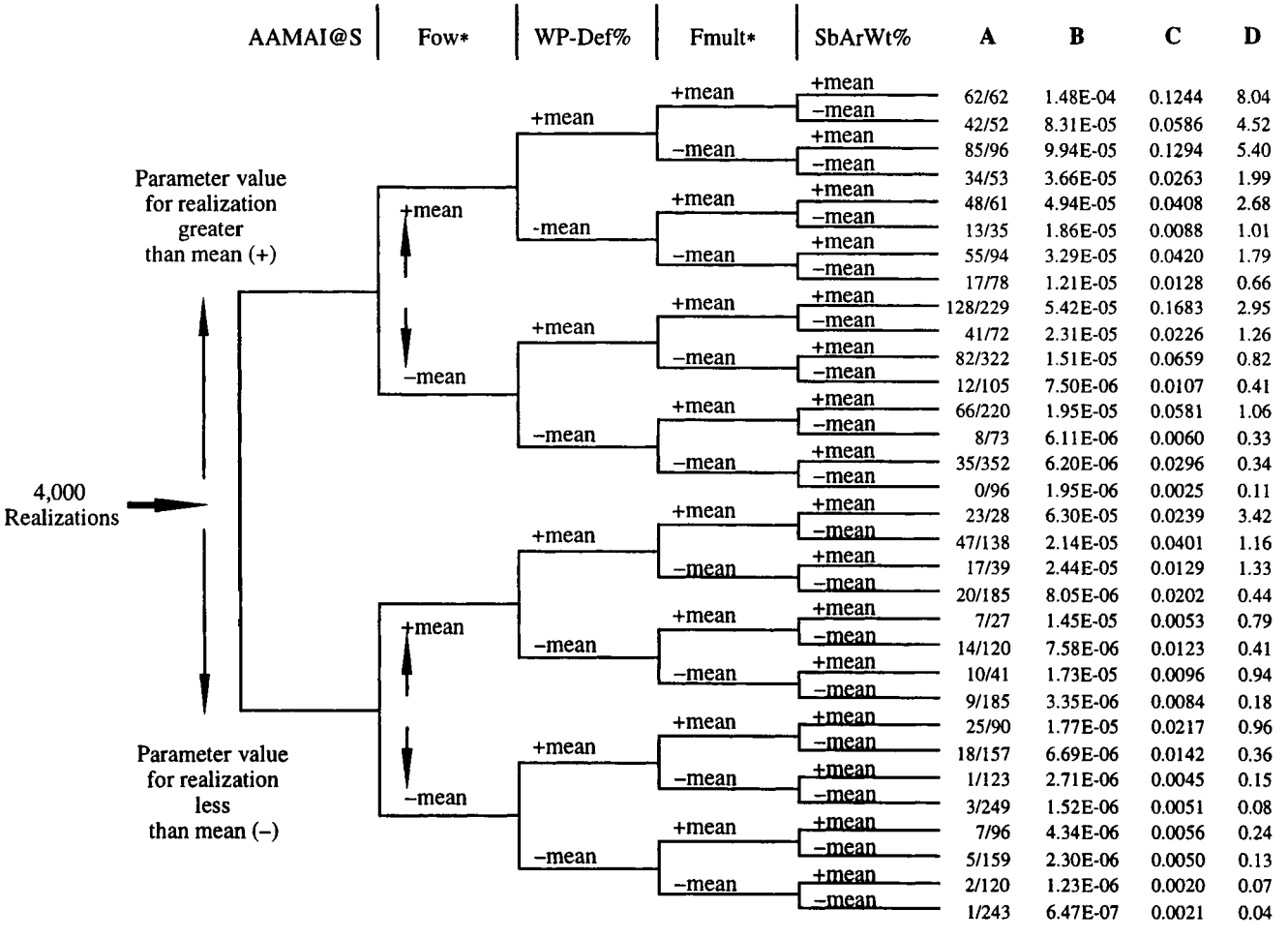

Figure 4-11. Mean-based parameter tree describing the technique for examining system sensitivity to groups of parameters

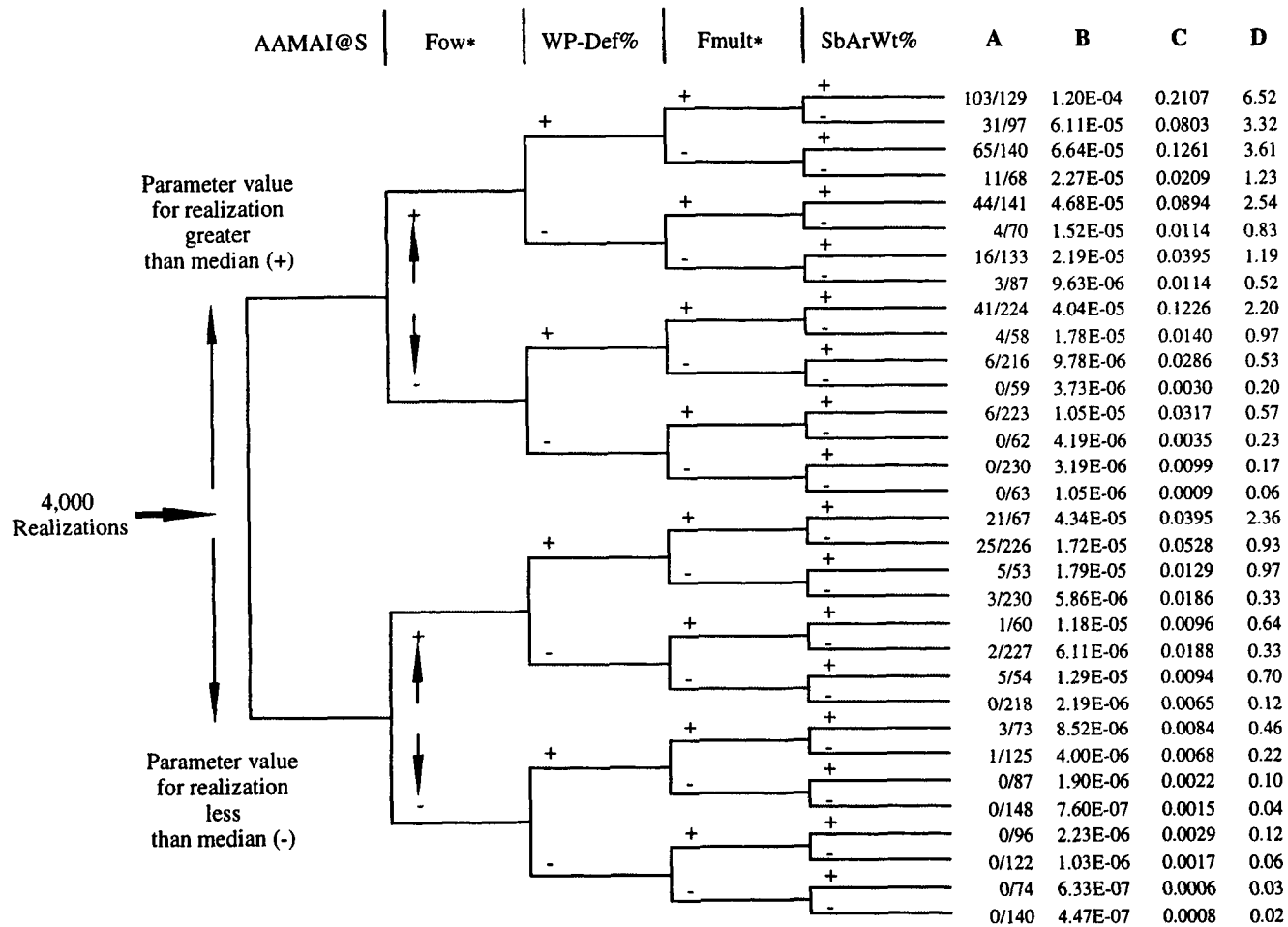

Figure 4-12. Mean-percentile-based parameter tree describing the technique for examining system sensitivity to groups of parameters; input parameters divided based on their median values and output variable divided based on its 90th percentile value from all 4,000 realizations

regression analysis are used in constructing the parameter tree. Figure 4-11 shows a tree where both the input parameters and the output variable have been partitioned based on their mean values. Again, the bins toward the top of the tree account for a disproportionate amount of the mean from all 4,000 realizations. In this example, sampling all five of the important input parameters above their mean values assures a peak dose above its mean value (see column A, row 1, in figure 4-11). The realizations where none or one of the input parameters is a - account for 55 percent of the mean from all realizations (includes 528 out of 4,000 realizations), which is a greater fraction on a per realizations basis than the example presented in figure 4-10. Column 3 of table 4-10 shows the ranking of the parameters according to sensitivity is slightly different with the mean than with the branching criterion; in this case, x_2 is the most influential parameter.

In figure 4-12, the input parameters are partitioned based on their median values, and the output variable is partitioned based on its 90th percentile. Columns B, C, and D of this figure contain numeric entries identical to those in figure 4-10. Row 1 of column A, however, shows that if all five of the important parameters are sampled above their median values (129 out of 4,000 realizations), the output variable is above its 90th percentile (4.97×10^{-5} rem/yr) in 103 of these realizations. That is, only 79.8 percent of the output above its 90th percentile is provided by the set of five parameters taking on values greater than their median. Comparing to corresponding values for Cases 1 and 2, it is clear that a significant number of extreme values (i.e., above 90th percentile) of the output are produced by combinations of parameters not represented by the group of five used in this calculation. Following the stepwise implementation described in the next section, it is possible to determine a set of parameters, different from the previous group, that most influences the 90th or other percentiles.

Table 4-10. Sensitivity coefficients calculated for various parameter trees

	Coefficient	Case 1 (Figure 4-10)	Case 2 (Figure 4-11)	Case 3 (Figure 4-12)	Case 4 (Figure 4-13)
Unconditional Sensitivities of Individual Parameters	S_{X_1}	0.351	0.26	0.134	0.351
	S_{X_2}	0.31	0.28	0.16	0.31
	S_{X_3}	0.202	0.173	0.119	0.202
	S_{X_4}	0.204	0.178	0.084	0.204
	S_{X_5}	0.192	0.15	0.102	0.081
Joint Sensitivities of Parameter Groups (see appendix C)	$\frac{\lvert p_H - p_L \rvert}{1 - \lvert p_H - p_L \rvert}$	0.541	0.351	0.155	0.541
		2.37	1.63	0.462	2.37
		6.75	4.68	0.938	6.75
		26	9.42	1.46	26
		33.5	249	3.95	26.8

Although these cases use parameter statistics as the branching criteria, other quantities could also be used. For example, total system failure could be defined as a peak dose to the hypothetical receptor greater than a predetermined limit defined by the regulation (Nuclear Regulatory Commission, 1999a). Similarly, input parameters could be partitioned based on a value that has some physical significance. For example, in the TPA Version 3.2 code, flow in fractures in the UZ begins when the infiltration exceeds the saturated matrix conductivity, currently estimated at about 3 mm/yr. This cutoff is important to performance of this subsystem because flow in fractures occurs more rapidly and dissolved contaminants experience much less chemical retardation than flow in the rock matrix. Hence, initiation of fracture flow in the UZ could be thought of as a transition from one performance regime to another for the UZ.

4.4.2 Stepwise Implementation of the Technique

The parameter tree technique was implemented in a stepwise fashion with the importance factor (Column D of figures 4-10 through 4-12) as the figure of merit for determining maximum polarity of the bins and the median value as the branching criterion. First, a one-parameter-depth tree was drawn for each sampled parameter. The parameter that yielded the greatest importance factor for one of the two branches was then used as the first-level parameter for the following iteration in the stepwise implementation. Next, for all remaining sampled parameters, a two-parameter-depth tree was drawn where the first-level parameter was determined as from the previous iteration. In this second iteration, the parameter that yielded the greatest importance factor on any branch of the tree was used as the second-level parameter for the third iteration. The procedure was repeated until the number of realizations in any bin dropped below 50, with the results of that iteration being discarded. This procedure resulted in a tree that was five parameters deep as shown in figure 4-13. The influential parameters identified by this method are compared with results from other methods in chapter 5. It may be noted that the first four parameters appear in the same order as in the stepwise regression conducted separately, however, the fifth parameter is the well-pumping rate at the receptor location 20 km down-gradient (WPRRG@20) instead of the subarea wet fraction (SbArWt%). This result is important because it shows that these parameters comprise the most important five-parameter set, which differs from the five individually most important parameters as determined by traditional methods. Also, note that WPRRG@20 is negatively correlated with the output variable (because in the TPA Version 3.2 code model, increased pumping merely increases the dilution volume and not the interception fraction of the contaminant plume by the well) and the procedure for assigning + and – was not reversed so the + + + + – bin represents the most pessimistic case in this example (i.e., the bin with the largest peak doses). In figure 4-13, note that this group of five parameters together produces a higher value of importance factor (7.06) for one of the branches (second branch from top of the tree) as compared to that in figure 4-10 (6.52 for the topmost branch). In contrast, the sensitivity measures in table 4-10 for Case 4 show that the combination of these five parameters (i.e., the last row) have a joint relative sensitivity less than that of Case 1 (26.8 versus 33.5). Thus, the nature of information provided by each sensitivity measure is somewhat different. In other words, if it had been decided to implement the stepwise procedure using the joint relative sensitivity measure, the five parameters would match exactly those of Case 1.

For all sensitivity analysis methods presented in this chapter, it should be noted that changes to the sampling ranges of the influential parameters (either expansion or contraction) should be made with greater caution than for other parameters because peak dose for the TPI shows the largest change per unit deviation in these parameters.

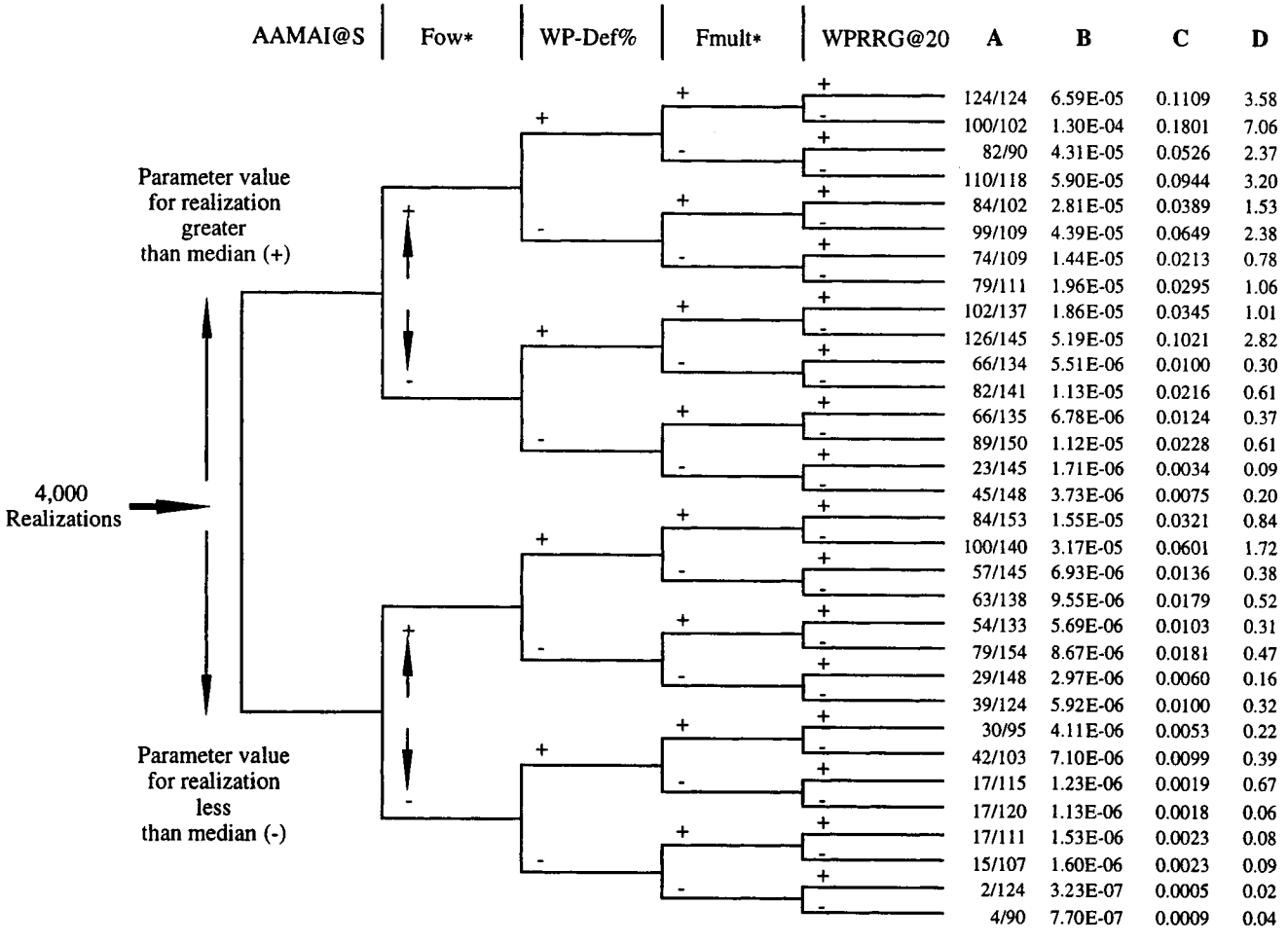

Figure 4-13. Tree developed using a stepwise implementation of the technique based on the importance factor

4.5 ALTERNATIVE CONCEPTUAL MODELS AND SCENARIO CASES STUDIED AT THE SYSTEM LEVEL

The system-level sensitivity studies cover alternative conceptual models and scenario cases. The analyses in this chapter include the full ranges of parameter variations for all modules. Two sets of results are presented. The first set of results reflects model runs that compare the basecase with alternative conceptual models. First, the basecase was evaluated with a 250-vector run. Alternative conceptual model tests were conducted with 250-vector runs, and the results were compared to the basecase. The alternative conceptual models were selected to evaluate (i) the effect on repository performance of several repository design features currently being considered by DOE, (ii) the effect on repository performance of plausible alternate thermo-hydrologic conditions in the repository near field, and (iii) bounding engineered or natural system behavior. The second set of results reflects the effects of disruptive scenarios, including igneous activity and major faulting. Seismicity is considered part of the basecase.

For both sets of analyses, the runs were limited to 10,000 and 50,000 yr. The number of realizations was limited to 250, to keep computer resources within reasonable limits. Runs up to 50,000 yr with 4,000 realizations are included in the sensitivity analyses in the previous sections of this chapter. Section 2.3.2 outlines the alternative conceptual models evaluated in this chapter.

For each alternative conceptual model, only the noted changes as described in section 2.3.2 to the TPA input file were made, with all other input parameters set to the values used in the basecase. Results are presented as the peak of the mean dose.

Figure 4-14 shows the results for the 10,000-yr TPI, while figure 4-15 is for the 50,000 yr results. The results for the NoInvert alternative were not plotted because they could not be distinguished from the basecase results.

Various observations can be made based on the calculational results shown in this chapter.

- Except for NoRet the relative effects of the alternative conceptual models (based on the peak of the mean dose) changed substantially between the 10,000- and 50,000-yr TPIs.

- The largest mean doses resulted from the NoRet assumption, demonstrating the importance of retardation in the alluvium of Pu, Am, and Th.

- The Flwthru-1 conceptual model led to a larger release in the 10,000-yr TPI, but was much less important for the 50,000-yr TPI. This probably can be attributed to the lack of a delay time caused by the necessity to fill the WP in the bathtub model. This effect is less important for the 50,000-yr TPI.

- Fast dissolution in the case of the dissolution (Model 1) and grain-size (Grain 1) alternatives led to an increased peak dose at 10,000-yr TPI, but it was not proportional simply to the increased rate of dissolution. In some cases, the high rate of dissolution did not contribute to an overall increase of dose for the 50,000-yr TPI. This is probably an indication that the high dissolution rate of the fuel led to near-total depletion of the SF.

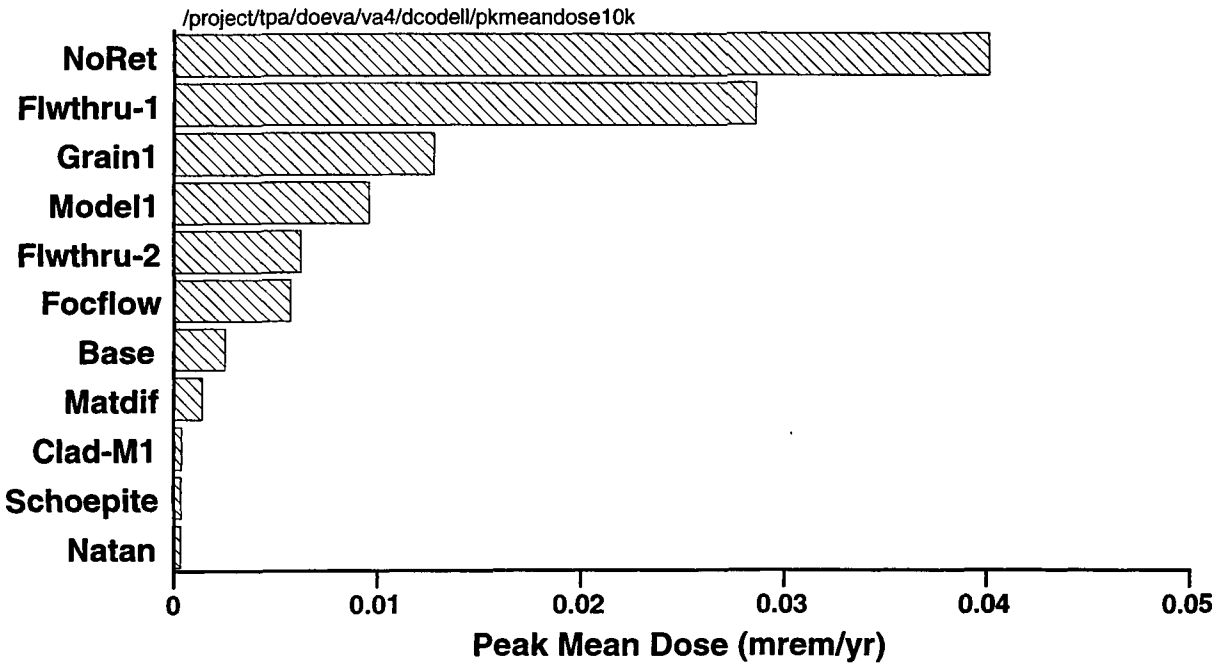

Figure 4-14. Bar chart showing the effects of alternative conceptual models at 10,000 yr

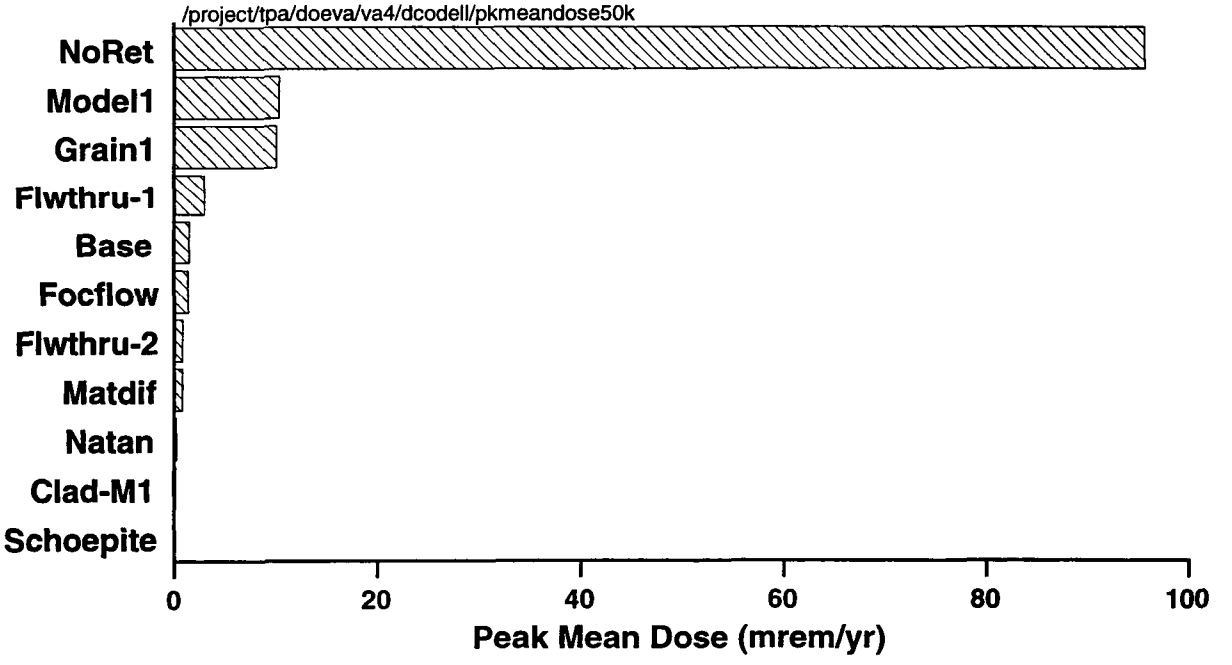

Figure 4-15. Bar chart showing the effects of alternative conceptual models at 50,000 yr

- Alternatives based on natural analog data (Natan) and assumptions about the behavior of radionuclides in secondary uranium minerals (Schoepite) led to much smaller peak doses.

- Protection of the fuel by cladding (Clad-M1) leads to a large reduction in peak doses.

- Matrix diffusion (Matdif) would reduce the peak of the mean dose for both the 10,000- and 50,000-yr TPI. Note, however, that the results from a single calculation, such as the mean value estimates in chapter 3, indicate that matrix diffusion might occasionally cause an increase in dose at later times.

5 SYNTHESIS OF SENSITIVITY RESULTS AND LINKAGE OF SENSITIVE PARAMETERS TO INTEGRATED SUBISSUES

This chapter attempts to identify influential parameters using the analyses presented in chapters 3 and 4. Chapter 4 presented the sensitivity analyses and their results, as well as results from alternative conceptual models. This chapter focuses on identifying the parameters and alternative models that significantly influence performance.

5.1 SELECTION OF INFLUENTIAL PARAMETERS

In the previous chapter, seven different sensitivity analyses methods (i.e., regression with normalized variables, regression with log-normalized variables, differential analysis, Morris method, FAST method, t-test on means, and parameter tree method) were used to determine the most influential parameters. The first five methods are scaled (i.e., standardized) so that the sensitivity results reflect the variability of the inputs. The last two are not scaled because their results are based on ranking the input variables using a set of predetermined criteria. Only six of the methods were used at a time for either the 10,000- or 50,000-yr TPI. The parameter tree method was used only for 10,000 yr and the t-test on means was used only for 50,000 yr. The seven methods have different approaches to determining sensitivity. For example, regression with log-transformed variables places greater emphasis on smaller doses than regression with untransformed variables. Also, the t-test on means was conducted to determine sensitive parameters relating only to relatively high doses. It is not clear that any one method is superior to another for this determination of sensitivity (or influence) and, consequently, no method can be fully relied on to provide a unique ranking of parameters. Therefore, the final list of parameters was selected on the basis of frequency of occurrence among various methods.

The selected parameters are presented in tables 5-1 and 5-2. The score in these tables specifies the number of methods that selected a particular parameter among the top ten. For example, a score of 6/6 for the subarea wet fraction parameter (SbArWt%) implies that the parameter ranked among the top 10 (five for the parameter tree method) in all six methods. Also note that, among the seven methods, there are two statistical methods (regression with normalized variables, and regression with log-normalized variables) and three nonstatistical methods (differential analysis, Morris method, and FAST method). It should be noted that the FAST method selected the most influential parameters only out of the top 20 listed in tables 4-1 and 4-2. The parameters that did not make the final list include those selected as influential by only one of the seven methods, those selected by only two statistical methods, and those selected by only two out of three nonstatistical methods. This resulted in only eight parameters being selected for 10,000- and 50,000-yr TPIs. Comparison of scores between these two TPIs also indicates that the influential parameters are common to most methods for the 10,000-yr TPI, whereas significant variation exists for the 50,000-yr TPI. Also note that for the 10,000-yr TPI, all parameters that ranked as the top five in the parameter tree method also were picked by other sensitivity analyses methods.

Table 5-1. Influential parameters for 10,000-yr time period of interest from sensitivity analysis studies

Parameter abbreviation	Parameter Name	Score
Fow*	Flow focusing factor	6/6
WP-Def%	Initially defective fraction of WPs	5/6
Fmult*	Fmult factor for flow entering a WP	5/6
AAMAI@S	Areal average mean annual infiltration at start	5/6
WPRRG@20	Well pumping rate at 20 km receptor group	5/5
ARDSAV-I	Alluvium R_d for ^{129}I	5/6
SbArWt%	Subarea wet fraction	5/5
ARDSAV-Tc	Alluvium R_d for ^{99}Tc	3/5**

**Parameter Tree method selected only the top 5 parameters of which ARDSAV-Tc is one. Hence, the score is 3/5 and not 3/6.

Table 5-2. Influential parameters for 50,000-yr time period of interest from sensitivity analysis studies

Parameter abbreviation	Parameter Name	Score
SbArWt%	Subarea wet fraction	6/6
WPRRG@20	Well pumping rate at 20-km receptor group	5/6
ARDSAV-Np	Alluvium R_d for ^{237}Np	4/6
ARDSAV-Tc	Alluvium R_d for ^{99}Tc	3/6
Fmult*	Fmult factor for flow entering a WP	3/6
ARDSAV-I	Alluvium R_d for ^{129}I	3/6
ARDSAV-U	Alluvium R_d for ^{234}U	3/6
AAMAI@S	Areal average mean annual infiltration at start	3/6

For both TPIs several parameters were found most influential for the basecase (the basecase is defined as the undisturbed scenario along with the effects of rockfall due to seismicity). The parameters include

- Areal fraction of the repository wetted by water infiltrating into the repository (SbArWt%)
- Well pumping rate at 20-km receptor group (WPRRG@20)
- Areal average mean annual infiltration at start (AAMAI@S)
- Alluvium R_d for ^{99}Tc (ARDSAV-Tc)
- Alluvium R_d for ^{129}I (ARDSAV-I)
- The fraction of water infiltrating to the repository from the UZ above the repository that will enter the WP and contribute to the release of radionuclides (Fmult*)

In addition, the parameters influential for the 10,000-yr TPI but not for the 50,000-yr, are

- A flow focusing factor that expresses the flow potentially reaching a wetted WP (Fow*)
- Initially defective fraction of WPs (WP-Def%)

Two parameters influential for the 50,000-yr TPI but not for the 10,000-yr, are

- Alluvium R_d for ^{237}Np (ARDSAV_Np)
- Alluvium R_d for ^{234}U (ARDSAV_U)

5.2 COMPARING INFLUENTIAL PARAMETERS TO INTEGRATED SUBISSUES

The influential parameters identified previously were crosswalked to the NRC integrated subissues [previously specified as key elements of subsystem abstraction in the Revision 1 TSPA&I Methodology KTI Issue Resolution Status Report (Nuclear Regulatory Commission, 1998)]. The crosswalking of these parameters for the basecase results and for the igneous activity disruptive events is presented in table 5-3. The alternative conceptual models investigated in this report are also cross-referenced to integrated subissues in table 5-3. The influential parameters corresponding to the disruptive events were determined from only differential analysis.

The influential parameters identified in tables 5-1 to 5-3 must be viewed in the proper context. The following are key points to consider when examining these tabulated results:

- All analysis results are based on the models and reference input values used in the TPA Version 3.2 code. Chapter 2 of this report gives a description of the conceptual models. TPA Version 3.2 Code User's Guide (Mohanty and McCartin, 1998) lays out the key assumptions for the conceptual models. Chapter 3 lists the reference input values.

- No consideration is given to corrosion or the defects of welds.

- No credit is given to retardation in fractures or matrix diffusion in the UZ.

- Fracture-only flow occurs in the UZ if the flux exceeds the saturated hydraulic conductivity of a stratigraphic unit.

- The DCFs are kept as constants in all the analyses performed, which implies that the DCFs are known with certainty.

- The receptor group is located 20 km from the repository and uses partially contaminated groundwater for drinking and farming.

- All WPs in a subarea fail from corrosion when the representative WP fails.

- No consideration is given to the effect of dripping of chloride-rich water on WP corrosion.

Table 5-3. A crosswalk between the integrated subissues, alternative conceptual models, and the influential parameters

Integrated Subissues	Alternative Models Investigated	Influential Parameters
WP degradation (temperature, humidity, and chemistry)	Not evaluated	-Initially defective fraction of waste packages (10,000-yr)
Mechanical disruption of WPs (seismicity, faulting, rockfall, and dike intrusion)	Not evaluated	-Time of next faulting event in the region of interest* -Spent fuel wetted fraction for faulting event* -North-East fault zone width*
Quantity and chemistry of water contacting WPs and waste forms	Clad-M1 Flwthru-1 Flwthru-2 Focflow Grain1	-Fmult factor for flow entering into a WP (10,000-yr, 50,000-yr) -Subarea wet fraction (10,000-yr, 50,000-yr) -Flow focusing factor (10,000-yr)
Radionuclide release rates and solubility limits	Model1 Flwthru-1 Flwthru-2 Natan Schoepite	— — — — —
Spatial and temporal distributions of flow	Focflow	-Areal average mean annual infiltration at start (10,000-yr, 50,000-yr)
Distribution of mass flux between fracture and matrix in unsaturated zone	—	—
Retardation in fractures in the unsaturated zone	Not evaluated	(No retardation or matrix diffusion in the unsaturated zone)
Flow rates in water production zones	Not evaluated	—
Retardation in water production zones and alluvium	NoRet Matdif	-Alluvium matrix R_d for ^{129}I (10,000-yr, 50,000-yr) -Alluvium matrix R_d for ^{237}Np (50,000-yr) -Alluvium matrix R_d for ^{99}Tc (10,000-yr, 50,000-yr) -Alluvium matrix R_d for ^{234}U (50,000-yr)

Table 5-3. A crosswalk between the integrated subissues, alternative conceptual models, and the influential parameters (cont'd)

Integrated Subissues	Alternative Models Investigated	Influential Parameters
Volcanic disruption of WPs	Evaluated as a special case	-Diameter of volcanic cone (10,000-yr, 50,000-yr) * -Volcanic event power (10,000-yr, 50,000-yr)* -Volcanic event duration (10,000-yr, 50,000-yr)* -Time of next volcanic event in region of interest (10,000-yr, 50,000-yr)*
Airborne transport of radionuclides	Evaluated as a special case	-Airborne mass load for igneous activity dose calculation (10,000-yr, 50,000-yr)* -Ash mean particle log diameter (10,000-yr, 50,000-yr) -Wind Speed (10,000-yr, 50,000-yr)*
Dilution of radionuclides in groundwater through well pumping	Not evaluated	-Well pumping rate at receptor group at 20 km (10,000-yr, 50,000-yr)
Dilution of radionuclides in soil through surface processes	Not evaluated	—
Critical group lifestyle	Not evaluated	(DCFs were set as constants)

*Sensitive parameters obtained directly from disruptive event scenario calculations without any consideration of event probability

The following conclusions, drawn solely on the basis of the sensitivity analyses, provide an indication of which integrated subissues may deserve more attention relative to others. Because the model abstractions are preliminary and data are continuously updated, results shown in this report provide a snapshot of the current relative importance and should not be used alone to determine the significance of any of the integrated subissues.

5.2.1 Key Integrated Subissues for 10,000-yr Time Period of Interest

For the 10,000-yr TPI, the basecase results have shown that total system performance is most sensitive to the following integrated subissues:

- WP degradation
- Quantity and chemistry of water contacting WPs and waste forms
- Spatial and temporal distribution of flow

- Retardation in water production zone and alluvium
- Dilution of radionuclides in groundwater due to well pumping

When disruptive events are included, the following two integrated subissues are the most important:

- Volcanic disruption of WPs
- Airborne transport of radionuclides

The predominance of the integrated subissues identified previously is the result of several processes and model abstractions that may merit further examination. These include (i) thermal period delays the onset of flow into the repository; (ii) bathtub fill-up could take several hundreds to thousands of years, thus delaying releases; and (iii) corrosion-resistant material significantly increases the life of the container, thus pushing the release time to late times or even beyond 10,000 yr. Consequently, the results are extremely sensitive to the initially defective failures and igneous activity disruptive event.

Based on the sensitivity and alternative conceptual model analyses results, the following specific points can be made with regard to the integrated subissues for the 10,000-yr TPI:

- Factors causing WPs to fail by mechanisms other than corrosion play a much more important role because of the long WP life. Total system performance is sensitive to the percent of initial defective WPs. Consistent with the deterministic analyses in chapter 3, repository performance is not sensitive to seismic rockfall or instantaneous fault displacement on new or under-appreciated faults (Integrated subissue—mechanical disruption of WPs).

- The number of WPs that are dripped on (immaterial prior to WP failure) and the amount of dripping water entering the WP are important to system performance (Integrated subissue—quantity and chemistry of water contacting WPs and waste forms).

- The alternative conceptual model that assumes no retardation in the SZ produced a much higher peak expected dose than the basecase and illustrates the importance of evaluating retardation in the SZ. By comparison to retardation, matrix diffusion does not have nearly as pronounced an effect on the system performance (Integrated subissues—retardation in water production zones and alluvium; quantity and chemistry of water contacting WPs and waste forms).

- Choice of the WP water retention model for release calculations (bathtub or flowthrough) has an effect on total system performance. The fuel dissolution rate also has an effect on total system performance (Integrated subissue—radionuclide release rates and solubility limits).

- Retardation of ^{129}I and ^{99}Tc in the alluvium is important to system performance (Integrated subissue—retardation in water production zones and alluvium).

- The alternative conceptual model that assumes partial cladding protection produced a much lower peak expected dose than the basecase, which illustrates the need to improve modeling capability and focus reviews in this area if the DOE decides to take credit for cladding (Integrated subissue—quantity and chemistry of water contacting WPs and waste forms).

- The peak expected dose resulting from the igneous activity scenario class is two orders of magnitude higher than the basecase after being weighted by its probability (Integrated subissues—volcanic disruption of WPs; airborne transport of radionuclides).

- The well pumping rate at the receptor group significantly influences the system performance. The well pumping rate is used in determining the dilution of radionuclide concentration. Dose is directly proportional to the radionuclide concentration in water. (Integrated subissue—dilution of radionuclides in groundwater through well pumping).

5.2.2 Key Integrated Subissues for 50,000-yr Time Period of Interest

For the 50,000-yr TPI, the results have shown that total system performance is most sensitive to the following integrated subissues (in the absence of igneous activity disruptive event):

- Quantity and chemistry of water contacting WPs and waste forms
- Radionuclide release rates and solubility limits
- Spatial and temporal distributions of flow
- Retardation in water production zones and alluvium
- Dilution of radionuclides in groundwater through well pumping

The peak expected dose resulting from the igneous activity scenario class was not computed for the 50,000-yr TPI because the peak expected dose due to igneous activity occurs during the first 1,000 yr following closure (see figure 3-50). The following specific points can be made with regard to the integrated subissues for the 10,000-yr TPI:

- The number of WPs that are dripped on and the amount of water contacting the waste affect the system performance (Integrated subissue—spatial and temporal distribution of flow; quantity and chemistry of water contacting WPs and waste forms).

- The choice of the release model (bathtub or flowthrough) has negligible effect on system performance. The fuel-dissolution rate has a relatively greater effect on the system performance. The grain/particle size has a relatively large effect on the system performance (Integrated subissue—radionuclide release rates and solubility limits).

- As in the 10,000-yr case, partial cladding protection significantly reduced peak expected dose (Integrated subissue—quantity and chemistry of water contacting WPs and waste forms).

- The alternative conceptual model that assumes no retardation in the SZ produced a much higher peak expected dose than the basecase, which illustrates the importance of evaluating radionuclide transport in the SZ. By comparison, matrix diffusion does not have a great effect on system performance (Integrated subissue—retardation in water production zones and alluvium).

- Retardation of ^{237}Np, ^{129}I, ^{99}Tc, and ^{234}U in the alluvium is important to system performance as indicated by sensitivity analysis (Integrated subissue—retardation in water production zones and alluvium).

- Total system performance is sensitive to dilution introduced by well pumping (Integrated subissue—dilution of radionuclides in groundwater through well pumping).

6 CONCLUSIONS

This report describes a series of computations performed for assessing the confidence in estimations of future repository performance in light of the uncertainty in conceptual models and the parameters of those models. These estimations allowed the staff to focus attention on what are likely to be the most important phenomena affecting repository performance and point out deficiencies in the current state of knowledge. The results of these analyses were also used to review the TSPA-VA and refine the issue resolution process, as described in chapter 5, tying the parameter sensitivities and alternative conceptual model results to the integrated subissues identified in the Total System Performance Assessment and Integration Methodology Issue Resolution Status Report.

6.1 BASECASE RESULTS

To gain insight into the basic functionality of the TPA code, the trend in results, and the influence of various code components on the overall results, TPA runs were analyzed using basecase data, scenario cases, and alternative conceptual model data sets. To explain the trend in the intermediate and final outputs, results from a single realization (using the mean value data set) were analyzed. Then the results from multiple realizations (250) using the basecase data set were presented to highlight the variability in dose as a function of variability in 246 sampled parameters.

At 0.002 mrem/yr, the peak dose from the mean value data set was found similar to a peak expected dose of 0.003 mrem/yr from multiple realizations for the 10,000-yr TPI. But for 100,000-yr TPI, the peak dose from the mean value data set was 0.3 mrem/yr compared to the 4-mrem/yr peak expected dose from multiple realizations. The analysis indicated that, though the expected dose from these two cases (mean value versus multiple realization) are quite similar, analysis using the mean value data set can be misleading. For example, for the 10,000-yr TPI, the major contributors to dose in the mean value data set case were ^{129}I and ^{36}Cl; for multiple realizations, ^{237}Np, ^{129}I, ^{99}Tc, and ^{234}U were the major contributors. For the multiple realizations, the minimum and maximum of the peak dose varied over five orders of magnitude for both TPIs. Dose at early times is primarily due to initially defective failures. A sharp rise in dose between 10,000 and 20,000 yr occurs predominantly because of corrosion failure. From 20,000 to 100,000 yr, the dose is generally constant except at about 85,000-yr, where the climatic conditions switch from pluvial back to nonpluvial. For the 10,000-yr TPI, the dose contributors were ^{237}Np, ^{129}I, ^{99}Tc, ^{234}U, ^{36}Cl, and ^{79}Se. For the 100,000-yr TPI, the dose contributors were ^{237}Np, ^{234}U, ^{99}Tc, and ^{129}I, with 92 percent of the contribution solely from ^{237}Np. When probability weighted, faulting did not influence the peak expected dose for either TPI, whereas igneous activity increased the dose from 0.003 mrem/yr for the basecase, which includes the effects of rockfall due to seismicity, to 0.6 mrem/yr.

6.2 ALTERNATIVE CONCEPTUAL MODELS

Chapters 3 and 4 describe results of the basecase compared to alternative conceptual model cases. The analyses in these chapters used the TPA Version 3.2 code and a WP design using an Alloy C-22 inner corrosion-resistant layer. Other stipulations about the basecase model were no backfilling of the repository drifts, no matrix diffusion into the rock matrix, no credit for cladding protection of fuel, even distribution of infiltrating water to WPs, and the bathtub model for fuel wetting. These basecase analyses considered seismically induced rockfall, but not the effects of fault displacement or igneous activity on repository performance. Separate analyses were conducted for the faulting and igneous activity disruptive scenarios.

Alternative conceptual models considered in this study were (i) matrix diffusion of radionuclides into the rock matrix in the SZ; (ii) a faster dissolution rate of exposed fuel, but offset by large credit for protection of fuel by cladding; (iii) focusing flow to a smaller number of WPs; (iv) flowthrough model with no pooling of water in WP; (v) flowthrough model, but with faster fuel dissolution; (vi) release rate based on a natural analog to SF; (vii) release based on the dissolution rate of schoepite; (viii) release based on fuel grain size rather than particle size; and (ix) no retardation of Pu, Th, and Am.

The results of the analyses of alternative conceptual models highlight the importance of some of the assumptions made about the processes modeled in the TPA code. Note, however, that the relative effects of the alternative conceptual models change substantially between the 10,000- and 50,000-yr TPIs and are not always intuitive. For example, matrix diffusion for the mean value run reduces the peak dose for the 10,000-yr TPI, but actually increases the peak dose for the 50,000-yr TPI. This result might be caused by a computational idiosyncracy of the code rather than a real phenomenon (see section 3.5.3.3). Results from the Monte Carlo runs in chapter 4 indicate that the peak mean dose is always decreased by matrix diffusion.

Elimination of major barrier components such as retardation and cladding protection resulted in the largest dose increases. The largest peak expected doses resulted from the no retardation assumption, demonstrating the importance of retardation of Pu, Am, and Th, especially if these radionuclides can travel as colloids unretarded through the geosphere.

Switching to models for fast dissolution increased peak expected dose at 10,000-yr TPI, but not at a rate proportional to the increased rate of dissolution. In some cases, the high rate of dissolution did not contribute to an overall increase in dose for the 50,000-yr TPI, indicating near-total depletion of the SF inventory. Conversely, results using alternative release rate models for phenomena such as cladding protection and observations of uranium transport at natural analog sites could result in considerably smaller doses. Tying the release rate to the dissolution of the secondary mineral schoepite also showed a large decrease in dose, which warrants further investigation to development of a better understanding of this geochemical process.

6.3 SENSITIVITY ANALYSES

The sensitivity analyses employed the TPA Version 3.2 code and applied a variety of statistical techniques to a large (>1,000 vector) set of Monte Carlo runs and nonstatistical techniques (differential analysis, Morris method, and FAST method) to 250–4,000 TPA realizations. Most of these analyses pertained to the basecase. Igneous activity and faulting were considered separately from the basecase, with their analyses limited to differential analysis. Statistical and nonstatistical analyses of the basecase were used to identify sensitive parameters for which a small input change can have a large effect on estimated repository performance. Other ranking techniques were applied to the Monte Carlo results to determine which parameters were important. The parameter tree method allowed the determination of combinations of variables that led to the highest doses. The Morris method and the FAST method were used in the current study to determine what further insights could be gained from techniques specifically designed for nonlinear models.

Regression analyses were performed on a 1,000-vector basecase run for 10,000- and 50,000-yr TPI. Results from the regression analyses were based on both normalized and log-transforms of the normalized inputs. The normalized results weight each result equally, whereas the log-normalized results tend to overemphasize smaller doses. However, the log-transformed results generally provide a better fit for the

regression equations. Results of the regression analyses are standardized to account for the ranges of the input variables and allow a more accurate ranking of sensitivity coefficients. The results from differential analysis, and the Morris and FAST methods were also scaled by the standard deviation of the input variables so that the ranks of these variables could be compared to those from the statistical analyses. Tables 4-6 and 4-7 summarize the results for the 10,000- and 50,000-yr TPIs from the regression, differential analysis, and the Morris and FAST methods.

Several of the other sensitivity analyses could not be ranked directly for sensitivity and were, therefore, not included in tables 4-6 and 4-7, but nevertheless supply insight to the sensitivity process. The parameter tree method fits into this category. Another is the statistical test in which the 1,000 vectors for the 50,000-yr TPI were sorted into two bins depending on whether the dose was greater or less than 10 millirem. The means of the input variables in each bin were then compared statistically for significant differences between the two bins.

To capture the information contained in all the sensitivity methods, tables 5-1 and 5-2 list the influential parameters for the 10,000- and 50,000-yr TPIs that appear from the results of at least three out of the six sensitivity methods explored in this report. Some important conclusions that can be drawn by examining the lists of parameters in tables 5-1, 5-2, and tables in chapter 4 include

- Numerous parameters affecting the flow of water onto and eventually into the failed WP (and onto SF) are important (e.g., Fow*, Fmult*, SF wetted fraction, and SbArWt%). There is no mechanistic basis for the input parameter ranges for these variables used in the TPA Version 3.2 code. Study continues to better understand the processes represented by these parameters.

- Regression techniques were able to distinguish as many as 18 statistically significant variables (at the 95th percent confidence level) for the 10,000-yr TPI and 20 variables at the 50,000-yr TPI. For the 10,000-yr TPI, 10 of the 18 significant variables were related to WP and fuel wetting, and 5 variables were related to retardation. For the 50,000-yr TPI, 8 of the 20 significant variables were related to WP and fuel wetting, 5 to retardation, and 3 to seismically induced rockfall. Study continues to better understand the reasons for these variables being significant.

- In the analysis of the mean value of input variables leading to the highest doses, there were 24 variables whose difference in means were determined statistically significant. Of these, 4 were associated with wetting, 13 with retardation, and 4 with UZ fracture and matrix flow. Thus, retardation factors take on added importance when considering the conditions that led to the largest doses. However, the dependence on UZ flow was for parameters that are not likely to have an effect on the results. It is likely that the sample size in the high-dose category (51 samples) was too small, and that some of these results are spurious.

6.4 IMPORTANCE OF RADIONUCLIDES

For a TPI of 10,000 yr, most of the peak mean dose came from the isotope ^{129}I, with ^{99}Tc and ^{237}Np (in descending order) accounting for most of the balance. For a TPI of 50,000 yr, most of the peak mean dose contribution came from ^{237}Np, with ^{129}I, ^{99}Tc, and ^{234}U (in descending order) accounting for most of the

balance. For either the 10,000- or 50,000-yr TPIs, however, the largest peak doses from any realization came from ^{237}Np.

6.5 INTEGRATED SUBISSUES REQUIRING FURTHER STUDIES

The influential parameters, identified using various statistical and nonstatistical sensitivity analysis methods and screened further by comparing the outcomes of these methods, were crosswalked to the NRC integrated subissues. Nine of the fourteen subissues were found to have at least one influential parameter (including the integrated subissues related to disruptive events). Because the staff has not yet developed an acceptable method for factoring event probability into sensitivity analysis, the influential parameters from the scenario events were crosswalked with the integrated subissues. Assuming an event probability of 1, the integrated subissues that deserve attention are summarized in table 5-3. The integrated subissues for the 10,000-yr TPI that deserve further examination are primarily because of the delay in radionuclide releases resulting from (i) corrosion-resistant material of the inner overpack pushing the WP failure time beyond 10,000 yr, (ii) thermal reflux delaying the onset of flow into the repository, (iii) bathtub filling time delaying the radionuclide release time by hundreds to thousands of years, and (iv) radionuclide sorption in the alluvium causing significant delay in the arrival time of radionuclides.

Conclusions drawn from these analyses may change as the models and assumptions are updated, and certain parameters or processes may become more or less important. Also, the assumptions and limitations, as described in chapter 2 of this report, should be considered when interpreting the results. Preparation by the NRC to review the DOE TSPA products is an iterative process, of which this report represents one facet.

7 REFERENCES

Baca, R.G., G.W. Wittmeyer, and R.W. Rice. 1996. Analysis of contaminant dilution in groundwater. *Scoping Calculations for Revisions to the EPA Standard.* NUREG–1538. Washington, DC: Nuclear Regulatory Commission.

Bell, M.J. 1998. Letter (July 6) to S.J. Brocoum, U.S. Department of Energy. Nuclear Regulatory Commission Comments on the U.S. Department of Energy Total System Performance Assessment. Washington, DC: Nuclear Regulatory Commission.

Benjamin, J.R., and C.A. Cornell. 1970. *Probability, Statistics, and Decision for Civil Engineers.* New York: McGraw-Hill.

Bowen, W.M., and C.A. Bennett, eds. 1988. *Statistical Methods for Nuclear Material Management.* NUREG/CR–4604. Washington, DC: Nuclear Regulatory Commission.

Codell, R.B, N. Eisenberg, D. Fehringer, W. Ford, T. Margulies, T. McCartin, J. Park, and J. Randall. 1992. *Initial Demonstration of the NRC's Capability to Conduct a Performance Assessment for a High-Level Waste Repository.* NUREG–1327. Washington, DC: Nuclear Regulatory Commission.

Cook, R.D., and S. Weisberg. 1994. *An Introduction to Regression Graphics.* New York: John Wiley and Sons, Inc.

Cukier, R.I., J.H. Schaibly, and K.E. Schuler. 1975. Study of the sensitivity of coupled reaction systems to uncertainties in rate coefficients. III: Analysis of the approximation. *Journal of Chemical Physics* 63(3): 1,140–1,149.

Cukier, R.I., C.M. Fortuin, K.E. Schuler, A.G. Petschek, and J.H. Schaibly. 1973. Study of the sensitivity of coupled reaction systems to uncertainties in rate coefficients. I: Theory. *Journal of Chemical Physics* 59(8): 3,873–3,878.

Cukier, R.I., H.B. Levine, and K.E. Schuler. 1978. Nonlinear standard sensitivity analysis of multiparameter model systems. *Journal of Computational Physics* 26: 1–42.

Draper, N.R.,and H. Smith, Jr. 1981. *Applied Regression Analysis.* 2nd Edition. New York: John Wiley and Sons, Inc.

Helton, J.C., J.W. Garner, R.D. McCurley, and D.K. Rudeen. 1991. *Sensitivity Analysis Techniques and Results for Performance Assessment at the Waste Isolation Pilot Plant.* SAND 90-7103. Albuquerque, NM: Sandia National Laboratories.

Iman, R.L., and W.J. Conover. 1979. The use of the rank transform in regression. *Techtonometrics* 21: 499–509.

Iman, R.L., J. Davenport, and D. Ziegler. 1980. *Latin Hypercube Sampling (Program User's Guide).* SAND-1473. Albuquerque, NM: Sandia National Laboratories.

Jarzemba, M.S., P.A. LaPlante, and K.J. Poor. 1997. *ASHPLUME Code Version 1.0 Model Description and User's Guide.* CNWRA 97-004. San Antonio, TX: Center for Nuclear Waste Regulatory Analyses.

Leigh, C.D., B.M. Thompson, J.E. Campbell, D.E. Longsine, R.A. Kennedy, and B.A. Napier. 1993. *User's Guide for GENII-S: A Code for Statistical and Deterministic Simulation of Radiation Doses to Humans from Radionuclides in the Environment.* SAND 91-0561. Albuquerque, NM: Sandia National Laboratories.

Lichtner, P.C., and M.S. Seth. 1996. *User's Manual for MULTIFLO: Part II—MULTIFLO 1.0 and GEM 1.0, Multicomponent-Multiphase Reactive Transport Model.* CNWRA 96-010. San Antonio, TX: Center for Nuclear Waste Regulatory Analyses.

Mason, R.L., R.F. Gunst, and J.L. Hess. 1989. *Statistical Design & Analysis of Experiments with Applications to Engineering and Science.* New York: John Wiley and Sons, Inc.

Mohanty, S., and T.J. McCartin, coordinators. 1998. *Total-system Performance Assessment (TPA) Version 3.2 Code: Module Description and User's Guide.* San Antonio, TX: Center for Nuclear Waste Regulatory Analyses.

Morgan, M.G., and M. Henrion. 1990. *Uncertainty: A Guide to Dealing with Uncertainty in Quantitative Risk and Policy Analysis.* New York: Cambridge University Press.

Morris, M.D. 1991. Factorial sampling plans for preliminary computational experiments. *Technometrics* 33(2): 161–174.

Nuclear Regulatory Commission. 1998. *Issue Resolution Status Report Key Technical Issues: Total-system Performance Assessment and Integration. Revision. 1.0.* Washington, DC: Nuclear Regulatory Commission.

Nuclear Regulatory Commission. 1999a. *Disposal of High-Level Radioactive Wastes in a Proposed Geological Repository at Yucca Mountain, Nevada: Proposed Rule.* Federal Register 64(34): 8640–8679. Washington, DC: U.S. Government Printing Office.

Nuclear Regulatory Commission. 1999b. *NRC Sensitivity and Uncertainty Analyses for a Proposed HLW Repository at Yucca Mountain, Nevada Using TPA 3.1. Volume II: Results and Conclusions.* NUREG–1668, Vol. 2. Washington, DC: Nuclear Regulatory Commission.

Olague, N.E., D.E. Longsine, J.E. Campbell, and C.D. Leigh. 1991. *User's Manual for the NEFTRAN II Computer Code.* NUREG/CR–5618. Washington, DC: Nuclear Regulatory Commission.

Seitz, R.R., A.S. Rood, G.A Harris, S.J. Maheras, and M. Kotechi. 1991. *Sample Application of Sensitivity/Uncertainty Analysis Techniques to a Groundwater Transport Problem.* DOE/LLW–108. Idaho Falls, ID: Idaho National Engineering Laboratory.

Sen, A., and M. Srivastava. 1990. *Regression Analysis-Theory, Methods and Applications.* New York: Springer-Verlag, Inc.

Stothoff, S.A., H.M. Castellaw, and A.C. Bagtzoglou. 1997. Simulating the spatial distribution of infiltration at Yucca Mountain, Nevada. *Water Resources Research.* Submitted for publication.

Stothoff, S.A. 1999 *Infiltration Abstraction for Shallow Soil Over Fractured Bedrock in a Semi-Arid Climate—Journal Paper.* San Antonio, TX: Center for Nuclear Waste Regulatory Analyses.

Strahler, A.N. 1969. *Physical Geography.* New York: John Wiley and Sons, Inc.

Suzuki, T. 1983. *A Theoretical Model for Dispersion of Tephra. Arc Volcanism: Physics and Tectonics.* Tokyo, Japan: Terra Scientific Publishing: 95–113.

Tschoepe, E., III, F. Lyle, Jr., D.M. Dancer, C.G. Interrante, and P.K. Nair. 1994. *Field Engineering Experience with Structural Materials.* San Antonio, TX: Center for Nuclear Waste Regulatory Analyses.

U.S. Department of Energy. 1998. Viability Assessment of a Repository at Yucca Mountain. Volume 3: Total System Performance Assessment. DOE/RW–0508/V3. Washington, DC: U.S. Department of Energy, Office of Civilian Radioactive Waste Management.

Wescott, R.G., M.P. Lee, N.A. Eisenberg, T.J. McCartin, and R.G. Baca, eds. 1995. *NRC Iterative Performance Assessment Phase 2.* NUREG–1464. Washington, DC: Nuclear Regulatory Commission.

Zimmerman, D.A. 1991. *A Review of Techniques for Propagating Data and Parameter Uncertainties in High-Level Waste Performance Assessment Models.* NUREG/CR–5395. Washington, DC: Nuclear Regulatory Commission.

APPENDIX A

DESIGN MATRIX FOR THE MORRIS METHOD

This appendix explains the steps necessary to obtain the matrix used by the TPA code as the input parameters. Let x_i, i = 1, 2, ..., I, be the elements of x, where x is the input parameter vector with I elements. Assuming $0 \le x_i \le 1$, the interval [0, 1] is now divided into p discrete levels. A randomly chosen base vector, x^*, is then obtained by assigning each element of x randomly from a set of discrete values: $\{0, 1/(p-1), 2/(p-1), \cdots, 1-\Delta\}$, where $\Delta = p/2(p-1)$. To obtain the matrix, first, a $(I+1)$-by-I sampling matrix, B, with elements of 0's and 1's is selected:

$$B = \begin{bmatrix} 0 & 0 & 0 & \cdots & 0 \\ 1 & 0 & 0 & \cdots & 0 \\ 1 & 1 & 0 & \cdots & 0 \\ \cdots & \cdots & \cdots & \cdots & \cdots \\ 1 & 1 & 1 & \cdots & 1 \end{bmatrix} \tag{A-1}$$

Matrix B has an important property that any row differs from its immediate neighboring rows only in one column. For instance, the second row differs from the first row only in the first column and the third row in the second column. A matrix obtained by multiplying B with Δ can be used to produce I values of $\partial y / \partial x_i$ based on (I + 1) runs. But the elements of the matrix are not randomly selected.

To randomize the matrix ΔB, the following operations are performed:

$$B^* = J_{(I+1),1}\, x^* + (\Delta/2)[(B - J_{(I+1),I})\, D^* + J_{(I+1),I}] \tag{A-2}$$

where

$$J_{(I+1),I} = \begin{bmatrix} 1 & 1 & 1 & \cdots & 1 \\ 1 & 1 & 1 & \cdots & 1 \\ 1 & 1 & 1 & \cdots & 1 \\ \cdots & \cdots & \cdots & \cdots & \cdots \\ 1 & 1 & 1 & \cdots & 1 \end{bmatrix}_{(I+1),I} \tag{A-3}$$

D^* is an I-dimensional diagonal matrix in which each diagonal element is either +1 or −1 with equal probability. The operations defined in Eq. (A-2) randomize the matrix ΔB. The matrix B^* is called design matrix.

Since the input variables are considered random, so is the output $y(x)$. If a distribution of r samples is required for each $\partial y/\partial x_i$, the previous process defined in Eq. (A-2) can be repeated r times to produce a r(I+1)-by-I design matrix X:

$$X_{r(I+1),I} = \begin{bmatrix} B_1^* \\ B_2^* \\ \cdots \\ B_r^* \end{bmatrix} \tag{A-4}$$

Each row of X will next be used as input to the TPA code to calculate $y(x)$, and the matrix X will be used to produce rI number of $\partial y/\partial x_i$, which, in turn, will produce I distributions for the input variables, each with r samples.

APPENDIX B

FORMALISM OF FOURIER AMPLITUDE SENSITIVITY TEST TECHNIQUE

Consider again the nonlinear computational model of Eq. (3-1), which has only one output variable and I input variables. The I input variables through I transformation functions can be represented as

$$x_i = g_i(\sin\omega_i s), i = 1, 2, \ldots, I \tag{B-1}$$

where g_i, $i = 1, \ldots, I$, are a set of trigonometric transform functions and ω_i, $i = 1, \ldots, I$, a set of integer frequencies, with one frequency assigned arbitrarily to each x_i of x (Cukier, 1973). Equation (B-1) is a parametric representation of a I-dimensional curve in the vector space of x. As s varies over the range $o \le s \le 2\pi$, $x_1, x_2, \ldots, x_I$ traverse the I-dimensional space simultaneously with a relative rate of traversal in each direction proportional to the frequency assigned to the direction.

After applying the transformation functions defined in Eq. (B-1) to the input vector x, the output variable $y(x)$ becomes a periodic function of s:

$$y(x) = y[g_1(\sin\omega_1 s), g_2(\sin\omega_2 s), \ldots, g_I(\sin\omega_I s)] = y(s) \tag{B-2}$$

and y can be expanded into a Fourier series:

$$y(s) = \frac{A_0}{2} + \sum_{i=1}^{I} A_i \sin(\omega_i s) = y(s + 2\pi) \tag{B-3}$$

The Fourier amplitudes A_i, $i = 1, 2, \ldots, I$, of the output variables corresponding to each frequency ω_i, $i = 1, \ldots, I$, can be obtained as (Schaibly and Schuler, 1973):

$$A_i = \frac{1}{\pi} \int_0^{2\pi} y(s)\sin(\omega_i s)ds, \; i = 1, 2, \ldots, I \tag{B-4}$$

The question now becomes whether the amplitudes A_i, $i = 1, 2, \ldots, I$, are strictly related to the input variable x_i, $i = 1, 2, \ldots, I$, and x_i only. If it can be shown that the Fourier amplitudes A_i, $i = 1, 2, \ldots, I$, are affected by the i^{th} parameter x_i only and not by any other parameters, then the Fourier amplitudes isolate, one by one, the sensitivity of the parameters x_i, $i = 1, 2, \ldots, I$, on the output. In other words, the magnitudes of the Fourier A_i, $i = 1, 2, \ldots, I$, give the quantitative measurements of sensitivities of the input variables x_i, $i = 1, 2, \ldots, I$. Because the measures are obtained by varying x_i, $i = 1, 2, \ldots, I$, simultaneously, the FAST method simulates a more realistic situation than other sensitivity analysis methods that vary only one parameter at a time.

The amplitudes A_i, $i = 1, 2, \ldots, I$, calculated according to Eq. (B-4) are truly related to the input variable x_i, $i = 1, 2, \ldots, I$, only if a set of incommensurate frequencies are used in Eq. (B-1), where "incommensurate" means that there does not exist a common divisor among the frequencies. But this would require that the Eq. (B-4) be evaluated over an infinite period. Instead, a set of integer frequencies is used. By using integer

frequencies, the output variable becomes a periodic function with a period of $2p$ and the amplitudes A_i, i = 1, 2, ..., I, can be obtained as

$$A_i = \frac{2}{N}\sum_{j=1}^{N} y(s_j)\sin(\omega_i s_j) \tag{B-5}$$

The use of integer frequencies causes some problems. For instance, if $\omega_4 = \omega_1 + \omega_2 - \omega_3$, then $A(\omega_4) = A(\omega_1 + \omega_2 - \omega_3)$, and A_4 will not only reflect the sensitivity of x_4, but also x_1, x_2, and x_3. In the FAST method, the integer frequency set is chosen such that

$$\sum_{i=1}^{I} r_i\omega_i \neq 0, \tag{B-6}$$

$$\sum_{i=1}^{I} |r_i| \leq M + 1 \tag{B-7}$$

where M and r_i, i = 1, 2, ..., I, are integers.

This set of frequencies is called approximately incommensurate to order M; it has the important property that no single frequency can be obtained by adding or subtracting any M frequencies. When the set of frequencies is used to determine the Fourier amplitudes A_i, i = 1, 2, ..., I, the amplitudes segregate the sensitivity of the input variables on the output to the order M. For instance, if M = 4, then there is no mutual interference between any four Fourier amplitudes, but there might be among five amplitudes coefficients. Therefore, the larger the value of M, the greater the likelihood that the Fourier amplitude of each input frequency reflects solely the influence of the corresponding rate coefficient. On the other hand, the larger the M, the more difficult it is to select integer frequencies that satisfy both Eqs. (B-6) and (B-7).

After selecting integer frequencies, N number of points are selected for s, which are used in Eq. (B-1) to generate x_i, i = 1, 2, ..., I, for numerical calculations:

$$s = \frac{2\pi j}{N}, \text{ j } = 1, 2, \ldots, N \tag{B-8}$$

But N cannot be an arbitrary integer. For instance, if $\omega_i = mN - \omega_k$, where m is an integer, then

$$y(\omega_i s) = y(mNs - \omega_k s) = y(2\pi im - \omega_k s) = y(\omega_k s) \tag{B-9}$$

and the amplitude A_i will not be distinguishable from A_k. To avoid this problem, N is chosen such that

$$\sum_{i=1}^{I} b_i \omega_i \neq mN \tag{B-10}$$

$$\sum_{i=1}^{I} |b_i| \leq M + 1 \tag{B-11}$$

where b_i, $i = 1, 2, ..., I$, and M is the same integer as in Eq. (B-7), in accordance to Eqs. (B-6) and (B-7).

The particular trigonometric transformation functions used are

$$x_i = \frac{1}{2} + \frac{1}{\pi} \arcsin[\sin(\omega_i s + r_i)], \; i = 1, 2, ..., I \tag{B-12}$$

where r_i, $i = 1, 2, ..., I$, are random numbers. The N points of s are then used in Eq. (B-12) to obtain x_i, $i = 1, 2, ..., I$ to calculate $y(x) = y(s)$. The values of x_i and y are then used in Eq. (B-5) to obtain the Fourier amplitudes A_i, $i = 1, 2, ..., I$.

REFERENCES

Schaibly, J.H., and K.E. Schuler. 1973. Study of the sensitivity of coupled reaction systems to uncertainties in rate coefficients. II: Applications. *Journal of Chemical Physics* 59(8): 3,879–3,888.

APPENDIX C

FORMALIZATION OF PARAMETER TREE SENSITIVITY ANALYSIS APPROACH

The following is a formal explanation of the parameter tree sensitivity analysis approach presented in section 4.1.5. Let $\hat{x}_i$ be the median value of x_i, $\hat{y}$ the median value of y, and I the total number of sampled parameters. In this development, median values are used for partitioning criteria, but any other statistical or physical branching criterion could also be used. The first step is to partition all of the realizations into two bins:

$$x_{I^+} = \left[\forall \text{ realizations with } x_{I,j} \geq x_I\right] \tag{C-1a}$$

$$x_{I^-} = \left[\forall \text{ realizations with } x_{I,j} < \hat{x}_1\right] \tag{C-1b}$$

where j represents a particular realization, assume that the two bins contain N_{I^+} and N_{I^-} members, where $N_{1^+} + N_{1^-} = N$ is the total number of samples or realizations. Note that when the partitioning criterion is the median value, $N_{I^+} = N_{I^-} = N/2$, but that will not be true for other branching criteria.

Now consider the N_{I^+} realizations of y that are produced by the x_{1^+} set. From these N_{I^+} realizations, we select those that meet the following criterion:

$$y_{1^+} = \left[\forall \textit{ realizations with } y_j \geq \hat{y} \,|\, x_{1,j} \in x_{1^+}\right] \tag{C-2}$$

Let the number of realizations satisfying this criteria be L_{1^+}. It follows that

$$p_{1^+} = P\{y \geq \hat{y} | x_1 \geq \hat{x}_1\} = \frac{L_{1^+}}{N_{1^+}} \tag{C-3}$$

The second branch of the tree is associated with the y_{1^-} bin containing L_{I^-} members, where

$$y_{1^-} = \left[\forall \text{ realizations with } y_j \geq \hat{y} | x_{1,j} \in x_{1^-}\right] \tag{C-4}$$

In this case, similar to Eq. (C-3),

$$p_{1^-} = P\{y \geq \hat{y} \;|\, x_1 < \hat{x}_1\} = \frac{L_{1^-}}{N_{1^-}} \tag{C-5}$$

Equal values of p_{1^+} and p_{1^-} would imply that whether x_1 takes values greater or smaller than its median, it does not affect the bin into which y values fall, thus indicating a lack of correlation or lack of sensitivity

of y to x_1. Consequently, a measure of relative sensitivity of y with respect to x_1 can be constructed as $|p_{1^+} - p_{1^-}|$. It is noted that the proposed measure provides only relative sensitivity because it does not provide a precise description of the change in y for a given change in x_1, as a measure for absolute sensitivity would provide. However, the relative sensitivity measure is sufficient for ranking important parameters. In general, one can partition the $x_{1,j}$ (and subsequent parameter realizations) into more than two bins but such a generalization will lead to a complicated tree structure (i.e., with potentially large numbers of branches per level) and is not pursued further here.

The branching strategy explained previously is now implemented for the second, third, and subsequent parameters until most of the output is sufficiently explained. For the second parameter, the procedure is as follows. Partition the bin x_{1^+} containing N_{1^+} realizations into two bins:

$$x_{1^+2^-} = \left[\forall \text{ realizations with } x_{1,j} \geq \hat{x}_1 \cap x_{2,j} < \hat{x}_2\right] \tag{C-6a}$$

and

$$x_{1^+2^+} = \left[\forall \text{ realizations with } x_{1,j} \geq \hat{x}_1 \cap x_{2,j} \geq \hat{x}_2\right] \tag{C-6b}$$

Similarly, the x_{1^-} bin can also be partitioned into two bins:

$$x_{1^-2^+} = \left[\forall \text{ realizations with } x_{1,j} < \hat{x}_1 \cap x_{2,j} \geq \hat{x}_2\right] \tag{C-6c}$$

and

$$x_{1^-2^-} = \left[\forall \text{ realizations with } x_{1,j} < \hat{x}_1 \cap x_{2,j} < \hat{x}_2\right]. \tag{C-6d}$$

Let the number of members in each of the four bins be $N_{1^+2^+}$, $N_{1^+2^-}$, $N_{1^-2^+}$, and $N_{1^-2^-}$. The output realizations associated with members of a bin are now scrutinized to count the number of realizations in which $y \geq \hat{y}$. Thus, the four output bins associated with the four branches of the tree at the second parameter level are

$$y_{1^+2^+} = \left[y_j \geq \hat{y} \middle| x_{1,j}, x_{2,j} \in x_{1^+2^+}\right] \tag{C-7a}$$

$$y_{1^+2^-} = \left[y_j \geq \hat{y} \middle| x_{1,j}, x_{2,j} \in x_{1^+2^-}\right] \tag{C-7b}$$

$$y_{1^-2^+} = \left[y_j \geq \hat{y} \middle| x_{1,j}, x_{2,j} \in x_{1^-2^+}\right] \tag{C-7c}$$

$$y_{1^-2^-} = \left[y_j \geq \hat{y} \middle| x_{1,j}, x_{2,j} \in x_{1^-2^-} \right] \tag{C-7d}$$

Let the number of realizations associated with the four bins of Eq. (C-7) be $L_{1^+2^+}$, $L_{1^+2^-}$, $L_{1^-2^+}$, and $L_{1^-2^-}$. Then at the second level of the tree, we can make the following probability statements:

$$p_{1^+2^+} = P\left\{ y \geq \hat{y} \middle| x_{1,j} \geq \hat{x}_1 \cap x_{2,k} \geq \hat{x}_2 \right\} = \frac{L_{1^+2^+}}{N_{1^+2^+}} \tag{C-8a}$$

and with similar interpretations,

$$p_{1^+2^-} = \frac{L_{1^+2^-}}{N_{1^+2^-}} \tag{C-8b}$$

$$p_{1^-2^+} = \frac{L_{1^-2^+}}{N_{1^-2^+}} \tag{C-8c}$$

$$p_{1^-2^-} = \frac{L_{1^-2^-}}{N_{1^-2^-}}. \tag{C-8d}$$

If $p_{1^+2^+} = p_{1^+2^-}$, then the second parameter, x_2, (given $x_1 \geq \hat{x}_1$) has no influence on y. Thus, relative sensitivities of x_2 can be partially measured by $\left| p_{1^+2^+} - p_{1^+2^-} \right|$ and $\left| p_{1^-2^+} - p_{1^-2^-} \right|$ for the cases of $x_1 \geq \hat{x}_1$ and $x_1 < \hat{x}_1$. The total relative sensitivity of y to x_2 can be determined from

$$S_{x_2} = \left| p_{1^+2^+} - p_{1^+2^-} \right| P\{x_1 \geq \hat{x}_1\} + \left| p_{1^-2^+} - p_{1^-2^-} \right| P\{x_1 < \hat{x}_1\} \tag{C-9}$$

Also, $p_{1^+2^+}$ equal to $p_{1^-2^-}$ implies that whether the first two parameters together had high (greater than their medians) or low (smaller than their medians) values, there is an equal chance of producing a y lower or higher than its median value. We use the quantity $\frac{\left| p_{1^+2^+} - p_{1^-2^-} \right|}{1 - \left| p_{1^+2^+} - p_{1^-2^-} \right|}$ as a measure of the relative sensitivity of y jointly to x_1 and x_2. For this example, it is assumed that both x_1 and x_2 are positively correlated with y (i.e., large values of x_1 and x_2 lead to large values of y and vice-versa). In general, this is not a valid assumption and input parameters can be positively or negatively correlated with the output variable. Hence, we now change our nomenclature for the joint relative sensitivity such that the coefficient is now defined

as $\frac{|p_H - p_L|}{1-|p_H - p_L|}$, where p_H and p_L are the greatest and least values of p among the bins. In this formulation, the numerator represents the "distance" of the output variable from perfect noncorrelation with the input parameter set (i.e., if y has no correlation with the input parameter set under study, then p is the same in all bins, and the numerator is zero). Similarly, the denominator represents the distance of the output variable from perfect correlation with the input parameter (i.e., if y shows perfect correlation with the input parameter set under study, p is unity in the highest bin and zero in the lowest bin, and the denominator is zero). With this formulation, the joint relative sensitivity is on the range $[0,\infty]$. This formulation can be extended to any number of parameters.

APPENDIX D

DESCRIPTION OF ABBREVIATIONS USED FOR TPA VERSION 3.2 CODE INPUT PARAMETERS

Short Name	Full Name	Description
AA_2_1	AA_2_1[C/m^2/yr]	A corrosion rate (passive current density) for the WP inner overpack in EBSFAIL.
AAMAI@S	ArealAverageMeanAnnualInfiltrationAtStart[mm/yr]	Mean areal average infiltration into the subsurface at the start of a TPA 3.2 run.
ABMLFVDC	AirborneMassLoadForVolcanismDoseCalculation[g/m3]	Mass load of ash/SF from volcanic event in the air available for inhalation by a receptor.
APrs_SAV	AlluviumMatrixPorosity_SAV	Amargosa Valley alluvium saturated zone matrix porosity.
AqThick5	AquiferThickness5km[m]	Thickness of the aquifer at a location 5 km south of Yucca Mountain.
ARDSAV_I	AlluviumMatrixRD_SAV_I	Matrix retardation for iodine in the saturated zone of the Amargosa Valley alluvium.
ARDSAV_U	AlluviumMatrixRD_SAV_U	Matrix retardation for uranium in the saturated zone of the Amargosa Valley alluvium.
ARDSAVAm	AlluviumMatrixRD_SAV_Am	Matrix retardation for americium in the saturated zone of the Amargosa Valley alluvium.
ARDSAVCs	AlluviumMatrixRD_SAV_Cs	Matrix retardation for cesium in the saturated zone of the Amargosa Valley alluvium.

DESCRIPTION OF ABBREVIATIONS USED FOR TPA VERSION 3.2 CODE INPUT PARAMETERS (cont'd)

Short Name	Full Name	Description
ARDSAVNb	AlluviumMatrixRD_SAV_Nb	Matrix retardation for niobium in the saturated zone of the Amargosa Valley alluvium.
ARDSAVNi	AlluviumMatrixRD_SAV_Ni	Matrix retardation for nickel in the saturated zone of the Amargosa Valley alluvium.
ARDSAVNp	AlluviumMatrixRD_SAV_Np	Matrix retardation for neptunium in the saturated zone of the Amargosa Valley alluvium.
ARDSAVPb	AlluviumMatrixRD_SAV_Pb	Matrix retardation for lead in the saturated zone of the Amargosa Valley alluvium.
ARDSAVPu	AlluviumMatrixRD_SAV_Pu	Matrix retardation for plutonium in the saturated zone of the Amargosa Valley alluvium.
ARDSAVRa	AlluviumMatrixRD_SAV_Ra	Matrix retardation for radium in the saturated zone of the Amargosa Valley alluvium.
ARDSAVSe	AlluviumMatrixRD_SAV_Se	Matrix retardation for selenium in the saturated zone of the Amargosa Valley alluvium.
ARDSAVTc	AlluviumMatrixRD_SAV_Tc	Matrix retardation for technetium in the saturated zone of the Amargosa Valley alluvium.
ARDSAVTh	AlluviumMatrixRD_SAV_Th	Matrix retardation for thorium in the saturated zone of the Amargosa Valley alluvium.

DESCRIPTION OF ABBREVIATIONS USED FOR TPA VERSION 3.2 CODE INPUT PARAMETERS (cont'd)

Short Name	Full Name	Description
AshMnPLD	AshMeanParticleLogDiameter[d_in_cm]	Relative size of ash/SF particulates from a volcanic event.
*Chlorid	ChlorideMultFactor	Factor by which chloride concentration in matrix is multiplied to compensate for dripping and drying that would lead to salt accumulation.
CladCorF	CladdingCorrectionFactor	A variable allowing for increased SF protection in a WP due to the presence of cladding on the SF.
CritRHAC	CriticalRelativeHumidityAqueousCorrosion	Critical relative humidity above which aqueous corrosion may initiate.
FEROI-Tn	TimeOfNextFaultingEventinRegionOfInterest[yr]	Time of the next faulting event in the repository area (years from present).
FEROI-X	XlocationOfFaultingEventInRegionOfInterest[m]	X location of the center of the faulting event within the repository area.
FEROI-Y	YlocationOfFaultingEventInRegionOfInterest[m]	Y location of the center of the faulting event within the repository area

DESCRIPTION OF ABBREVIATIONS USED FOR TPA VERSION 3.2 CODE INPUT PARAMETERS (cont'd)

Short Name	Full Name	Description
Fmult*	FmultFactor	The fraction of water infiltrating to the repository from the unsaturated zone above the repository that will enter the WP and contribute to the release of radionuclides. Water dripping toward the drifts may be diverted around the drift due to capillary action, may be diverted down the side of the drift, or may not enter the WP for other reasons.
FO-Rn#Sd	RntoDetermineFaultOrientation	Random number selected to determine the orientation of the fault within the repository area.
FOC-R	FractionOfCondensateRemoved[1/yr]	Fraction of water condensate removed in each reflux3 time step.
FOCTR	FractionOfCondensateTowardRepository[1/yr]	Fraction of water condensate moving towards the repository.
FOCTR-R	FractionOfCondensateTowardRepositoryRemoved[1/yr]	Fraction of water condensate moving towards the repository but escaped before entering the repository.
Fow*	FowFactor	A flow focusing factor which expresses the flow potentially reaching a wetted WP (can be greater or less than 1.0).
FPrm_BFw	FracturePermeability_BFw_[m^2]	Bullfrog-welded fracture permeability (UZ).
FPrm_CHv	FracturePermeability_CHnv[m^2]	Calico Hills-nonwelded vitric fracture permeability (UZ).
FPrm_CHz	FracturePermeability_CHnz[m^2]	Calico Hills-nonwelded zeolitic fracture permeability (UZ).
FPrm_PPw	FracturePermeability_PPw_[m^2]	Prow Pass-welded fracture permeability (UZ).

DESCRIPTION OF ABBREVIATIONS USED FOR TPA VERSION 3.2 CODE INPUT PARAMETERS (cont'd)

Short Name	Full Name	Description
FPrm_TSw	FracturePermeability_TSw_[m^2]	Topopah Spring-welded fracture permeability (UZ).
FPrm_UCF	FracturePermeability_UCF_[m^2]	Upper Crater Flat fracture permeability (UZ).
FPrm_UFZ	FracturePermeability_UFZ_[m^2]	Unsaturated Fracture Zone fracture permeability (UZ).
FPrs_BFw	FracturePorosity_BFw_	Bullfrog-welded fracture porosity (UZ).
FPrs_CHv	FracturePorosity_CHnv	Calico Hills-nonwelded vitric fracture porosity (UZ).
FPrs_CHz	FracturePorosity_CHnz	Calico Hills-nonwelded zeolitic fracture porosity (UZ).
FPrs_PPw	FracturePorosity_PPw_	Prow Pass-welded fracture porosity (UZ).
FPrs_STF	FracturePorosity_STFF	Fracture porosity of saturated tuff (SZ)
FPrs_TSw	FracturePorosity_TSw_	Topopah Spring-welded fracture porosity (UZ).
FPrs_UCF	FracturePorosity_UCF_	Upper Crater Flat fracture porosity (UZ).
FPrs_UFZ	FracturePorosity_UFZ_	Unsaturated Fracture Zone fracture porosity (UZ).
H2O-FThk	ThicknessOfWaterFilm[m]	Thickness of water film on WP surface
InitRSFP	InitialRadiusOfSFParticle[m]	Initial radium of spent fuel particle - affects SF alteration rate and transport out of a failed WP in EBSREL.

DESCRIPTION OF ABBREVIATIONS USED FOR TPA VERSION 3.2 CODE INPUT PARAMETERS (cont'd)

Short Name	Full Name	Description
InnOvrEI	InnerOverpackErpIntercept	Inner overpack E_{rp} intercept.
InvMPerm	InvertMatrixPermeability[m^2]	Matrix permeability of the invert.
MAPM@GM	MeanAveragePrecipitationMultiplierAtGlacialMaximum	Mean annual precipitation increase at glacial maximum - affects infiltration from the land surface in UZFLOW.
MATI@GM	MeanAverageTemperatureIncreaseAtGlacialMaximum[°C]	Magnitude of mean annual temperature change at glacial maximum—affects infiltration from the land surface in UZFLOW.
MixZnT20	MixingZoneThickness20km[m]	Mixing zone thickness in a well at a receptor group 20 km from YM.
MKD_BFwU	MatrixKD_BFw_U[m3/kg]	Bullfrog-welded matrix K_d for U
MKD_CHvU	MatrixKD_CHnvU[m3/kg]	Calico Hills-nonwelded vitric matrix K_d for U
MKD_CHzU	MatrixKD_CHnzU[m3/kg]	Calico Hills-nonwelded zeolitic matrix K_d for U
MKD_PPwU	MatrixKD_PPw_U[m3/kg]	Prow Pass-welded matrix K_d for U
MKD_TSwU	MatrixKD_TSw_U[m3/kg]	Topopah Spring-welded matrix K_d for U
MKD_UCFU	MatrixKD_UCF_U[m3/kg]	Upper Crater Flat matrix K_d for U
MKDBFwAm	MatrixKD_BFw_Am[m3/kg]	Bullfrog-welded matrix K_d for Am

DESCRIPTION OF ABBREVIATIONS USED FOR TPA VERSION 3.2 CODE INPUT PARAMETERS (cont'd)

Short Name	Full Name	Description
MKDBFwCs	MatrixKD_BFw_Cs[m3/kg]	Bullfrog-welded matrix K_d for Cs
MKDBFwNi	MatrixKD_BFw_Ni[m3/kg]	Bullfrog-welded matrix K_d for Ni
MKDBFwNp	MatrixKD_BFw_Np[m3/kg]	Bullfrog-welded matrix K_d for Np
MKDBFwPb	MatrixKD_BFw_Pb[m3/kg]	Bullfrog-welded matrix K_d for Pb
MKDBFwPu	MatrixKD_BFw_Pu[m3/kg]	Bullfrog-welded matrix K_d for Pu
MKDBFwRa	MatrixKD_BFw_Ra[m3/kg]	Bullfrog-welded matrix K_d for Ra
MKDBFwSe	MatrixKD_BFw_Se[m3/kg]	Bullfrog-welded matrix K_d for Se
MKDBFwTh	MatrixKD_BFw_Th[m3/kg]	Bullfrog-welded matrix K_d for Th
MKDCHvAm	MatrixKD_CHnvAm[m3/kg]	Calico Hills-nonwelded vitric matrix K_d for Am
MKDCHvCs	MatrixKD_CHnvCs[m3/kg]	Calico Hills-nonwelded vitric matrix K_d for Cs
MKDCHvNi	MatrixKD_CHnvNi[m3/kg]	Calico Hills-nonwelded vitric matrix K_d for Ni
MKDCHvNp	MatrixKD_CHnvNp[m3/kg]	Calico Hills-nonwelded vitric matrix K_d for Np
MKDCHvPb	MatrixKD_CHnvPb[m3/kg]	Calico Hills-nonwelded vitric matrix K_d for Pb
MKDCHvPu	MatrixKD_CHnvPu[m3/kg]	Calico Hills-nonwelded vitric matrix K_d for Pu

DESCRIPTION OF ABBREVIATIONS USED FOR TPA VERSION 3.2 CODE INPUT PARAMETERS (cont'd)

Short Name	Full Name	Description
MKDCHvRa	MatrixKD_CHnvRa[m3/kg]	Calico Hills-nonwelded vitric matrix K_d for Ra
MKDCHvSe	MatrixKD_CHnvSe[m3/kg]	Calico Hills-nonwelded vitric matrix K_d for Se
MKDCHvTh	MatrixKD_CHnvTh[m3/kg]	Calico Hills-nonwelded vitric matrix K_d for Th
MKDCHzAm	MatrixKD_CHnzAm[m3/kg]	Calico Hills-nonwelded zeolitic matrix K_d for Am
MKDCHzCs	MatrixKD_CHnzCs[m3/kg]	Calico Hills-nonwelded zeolitic matrix K_d for Cs
MKDCHzNi	MatrixKD_CHnzNi[m3/kg]	Calico Hills-nonwelded zeolitic matrix K_d for Ni
MKDCHzNp	MatrixKD_CHnzNp[m3/kg]	Calico Hills-nonwelded zeolitic matrix K_d for Np
MKDCHzPb	MatrixKD_CHnzPb[m3/kg]	Calico Hills-nonwelded zeolitic matrix K_d for Pb
MKDCHzPu	MatrixKD_CHnzPu[m3/kg]	Calico Hills-nonwelded zeolitic matrix K_d for Pu
MKDCHzRa	MatrixKD_CHnzRa[m3/kg]	Calico Hills-nonwelded zeolitic matrix K_d for Ra
MKDCHzSe	MatrixKD_CHnzSe[m3/kg]	Calico Hills-nonwelded zeolitic matrix K_d for Se
MKDCHzTh	MatrixKD_CHnzTh[m3/kg]	Calico Hills-nonwelded zeolitic matrix K_d for Th
MKDPPwAm	MatrixKD_PPw_Am[m3/kg]	Prow Pass-welded matrix K_d for Am
MKDPPwCs	MatrixKD_PPw_Cs[m3/kg]	Prow Pass-welded matrix K_d for Cs

DESCRIPTION OF ABBREVIATIONS USED FOR TPA VERSION 3.2 CODE INPUT PARAMETERS (cont'd)

Short Name	Full Name	Description
MKDPPwNi	MatrixKD_PPw_Ni[m3/kg]	Prow Pass-welded matrix K_d for Ni
MKDPPwNp	MatrixKD_PPw_Np[m3/kg]	Prow Pass-welded matrix K_d for Np
MKDPPwPb	MatrixKD_PPw_Pb[m3/kg]	Prow Pass-welded matrix K_d for Pb
MKDPPwPu	MatrixKD_PPw_Pu[m3/kg]	Prow Pass-welded matrix K_d for Pu
MKDPPwRa	MatrixKD_PPw_Ra[m3/kg]	Prow Pass-welded matrix K_d for Ra
MKDPPwSe	MatrixKD_PPw_Se[m3/kg]	Prow Pass-welded matrix K_d for Se
MKDPPwTh	MatrixKD_PPw_Th[m3/kg]	Prow Pass-welded matrix K_d for Th
MKDTSwAm	MatrixKD_TSw_Am[m3/kg]	Topopah Spring-welded matrix K_d for Am
MKDTSwCs	MatrixKD_TSw_Cs[m3/kg]	Topopah Spring-welded matrix K_d for Cs
MKDTSwNi	MatrixKD_TSw_Ni[m3/kg]	Topopah Spring-welded matrix K_d for Ni
MKDTSwNp	MatrixKD_TSw_Np[m3/kg]	Topopah Spring-welded matrix K_d for Np
MKDTSwPb	MatrixKD_TSw_Pb[m3/kg]	Topopah Spring-welded matrix K_d for Pb
MKDTSwPu	MatrixKD_TSw_Pu[m3/kg]	Topopah Spring-welded matrix K_d for Pu
MKDTSwRa	MatrixKD_TSw_Ra[m3/kg]	Topopah Spring-welded matrix K_d for Ra

DESCRIPTION OF ABBREVIATIONS USED FOR TPA VERSION 3.2 CODE INPUT PARAMETERS (cont'd)

Short Name	Full Name	Description
MKDTSwSe	MatrixKD_TSw_Se[m3/kg]	Topopah Spring-welded matrix K_d for Se
MKDTSwTh	MatrixKD_TSw_Th[m3/kg]	Topopah Spring-welded matrix K_d for Th
MKDUCFAm	MatrixKD_UCF_Am[m3/kg	Upper Crater Flat matrix K_d for Am
MKDUCFCs	MatrixKD_UCF_Cs[m3/kg]	Upper Crater Flat matrix K_d for Cs
MKDUCFNi	MatrixKD_UCF_Ni[m3/kg]	Upper Crater Flat matrix K_d for Ni
MKDUCFNp	MatrixKD_UCF_Np[m3/kg]	Upper Crater Flat matrix K_d for Np
MKDUCFPb	MatrixKD_UCF_Pb[m3/kg]	Upper Crater Flat matrix K_d for Pb
MKDUCFPu	MatrixKD_UCF_Pu[m3/kg]	Upper Crater Flat matrix K_d for Pu
MKDUCFRa	MatrixKD_UCF_Ra[m3/kg]	Upper Crater Flat matrix K_d for Ra
MKDUCFSe	MatrixKD_UCF_Se[m3/kg]	Upper Crater Flat matrix K_d for Se
MKDUCFTh	MatrixKD_UCF_Th[m3/kg]	Upper Crater Flat matrix K_d for Th
MKDUFZ_U	MatrixKD_UFZ_U[m3/kg]	Unsaturated Fracture Zone matrix K_d for U
MKDUFZAm	MatrixKD_UFZ_Am[m3/kg]	Unsaturated Fracture Zone matrix K_d for Am
MKDUFZCs	MatrixKD_UFZ_Cs[m3/kg]	Unsaturated Fracture Zone matrix Kd for Cs

DESCRIPTION OF ABBREVIATIONS USED FOR TPA VERSION 3.2 CODE INPUT PARAMETERS (cont'd)

Short Name	Full Name	Description
MKDUFZNi	MatrixKD_UFZ_Ni[m3/kg]	Unsaturated Fracture Zone matrix K_d for Ni
MKDUFZNp	MatrixKD_UFZ_Np[m3/kg]	Unsaturated Fracture Zone matrix K_d for Np
MKDUFZPb	MatrixKD_UFZ_Pb[m3/kg]	Unsaturated Fracture Zone matrix K_d for Pb
MKDUFZPu	MatrixKD_UFZ_Pu[m3/kg]	Unsaturated Fracture Zone matrix K_d for Pu
MKDUFZRa	MatrixKD_UFZ_Ra[m3/kg]	Unsaturated Fracture Zone matrix K_d for Ra
MKDUFZSe	MatrixKD_UFZ_Se[m3/kg]	Unsaturated Fracture Zone matrix K_d for Se
MKDUFZTh	MatrixKD_UFZ_Th[m3/kg]	Unsaturated Fracture Zone matrix K_d for Th
Mprm_BFw	MatrixPermeability_BFw_[m2]	Bullfrog-welded matrix permeability
MPrm_CHv	MatrixPermeability_CHnv[m2]	Calico Hills-nonwelded vitric matrix permeability
MPrm_CHz	MatrixPermeability_CHnz[m2]	Calico Hills-nonwelded zeolitic matrix permeability
MPrm_PPw	MatrixPermeability_PPw_[m2]	Prow Pass-welded matrix permeability
MPrm_TSw	MatrixPermeability_TSw_[m2]	Topopah Spring-welded matrix permeability
MPrm_UCF	MatrixPermeability_UCF_[m2]	Upper Crater Flat matrix permeability
MPrm_UFZ	MatrixPermeability_UFZ_[m2]	Unsaturated Fracture Zone matrix permeability

DESCRIPTION OF ABBREVIATIONS USED FOR TPA VERSION 3.2 CODE INPUT PARAMETERS (cont'd)

Short Name	Full Name	Description
NEFZnW	NEFaultZoneWidth[m]	North East fault zone width
NELCDAmt	NEAmountOfLargestCredibleDisplacement[m]	North East largest credible displacement
NWFZnW	NWFaultZoneWidth[m]	North West fault zone width
NWLCDAmt	NWAmountOfLargestCredibleDisplacement[m]	North West largest credible displacement
OO-CofLC	CoefForLocCorrOfOuterOverpack	Coefficient for localized corrosion rate of outer overpack
PlumeTh5	PlumeThickness5km[m]	Plume thickness at 5 km
SbArWt%	SubAreaWetFraction	Subarea wet fraction
SbGFRATF	SubGrainFragmentRadiusAfterTransFrac[m]	Subgrain fragment radius of UO_2 particle after transgranular fracture; used only if fuel conversion takes place from UO_2 to $UO_{2.4}$ and U_3O_8; used only by the SF dissolution models that are dependent on exposed surface area
SFWt%C1	SFWettedFraction_Corrosion_1	Spent fuel wet fraction for corrosion failures in subarea 1
SFWt%C2	SFWettedFraction_Corrosion_2	Spent fuel wet fraction for corrosion failures in subarea 2
SFWt%C3	SFWettedFraction_Corrosion_3	Spent fuel wet fraction for corrosion failures in subarea 3
SFWt%C4	SFWettedFraction_Corrosion_4	Spent fuel wet fraction for corrosion failures in subarea 4

DESCRIPTION OF ABBREVIATIONS USED FOR TPA VERSION 3.2 CODE INPUT PARAMETERS (cont'd)

Short Name	Full Name	Description
SFWt%C5	SFWettedFraction_Corrosion_5	Spent fuel wet fraction for corrosion failures in subarea 5
SFWt%C6	SFWettedFraction_Corrosion_6	Spent fuel wet fraction for corrosion failures in subarea 6
SFWt%C7	SFWettedFraction_Corrosion_7	Spent fuel wet fraction for corrosion failures in subarea 7
SFWt%F0	SFWettedFraction_FAULTO	Spent fuel wet fraction for faulting failures
SFWt%I1	SFWettedFraction_Initial_1	Spent fuel wet fraction for initial failures in subarea 1
SFWt%I2	SFWettedFraction_Initial_2	Spent fuel wet fraction for initial failures in subarea 2
SFWt%I3	SFWettedFraction_Initial_3	Spent fuel wet fraction for initial failures in subarea 3
SFWt%I4	SFWettedFraction_Initial_4	Spent fuel wet fraction for initial failures in subarea 4
SFWt%I5	SFWettedFraction_Initial_5	Spent fuel wet fraction for initial failures in subarea 5
SFWt%I6	SFWettedFraction_Initial_6	Spent fuel wet fraction for initial failures in subarea 6
SFWt%I7	SFWettedFraction_Initial_7	Spent fuel wet fraction for initial failures in subarea 7
SFWt%S11	SFWettedFraction_SEISMO1_1	Spent fuel wet fraction for seismic failures for seismic interval 1 in subarea 1
SFWt%S12	SFWettedFraction_SEISMO1_2	Spent fuel wet fraction for seismic failures for seismic interval 1 in subarea 2

DESCRIPTION OF ABBREVIATIONS USED FOR TPA VERSION 3.2 CODE INPUT PARAMETERS (cont'd)

Short Name	Full Name	Description
SFWt%S13	SFWettedFraction_SEISMO1_3	Spent fuel wet fraction for seismic failures for seismic interval 1 in subarea 3
SFWt%S14	SFWettedFraction_SEISMO1_4	Spent fuel wet fraction for seismic failures for seismic interval 1 in subarea 4
SFWt%S15	SFWettedFraction_SEISMO1_5	Spent fuel wet fraction for seismic failures for seismic interval 1 in subarea 5
SFWt%S16	SFWettedFraction_SEISMO1_6	Spent fuel wet fraction for seismic failures for seismic interval 1 in subarea 6
SFWt%S17	SFWettedFraction_SEISMO1_7	Spent fuel wet fraction for seismic failures for seismic interval 1 in subarea 7
SFWt%S21	SFWettedFraction_SEISMO2_1	Spent fuel wet fraction for seismic failures for seismic interval 2 in subarea 1
SFWt%S22	SFWettedFraction_SEISMO2_2	Spent fuel wet fraction for seismic failures for seismic interval 2 in subarea 2
SFWt%S23	SFWettedFraction_SEISMO2_3	Spent fuel wet fraction for seismic failures for seismic interval 2 in subarea 3
SFWt%S24	SFWettedFraction_SEISMO2_4	Spent fuel wet fraction for seismic failures for seismic interval 2 in subarea 4

DESCRIPTION OF ABBREVIATIONS USED FOR TPA VERSION 3.2 CODE INPUT PARAMETERS (cont'd)

Short Name	Full Name	Description
SFWt%S25	SFWettedFraction_SEISMO2_5	Spent fuel wet fraction for seismic failures for seismic interval 2 in subarea 5
SFWt%S26	SFWettedFraction_SEISMO2_6	Spent fuel wet fraction for seismic failures for seismic interval 2 in subarea 6
SFWt%S27	SFWettedFraction_SEISMO2_7	Spent fuel wet fraction for seismic failures for seismic interval 2 in subarea 7
SFWt%S31	SFWettedFraction_SEISMO3_1	Spent fuel wet fraction for seismic failures for seismic interval 3 in subarea 1
SFWt%S32	SFWettedFraction_SEISMO3_2	Spent fuel wet fraction for seismic failures for seismic interval 3 in subarea 2
SFWt%S33	SFWettedFraction_SEISMO3_3	Spent fuel wet fraction for seismic failures for seismic interval 3 in subarea 3
SFWt%S34	SFWettedFraction_SEISMO3_4	Spent fuel wet fraction for seismic failures for seismic interval 3 in subarea 4
SFWt%S35	SFWettedFraction_SEISMO3_5	Spent fuel wet fraction for seismic failures for seismic interval 3 in subarea 5
SFWt%S36	SFWettedFraction_SEISMO3_6	Spent fuel wet fraction for seismic failures for seismic interval 3 in subarea 6

DESCRIPTION OF ABBREVIATIONS USED FOR TPA VERSION 3.2 CODE INPUT PARAMETERS (cont'd)

Short Name	Full Name	Description
SFWt%S37	SFWettedFraction_SEISMO3_7	Spent fuel wet fraction for seismic failures for seismic interval 3 in subarea 7
SFWt%S41	SFWettedFraction_SEISMO4_1	Spent fuel wet fraction for seismic failures for seismic interval 4 in subarea 1
SFWt%S42	SFWettedFraction_SEISMO4_2	Spent fuel wet fraction for seismic failures for seismic interval 4 in subarea 2
SFWt%S43	SFWettedFraction_SEISMO4_3	Spent fuel wet fraction for seismic failures for seismic interval 4 in subarea 3
SFWt%S44	SFWettedFraction_SEISMO4_4	Spent fuel wet fraction for seismic failures for seismic interval 4 in subarea 4
SFWt%S45	SFWettedFraction_SEISMO4_5	Spent fuel wet fraction for seismic failures for seismic interval 4 in subarea 5
SFWt%S46	SFWettedFraction_SEISMO4_6	Spent fuel wet fraction for seismic failures for seismic interval 4 in subarea 6
SFWt%S47	SFWettedFraction_SEISMO4_7	Spent fuel wet fraction for seismic failures for seismic interval 4 in subarea 7
SFWt%V0	SFWettedFraction_VOLCANO	Spent fuel wet fraction for volcanic failures
Solbl-Am	SolubilityAm[kg/m3]	Solubility limit for americium

DESCRIPTION OF ABBREVIATIONS USED FOR TPA VERSION 3.2 CODE INPUT PARAMETERS (cont'd)

Short Name	Full Name	Description
Solbl-Np	SolubilityNp[kg/m3]	Solubility limit for neptunium
Solbl-Pu	SolubilityPu[kg/m3]	Solubility limit for plutonium
SSMO-JS3	SEISMOJointSpacing3[m]	Joint spacing (JS) for rock condition 3. Not all rocks falling from the roof of the emplacement will impact WPs. The effective size of the rock that impacts WPs will be controlled by JS.
SSMO-JS4	SEISMOJointSpacing4[m]	Joint spacing (JS) for rock condition 4
SSMO-JS1	SEISMOJointSpacing1[m]	Joint spacing (JS) for rock condition 1
SSMO-RE	RockModulusOfElasticityforSEISMO[Pa]	Rock modulus of elasticity
SSMO-JS2	SEISMOJointSpacing2[m]	Joint spacing (JS) for rock condition 2
SSMO-JS5	SEISMOJointSpacing5[m]	Joint spacing (JS) for rock condition 5
SSMO-RPR	RockPoissonRatioforSEISMO[]	Rock poisson ratio
SSMOV201	VerticalExtentOfRockFall2_1[m]	Vertical extent of rock fall for rock condition 2 and ground acceleration 0.05 g. The lower limit is approximately equivalent to the average rock joint spacing of rock condition 1. The upper limit is estimated from numerical results.
SSMOV202	VerticalExtentOfRockFall2_2[m]	Same as above except with ground acceleration 0.10g

DESCRIPTION OF ABBREVIATIONS USED FOR TPA VERSION 3.2 CODE INPUT PARAMETERS (cont'd)

Short Name	Full Name	Description
SSMOV203	VerticalExtentOfRockFall2_3[m]	Same as above except with ground acceleration 0.15g
SSMOV204	VerticalExtentOfRockFall2_4[m]	Same as above except with ground acceleration 0.20g
SSMOV205	VerticalExtentOfRockFall2_5[m]	Same as above except with ground acceleration 0.25g
SSMOV206	VerticalExtentOfRockFall2_6[m]	Same as above except with ground acceleration 0.30g
SSMOV207	VerticalExtentOfRockFall2_7[m]	Same as above except with ground acceleration 0.35g
SSMOV208	VerticalExtentOfRockFall2_8[m]	Same as above except with ground acceleration 0.40g
SSMOV209	VerticalExtentOfRockFall2_9[m]	Same as above except with ground acceleration 0.45g
SSMOV210	VerticalExtentOfRockFall2_10[m]	Same as above except with ground acceleration 0.50g
SSMOV301	VerticalExtentOfRockFall3_1[m]	Vertical extent of rock fall for rock condition 3 and ground acceleration 0.05 g
SSMOV302	VerticalExtentOfRockFall3_2[m]	Same as above except with ground acceleration 0.10g
SSMOV303	VerticalExtentOfRockFall3_3[m]	Same as above except with ground acceleration 0.15g
SSMOV304	VerticalExtentOfRockFall3_4[m]	Same as above except with ground acceleration 0.20g
SSMOV305	VerticalExtentOfRockFall3_5[m]	Same as above except with ground acceleration 0.25g

DESCRIPTION OF ABBREVIATIONS USED FOR TPA VERSION 3.2 CODE INPUT PARAMETERS (cont'd)

Short Name	Full Name	Description
SSMOV306	VerticalExtentOfRockFall3_6[m]	Same as above except with ground acceleration 0.30g
SSMOV307	VerticalExtentOfRockFall3_7[m]	Same as above except with ground acceleration 0.35g
SSMOV308	VerticalExtentOfRockFall3_8[m]	Same as above except with ground acceleration 0.40g
SSMOV309	VerticalExtentOfRockFall3_9[m]	Same as above except with ground acceleration 0.45g
SSMOV310	VerticalExtentOfRockFall3_10[m]	Same as above except with ground acceleration 0.50g
SSMOV401	VerticalExtentOfRockFall4_1[m]	Vertical extent of rock fall for rock condition 4 and ground acceleration 0.05 g
SSMOV402	VerticalExtentOfRockFall4_2[m]	Same as above except with ground acceleration 0.10g
SSMOV403	VerticalExtentOfRockFall4_3[m]	Same as above except with ground acceleration 0.15g
SSMOV404	VerticalExtentOfRockFall4_4[m]	Same as above except with ground acceleration 0.20g
SSMOV405	VerticalExtentOfRockFall4_5[m]	Same as above except with ground acceleration 0.25g
SSMOV406	VerticalExtentOfRockFall4_6[m]	Same as above except with ground acceleration 0.30g
SSMOV407	VerticalExtentOfRockFall4_7[m]	Same as above except with ground acceleration 0.35g
SSMOV408	VerticalExtentOfRockFall4_8[m]	Same as above except with ground acceleration 0.40g

DESCRIPTION OF ABBREVIATIONS USED FOR TPA VERSION 3.2 CODE INPUT PARAMETERS (cont'd)

Short Name	Full Name	Description
SSMOV409	VerticalExtentOfRockFall4_9[m]	Same as above except with ground acceleration 0.45g
SSMOV410	VerticalExtentOfRockFall4_10[m]	Same as above except with ground acceleration 0.50g
SSMOV501	VerticalExtentOfRockFall5_1[m]	Vertical extent of rock fall for rock condition 5 and ground acceleration 0.05 g
SSMOV502	VerticalExtentOfRockFall5_2[m]	Same as above except with ground acceleration 0.10g
SSMOV503	VerticalExtentOfRockFall5_3[m]	Same as above except with ground acceleration 0.15g
SSMOV504	VerticalExtentOfRockFall5_4[m]	Same as above except with ground acceleration 0.20g
SSMOV505	VerticalExtentOfRockFall5_5[m]	Same as above except with ground acceleration 0.25g
SSMOV506	VerticalExtentOfRockFall5_6[m]	Same as above except with ground acceleration 0.30g
SSMOV507	VerticalExtentOfRockFall5_7[m]	Same as above except with ground acceleration 0.35g
SSMOV508	VerticalExtentOfRockFall5_8[m]	Same as above except with ground acceleration 0.40g
SSMOV509	VerticalExtentOfRockFall5_9[m]	Same as above except with ground acceleration 0.45g
SSMOV510	VerticalExtentOfRockFall5_10[m]	Same as above except with ground acceleration 0.50g
TempGrBI	TemperatureGradientInVicinityOfBoilingIsotherm[K/m]	Temperature gradient in the vicinity of the boiling isotherm. (Parameter specific to reflux3 model)

DESCRIPTION OF ABBREVIATIONS USED FOR TPA VERSION 3.2 CODE INPUT PARAMETERS (cont'd)

Short Name	Full Name	Description
VC-Dia	DiameterOfVolcanicCone[m]	Cone diameter
VD-Angle	AngleOfVolcanicDikeMeasuredFromNorthClockwise[degrees]	Volcanic dike angle
VD-Width	WidthOfVolcanicDike[m]	Volcanic dike width
VD-Lengt	LengthOfVolcanicDike[m]	Volcanic dike length
VE-Power	VolcanicEventPower[W]	Volcanic event power
VE-Durat	VolcanicEventDuration[s]	Volcanic event duration
VEi/e-R#	RNtoDetermineIfExtrusiveOrIntrusiveVolcanicEvent	Random number to determine volcanic event type
VEROI-Tn	TimeOfNextVolcanicEventinRegionOfInterest[yr]	Time of next volcanic event
WindSpd	WindSpeed[cm/s]	Wind speed
WP-Def%	DefectiveFractionOfWPs/cell	Fraction of total waste packages in a subarea that fail at time t=0
WPFD-ThD	ThresholdDisplacementforFaultDisruptionOfWP[m]	Threshold fault displacement for disruption. Data input order: number of fault displacement values to be provided followed by equiprobable displacement values
WPRRG@10	WellPumpingRateAtReceptorGroup10km[gal/day]	Well pumping rate for residential receptor group located less than 10 km from Yucca Mountain

DESCRIPTION OF ABBREVIATIONS USED FOR TPA VERSION 3.2 CODE INPUT PARAMETERS (cont'd)

Short Name	Full Name	Description
WPRRG@20	WellPumpingRateAtReceptorGroup20km[gal/day]	Well pumping rate for residential receptor group located less than 20 km from Yucca Mountain
YMR-TC	ThermalConductivityofYMRock[W/(m-K)]	Thermal conductivity of rock

APPENDIX E

APPENDIX E
DETAILED RESULTS FROM DIFFERENTIAL ANALYSES

The tables in this appendix present the results of the differential analysis. Tables E-1 and E-2 present the results for the basecase analysis for 10,000-yr and 50,000-yr TPI. Tables E-3 and E-4 present the results for the faulting scenario for 10,000-yr and 50,000-yr TPI. Table E-5 presents the results for the volcanism scenario. The results for the 50,000-yr TPI are not expected to be different than the 10,000-yr results, because after the 10,000-yr TPI when the groundwater dose dominates, the primary contributors to ground surface dose have decreased (see section 4.3.1). Therefore, only the table for the 10,000-yr TPI is shown.

The tables are organized in the following manner. The first column lists an abbreviation of the parameter that was tested. Only those parameters that had a non-zero result in any of the seven runs are included on the table. The second column contains the arithmetic average of the sigma-weighted sensitivity coefficients of the seven runs. This value considers the uncertainty of the parameter as well as the magnitude of the dose for the given run in calculating the sensitivity of a parameter and is the result by which the parameters are sorted. The third column contains the arithmetic average of the scaled sensitivity coefficients, which show the absolute sensitivity that a parameter has on the results of the TPA code without taking the input range of the parameter into account. The fourth column shows the geometric average of the same value to weight more highly those parameters that show high sensitivity for all runs instead of just a high sensitivity for a couple of runs. The fifth column contains the highest value of the scaled sensitivity coefficients calculated in any of the runs. The remainder of the columns show the individual run results for both the sigma-weighted sensitivity coefficient and the scaled sensitivity coefficients.

Table E-1. Differential analysis results for the basecase for a time period of interest of 10,000 yr

Parameter Name— 10,000-yr, Ranked by Sigma	Arith. Mean of Sigma Weighted Values	S - Arith. Mean	S - Geom. Mean	S - High Value	R1 - Sigma	R2 - Sigma	R3 - Sigma	R4 - Sigma	R5 - Sigma	R6 - Sigma	R7 - Sigma	R1 - S	R2 - S	R3 - S	R4 - S	R5 - S	R6 - S	R7 - S
Base Value Peak Total Effective Dose Equivalent (rem/yr)					3.85e-06	1.33e-07	1.44e-07	6.48e-06	4.01e-08	2.00e-06	4.02e-06	3.85e-06	1.33e-07	1.44e-07	6.48e-06	4.01e-08	2.00e-06	4.02e-06
ARDSAVTc	1.138e-05	6.139e-01	4.766e-02	1.791e+00	1.11e-08	0.00e+00	1.86e-07	7.92e-05	2.31e-07	9.02e-09	0.00e+00	2.60e-03	7.51e-03	7.31e-01	1.76e+00	1.79e+00	5.00e-03	2.49e-03
FOCTR-R	9.574e-06	9.796e-02	3.942e-02	2.753e-01	2.68e-08	7.02e-09	0.00e+00	5.77e-11	0.00e+00	6.70e-05	7.41e-11	2.75e-01	1.95e-01	6.96e-03	2.62e-02	2.49e-03	4.50e-02	1.34e-01
Fow*	3.822e-06	6.792e-01	4.682e-01	2.291e+00	2.09e-05	2.54e-07	4.54e-07	3.50e-06	7.90e-08	1.68e-07	1.44e-06	2.29e+00	4.66e-01	7.73e-01	3.30e-01	4.81e-01	1.35e-01	2.79e-01
ARDSAV_I	2.982e-06	2.137e+00	1.736e+00	4.264e+00	7.88e-06	7.80e-08	1.37e-07	3.85e-06	1.81e-08	8.31e-07	8.07e-06	2.82e+00	9.54e-01	3.81e+00	8.60e-01	1.10e+00	1.15e+00	4.26e+00
SFWt%I3	2.618e-06	2.058e+00	5.144e-01	7.021e+00	6.78e-06	3.92e-08	5.63e-08	2.18e-06	0.00e+00	4.02e-07	8.86e-06	4.94e+00	7.06e-01	3.20e-01	8.06e-01	2.49e-03	6.05e-01	7.02e+00
WP-Def%	2.167e-06	1.336e+00	1.212e+00	2.539e+00	1.05e-06	1.48e-07	4.57e-08	9.17e-06	3.29e-08	2.69e-06	2.03e-06	6.43e-01	1.38e+00	8.96e-01	2.54e+00	1.87e+00	9.74e-01	1.04e+00
ARDSAVSe	1.808e-06	5.714e-02	1.111e-02	3.090e-01	1.18e-05	0.00e+00	0.00e+00	0.00e+00	8.72e-07	0.00e+00	0.00e+00	6.75e-02	7.51e-03	6.96e-03	1.54e-03	3.09e-01	5.00e-03	2.49e-03
SbArWt%	1.681e-06	1.000e+00	1.000e+00	1.002e+00	1.27e-06	1.82e-06	1.32e-07	5.77e-06	5.23e-08	1.12e-06	1.61e-06	1.00e+00	9.99e-01	1.00e+00	1.00e+00	9.99e-01	1.00e+00	9.98e-01
Fmult*	1.478e-06	6.823e-01	4.721e-01	2.290e+00	8.10e-06	2.10e-08	3.20e-08	9.05e-07	1.82e-08	1.94e-07	1.07e-06	2.29e+00	4.81e-01	7.73e-01	3.33e-01	4.81e-01	1.35e-01	2.84e-01
FOC-R	1.037e-06	4.578e-02	2.877e-02	9.347e-02	2.81e-08	1.84e-08	2.18e-13	1.08e-10	2.28e-10	7.21e-06	0.00e+00	9.35e-02	2.25e-02	2.09e-02	6.64e-02	8.97e-02	2.50e-02	2.49e-03
WPRRG@20	8.463e-07	9.956e-01	9.956e-01	1.010e+00	7.22e-07	4.57e-08	4.28e-08	2.74e-06	8.05e-09	7.29e-07	1.64e-06	9.89e-01	9.91e-01	1.01e+00	9.89e-01	9.89e-01	1.01e+00	9.91e-01
SfWt%I4	6.774e-07	3.365e-01	1.332e-01	1.468e+00	2.89e-07	5.28e-09	2.67e-08	4.20e-06	1.65e-08	5.48e-08	1.45e-07	3.37e-02	1.50e-02	2.51e-01	1.47e+00	3.84e-01	9.50e-02	1.10e-01
APrs_SAV	6.615e-07	2.522e+00	2.159e+00	4.780e+00	9.72e-07	2.25e-08	7.91e-08	1.37e-06	1.45e-08	2.08e-07	1.97e-06	2.00e+00	1.37e+00	4.78e+00	1.52e+00	3.28e+00	8.75e-01	3.83e+00
AAMAI@S	4.890e-07	8.722e-01	4.354e-01	2.446e+00	2.71e-06	6.07e-08	7.76e-08	3.18e-07	1.68e-08	7.36e-08	1.65e-07	2.45e+00	1.13e+00	1.43e+00	9.41e-02	8.12e-01	9.00e-02	1.10e-01
SFWt%I5	4.449e-07	5.342e-01	2.791e-01	1.672e+00	8.38e-08	4.86e-08	1.50e-08	1.07e-06	2.23e-07	2.68e-07	1.41e-06	6.75e-02	1.03e+00	2.37e-01	4.94e-02	1.67e+00	2.00e-01	4.86e-01
MAPM@GM	4.374e-07	1.116e+00	7.458e-01	3.323e+00	1.79e-06	6.59e-09	2.29e-08	5.51e-07	6.07e-09	3.15e-08	6.52e-07	3.32e+00	4.13e-01	1.38e+00	4.89e-01	8.17e-01	1.35e-01	1.26e+00
InitRSFP	4.032e-07	7.456e-01	7.433e-01	8.660e-01	5.68e-07	2.22e-08	2.20e-08	1.25e-06	7.15e-09	3.15e-07	6.40e-07	7.24e-01	7.44e-01	6.82e-01	8.66e-01	7.92e-01	7.00e-01	7.10e-01
SFWt%I1	3.661e-07	2.806e-01	7.829e-02	1.119e+00	2.20e-06	7.06e-08	1.53e-08	1.32e-07	0.00e+00	1.03e-07	4.13e-08	5.14e-01	1.12e+00	1.95e-01	5.40e-02	2.49e-03	6.00e-02	1.99e-02
TempGrBI	3.256e-07	2.104e-01	1.041e-01	4.801e-01	1.64e-06	1.04e-08	1.13e-09	1.30e-07	6.62e-09	3.69e-07	1.26e-07	2.91e-01	2.10e-01	6.96e-03	3.09e-02	4.01e-01	4.80e-01	5.23e-02
SFWt%I6	3.241e-07	1.500e-01	6.516e-02	3.551e-01	1.14e-07	1.29e-08	2.63e-09	9.99e-07	0.00e+00	5.86e-07	5.53e-07	8.57e-02	1.50e-02	6.26e-02	2.58e-01	2.49e-03	3.55e-01	2.71e-01
MPrm_CHv	2.681e-07	1.063e-01	1.048e-02	6.957e-01	1.83e-06	5.53e-09	0.00e+00	0.00e+00	0.00e+00	4.59e-08	0.00e+00	6.96e-01	1.50e-02	6.96e-03	1.54e-03	2.49e-03	2.00e-02	2.49e-03
SFWt%I7	2.057e-07	2.087e-01	6.076e-02	6.154e-01	9.49e-07	1.45e-09	6.36e-08	1.11e-07	0.00e+00	1.30e-07	1.85e-07	6.15e-01	3.76e-02	5.71e-01	7.72e-03	2.49e-03	8.50e-02	1.42e-01
YMR-TC	1.652e-07	1.285e+00	1.252e+00	1.692e+00	1.92e-07	1.20e-08	9.48e-09	4.89e-07	4.09e-09	1.86e-07	2.64e-07	8.39e-01	1.40e+00	1.06e+00	1.32e+00	1.69e+00	1.61e+00	1.07e+00
SFWt%I2	1.537e-07	9.565e-02	3.249e-02	2.854e-01	0.00e+00	5.29e-08	4.26e-08	5.31e-08	0.00e+00	2.60e-08	9.01e-07	2.60e-03	2.85e-01	2.09e-01	2.31e-02	2.49e-03	4.00e-02	1.07e-01
FPrs_STF	1.359e-07	3.274e-02	3.021e-02	5.725e-02	2.31e-07	3.73e-09	6.83e-09	3.15e-07	2.13e-09	2.13e-08	3.71e-07	5.19e-02	2.25e-02	2.78e-02	2.47e-02	1.99e-02	2.50e-02	5.73e-02
FOCTR	6.167e-08	1.745e-01	5.696e-02	5.456e-01	1.18e-08	1.65e-08	4.55e-09	1.67e-07	7.59e-09	1.99e-07	2.54e-08	7.79e-03	3.46e-01	1.39e-02	5.09e-02	5.46e-01	2.50e-01	7.47e-03
MATI@GM	2.717e-08	1.245e-01	4.904e-02	5.580e-01	8.13e-08	1.47e-09	3.08e-10	4.66e-08	3.86e-09	0.00e+00	5.67e-08	1.14e-01	6.01e-02	1.39e-02	2.78e-02	5.58e-01	5.00e-03	9.21e-02
FPrm_UCF	3.686e-09	4.084e-03	3.504e-03	7.507e-03	0.00e+00	2.58e-08	0.00e+00	0.00e+00	0.00e+00	0.00e+00	0.00e+00	2.60e-03	7.51e-03	6.96e-03	1.54e-03	2.49e-03	5.00e-03	2.49e-03

Table E-2. Differential analysis results for the basecase for a time period of interest of 50,000 yr

Parameter Name—50,000-yr, Ranked by Sigma	Arith. Mean of Sigma Weighted Values	S - Arithmatic Mean	S - Geometric Mean	S - High Value	R1 - Sigma	R2 - Sigma	R3 - Sigma	R4 - Sigma	R5 - Sigma	R6 - Sigma	R7 - Sigma	R1 - S	R2 - S	R3 - S	R4 - S	R5 - S	R6 - S	R7 - S
Base Value Peak Total Effective Dose Equivalent (rem/yr)					5.60e-04	1.90e-05	9.60e-05	4.40e-04	1.50e-04	5.40e-04	4.70e-04	5.60e-04	1.90e-05	9.60e-05	4.40e-04	1.50e-04	5.40e-04	4.70e-04
ARDSAVNp	2.372e-03	1.205e+00	8.297e-03	8.416e+00	1.66e-02	0.00e+00	0.00e+00	0.00e+00	0.00e+00	0.00e+00	0.00e+00	8.42e+00	5.19e-03	1.04e-03	2.29e-03	6.53e-03	1.86e-03	2.14e-03
Fow*	2.131e-04	4.145e-01	2.794e-01	7.334e-01	1.66e-04	5.53e-05	6.92e-05	4.51e-04	3.11e-04	1.25e-06	4.38e-04	1.26e-01	7.01e-01	1.76e-01	6.33e-01	4.96e-01	3.73e-02	7.33e-01
OO-CofLC	2.105e-04	1.590e+00	7.834e-02	8.939e+00	0.00e+00	0.00e+00	9.12e-08	1.81e-04	1.43e-04	1.14e-03	1.13e-05	1.80e-03	5.19e-03	3.12e-03	6.26e-01	1.48e+00	8.94e+00	7.51e-02
AA_2_1	1.920e-04	1.268e+00	2.346e-01	3.513e+00	5.75e-04	1.53e-07	2.38e-06	6.25e-05	7.93e-05	0.00e+00	6.25e-04	3.15e+00	4.15e-02	4.89e-02	6.28e-01	1.49e+00	1.86e-03	3.51e+00
SbArWt%	1.914e-04	1.000e+00	1.000e+00	1.006e+00	1.83e-04	2.63e-04	8.79e-05	3.87e-04	2.01e-04	3.01e-05	1.87e-04	1.00e+00	9.96e-01	9.99e-01	9.99e-01	1.01e+00	9.99e-01	1.00e+00
ARDSAVTc	1.762e-04	2.593e-01	1.349e-01	5.392e-01	9.80e-05	6.14e-08	9.19e-05	8.21e-04	1.80e-04	2.10e-05	2.11e-05	1.58e-01	5.19e-03	5.39e-01	2.70e-01	3.66e-01	4.34e-01	4.29e-02
Fmult*	8.428e-05	4.160e-01	2.785e-01	7.464e-01	6.52e-05	4.47e-06	4.91e-06	1.15e-04	7.06e-05	1.36e-06	3.28e-04	1.27e-01	7.06e-01	1.77e-01	6.30e-01	4.90e-01	3.54e-02	7.46e-01
WPRRG@20	8.060e-05	9.949e-01	9.949e-01	1.010e+00	1.04e-04	6.61e-06	2.86e-05	1.84e-04	3.06e-05	1.96e-05	1.90e-04	9.89e-01	9.91e-01	1.01e+00	9.90e-01	9.86e-01	1.01e+00	9.89e-01
APrs_SAV	7.848e-05	1.392e+00	4.233e-01	6.021e+00	4.24e-04	6.14e-08	6.85e-06	2.23e-06	7.95e-06	5.39e-06	1.03e-04	6.02e+00	2.59e-02	6.19e-01	3.67e-02	4.70e-01	8.46e-01	1.73e+00
ARDSAV_I	6.033e-05	3.891e-01	2.021e-01	1.389e+00	7.25e-06	1.66e-06	4.26e-06	8.37e-05	8.66e-06	1.13e-05	3.05e-04	1.80e-02	1.40e-01	1.77e-01	2.77e-01	1.37e-01	5.85e-01	1.39e+00
MAPM@GM	4.974e-05	2.108e+00	9.541e-01	8.692e+00	4.83e-05	2.01e-05	6.01e-06	1.15e-04	3.74e-05	3.85e-07	1.21e-04	6.19e-01	8.69e+00	5.41e-01	1.51e+00	1.32e+00	6.15e-02	2.01e+00
AAMAI@S	4.432e-05	3.256e-01	2.190e-01	7.570e-01	2.93e-05	2.96e-06	2.88e-06	1.14e-04	2.73e-05	7.36e-07	1.33e-04	1.83e-01	3.79e-01	7.91e-02	5.02e-01	3.46e-01	3.35e-02	7.57e-01
SFWt%C6	4.162e-05	2.129e-01	1.365e-01	6.713e-01	7.18e-05	1.65e-06	8.79e-06	8.09e-05	7.43e-06	5.53e-06	1.15e-04	5.57e-02	2.75e-01	9.58e-02	2.50e-01	3.26e-02	1.10e-01	6.71e-01
SFWt%C3	4.086e-05	2.989e-01	1.644e-01	4.619e-01	1.24e-04	3.67e-06	1.27e-05	1.15e-04	1.61e-05	7.26e-06	7.40e-06	2.41e-01	4.62e-01	3.53e-01	4.40e-01	2.74e-01	3.20e-01	2.14e-03
SFWt%C2	3.250e-05	2.696e-01	1.330e-01	4.440e-01	3.15e-05	5.42e-06	1.98e-05	1.37e-04	2.88e-05	5.40e-06	0.00e+00	1.47e-01	4.41e-01	3.62e-01	4.10e-01	4.44e-01	8.01e-02	2.14e-03
SFWt%C4	3.239e-05	1.714e-01	1.478e-01	3.160e-01	1.22e-04	1.62e-06	4.47e-06	5.16e-05	6.57e-06	6.87e-07	4.01e-05	3.16e-01	1.25e-01	1.51e-01	1.67e-01	1.31e-01	4.47e-02	2.66e-01
SFWt%C5	3.144e-05	1.410e-01	1.071e-01	2.693e-01	9.99e-05	1.39e-06	7.04e-06	7.72e-05	1.18e-05	5.03e-06	1.78e-05	2.69e-01	4.15e-02	5.73e-02	1.53e-01	1.83e-01	2.46e-01	3.65e-02
SFWt%C1	3.014e-05	2.782e-01	1.902e-01	5.453e-01	2.24e-05	3.48e-06	1.56e-05	8.54e-05	1.57e-05	5.30e-06	6.31e-05	1.97e-02	4.15e-01	2.60e-01	5.45e-01	3.20e-01	7.83e-02	3.09e-01
InitRSFP	3.006e-05	5.978e-01	5.170e-01	1.012e+00	9.42e-05	9.89e-07	2.00e-05	3.34e-05	1.89e-05	1.22e-05	3.08e-05	8.31e-01	2.28e-01	9.27e-01	3.44e-01	5.49e-01	1.01e+00	2.94e-01
ARDSAVSe	2.994e-05	3.938e-03	3.538e-03	6.531e-03	1.36e-04	9.42e-07	1.92e-06	0.00e+00	7.03e-05	4.17e-07	0.00e+00	5.39e-03	5.19e-03	4.16e-03	2.29e-03	6.53e-03	1.86e-03	2.14e-03
MKDCHvNp	2.258e-05	4.043e-02	5.060e-03	2.639e-01	1.58e-04	0.00e+00	0.00e+00	0.00e+00	0.00e+00	0.00e+00	0.00e+00	2.64e-01	5.19e-03	1.04e-03	2.29e-03	6.53e-03	1.86e-03	2.14e-03
SFWt%C7	1.881e-05	4.681e-02	3.565e-02	1.029e-01	7.11e-05	7.45e-07	2.13e-06	1.91e-05	3.66e-06	2.77e-06	3.22e-05	1.62e-02	6.23e-02	7.29e-03	4.58e-02	3.92e-02	5.40e-02	1.03e-01
MATI@GM	1.438e-05	2.448e-01	1.404e-01	7.635e-01	1.46e-05	6.23e-07	1.45e-06	2.02e-05	9.13e-06	9.83e-08	5.46e-05	1.42e-01	1.76e-01	9.79e-02	1.79e-01	3.46e-01	9.32e-03	7.63e-01
YMR-TC	1.392e-05	7.965e-01	6.034e-01	1.861e+00	5.58e-05	3.20e-07	3.15e-06	8.52e-06	1.72e-05	1.61e-06	1.10e-05	1.68e+00	2.60e-01	5.26e-01	3.41e-01	1.86e+00	5.20e-01	3.84e-01
Solbl-Np	1.015e-05	2.376e-02	4.655e-03	1.472e-01	7.11e-05	0.00e+00	0.00e+00	0.00e+00	0.00e+00	0.00e+00	0.00e+00	1.47e-01	5.19e-03	1.04e-03	2.29e-03	6.53e-03	1.86e-03	2.14e-03
WP-Def%	8.342e-06	3.750e-02	7.792e-03	2.331e-01	5.51e-05	6.40e-08	2.77e-07	1.73e-06	2.62e-07	0.00e+00	9.72e-07	2.33e-01	4.15e-03	8.12e-03	7.10e-03	3.92e-03	1.86e-03	4.29e-03
FPrs_STF	2.503e-06	8.337e-03	6.352e-03	1.863e-02	6.94e-06	1.24e-07	3.42e-07	0.00e+00	0.00e+00	4.27e-07	9.69e-06	1.08e-02	5.19e-03	2.08e-03	2.29e-03	6.53e-03	1.86e-02	1.29e-02
SFWt%I4	2.378e-06	5.130e-03	3.833e-03	1.256e-02	1.56e-05	0.00e+00	7.42e-08	0.00e+00	0.00e+00	0.00e+00	9.88e-07	1.26e-02	5.19e-03	1.04e-03	2.29e-03	6.53e-03	1.86e-03	6.43e-03
ARDSAVNi	1.150e-06	2.978e-03	2.480e-03	6.529e-03	0.00e+00	0.00e+00	8.05e-06	0.00e+00	0.00e+00	0.00e+00	0.00e+00	1.80e-03	5.19e-03	1.04e-03	2.29e-03	6.53e-03	1.86e-03	2.14e-03
SFWt%I7	1.023e-06	6.826e-03	3.687e-03	2.873e-02	6.41e-06	0.00e+00	7.75e-08	0.00e+00	3.48e-07	0.00e+00	3.24e-07	2.87e-02	5.19e-03	1.04e-03	2.29e-03	6.53e-03	1.86e-03	2.14e-03
SFWt%I2	7.838e-07	6.332e-03	5.027e-03	1.304e-02	0.00e+00	0.00e+00	5.68e-07	1.77e-06	8.26e-07	2.27e-07	2.10e-06	1.80e-03	5.19e-03	4.16e-03	1.15e-02	6.53e-03	1.30e-02	2.14e-03
SFWt%I1	7.633e-07	7.893e-03	6.537e-03	1.306e-02	0.00e+00	0.00e+00	6.02e-07	1.88e-06	6.24e-07	1.72e-07	2.06e-06	1.80e-03	5.19e-03	1.15e-02	1.15e-02	1.31e-02	3.73e-03	8.58e-03
SFWt%I3	6.962e-07	5.703e-03	4.411e-03	1.257e-02	2.49e-06	0.00e+00	1.22e-07	4.18e-07	5.16e-07	6.64e-08	1.26e-06	1.26e-02	5.19e-03	1.04e-03	2.29e-03	6.53e-03	3.73e-03	8.58e-03
TempGrBI	6.230e-07	1.789e-02	4.422e-03	1.062e-01	1.46e-06	0.00e+00	1.13e-07	0.00e+00	0.00e+00	2.19e-06	5.98e-07	1.80e-03	5.19e-03	1.04e-03	2.29e-03	6.53e-03	1.06e-01	2.14e-03
SFWt%I6	5.317e-07	4.766e-03	4.034e-03	8.977e-03	1.73e-06	0.00e+00	5.84e-08	0.00e+00	3.29e-07	8.26e-08	1.52e-06	8.98e-03	5.19e-03	2.08e-03	2.29e-03	6.53e-03	1.86e-03	6.43e-03
SFWt%I5	4.526e-07	4.311e-03	3.448e-03	8.977e-03	1.61e-06	0.00e+00	4.41e-08	0.00e+00	0.00e+00	6.70e-08	1.45e-06	8.98e-03	5.19e-03	1.04e-03	2.29e-03	6.53e-03	1.86e-03	4.29e-03
MPrm_CHv	3.056e-07	7.332e-03	4.140e-03	2.076e-02	0.00e+00	1.11e-06	0.00e+00	0.00e+00	0.00e+00	1.03e-06	0.00e+00	1.80e-03	2.08e-02	1.04e-03	2.29e-03	6.53e-03	1.68e-02	2.14e-03
MKDCHvSe	1.783e-07	2.978e-03	2.480e-03	6.528e-03	0.00e+00	0.00e+00	0.00e+00	0.00e+00	1.25e-06	0.00e+00	0.00e+00	1.80e-03	5.19e-03	1.04e-03	2.29e-03	6.53e-03	1.86e-03	2.14e-03
FOCTR	1.686e-07	6.439e-03	3.617e-03	2.609e-02	3.95e-07	0.00e+00	2.27e-07	0.00e+00	0.00e+00	5.58e-07	0.00e+00	1.80e-03	5.19e-03	1.04e-03	2.29e-03	6.53e-03	2.61e-02	2.14e-03
CritRHAC	1.548e-07	1.393e-01	6.050e-03	9.558e-01	0.00e+00	0.00e+00	0.00e+00	0.00e+00	0.00e+00	1.08e-06	0.00e+00	1.80e-03	5.19e-03	1.04e-03	2.29e-03	6.53e-03	9.56e-01	2.14e-03
FOC-R	1.115e-08	3.127e-03	2.738e-03	6.529e-03	7.81e-08	0.00e+00	1.45e-11	0.00e+00	0.00e+00	0.00e+00	0.00e+00	1.80e-03	5.19e-03	2.08e-03	2.29e-03	6.53e-03	1.86e-03	2.14e-03
FOCTR-R	3.631e-09	2.979e-03	2.481e-03	6.529e-03	2.53e-08	0.00e+00	0.00e+00	0.00e+00	0.00e+00	0.00e+00	1.37e-10	1.80e-03	5.19e-03	1.04e-03	2.29e-03	6.53e-03	1.86e-03	2.14e-03

Table E-3. Differential analysis results for the faulting scenario for a time period of interest of 10,000 yr

10,000-yr, Faulting, Random4 Values Increased by 1%	dD/dx	Sigma	X bar	Mean Dose	dD/dx*sigma	S
SFWT%F0	5.09e-04	2.89e-01	2.66e-01	4.34e-04	0.0001471003	0.3124591
FEROI-Tn	-1.16e-07	2.86e+03	7.14e+03	4.34e-04	0.0003312564	1.9061315
WPFD-ThD	0.00e+00	1.12e-01	1.00e-01	4.34e-04	0	0
FEROI-X	0.00e+00	3.47e+03	5.48e+05	4.34e-04	0	0
FEROI-Y	0.00e+00	8.20e+03	4.08e+06	4.34e-04	0	0
FO-Rn#Sd	0.00e+00	2.89e-01	6.56e-01	4.34e-04	0	0
NWFZnW	0.00e+00	1.74e+01	2.50e+01	4.34e-04	0	0
NEFZnW	-6.24e-07	2.32e+01	1.46e+01	4.34e-04	0.0000144944	0.0209178
NWLCDAmt	0.00e+00	1.00e-01	2.03e-01	4.34e-04	0	0
NELCDAmt	0.00e+00	1.00e-01	1.64e-01	4.34e-04	0	0

Table E-4. Differential analysis results for the faulting scenario for a time period of interest of 50,000 yr

50,000-yr, Faulting, Random4 Values Increased by 1%	dD/dx	Sigma	X bar	Mean Dose	dD/dx*sigma	S
NELCDAmt	0.00e+00	1.00e-01	1.64e-01	4.34e-04	0	0
NEFZnW	-6.87e-08	2.32e+01	1.46e+01	4.34e-04	0.0000015956	0.0023027
NWLCDAmt	0.00e+00	1.00e-01	2.03e-01	4.34e-04	0	0
NWFZnW	0.00e+00	1.74e+01	2.50e+01	4.34e-04	0	0
FO-Rn#Sd	0.00e+00	2.89e-01	6.56e-01	4.34e-04	0	0
SFWt%F0	1.50e-05	2.89e-01	2.66e-01	4.34e-04	0.0000043366	0.0092115
WPFD-ThD	0.00e+00	1.12e-01	1.00e-01	4.34e-04	0	0
FEROI-Tn	0.00e+00	2.86e+03	7.14e+03	4.34e-04	0	0
FEROI-X	0.00e+00	3.47e+03	5.48e+05	4.34e-04	0	0
FEROI-Y	0.00e+00	8.20e+03	4.08e+06	4.34e-04	0	0

Table E-5. Differential analysis results for the igneous activities scenario for a time period of interest of 10,000 yr

Parameter	Arith. Mean of Sigma Weighted	S - Arith. Mean	S - Geom. Mean	S - High Value	R1 - Sigma	R2 - Sigma	R3 - Sigma	R4 - Sigma	R5 - Sigma	R6 - Sigma	R7 - Sigma	R1 - S	R2 - S	R3 - S	R4 - S	R5 - S	R6 - S	R7 - S
Base Value Peak Total Effective Dose Equivalent(rem/yr)*					2.35e-01	1.51e+00	1.89e+00	9.34e-01	5.90e-02	2.28e+00	2.12e+00	2.35e-01	1.51e+00	1.89e+00	9.34e-01	5.90e-02	2.28e+00	2.12e+00
VE-Power	3.672e+00	8.051e-01	7.434e-01	1.328e+00	7.75e-02	1.55e+01	2.41e+00	1.23e+00	5.12e-02	2.30e+00	4.15e+00	7.88e-01	3.05e-01	9.16e-01	9.13e-01	7.94e-01	5.92e-01	1.33e+00
ABMLFVDC	2.835e+00	7.526e-01	5.856e-01	9.695e-01	6.02e-02	1.39e+01	2.22e+00	1.17e+00	7.37e-02	9.04e-01	1.53e+00	8.23e-01	8.36e-01	9.53e-01	9.70e-01	8.99e-01	7.32e-01	5.65e-02
VE-Durat	2.014e+00	6.285e-01	2.945e-01	9.695e-01	5.70e-01	0.00e+00	7.50e+00	4.70e+00	1.45e-02	1.31e+00	8.16e-03	8.14e-01	6.63e-03	9.43e-01	9.70e-01	8.95e-01	7.10e-01	6.12e-02
VEROI-Tn	1.300e+00	5.050e-01	4.627e-01	8.700e-01	4.06e-02	2.29e+00	6.66e-01	2.10e-01	1.32e-02	4.31e-01	5.45e+00	5.03e-01	8.18e-01	3.32e-01	3.24e-01	3.24e-01	3.64e-01	8.70e-01
VC-Dia	7.689e-01	2.026e+00	2.026e+00	2.071e+00	1.02e-01	1.34e+00	1.14e+00	8.29e-01	4.18e-02	9.63e-01	9.64e-01	2.00e+00	2.02e+00	2.07e+00	1.99e+00	2.04e+00	2.03e+00	2.03e+00
WindSpd	6.267e-01	4.548e-01	2.324e-01	1.930e+00	3.11e-01	1.82e+00	3.90e-01	2.90e-01	6.95e-02	1.14e+00	3.66e-01	3.11e-01	1.93e+00	1.06e-01	1.17e-01	5.94e-02	4.91e-01	1.69e-01
AshMnPLD	2.306e-01	1.546e-01	1.137e-01	4.841e-01	2.26e-02	5.83e-01	1.06e-01	4.59e-02	9.68e-03	3.02e-01	5.45e-01	1.15e-01	4.84e-01	6.89e-02	3.32e-02	9.84e-02	1.23e-01	1.60e-01
VD-Angle	0.000e+00	4.007e-03	3.432e-03	6.632e-03	0.00e+00	0.00e+00	0.00e+00	0.00e+00	0.00e+00	0.00e+00	0.00e+00	4.26e-03	6.63e-03	5.30e-03	1.07e-03	1.70e-03	4.38e-03	4.71e-03
VD-Lengt	0.000e+00	4.007e-03	3.432e-03	6.632e-03	0.00e+00	0.00e+00	0.00e+00	0.00e+00	0.00e+00	0.00e+00	0.00e+00	4.26e-03	6.63e-03	5.30e-03	1.07e-03	1.70e-03	4.38e-03	4.71e-03
SFWT%V0	0.000e+00	4.007e-03	3.432e-03	6.632e-03	0.00e+00	0.00e+00	0.00e+00	0.00e+00	0.00e+00	0.00e+00	0.00e+00	4.26e-03	6.63e-03	5.30e-03	1.07e-03	1.70e-03	4.38e-03	4.71e-03
VD-Width	0.000e+00	4.007e-03	3.432e-03	6.632e-03	0.00e+00	0.00e+00	0.00e+00	0.00e+00	0.00e+00	0.00e+00	0.00e+00	4.26e-03	6.63e-03	5.30e-03	1.07e-03	1.70e-03	4.38e-03	4.71e-03

*Conditional results not weighted by the scenario probability